



National Library
of Canada

Bibliothèque nationale
du Canada

Acquisitions and
Bibliographic Services Branch

Direction des acquisitions et
des services bibliographiques

395 Wellington Street
Ottawa, Ontario
K1A 0N4

395, rue Wellington
Ottawa (Ontario)
K1A 0N4

Your file Votre référence

Our file Notre référence

NOTICE

The quality of this microform is heavily dependent upon the quality of the original thesis submitted for microfilming. Every effort has been made to ensure the highest quality of reproduction possible.

If pages are missing, contact the university which granted the degree.

Some pages may have indistinct print especially if the original pages were typed with a poor typewriter ribbon or if the university sent us an inferior photocopy.

Reproduction in full or in part of this microform is governed by the Canadian Copyright Act, R.S.C. 1970, c. C-30, and subsequent amendments.

AVIS

La qualité de cette microforme dépend grandement de la qualité de la thèse soumise au microfilmage. Nous avons tout fait pour assurer une qualité supérieure de reproduction.

S'il manque des pages, veuillez communiquer avec l'université qui a conféré le grade.

La qualité d'impression de certaines pages peut laisser à désirer, surtout si les pages originales ont été dactylographiées à l'aide d'un ruban usé ou si l'université nous a fait parvenir une photocopie de qualité inférieure.

La reproduction, même partielle, de cette microforme est soumise à la Loi canadienne sur le droit d'auteur, SRC 1970, c. C-30, et ses amendements subséquents.

UNIVERSITY OF ALBERTA

**STATISTICAL PROPERTIES OF ERBIUM DOPED FIBER
AMPLIFIERS**

BY

BENJAMIN CHAN ©

A thesis submitted to the Faculty of Graduate Studies and Research in partial fulfillment of the requirements for the degree of **MASTER OF SCIENCE.**

DEPARTMENT OF ELECTRICAL ENGINEERING

EDMONTON, ALBERTA
FALL 1995



National Library
of Canada

Bibliothèque nationale
du Canada

Acquisitions and
Bibliographic Services Branch

Direction des acquisitions et
des services bibliographiques

395 Wellington Street
Ottawa, Ontario
K1A 0N4

395, rue Wellington
Ottawa (Ontario)
K1A 0N4

Your file Votre référence

Our file Notre référence

THE AUTHOR HAS GRANTED AN
IRREVOCABLE NON-EXCLUSIVE
LICENCE ALLOWING THE NATIONAL
LIBRARY OF CANADA TO
REPRODUCE, LOAN, DISTRIBUTE OR
SELL COPIES OF HIS/HER THESIS BY
ANY MEANS AND IN ANY FORM OR
FORMAT, MAKING THIS THESIS
AVAILABLE TO INTERESTED
PERSONS.

L'AUTEUR A ACCORDE UNE LICENCE
IRREVOCABLE ET NON EXCLUSIVE
PERMETTANT A LA BIBLIOTHEQUE
NATIONALE DU CANADA DE
REPRODUIRE, PRETER, DISTRIBUER
OU VENDRE DES COPIES DE SA
THESE DE QUELQUE MANIERE ET
SOUS QUELQUE FORME QUE CE SOIT
POUR METTRE DES EXEMPLAIRES DE
CETTE THESE A LA DISPOSITION DES
PERSONNE INTERESSEES.

THE AUTHOR RETAINS OWNERSHIP
OF THE COPYRIGHT IN HIS/HER
THESIS. NEITHER THE THESIS NOR
SUBSTANTIAL EXTRACTS FROM IT
MAY BE PRINTED OR OTHERWISE
REPRODUCED WITHOUT HIS/HER
PERMISSION.

L'AUTEUR CONSERVE LA PROPRIETE
DU DROIT D'AUTEUR QUI PROTEGE
SA THESE. NI LA THESE NI DES
EXTRAITS SUBSTANTIELS DE CELLE-
CI NE DOIVENT ETRE IMPRIMES OU
AUTREMENT REPRODUITS SANS SON
AUTORISATION.

ISBN 0-612-06451-4

Canada

UNIVERSITY OF ALBERTA

RELEASE FORM

NAME OF AUTHOR: **BENJAMIN CHAN**

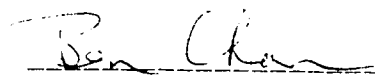
TITLE OF THESIS: **STATISTICAL PROPERTIES OF
ERBIUM DOPED FIBER AMPLIFIERS**

DEGREE: **MASTER OF SCIENCE**

YEAR THIS DEGREE GRANTED: **FALL 1995**

Permission is hereby granted to the University of Alberta Library to reproduce single copies of this thesis and to lend or sell such copies for private, scholarly or scientific research purposes only.

The author reserves all other publication and other rights in association with the copyright in the thesis, and except as hereinbefore provided neither the thesis nor any substantial portion thereof may be printed or otherwise reproduced in any material form without the author's prior written permission.

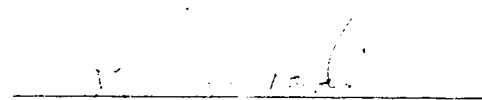

'E', 19/F., Tower 4,
Miami Beach Towers,
268 Wu Chui Road,
Tuen Mun, N.T.,
Hong Kong

DATE: August 15, 1995

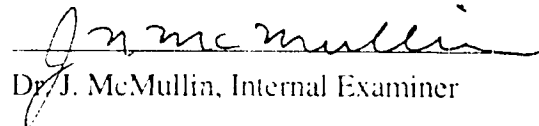
UNIVERSITY OF ALBERTA

FACULTY OF GRADUATE STUDIES AND RESEARCH

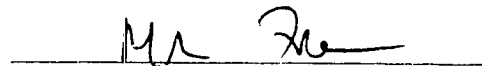
The undersigned certify that they have read, and recommended to the Faculty of Graduate Studies and Research for acceptance a thesis entitled **STATISTICAL PROPERTIES OF ERBIUM DOPED FIBER AMPLIFIERS** in partial fulfillment of the requirements for the degree of **MASTER OF SCIENCE**



Dr. J. Conradi, Supervisor



Dr. J. McMullin, Internal Examiner



Dr. M. Freeman, External Examiner

DATE : August 1, 2001

Dedicated To

My father, mother and brother for their love and support.

Abstract

The non-Gaussian statistics in an Erbium Doped Fiber Amplifier (EDFA) preamplified digital lightwave transmission system have been theoretically studied and experimentally verified. The probability density functions (PDFs) of logical ones and logical zeros are theoretically shown to be the Non-Central and Central Chi-Square distributions respectively when the thermal and shot noises are neglected. The Steepest Descent Method can be used to find the approximated PDFs of logical ones and logical zeros with less than 1% of error when the post-detection Gaussian noises (the thermal and shot noises) are included. The difference between the more commonly used Gaussian approximation to the PDFs and the non-Gaussian PDFs is more apparent when the EDFA small signal gain is large and the receiver electrical bandwidth is sufficiently wide. The Gaussian approximations to the distributions of logical zeros and logical ones can be used to predict receiver sensitivity of EDFA preamplified digital systems within 0.3 dB of the sensitivity predicted using the non-Gaussian PDFs. However in predicting the optimum thresholds for the receiver decision circuit, the Gaussian approximation is less accurate than the non-Gaussian theory. An experimental method has been devised to measure the noise distributions of logical ones and logical zeros. The measured PDFs fit well the shapes of the theoretical non-Gaussian PDFs. The optimum thresholds have also been experimentally measured and the results agree more with the non-Gaussian theory.

Acknowledgments

I would like to express my sincere thanks to my supervisor, Dr. Jan Conradi, for his guidance, support and encouragement.

I would like to sincerely thank Dr. J. McMullin and Dr. M. Freeman for reviewing this thesis.

In addition, I would like to thank Sheldon Walklin, Ping Wan, Tom Young, Dave Moore, Nicole Sat and Stephen Lai for many stimulating and helpful discussions.

I would also like to acknowledge Bruce Beggs and his co-workers at division five of BNR for their help in learning the operation of equipment and devices, and for many helpful suggestions and advice. Finally, I would like to acknowledge Derrick Remedios and Dave Daniger at division one of BNR for many helpful discussions and suggestions.

This work was supported by the Natural Sciences and Engineering Research Council of Canada (NSERC), Bell Northern Research (BNR) and TRILabs through the NSERC/BNR/TRILabs Industrial Research Chair in Fiber Optic Communications at the University of Alberta.

Table of Contents

1. Introduction.....	1
1.1. Optically Preamplified Digital Transmission System.....	1
1.2. Noises in the Optically Preamplified Digital System	3
1.3. The Distributions of the Noises.....	4
1.4. Objectives and Accomplishment	5
1.5. Organization of Thesis	6
2. Non-Gaussian Noise Theory-Part I.....	7
2.1. The Origin of the Non-Gaussian Distribution.....	7
2.2. The Theoretical Model of the System	10
2.3. The Integrate-and-Dump Filter.....	10
2.4. Bandpass Representation of Signal and Noise.....	13
2.5. Fourier Series Representation of Signal and Noise.....	13
2.6. The Dimensionality of Finite Energy Signals	16
2.7. The magnitude spectra of signal and ASE	17
2.8. The Moment Generating Functions and The PDFs.....	19
2.9. The Means and Variances of the PDFs.....	20
2.10. Expressing PDFs in Physical Parameters	21
2.10.1. The autocorrelation function.....	21
2.10.2. The power spectral density of ASE.....	22
2.10.3. The EDFA small signal gain.....	23
2.10.4. The new expressions for the PDFs.....	25
2.11. Comparison of Beat Noises with Olsson's Expressions	26
2.12. The Probability of Error and the Bit Error Rate	28
2.13. Gaussian Approximation.....	31
2.14. Modification of Equations When Polarizer is Omitted	32
2.15. The Optimum Threshold	33

2.16. The Coupling and Insertion Losses.....	34
2.17. Comparison of Gaussian and Chi-Square PDFs.....	34
2.18. On The Computation of Functions.....	39
3. Non-Gaussian Noise Theory-Part II.....	41
3.1. The MGF of Gaussian PDF.....	41
3.2. The Variances of Thermal and Shot Noises.....	41
3.3. The Overall MGF.....	43
3.4. The Steepest Descent Method.....	45
3.4.1. The paths of constant $\text{Im}\{f(r)\}$	46
3.4.2. The path of steepest descent.....	49
3.4.3. The evaluation of $J(z)$	50
3.5. The Inverse Laplace Transform of the Overall MGF.....	52
3.5.1. The saddle point.....	52
3.5.2. The path of steepest descent.....	53
3.5.3. The closed form expression of PDFs.....	58
3.6. The Accuracy of the Steepest Descent Method.....	59
3.7. The Conversion of Current to Voltage.....	60
3.8. The Impact of Values of Parameters on PDFs.....	62
3.9. The Probability of Error and the Bit Error Rate.....	68
4. Simulation of System Performance.....	70
4.1. The BER as a Function of the Received Power.....	70
4.2. The Sensitivity of the System.....	77
4.2.1. The EDFA gain dependence of beat noises.....	80
4.3. The Impacts of Values of Parameters on BER.....	82
4.4. The BER as a Function of the Decision Threshold.....	86
4.4.1. The loci of the percentage optimum threshold.....	89
4.5. The Impacts of Values of Parameters on Threshold.....	90

4.6. Implications of Simulation Results	94
5. Experimental Non-Gaussian PDFs	95
5.1. Experimental Setup and Methods.....	95
5.2. Experimental Results	101
5.3. Comparison of Measured PDFs with Theories.....	105
5.4. Measurement of PDFs with 10 GHz Electrical Amplifiers	109
5.5. The Function of the Decision Circuit.....	110
5.6. Results On PDFs Using 10 GHz Electrical Amplifiers	113
5.7. The Percentage Optimum Threshold Measurement.....	120
5.8. Experimental Results on Percentage Optimum Threshold	124
6. The OC-192 System.....	132
6.1. Back to Back OC-192 System	133
6.2. Back to Back OC-192 System With EDFA and Optical BPF	137
6.3. Characteristics of the Tek EDFA.....	142
6.4. Experimental Results.....	146
6.4.1. Sensitivity of OC-192 Receiver	146
6.4.2. Constant BER contours of OC-192 system.....	148
6.4.3. Optimum Threshold versus Received Power	151
7. Conclusions.....	153
7.1. Future works.....	154
References.....	156
Appendix A1.....	160
Derivations of MGFs, PDFs, Means and Variances	160
Appendix A2.....	165
Derivation of equation (2.10.4.1)	165
Appendix A3.....	166
Derivation of probability of error for logical ones.....	166

Derivation of probability of error for logical zeros	167
Appendix A4.....	169
Derivation of error upper bound.....	169
Appendix A5.....	171
Equations of PDFs When Polarizer is Omitted	171
Appendix B	173
Derivations of The Probabilities of Errors.....	173
Appendix C	179
Derivation of the Value of Gauss Integral With Complex Argument.....	179
Appendix D	182
Matlab Programs	182
Parameters.....	182
Program 1	182
Program 2	184
Program 3	186
Program 4	189
Program 5	192
Program 6	193
Program 7	194
Program 8	198
Program 9	200

List of Tables

Table 4.1.1. Simulation parameters.	71
Table 5.3.1. Simulation and experimental parameters for PDF measurements using Mini-Circuits amplifiers.	105
Table 5.6.1. Simulation and experimental parameters for PDF measurements using SHF and Veritech amplifiers.	114
Table 5.8.1. Simulation and experimental parameters for threshold measurements using SHF and Veritech amplifiers.	125

List of Figures

Fig. 1.1.1. Optically preamplified system.....	1
Fig. 1.3.1. Illustration of Gaussian and Non-Gaussian PDFs.....	4
Fig. 2.1.1. Responsivity of PIN diode.....	8
Fig. 2.2.1. Theoretical model of system.....	10
Fig. 2.3.1.a. Magnitude response of integrate-and-dump filter.....	11
Fig. 2.3.1.b. Phase response of integrate-and-dump filter.....	12
Fig. 2.7.1.a. The baseband magnitude spectrum of signal in a time interval $[0,T]$	18
Fig. 2.7.1.b. The baseband magnitude spectrum of ASE in a time interval $[0,T]$	18
Fig. 2.11.1. The ratio of the sp-sp beat noise terms versus M	27
Fig. 2.17.1.a. PDFs of logical zeros with polarizer.....	35
Fig. 2.17.1.b. PDFs of logical ones with polarizer.....	36
Fig. 2.17.1.c. PDFs of logical zeros without polarizer.....	36
Fig. 2.17.1.d. PDFs of logical ones without polarizer.....	37
Fig. 2.17.2.a. Crossing points of PDFs with polarizer.....	38
Fig. 2.17.2.b. Crossing points of PDFs without polarizer.....	39
Fig. 3.4.2.1. Paths of constant $\text{Im}\{f(t)\}$	49
Fig. 3.5.1. The contour of integration.....	52
Fig. 3.5.2.1. Saddle point and constant $\text{Im}\{F(u)\}$ paths.....	55
Fig. 3.5.2.2. Surface plot of $\text{Re}\{F(u)\}$, the path of steepest descent and the location of the saddle point.....	57
Fig. 3.6.1.a. Comparison of PDFs evaluated by Chi-Square distributions and Steepest Descent Method.....	59
Fig. 3.6.1.b. Relative error in Steepest Descent Method.....	60
Fig. 3.7.1. Receiver with current to voltage conversion block.....	61
Fig. 3.8.1.a. PDFs of logical zeros with $B_{elec}=1, 20$ GHz.....	63
Fig. 3.8.1.b. PDFs of logical ones with $B_{elec}=1, 20$ GHz.....	64

Fig. 3.8.2.a. PDFs of logical zeros with $B_o=1, 3$ nm.....	65
Fig. 3.8.2.b. PDFs of logical ones with $B_o=1, 3$ nm.	66
Fig. 3.8.3.a. PDFs of logical zeros with $G_o=20, 30$ dB.....	67
Fig. 3.8.3.b. PDFs of logical ones with $G_o=20, 30$ dB.	68
Fig. 4.1.1.a. BER versus Received Power with $B_{elec}=1$ GHz.....	72
Fig. 4.1.1.b. BER versus Received Power with $B_{elec}=20$ GHz.....	73
Fig. 4.1.2.a. BER versus Received Power with $B_{elec}=1, 10, 20$ GHz.	74
Fig. 4.1.2.b. BER versus Received Power with $B_o=1, 2, 4$ nm.....	75
Fig. 4.1.3. Noise Power versus Received Power.....	76
Fig. 4.2.1.a. Sensitivity versus Electrical Bandwidth.	77
Fig. 4.2.1.b. Sensitivity versus Optical Bandwidth.....	78
Fig. 4.2.2.a. Sensitivity versus Extinction Ratio.....	79
Fig. 4.2.2.b. Sensitivity versus Spontaneous Emission Factor.	80
Fig. 4.2.1.1. Sensitivity versus EDFA Small Signal Gain.....	81
Fig. 4.3.1. BER versus Extinction Ratio.....	83
Fig. 4.3.2. BER versus EDFA Small Signal Gain.....	84
Fig. 4.3.3. BER versus μ (by varying B_{elec}).....	85
Fig. 4.3.4. BER versus M (by varying B_o).....	86
Fig. 4.4.1.a. BER versus Percentage Threshold, $B_{elec}=1$ GHz.....	87
Fig. 4.4.1.b. BER versus Percentage Threshold, $B_{elec}=20$ GHz.....	88
Fig. 4.4.1.1. Percentage Optimum Threshold versus Received Power, $B_{elec}=1$ GHz.....	89
Fig. 4.4.1.2. Percentage Optimum Threshold versus Received Power, $B_{elec}=20$ GHz.....	90
Fig. 4.5.1. Percentage Optimum Threshold versus Extinction Ratio.	91
Fig. 4.5.2. Percentage Optimum Threshold versus EDFA Small Signal Gain.....	92
Fig. 4.5.3. Percentage Optimum Threshold versus M (varying B_{elec}).	93

Fig. 4.5.4. Percentage Optimum Threshold versus M (varying B_o).....	94
Fig. 5.1.1.a. The optical signal source for PDF experiment.....	95
Fig. 5.1.1.b. The cascaded EDFAs for PDF experiment.....	96
Fig. 5.1.1.c. The receiver for PDF experiment.....	97
Fig. 5.1.2. The setup of the BERT.....	98
Fig. 5.1.3. The threshold detection of noise.....	99
Fig. 5.2.1. Experimental PDFs of thermal and beat noises, $G=33$ dB, Mini-Circuits amplifiers.....	102
Fig. 5.2.2. Experimental PDFs of beat noises at different laser powers, $G=29.5$ dB, Mini-Circuits amplifiers.....	103
Fig. 5.2.3. Experimental PDFs of beat noises with polarizer, $G=32.4$ dB, $m_t=1$, Mini-Circuits amplifiers.	104
Fig. 5.3.1.a. Comparison of experimental PDF for ASE only with theories, $m_t=1$	107
Fig. 5.3.1.b. Comparison of experimental PDF for ASE only with theories, $m_t=2$	107
Fig. 5.3.2.a. Comparison of experimental PDF with theories, $m_t=1$, $P_{in}=-36.3$ dBm.....	108
Fig. 5.3.2.b. Comparison of experimental PDF with theories, $m_t=2$, $P_{in}=-37.6$ dBm.....	108
Fig. 5.4.1. Receiver for measuring PDFs with 10 GHz microwave amplifiers.	109
Fig. 5.5.1. Block diagram of the decision circuit.....	109
Fig. 5.5.2.a. Eye diagram of pulses at decision circuit output, $BER=4 \times 10^{-1}$	112
Fig. 5.5.2.b. Eye diagram of pulses at decision circuit output with $BER=1 \times 10^{-3}$	112
Fig. 5.6.1. Comparison of PDFs, $m_t=2$, ASE=-10.7 dBm.....	115
Fig. 5.6.2. Comparison of PDFs, $m_t=1$, ASE=-14 dBm.....	115

Fig. 5.6.3. Comparison of experimental PDFs obtained from using different clock frequency and from using the BERT directly.....	116
Fig. 5.6.4. Comparison of PDFs, $m_I=2$, $P_{in}=-39.7$ dBm.....	117
Fig. 5.6.5. Comparison of PDFs, $m_I=1$, $P_{in}=-32.3$ dBm.....	118
Fig. 5.6.6. Comparison of PDFs, $m_I=2$, $P_{in}=-35$ dBm.	119
Fig. 5.6.7. Comparison of PDFs, $m_I=1$, $P_{in}=-30.3$ dBm.....	119
Fig. 5.7.1. Direct modulation of 1550 nm DFB laser.....	120
Fig. 5.7.2. The transfer characteristic of 1550 nm DFB laser.	121
Fig. 5.7.3.a. Pulses used to drive the laser.	122
Fig. 5.7.3.b. Waveform of received pulses.....	122
Fig. 5.7.3.c. Received pulses with noise, $G=32$ dB, $m_I=2$	123
Fig. 5.7.3.d. Received pulses with noise, $G=31$ dB, $m_I=1$	123
Fig. 5.8.1.a. BER versus Received Power, $G=32$ dB, $m_I=2$	126
Fig. 5.8.1.b. BER versus Percentage Optimum Threshold, $G=32$ dB, $m_I=2$	127
Fig. 5.8.1.c. Percentage Optimum Threshold versus Received Power, $G=32$ dB, $m_I=2$	128
Fig. 5.8.2.a. BER versus Received Power, $G=31$ dB, $m_I=1$	129
Fig. 5.8.2.b. BER versus Percentage Optimum Threshold, $G=31$ dB, $m_I=1$	130
Fig. 5.8.2.c. Percentage Optimum Threshold versus Received Power, $G=31$ dB, $m_I=1$	131
Fig. 6.1.1. Transmitter block diagram of OC-192 system.	133
Fig. 6.1.2.a. Optical eye of MZ output.....	134
Fig. 6.1.2.b. Histograms of MZ optical eye.....	134
Fig. 6.1.3. Receiver block diagram of OC-192 system.....	135
Fig. 6.1.4. Block diagram of clock recovery circuit.	136
Fig. 6.1.5. A data eye at the input of decoder.....	136

Fig. 6.2.1. Block diagram of back to back OC-192 system with EDFA and optical BPF.....	137
Fig. 6.2.2.a. Data eye diagram at the input of decoder (BER=10 ⁻⁶).....	138
Fig. 6.2.2.b. Histograms of the data eye (BER=10 ⁻⁶).....	138
Fig. 6.2.3.a. Data eye diagram at the input of decoder (BER=10 ⁻⁹).....	139
Fig. 6.2.3.b. Histograms of the data eye (BER=10 ⁻⁹).....	139
Fig. 6.2.4. Double traces in the data eye.	140
Fig. 6.2.5. Nonlinear transfer function of amplifier.	141
Fig. 6.3.1. Relation between EDFA small signal gain and EDFA number.....	142
Fig. 6.3.2.a. EDFA gain as a function of input signal power.....	143
Fig. 6.3.2.b. EDFA gain as a function of output signal power.....	143
Fig. 6.3.3. N_{sp} as function of EDFA small signal gain.....	144
Fig. 6.3.4. Sensitivity of receiver as function of EDFA small signal gain.	145
Fig. 6.4.1.1. Sensitivity curves of receiver.....	146
Fig. 6.4.1.2. Sensitivity curves for 0 and 81 km of fiber.....	147
Fig. 6.4.2.1.a. Constant BER contour for 0 km, no EDFA.....	148
Fig. 6.4.2.1.b. Constant BER contour for 0 km with Tek EDFA and optical BPF.....	149
Fig. 6.4.2.1.c. Constant BER contour for 81 km with nt EDFA.....	150
Fig. 6.4.2.2. Data eye at input of decoder with nt EDFA and 81 km of fibers.	151
Fig. 6.4.3.1. Optimum threshold versus received power.	152
Fig. B.1. Taylor series approximation to $G_1(u)$	175
Fig. B.2. Absolute percentage error of P_1	176
Fig. B.3. Taylor series approximation to $G_0(u)$	177
Fig. B.4. Absolute percentage error of P_0	178
Fig. C1 Closed contour of (C5).	180

List of Symbols

$\hat{A}_{sp}(t)$:	Real amplitude of $\hat{E}_s(t)$
B_c :	One-sided electrical bandwidth
B_{elec} :	Two-sided electrical bandwidth
B_o :	Optical bandwidth
$BPPSD_{sp}(f)$:	Bandpass power spectral density of ASE
c_o :	Speed of light in free space
c_{nI} :	Fourier series expansion coefficient of $e_{spI}(t)$
c_{nIr} :	Real part of c_{nI}
c_{nIi} :	Imaginary part of c_{nI}
c_{nQ} :	Fourier series expansion coefficient of $e_{spQ}(t)$
c_{nQr} :	Real part of c_{nQ}
c_{nQi} :	Imaginary part of c_{nQ}
c_n :	Fourier series expansion coefficient of $\hat{e}_{sp}(t)$
c_{rn} :	Real part of c_n
c_{in} :	Imaginary part of c_n
$\delta(t)$:	Delta function
δ :	Extinction ratio (Powers of logical zeros over ones)
$e_{sp}(t)$:	ASE electric field at EDFA output
$e_{spI}(t)$:	In-phase component of $e_{sp}(t)$
$e_{spQ}(t)$:	Quadrature component of $e_{sp}(t)$
$\hat{e}_{sp}(t)$:	Bassband optically filtered ASE electric field
$\hat{e}_{sp}^*(t)$:	Conjugate of $\hat{e}_{sp}(t)$
$E_s(t)$:	Signal electric field at EDFA output
$E_{sI}(t)$:	In-phase component of $E_s(t)$
$E_{sQ}(t)$:	Quadrature component of $E_s(t)$:
E_{nI} :	Fourier series expansion coefficient of $E_{sI}(t)$

E_{nIr} :	Real part of E_{nI}
E_{nIi} :	Imaginary part of E_{nI}
E_{nQ} :	Fourier series expansion coefficient of $E_{sQ}(t)$
E_{nQr} :	Real part of E_{nQ}
E_{nQi} :	Imaginary part of E_{nQ}
$\hat{E}_s(t)$:	Bassband optically filtered signal electric field
E_n :	Fourier series expansion coefficient of $\hat{E}_s(t)$
E_{rn} :	Real part of E_n
E_{in} :	Imaginary part of E_n
$\hat{E}_{sp}(t)$:	Bandpass optically filtered ASE electric field
$\hat{E}_{sp}^*(t)$:	Conjugate of $\hat{E}_{sp}(t)$
$E_{rr}(\cdot)$:	Truncation error of Generalized Q-function
f :	Photon frequency
f_c :	Light carrier frequency
$f_0(y)$:	Non-Gaussian PDF of logical zeros
$f_{0g}(y)$:	Gaussian PDF of logical zeros
$f_1(y)$:	Non-Gaussian PDF of logical ones
$f_{1g}(y)$:	Gaussian PDF of logical ones
F :	Noise figure of electrical amplifier
$F(s)$:	MGF including thermal and shot noises
$F_0(s)$:	MGF of Non-Gaussian PDF of logical zeros
$F_1(s)$:	MGF of Non-Gaussian PDF of logical ones
$F_g(s)$:	MGF of Gaussian PDF
G :	EDFA gain
G_0 :	EDFA small signal gain
G_{elec} :	Gain of electrical amplifier
h :	Planck's constant

η_{eff} :	Photodetector quantum efficiency
$h_{int}(t)$:	Impulse response of integrate-and dump filter
$H_{int}(f)$:	Frequency response of integrate-and dump filter
I_d :	Decision current
I_{dopt} :	Optimum decision current of Non-Gaussian PDFs
$I_{doptgauss}$:	Optimum decision current of Gaussian PDFs
$I_M(\cdot)$:	Modified Bessel of the first kind with order M
$I_{ph}(t)$:	Photocurrent
\bar{I}_{ph} :	Time and statistical average of photocurrent
I_s :	Average photocurrent of signal
I_{sp} :	Average photocurrent of ASE
k :	Boltzmann's constant
K :	Proportionality constant
L :	Loss between EDFA and photodetector
λ :	Photon Wavelength
λ_c :	Light carrier wavelength
μ_{in} :	Input coupling loss of EDFA
μ_{out} :	Output coupling loss of EDFA
m_t :	Polarization state parameter
M :	Ratio of optical to two-sided electrical bandwidths
N_{sp} :	Spontaneous emission factor of EDFA
N_{s-sp} :	Signal-spontaneous beat noise power
N_{sp-sp} :	Spontaneous-spontaneous beat noise power
ω_n :	Angular frequency
$P_0(I_d)$:	Probability of error of logical zeros at I_d for Non-Gaussian PDF

$P_{0g}(I_d)$:	Probability of error of logical zeros at I_d for Gaussian PDF
$P_{1l}(I_d)$:	Probability of error of logical ones at I_d for Non-Gaussian PDF
$P_{lg}(I_d)$:	Probability of error of logical ones at I_d for Gaussian PDF
P_{ase} :	ASE power at photodetector
\hat{P}_{ase} :	ASE power at photodetector including losses
P_{in0} :	Average input power to EDFA for logical zeros
P_{in1} :	Average input power to EDFA for logical ones
P_{inav} :	Average input power to EDFA
$P_{opt}(t)$:	Total optical power at photodetector
P_{sat} :	Saturation power of EDFA
P_{sig} :	Average signal power at photodetector
\hat{P}_{sig} :	P_{sig} including losses
$PSD_{sp}(f)$:	Baseband equivalent of $BPPSD_{sp}(f)$
PSD_{sh} :	Shot noise power spectral density
PSD_{th} :	Thermal noise power spectral density
q :	Electron charge
$Q(\cdot)$:	Q-function for Gaussian PDF
$Q_M(a,b)$:	Generalized Q-function for Non-Gaussian PDF
$\hat{Q}_M(a,b)$:	Approximated generalized Q-function
\mathfrak{R} :	Responsivity of photodetector
$R(\tau)$:	Autocorrelation function
R_{eq} :	Equivalent noise resistance for thermal noise
R_{in} :	Input resistance of electrical amplifier
σ^2 :	Variance of c_{rn} and c_{in}

σ_g^2 :	Variance of Gaussian PDF
σ_0^2 :	Variance of logical zeros
σ_1^2 :	Variance of logical ones
σ_{sh}^2 :	Variance of shot noise
σ_{sp-sp}^2 :	Variance of spontaneous-spontaneous beat noise
σ_{sig-sp}^2 :	Variance of signal-spontaneous beat noise
σ_{th}^2 :	Variance of thermal noise
θ_n :	Phase of E_n
$\theta(t)$:	Phase of $\hat{E}_{sp}(t)$
T :	Time interval
T_k :	Temperature in Kelvin
u_{d0} :	Saddle point of logical zeros at decision threshold
u_{d1} :	Saddle point of logical ones at decision threshold
y :	Time averaged photocurrent
$\langle y \rangle$:	Expectation of y
\bar{y}_0 :	Mean value of logical zeros
\bar{y}_1 :	Mean value of logical ones
y_g :	Gaussian current random variable

List of Abbreviations

ac	alternating current
APD	Avalanche Photodiode
ASE	Amplified Spontaneous Emission
ASK	Amplitude Shift Keying
BER	Bit Error Rate
BERT	Bit Error Rate Tester
BNR	Bell Northern Research
BPF	Bandpass Filter
CDF	Cumulative Distribution Function
dc	direct current
DFB	Distributed Feedback
EDF	Erbium Doped Fiber
EDFA	Erbium Doped Fiber Amplifier
FD	Frequency Doubler
FWHM	Full Width Half Maximum
FSK	Frequency Shift Keying
HP	Hewlett Packard
ISI	Intersymbol Interference
LOO	Local Optical Oscillator
MGF	Moment Generating Function
MZ	Mach Zehnder
NRZ	Non-Return-Zero
nt	northern telecom
OC-12	Optical Carrier 12
OC-192	Optical Carrier 192
OOK	On-Off Keying or On-Off Keyed

PDF	Probability Density Function
PIN	P-Intrinsic-N
PRBS	Pseudo Random Bit Sequence
PSK	Phase Shift Keying
sig-sp	signal-spontaneous
SNR	Electrical Signal-to-Noise Ratio
SOA	Semiconductor Optical Amplifier
sp-sp	spontaneous-spontaneous
Tek	Tektronics
TRLabs	Telecommunications Research Laboratories
VOA	Variable Optical Attenuator

1. Introduction

The conventional way of compensating the losses in an optical digital communication system utilizes electrical regenerative repeaters. The losses could be due to fiber losses in a long haul system, splitting or coupling losses, etc. The regeneration process includes optical to electrical conversion, electrical amplification, retiming, pulse shaping, and electrical to optical conversion. Although the signal can be successfully regenerated, the process is complicated from a system point of view. However, with the advent of optical amplifiers, direct amplification of the signal in the optical domain is made possible. The optical amplifiers not only reduce the amount of components needed in the system. They can also provide high signal gain in a much wider bandwidth than the electrical repeater. When the optical amplifiers are used in conjunction with the dispersion shifted fiber in the 1.55 μm region, the necessity of the regeneration process is virtually eliminated.

1.1. Optically Preamplified Digital Transmission System

One of the many applications of optical amplifiers is to use them as preamplifiers in an optical digital transmission system. An optical amplifier acting like a preamplifier is placed in front of the receiver as shown in Fig. 1.1.1. The optical bandpass filter (BPF) is used to filter out part of the amplified spontaneous emission (ASE) from the optical preamplifier.

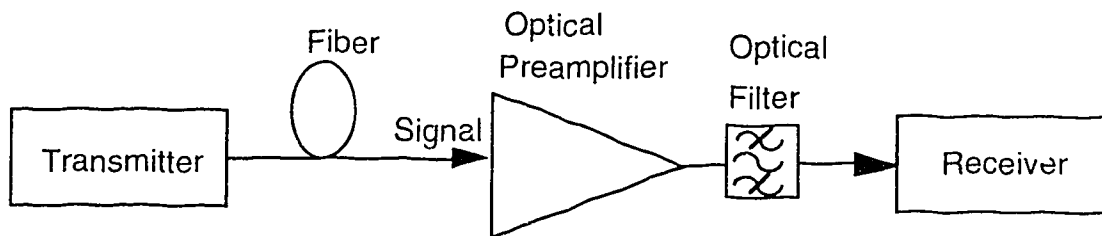


Fig. 1.1.1. Optically preamplified system.

The advantage of doing this is that the sensitivity of the receiver, which is defined as the optical power (received power) required to achieve a certain bit error rate (BER), can be significantly improved.

This is because now the optical amplifier is treated as part of the receiver. The definition of the received power is changed from the power at the photodetector to the power at the input of the optical amplifier. As an example, for the 10 Gb/s direct detection system in [1], when the optical amplifier is a semiconductor optical amplifier (SOA), the sensitivity at a BER of 10^{-9} is improved by more than 11 dB. When the optical amplifier is an Erbium Doped Fiber Amplifier (EDFA), the improvement is as much as 17 dB. It is because of this great improvement in sensitivity, there has been an increase in interest in the performance of such a system in terms of the sensitivity, the BER and the noise [2, 3, 4, 5].

The transmitter in Fig. 1.1.1 may contain a laser which can be directly modulated for low bit rate applications. Alternatively it may contain a laser source and an external modulator such as the Mach-Zehnder (MZ) for high bit rate applications. The receiver will contain a photodiode such as a PIN diode or an avalanche photodiode (APD) for direct detection, or a local optical oscillator (LOO) and a photodiode for coherent detection. The photodiode is followed by electrical filters and amplifiers, and a digital decision circuit. Direct detection without using the optical amplifier has poorer sensitivity performance than coherent detection. However when an optical amplifier is used, the sensitivity is improved significantly. Therefore the high sensitivity offered by coherent detection becomes less attractive. The ease of implementation of direct detection also provides it with an advantage over coherent detection. Nevertheless the optical amplifier can still be used in conjunction with a coherent receiver to suppress beat noise [6]. The beat noise will be discussed in the next section. The digital signal can be modulated by using amplitude shift keying (ASK), frequency shift keying (FSK), or phase shift keying (PSK). Each modulation scheme has its advantages and disadvantages in terms of system performance and implementation. The optical amplifier can be a SOA or an EDFA. The SOA can provide wider optical bandwidth than the EDFA but it has lower gain than the EDFA and is usually polarization sensitive. However the compact size of the SOA is a very attractive feature.

There could be many different combinations of the various modulation formats, SOAs and EDFAs, coherent and direct detection. Extensive research is still underway to investigate the potential application, the advantages and disadvantages of each combination. The discussions in the following sections will be focused on the EDFA preamplified, directly detected, optical digital transmission system.

1.2. Noises in the Optically Preamplified Digital System

The EDFAs are low noise optical amplifiers with typical noise figures of about 5 to 7 dB (3 dB for an ideal optical amplifier). Using the EDFA preamplifier is not completely without disadvantages. Without the EDFA preamplifier, the thermal noise and the shot noise are the two dominant noise sources in digital receivers with the thermal noise being dominant provided the signal power is not very large. However when an EDFA preamplifier is inserted into the optical digital transmission system, the ASE originating from the EDFA generates two additional beat noises in the receiver. The beat noises result from the electric field mixing due to the square-law detection characteristic of the PIN diode. This field mixing effect can be seen from equations (1.2.1) and (1.2.2):

$$I_{ph}(t) = K \left| \hat{E}_s(t) + \hat{e}_{sp}(t) \right|^2 \quad (1.2.1)$$

where $I_{ph}(t)$ is the detected photocurrent, K is a proportionality constant, $\hat{E}_s(t)$ is the optically filtered bandpass signal electric field which is complex, $\hat{e}_{sp}(t)$ is the optically filtered bandpass ASE electric field which is complex and random. At a fixed instant of time, (1.2.1) can be expanded as:

$$I_{ph} = K \left| \hat{E}_s \right|^2 + 2K \operatorname{Re} \{ \hat{E}_s \hat{e}_{sp}^* \} + K \left| \hat{e}_{sp} \right|^2. \quad (1.2.2)$$

The first term in (1.2.2) is the signal. The second term is the signal-spontaneous (sig-sp) beat noise which is the dominant noise for the logical one because of the presence of large signal power. The third term is spontaneous-spontaneous (sp-sp) beat noise which is the

dominant noise for the logical zero provided the ASE power is sufficiently high and the signal power level is low during the logical zero. The thermal noise and the shot noise are relatively insignificant now compared with the beat noises [7].

1.3. The Distributions of the Noises

The probability density functions (PDFs) of the thermal noise and shot noise in the receiver can be well approximated by a Gaussian distribution. However the beat noises in the logical one and the logical zero have been theoretically shown to be non-Gaussian [7, 8, 9, 10]. The source of the non-Gaussian distributions comes from the distribution of the sp-sp beat noise which has a non-Gaussian shape. The distribution of the sig-sp beat noise however assumes a Gaussian shape [8]. The Gaussian and the non-Gaussian PDFs of logical ones and logical zeros are sketched in Fig. 1.3.1.

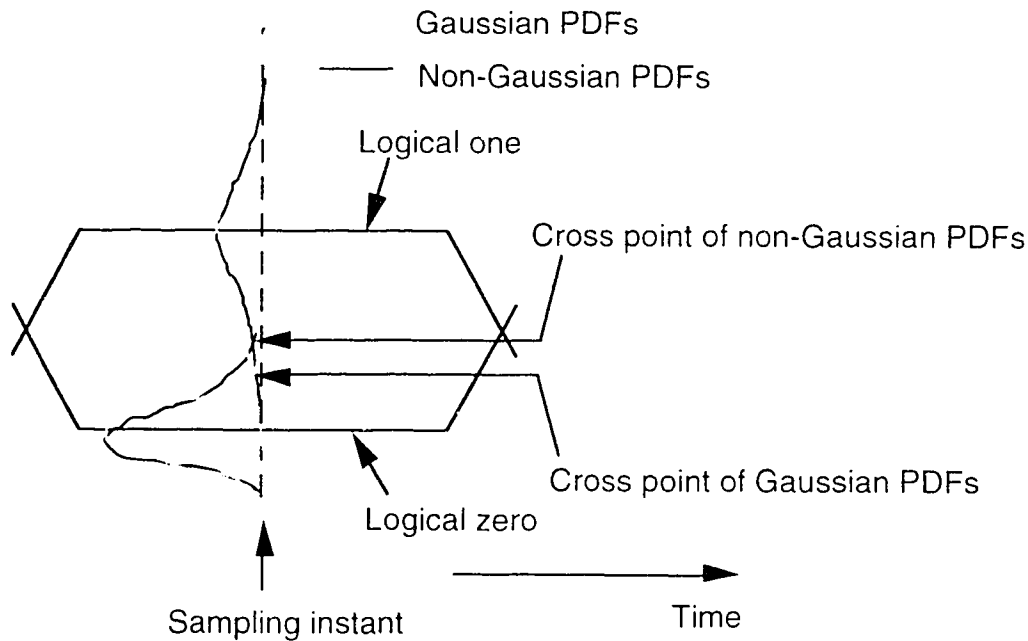


Fig. 1.3.1. Illustration of Gaussian and Non-Gaussian PDFs.

The Gaussian PDFs are symmetrical about the peaks whereas the non-Gaussian PDFs are not. The cross point of the extreme tails or the optimum threshold of the Gaussian PDFs is different from that of the non-Gaussian PDFs. Although the optimum thresholds of the two

distributions are very different, it is surprising to know that using the Gaussian approximation to the distributions of logical zeros and logical ones is sufficient to predict the sensitivity of the receiver with only about 0.3 dB discrepancy [9]. Moreover the Gaussian distribution is very easy to handle computationally and hence it is very tempting to just use the Gaussian approximation in all the analyses of system performance as in [11]. However the Gaussian approximation is less accurate in predicting the optimum threshold that should be used in the decision circuit [10]. It is for this reason that an exact theoretical model is preferable.

1.4. Objectives and Accomplishment

The first objective of this project is to understand the theories that formulate the non-Gaussian distributions. These theories were developed by Marcuse [7, 8], and by Humblet and Azizoglu [10]. They belong to a general class of theory that deals with the square-law detection of signal and noise, and it has already been considered in the years of 40's to 60's [12, 13, 14]. However optical amplifiers were not yet available and the theory was not used in the field of fiber optic communications with optical amplifiers. The performance of the EDFA preamplified optical digital system will be analyzed by making use of these theories. Other authors have done similar analysis to the system [9, 15] but only the theories proposed by Marcuse, Humblet and Azizoglu give rises to closed form solutions. The second objective is to experimentally verify the non-Gaussian distributions since there is no practical evidence that the statistics are non-Gaussian.

The non-Gaussian theory has been used to study the system performance and it has been found that the Gaussian theory provides satisfactory results in predicting the sensitivity of the system. However in the analyses that require knowledge of the optimum decision threshold, the Gaussian theory is less accurate and the non-Gaussian theory must be used. A simple method has also been devised and used to demonstrate experimentally that the distributions of logical ones and logical zeros in an EDFA preamplified, directly detected system are indeed non-Gaussian. The

experimentally measured PDFs have been compared with the non-Gaussian theoretical PDFs. Good agreement has been found between the theoretical and experimental results.

1.5. Organization of Thesis

This thesis is divided into 7 chapters and 4 appendices. Chapter 1 gave a brief introduction to the EDFA preamplified digital transmission system studied. Chapters 2 and 3 provide discussions on the theoretical study of the noise distributions in the system. Some simulation results that are obtained from using the theories are presented and discussed in chapter 4. The experimental method and setup for measuring the noise distributions are described in chapter 5. Experimental results are also presented and discussed in chapter 5. The performance of the OC-192 system (10 Gb/s digital fiber optic system) using EDFA preamplifier is evaluated and shown in chapter 6. Chapter 7 gives the conclusions of this thesis work and possible future works. The detailed derivations of the theories can be found in Appendices A to C. The Matlab simulation programs are included in Appendix D.

2. Non-Gaussian Noise Theory-Part I

The origin of the non-Gaussian noise distribution will be discussed in this chapter. The non-Gaussian PDFs for logical ones and logical zeros will be presented. Some crucial derivation steps will be shown and discussed. The detailed derivations can be found in Appendices A1 to A5. The ideas of the derivations are based on the work of Marcuse [7], and Humblet and Azizoglu [10]. The mathematics used in analyzing the statistics assumes that the statistics of the signal and noise are at least wide-sense stationary in time, and homogeneous in space. Stationary means that the statistics are invariant with time and homogeneous means that the statistics are independent of position in space. These assumptions greatly simplify the mathematics and give rise to the closed forms of the PDFs. This part of the theoretical study does not include the thermal and the shot noises. These two noises will be included in the second part of the theoretical study in chapter 3 where the Steepest Descent Method will be used. Intersymbol interference (ISI) will be ignored in all the following analyses as the degree of ISI varies from electrical filter to electrical filter.

2.1. The Origin of the Non-Gaussian Distribution

The non-Gaussian shape of the PDF of the sp-sp beat noise originates from the square-law detection characteristic of the PIN diode. The detected photocurrent is directly proportional to the optical power as given by:

$$I_{ph}(t) = \Re P_{opt}(t) \quad (2.1.1)$$

where \Re is responsivity of the PIN diode given by [16]:

$$\Re = \frac{\eta_{eff} q}{hf} = \frac{\eta_{eff} \lambda}{1.24} \quad (2.1.2)$$

where $c_o = f\lambda$ has been used, $c_o = 3 \times 10^8$ m/s (speed of light in free space) is assumed, η_{eff} is the quantum efficiency of the PIN diode, $q = 1.6 \times 10^{-19}$ C is the electron charge, $h = 6.6262 \times 10^{-34}$ J-s is the

Planck's constant, f is the frequency of photon, λ is the photon wavelength in μm . Equation (2.1.2) shows that the responsivity is linearly proportional to the wavelength. However in practice, the region over which the responsivity increases with the wavelength is limited as sketched in Fig. 2.1.1.

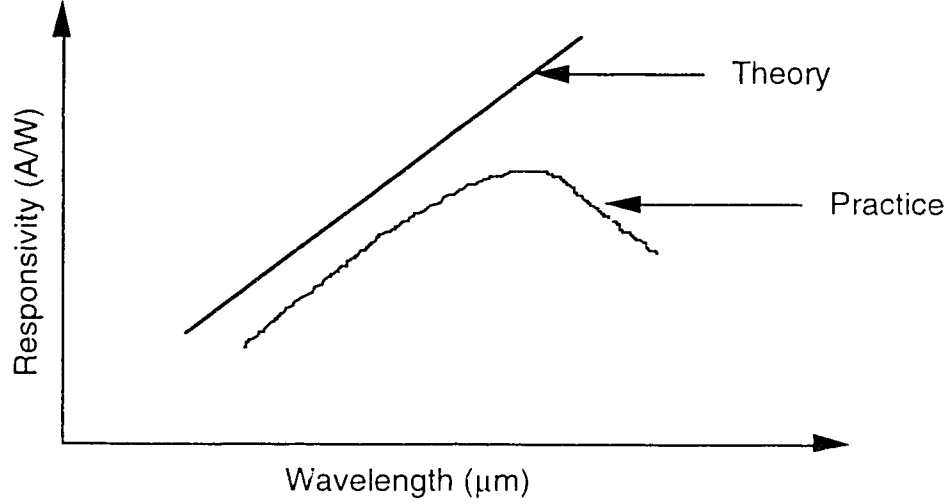


Fig. 2.1.1. Responsivity of PIN diode.

The responsivity is a weak function of the wavelength in a narrow range of wavelengths. Such is the case when a narrow-band optical BPF (bandwidth on the order of nanometer) is placed in front of the PIN diode. The wavelength λ in (2.1.2) can then be replaced by the centre wavelength λ_c of the signal.

The optical power is proportional to the magnitude squared of the total filtered electric field given by:

$$P_{opt}(t) = \frac{K}{\Re} |\hat{E}_s(t) + \hat{e}_{sp}(t)|^2 \quad (2.1.3)$$

where equation (1.2.1) has been used. The ASE spectrum at the output of the EDFA is very broad relative to the bandwidth of the optical BPF. Therefore the optically filtered bandpass ASE electric field $\hat{e}_{sp}(t)$ can be modeled as a zero-mean white noise Gaussian process [9]. This means the optical power and the photocurrent in

(2.1.1) and (2.1.3) are also random. The Gaussian process of the ASE electric field means that negative values are possible for the ASE electric field. However the optical power in (2.1.3) must be positive, which means the photocurrent must be positive. It is then clear that the distribution of the photocurrent cannot assume a Gaussian shape. Equation (2.1.1) can be expanded by using (2.1.3) to give the expression of the photocurrent as shown in equation (1.2.2). Using (1.2.2), it can be seen that within one bit time interval, the signal electric field is not random or its randomness is negligible compared with the ASE electric field. Therefore the sig-sp beat noise retains the Gaussian distribution of \hat{e}_{sp} which means negative values are possible [8]. The sp-sp beat noise term, however, will assume a distribution which is the square of the Gaussian so that only positive values are allowed. At first glance, the Gaussian distribution of sig-sp beat noise seems to contradict the non-negative photocurrent. However note that only when \hat{e}_{sp} is small compared to \hat{E}_s , is the distribution of the photocurrent dominated by the Gaussian shape of the sig-sp beat noise. When \hat{e}_{sp} is large, the distribution is dominated by the distribution of $|\hat{e}_{sp}|^2$. In other words, the tails of the final distribution are dominated by the distribution of $|\hat{e}_{sp}|^2$ and this justifies that the photocurrent is positive. For digital transmission, in the case of a logical zero, \hat{E}_s is small and hence the distribution of logical zeros is non-Gaussian. For logical ones, \hat{E}_s is large so that only in the extreme tails of the PDF would we find a non-Gaussian distribution. The noise current generated by thermal noise can be added to (2.1.1) so that during a logical zero, the Gaussian distribution of the thermal noise could be competing with the distribution of $|\hat{e}_{sp}|^2$ if the sp-sp beat noise power is not sufficiently large. In order for the sp-sp beat noise to dominate over the thermal noise, the small signal gain of the EDFA should be increased since the sp-sp beat noise is proportional to the square of the EDFA small signal gain [11].

2.2. The Theoretical Model of the System

The theoretical system being analyzed is an optical digital system employing an EDFA as optical preamplifier. The ASE is polarized in the same spatial state as the signal by using a polarizer. An ideal optical bandpass filter is used to reduce the amount of ASE power at the receiver. The block diagram of the system is shown in Fig 2.2.1.

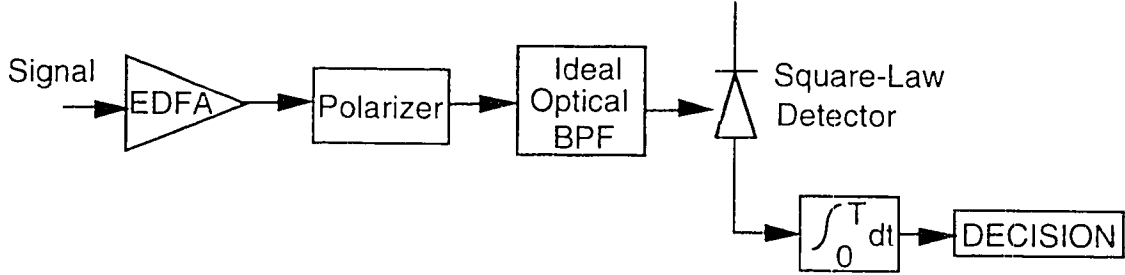


Fig. 2.2.1. Theoretical model of system.

The signal at the EDFA input is assumed to be ASK modulated. The EDFA has a small signal power gain of G . The output of the EDFA contains the amplified signal and the ASE. The optical BPF is assumed to be ideal with bandwidth B_o . The photodiode is modeled as a square-law detector. After square-law detection, the signal becomes an on-off keyed (OOK) signal as the optical carrier is removed. The electrical low-pass filter is modeled as an integrate-and-dump filter which will be discussed in section 2.3. The decision circuit is used to decode the noise corrupted OOK signal based on the amplitudes of the pulses received.

2.3. The Integrate-and-Dump Filter

The impulse response of the integrate-and-dump filter is given by:

$$h_{int}(t) = \int_0^T \delta(t) dt \quad (2.3.1)$$

$$= 1 \quad 0 \leq t \leq T \quad (2.3.2)$$

$$= 0 \quad \text{otherwise} \quad (2.3.3)$$

where T is the time at which the output of the filter is reset to zero. The impulse response is just a rectangular pulse with duration T and centered at time $t=T/2$. The frequency response of the filter can be easily obtained by applying the Fourier transform to the impulse response in (2.3.2) and (2.3.3) [17]:

$$H_{\text{int}}(f) = T \text{sinc}(fT) \exp(-j\pi fT). \quad (2.3.4)$$

The magnitude response $|H_{\text{int}}(f)|$ is normalized with respect to T and is plotted in Fig. 2.3.1.a. The phase response is normalized with respect to π and is shown in Fig. 2.3.1.b.

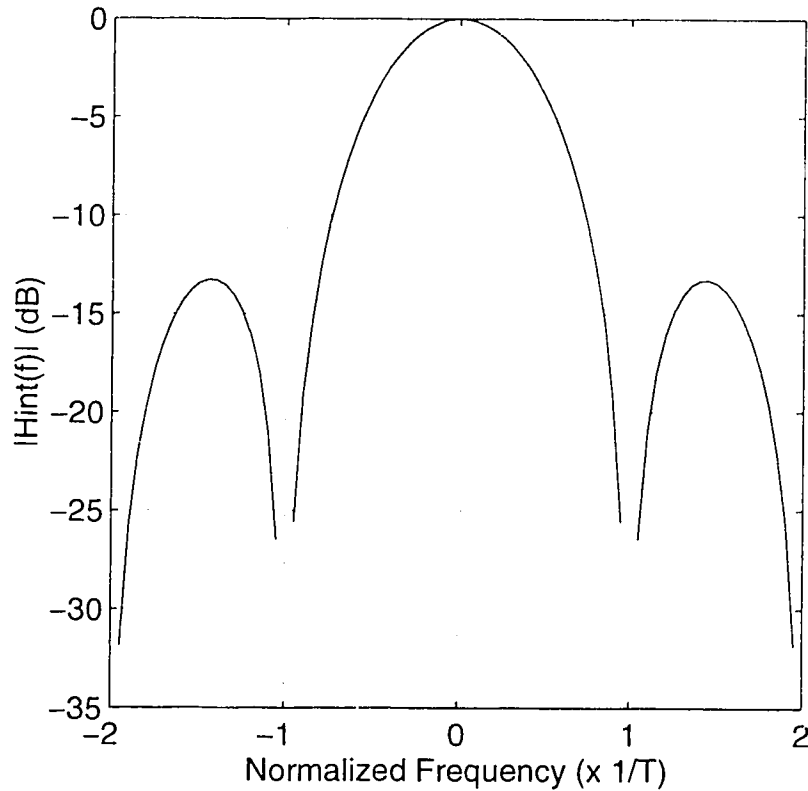


Fig. 2.3.1.a. Magnitude response of integrate-and-dump filter.

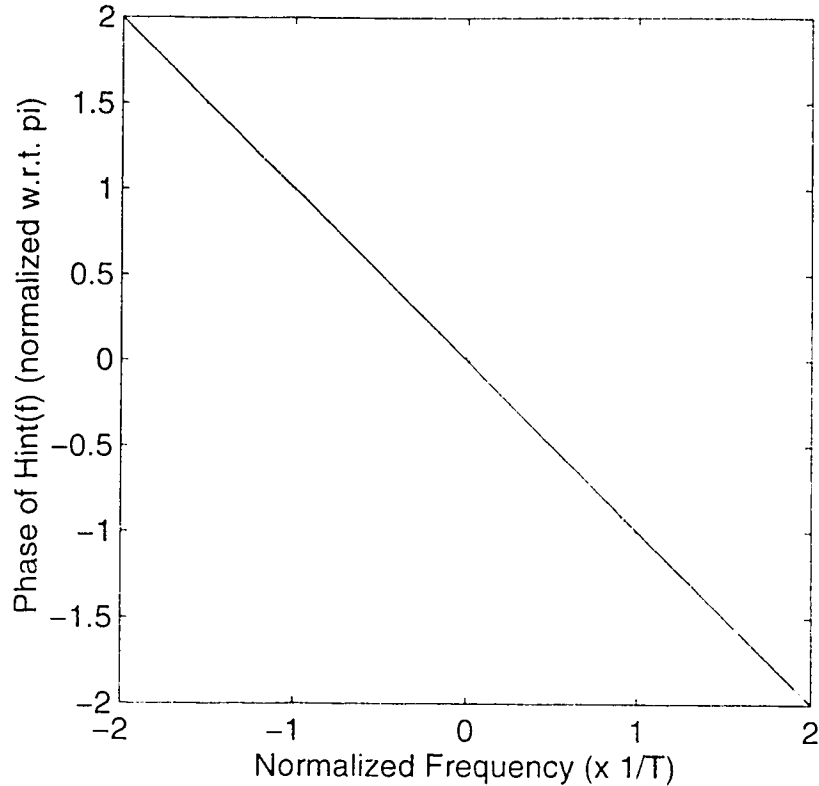


Fig. 2.3.1.b. Phase response of integrate-and-dump filter.

The one-sided 3-dB electrical bandwidth of the integrate-and-dump filter can be calculated approximately as $1/2T$. The choice of the integrate-and-dump is purely for mathematical convenience in the derivations of the PDFs which will be shown in the following sections. The use of the integrate-and-dump filter has been criticized to be impractical in a high bit rate transmission system [9]. However from section 2.1, we have learned that the non-Gaussian shape of the PDFs originates from the square-law detection characteristic of the photodiode. The characteristics of the electrical filter have very little to do with the shape of the PDFs. The filter has an effect on the way the noise power is accumulated and the amount of noise power accumulated determines the variance of the PDFs but not the shape of the PDFs. For example, with a wide-band filter, more noise is accumulated and hence the PDFs are broadened. However the shapes of the PDFs remain the same; they could be either Gaussian or non-

Gaussian. The work of Lee and Shim [9] has adopted a complicated approach in their analysis in which a more realistic electrical filter has been used. The PDFs are expressed in a more complicated way and are non-Gaussian. However the sensitivity analysis by Lee and Shim [9] turns out to be very close to the result obtained by the approach that will be adopted here, in which the integrate-and-dump filter will be used.

2.4. Bandpass Representation of Signal and Noise

Having learned the origin of the non-Gaussian distributions and established the theoretical model, we are now ready to consider the representation of the signal and noise in the optical field domain. The complex bandpass signal electric field at the output of the EDFA can be written as [18]:

$$E_s(t) = (E_{sI}(t) + jE_{sQ}(t)) \exp(j2\pi f_c t) \quad (2.4.1)$$

where the subscripts I and Q signify the in-phase and the quadrature components of the signal, f_c is the optical carrier frequency. Similarly the complex ASE electric field can be expressed as:

$$e_{sp}(t) = (e_{spI}(t) + je_{spQ}(t)) \exp(j2\pi f_c t). \quad (2.4.2)$$

The optical carrier is removed after the signal and noise are detected by the photodiode. Therefore the exponential terms in (2.4.1) and (2.4.2) will be ignored in the following analysis.

2.5. Fourier Series Representation of Signal and Noise

It is known that if a function is at least piece-wise continuous in an interval $[a, b]$, and if there exists a set of orthogonal functions in $[a, b]$, then the function can be approximated as a weighted sum of the orthogonal functions [19]. In a time interval $[0, T]$, where T is assumed to be the duration of a single level pulse, both the signal and ASE electric fields are at least piece-wise continuous functions. The interpretation of the pulse is not important for the analysis. It could represent a logical one or a logical zero, two logical ones or two

logical zeros, half of a logical one or a logical zero, and so on. The complex exponential functions $\exp(j\omega_n t)$, where $\omega_n = 2\pi n / T$ and $n = 0, \pm 1, \pm 2, \dots$, are known to be orthogonal in $[0, T]$. Therefore the in-phase and quadrature components in (2.4.1) and (2.4.2) can be expanded as Fourier series in $[0, T]$:

$$E_{sI}(t) = \sum_{n=-\infty}^{\infty} E_{nI} \exp(j\omega_n t) \quad 0 \leq t \leq T \quad (2.5.1)$$

$$E_{sQ}(t) = \sum_{n=-\infty}^{\infty} E_{nQ} \exp(j\omega_n t) \quad 0 \leq t \leq T \quad (2.5.2)$$

$$e_{spI}(t) = \sum_{n=-\infty}^{\infty} c_{nI} \exp(j\omega_n t) \quad 0 \leq t \leq T \quad (2.5.3)$$

$$e_{spQ}(t) = \sum_{n=-\infty}^{\infty} c_{nQ} \exp(j\omega_n t) \quad 0 \leq t \leq T \quad (2.5.4)$$

where E_{nI} , E_{nQ} , c_{nI} , c_{nQ} are the expansion coefficients given by:

$$E_{nI} = E_{nIr} + jE_{nIi} \quad (2.5.5)$$

$$E_{nQ} = E_{nQr} + jE_{nQi} \quad (2.5.6)$$

$$c_{nI} = c_{nIr} + jc_{nIi} \quad (2.5.7)$$

$$c_{nQ} = c_{nQr} + jc_{nQi} \quad (2.5.8)$$

The coefficients c_{nIr} , c_{nIi} , c_{nQr} and c_{nQi} are assumed to be independent Gaussian random variables with zero mean and the same variance $\sigma^2/2$. Using (2.5.1) to (2.5.8) in (2.4.1) and (2.4.2), we have:

$$E_s(t) = \sum_{n=-\infty}^{\infty} \left[(E_{nIr} - E_{nQi}) + j(E_{nIi} + E_{nQr}) \right] \exp(j\omega_n t) \quad (2.5.9)$$

$$e_{sp}(t) = \sum_{n=-\infty}^{\infty} \left[(c_{nlr} - c_{nQi}) + j(c_{nli} + c_{nQr}) \right] \exp(j\omega_n t). \quad (2.5.10)$$

After the optical BPF, the infinite sums in (2.5.9) and (2.5.9) need to be replaced by finite sums. Since the summation or the subtraction of two independent Gaussian random variables will also result in a Gaussian random variable [18], (2.5.9) and (2.5.10) can be written as:

$$\hat{E}_s(t) = \sum_{n=-\frac{M}{2}}^{\frac{M}{2}} E_n \exp(j\omega_n t) \quad (\text{filtered signal}) \quad (2.5.11)$$

$$\hat{e}_{sp}(t) = \sum_{n=-\frac{M}{2}}^{\frac{M}{2}} c_n \exp(j\omega_n t) \quad (\text{filtered ASE}) \quad (2.5.12)$$

where $E_n = E_{rn} + jE_{in} = (E_{nlr} - E_{nQi}) + j(E_{nli} + E_{nQr}) \quad (2.5.13)$

or $E_n = |E_n| \exp(j\theta_n) \quad (2.5.14)$

$$\theta_n = \tan^{-1} \left(\frac{E_{in}}{E_{rn}} \right) \quad (2.5.15)$$

$$c_n = c_{rn} + jc_{in} = (c_{nlr} - c_{nQi}) + j(c_{nli} + c_{nQr}) \quad (2.5.16)$$

where c_{rn} and c_{in} are identically distributed, independent, zero-mean Gaussian random variables with variance σ^2 . The summations in (2.5.11) and (2.5.12) are over $(M+1)$ components. The parameter M is assumed to be a positive even integer for mathematical convenience.

Filtering causes the signal to spread in time. If the optical filter bandwidth is much larger than the signal spectrum, the effect will be insignificant. Similarly filtering will bandlimit the ASE. Since the ASE spectrum is much wider than the optical filter bandwidth, this

might cause significant correlation of the noises in adjacent time slots. If the correlation is significant, equation (2.5.12) will no longer hold in just one time slot $[0, T]$. Marcuse has numerically shown that for both the sig-sp beat and sp-sp beat noises, the correlation is negligible provided that $M > 1$. In a practical system, M will also be much greater than one. Therefore it can be assumed that the noise in one time slot is uncorrelated with noises in other time slots.

2.6. The Dimensionality of Finite Energy Signals

The dimensionality of the space (the number of discrete frequency components) of baseband finite energy signals with one-sided bandwidth B and time spread about T is approximately $2BT+1$ [10, 20]. The filtered signal and ASE in equations (2.5.11) and (2.5.12) have $M+1$ frequency components spaced at $1/T$ and bandwidth B_o which is the bandwidth of the optical BPF (in Hz). Therefore we have:

$$2BT+1 = B_o T + 1 = M+1 \quad (2.6.1)$$

$$\text{or} \quad B_o = \frac{M}{T}. \quad (2.6.2)$$

Since the 3-dB one-sided electrical bandwidth of the integrate-and-dump filter is $1/2T$, we have:

$$B_o = M \frac{2}{2T} = M(2B_e) = MB_{elec} \quad (2.6.3)$$

$$\text{or} \quad M = \frac{B_o}{B_{elec}}. \quad (2.6.4)$$

Hence M is the ratio of the optical bandwidth B_o to the two-sided electrical bandwidth B_{elec} . Now that the physical meaning of the parameter M has been identified. We can relax the assumption that M is an even integer, which has been used in section 2.5 for mathematical convenience. We now treat M as the ratio of the optical bandwidth to the two-sided electrical bandwidth. The

derivation of (2.6.4) has used the bandwidth of the integrate-and-dump filter. If the time T represents one bit time interval of a non-return-zero (NRZ) signal, the 3-dB one-sided electrical bandwidth of the integrate-and-dump filter will be half of the bit rate which is the Nyquist rate and is the minimum bandwidth required to decode the NRZ signal. However T could also represent two consecutive logical ones (or logical zeros), or half of a logical one (or logical zero). Therefore it is not meaningful to relate the time T to the bit rate. The meaning of the electrical bandwidth can then be relaxed. It does not have to represent the Nyquist rate. In the simulations that will be shown in chapter 4, the two-sided electrical bandwidth B_{elec} is specified in order to calculate the parameter M . The value of T is not needed. For example, if $B_{elec}=20$ GHz, then the filter can pass NRZ signals from low bit rates up to 20 Gb/s. Therefore the actual bit rate is not important. The 20 GHz bandwidth only determines how much noise power is accumulated. The time T acts like a dummy parameter in the derivation. Also the PDFs that will be derived represent the noise distributions at one instant in time and hence how the time T is interpreted is not important to this work.

2.7. The magnitude spectra of signal and ASE

Equations (2.5.11) and (2.5.12) show that the signal and noise in a time interval $[0,T]$ contain discrete frequency components spaced at $1/T$. The magnitude spectra of the signal and noise in a time interval $[0,T]$ are shown in Fig. 2.7.1.(a-b).

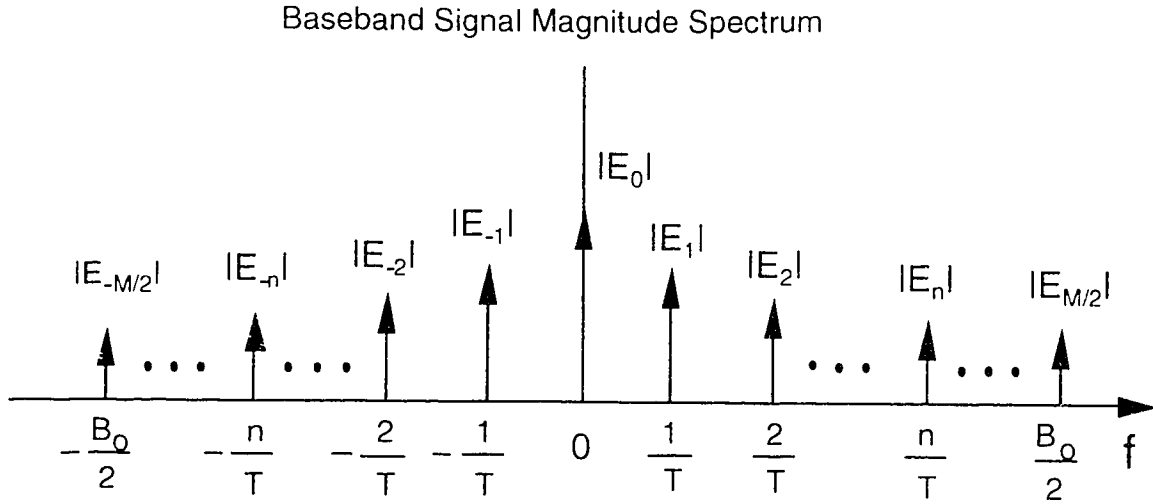


Fig. 2.7.1.a. The baseband magnitude spectrum of signal in a time interval $[0, T]$.

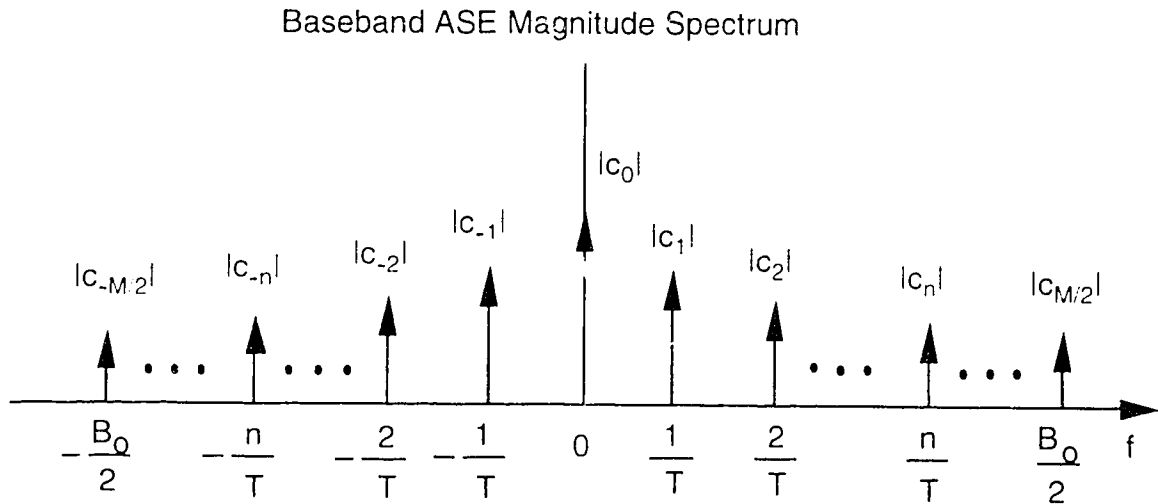


Fig. 2.7.1.b. The baseband magnitude spectrum of ASE in a time interval $[0, T]$.

If the optical bandwidth is much greater than the signal spectrum in the time interval $[0, T]$, the expansion coefficients $|E_{\pm n}|$ and $|E_{\pm M/2}|$ for the signal will approach zero.

2.8. The Moment Generating Functions and The PDFs

The photocurrent in (2.1.1) is a random process because it is time-dependent. The advantage of using the integrate-and-dump filter is now clear. At the output of the filter, the current is the time average of the photocurrent and is time-independent. It is a random variable instead of a process and is given by:

$$y = \frac{1}{T} \int_0^T I_{ph}(t) dt. \quad (2.8.1)$$

Now that the random variable has been identified, calculating its PDF is straightforward. Before performing the integration in (2.8.1), it is advantageous to make slight modifications to the summations in (2.5.15) and (2.5.16). We shall let the coefficient E_0 equal zero such that only M components instead of $(M+1)$ components will enter the calculations. The purpose of doing this will be clear in section 2.11. In addition, the summation symbol will be replaced by \sum and that it is understood the summation is over M components. The detailed calculations for the moment generating functions (MGFs), which are the Laplace transforms of the PDFs, the PDFs are shown in Appendix A1.

The MGF and the PDF of logical ones can be calculated to be:

$$F_1(s) = \frac{1}{(1 + 2\sigma^2 K s)^M} \exp\left(\frac{-sK \sum |E_n|^2}{1 + 2\sigma^2 K s}\right) \quad (\text{MGF}) \quad (2.8.2)$$

$$f_1(y) = \frac{\exp\left(-\frac{K \sum |E_n|^2 + y}{2\sigma^2 K}\right)}{2\sigma^2 K} \left(\frac{y}{K \sum |E_n|^2}\right)^{\frac{M-1}{2}} I_{M-1}\left(\frac{\sqrt{yK \sum |E_n|^2}}{\sigma^2 K}\right) \quad (\text{PDF}) \quad (2.8.3)$$

and the MGF and the PDF for logical zeros are:

$$F_0(s) = \frac{1}{(1 + 2\sigma^2 K s)^M} \quad (\text{MGF}) \quad (2.8.4)$$

$$f_0(y) = \frac{1}{(2\sigma^2 K)^M} \frac{y^{M-1}}{(M-1)!} \exp\left(-\frac{y}{2\sigma^2 K}\right). \quad (\text{PDF}) \quad (2.8.5)$$

The PDFs in (2.8.3) and (2.8.5) are recognized as the Non-Central and Central Chi-Square distributions that have been derived in [7]. The expressions of the PDFs involve parameters such as σ^2 and K which are not physically measurable and hence it is difficult to evaluate the PDFs by using (2.8.3) and (2.8.5). However it will be shown in section 2.10 that the PDFs can be expressed in terms of physical parameters that are measurable.

2.9. The Means and Variances of the PDFs

The detailed calculations of the means and variances can be found in Appendix A1. The means of logical zeros \bar{y}_0 and logical ones \bar{y}_1 are given by:

$$\bar{y}_0 = (2\sigma^2 K)M \quad (\text{zero}) \quad (2.9.1)$$

$$\bar{y}_1 = (2\sigma^2 K)M + K \sum |E_n|^2. \quad (\text{one}) \quad (2.9.2)$$

The corresponding variances are given by:

$$\sigma_0^2 = M(2\sigma^2 K)^2 \quad (\text{zero}) \quad (2.9.3)$$

$$\sigma_1^2 = M(2\sigma^2 K)^2 + 2(2\sigma^2 K)(K \sum |E_n|^2). \quad (\text{one}) \quad (2.9.4)$$

It will be shown in section 2.10 that the means and variances can also be expressed in measurable physical parameters.

2.10. Expressing PDFs in Physical Parameters

2.10.1. The autocorrelation function

The mean of the photocurrent y is given by the temporal and statistical mean of the time-dependent photocurrent $I_{ph}(t)$:

$$\langle y \rangle = \langle \frac{1}{T} \int_0^T I_{ph}(t) dt \rangle \quad (2.10.1.1)$$

$$= \frac{1}{T} \int_0^T \langle I_{ph}(t) \rangle dt \quad (2.10.1.2)$$

where equation (2.8.1) has been used. The symbol $\langle \cdot \rangle$ represents the expectation operator. For a logical zero, assuming there is no signal present, the time-dependent photocurrent is given by:

$$I_{ph}(t) = \Re P_{ase}(t) \quad (2.10.1.3)$$

$$= K \hat{E}_{sp}(t) \hat{E}_{sp}^*(t) \quad (2.10.1.4)$$

$$= K \hat{A}_{sp}^2(t) \quad (2.10.1.5)$$

where K is a proportionality constant, $\hat{E}_{sp}(t) = \hat{A}_{sp}(t) \exp[j2\pi f_c t + j\theta(t)]$ is the complex bandpass representation of the optically filtered random ASE electric field, $\hat{A}_{sp}(t)$ is the random electric field envelope and is a real function, f_c is the frequency of the light carrier, $\theta(t)$ is the random phase.

The random electric field envelope $\hat{A}_{sp}(t)$ can be modeled as a random process and since the statistical process has been assumed to be at least wide-sense stationary, the autocorrelation function of the envelope $\hat{A}_{sp}(t)$ is given by [17]:

$$R(\tau) = \langle \hat{A}_{sp}(t) \hat{A}_{sp}(t + \tau) \rangle \quad (2.10.1.6)$$

where τ is an arbitrary time constant. When $\tau = 0$, we have:

$$R(0) = \langle \hat{A}_{sp}^2(t) \rangle. \quad (2.10.1.7)$$

2.10.2. The power spectral density of ASE

The autocorrelation function is also the inverse Fourier transform of the power spectral density $PSD_{sp}(f)$ (in $V^2/m^2/Hz$) of the random electric field envelope $\hat{A}_{sp}(t)$:

$$R(\tau) = \int_{-\infty}^{\infty} PSD_{sp}(f) \exp(j2\pi f\tau) df \quad (2.10.2.1)$$

and
$$R(0) = \int_{-\infty}^{\infty} PSD_{sp}(f) df \quad (2.10.2.2)$$

where $f \in [0, B_o]$ since $\hat{A}_{sp}(t)$ is the baseband envelope of the optically filtered ASE electric field $\hat{E}_{sp}(t)$. The quantity in (2.10.2.2) is related to the ASE power P_{ase} in watts as:

$$P_{ase} = \frac{K}{\Re} R(0) = \int_{-\infty}^{\infty} \frac{K}{\Re} PSD_{sp}(f) df \quad (2.10.2.3)$$

where the proportionality constant K and the responsivity \Re have units of Am^2/V^2 and A/W respectively. These two constants serve to convert the unit of the power spectral density to W/Hz . The ASE power can also be calculated using the one-sided bandpass power spectral density $BPPSD_{sp}(f)$ given by [21]:

$$BPPSD_{sp}(f) = m_t N_{sp} (G - 1) hf \quad (2.10.2.4)$$

where the polarization state parameter m_t is equal to one if the polarizer is used, and is equal to two when the polarizer is omitted. The polarizer is essentially a spatial filter which can be used to filter out the ASE electric field component that is orthogonal to the signal electric field. The parameter N_{sp} is the spontaneous emission factor of the EDFA. The EDFA small signal gain is denoted by G , h is the

Planck's constant and f is the photon frequency. Within a narrow range of wavelengths, such as the case when a narrow-band optical filter is placed at the output of the EDFA, the spontaneous emission factor and the EDFA small signal gain are weak functions of the wavelength (or frequency). The bandpass power spectral density in (2.10.2.4) is then linearly proportional to the frequency with $f \in [f_c - B_o/2, f_c + B_o/2]$. Using (2.10.2.4), the ASE power in (2.10.2.3) can be calculated as [11]:

$$P_{ase} = \int_{f_c - B_o/2}^{f_c + B_o/2} m_t N_{sp} (G - 1) h f df \quad (2.10.2.5)$$

$$= m_t N_{sp} (G - 1) h f_c B_o. \quad (2.10.2.6)$$

Using (2.10.1.5), (2.10.1.7) and (2.10.2.3) in (2.10.1.2), the mean of a logical zero can be expressed as:

$$\langle y \rangle_0 = \Re P_{ase} \quad (2.10.2.7)$$

where the ASE power P_{ase} is given by (2.10.2.6). Equating (2.9.1) and (2.10.2.7), the mean of y for logical zeros is:

$$\bar{y}_0 = (2\sigma^2 K) M = \langle y \rangle_0 = \Re P_{ase} \quad (2.10.2.8)$$

so that
$$2\sigma^2 K = \frac{\Re P_{ase}}{M}. \quad (2.10.2.9)$$

Equation (2.10.2.9) can be used to rewrite the equations of the PDFs and the new equations will be shown in section 2.10.4.

2.10.3. The EDFA small signal gain

The EDFA small signal gain can be calculated by using the transcendental equation [22]:

$$G = G_o \exp \left[\frac{(1 - G) P_{inav}}{P_{sat}} \right] \quad (2.10.3.1)$$

where G_o is the EDFA small signal gain, P_{sat} is the saturation power, and P_{inav} is the average signal power at the input of the EDFA and is given by (assuming logical zeros and logical ones are equiprobable):

$$P_{inav} = \frac{1}{2}(P_{in1} + P_{in0}) \quad (2.10.3.2)$$

where P_{in1} and P_{in0} are the average powers during a logical one and a logical zero respectively and are related through the extinction ratio δ :

$$P_{in0} = \delta P_{in1}. \quad (2.10.3.3)$$

The average signal power is used in (2.10.3.1) instead of the individual signal powers for logical ones and logical zeros because the EDFA cannot respond to fast varying powers [23]. The definition of the extinction ratio used here is the average power of a logical zero divided by the average power of a logical one. The transcendental equation in (2.10.3.1) can be solved numerically using methods such as the Newton Raphson method [24].

2.10.4. The new expressions for the PDFs

The term in (2.8.2) that sums the expansion coefficients of the signal electric field can be recognized as the photocurrent generated by the signal. Therefore it can be rewritten as:

$$K \sum |E_n|^2 = \Re P_{sig} \quad (2.10.4.1)$$

where \Re is the responsivity of the photodiode and P_{sig} is the average signal power in the time interval $[0, T]$ for logical ones. The detailed proof of (2.10.4.1) can be found in Appendix A2. The means and variances can then be expressed by using (2.10.2.9) and (2.10.4.1) as:

$$\bar{y}_0 = \Re P_{ase} \quad (2.10.4.2)$$

$$\bar{y}_1 = \Re (P_{ase} + P_{sig}) \quad (2.10.4.3)$$

$$\sigma_0^2 = \frac{(\Re P_{ase})^2}{M} \quad (2.10.4.4)$$

$$\sigma_1^2 = \frac{(\Re P_{ase})^2}{M} + \frac{2 \Re^2 P_{ase} P_{sig}}{M}. \quad (2.10.4.5)$$

The variance σ_0^2 of logical zeros represents the sp-sp beat noise whereas the second term in equation (2.10.4.5) represents the sig-sp beat noise. The PDFs can be expressed as:

$$f_0(y) = \left(\frac{M}{\Re P_{ase}} \right)^M \frac{y^{M-1}}{(M-1)!} \exp \left(-\frac{yM}{\Re P_{ase}} \right) \quad (2.10.4.6)$$

$$f_1(y) = \left(\frac{M}{\Re P_{ase}} \right) \left(\frac{y}{\Re P_{sig}} \right)^{M-1} \exp \left(- \frac{M(y + \Re P_{sig})}{\Re P_{ase}} \right) I_{M-1} \left(\frac{2M \sqrt{y \Re P_{sig}}}{\Re P_{ase}} \right). \quad (2.10.4.7)$$

Now equations (2.10.4.6) and (2.10.4.7) can be used to evaluate the PDFs by properly choosing the values of the physical parameters such as the EDFA small signal gain, etc.

2.11. Comparison of Beat Noises with Olsson's Expressions

The sig-sp and sp-sp beat noises derived by Olsson, ignoring losses, are given by [11]:

$$N_{s-sp} = 4 I_s I_{sp} \frac{B_c}{B_o} \quad (2.11.1)$$

$$N_{sp-sp} = I_{sp}^2 \frac{B_c (2 B_o - B_c)}{B_o^2}. \quad (2.11.2)$$

Using equation (2.6.4) and $I_s = \Re P_{sig}$, $I_{sp} = \Re P_{ase}$, the variances in equations (2.10.4.4) and (2.10.4.5) can be rewritten as:

$$\sigma_0^2 = I_{sp}^2 \frac{B_{elec}}{B_o} \quad (2.11.3)$$

$$\sigma_1^2 = I_{sp}^2 \frac{B_{elec}}{B_o} + \frac{2 I_s I_{sp} B_{elec}}{B_o}. \quad (2.11.4)$$

Since $B_{elec} = 2 B_c$, the sig-sp noise terms in equations (2.11.1) and (2.11.4) are identical. The sp-sp beat noise terms are slightly different. The difference can be examined by forming the ratio of the sp-sp noise terms:

$$ratio = \frac{\sigma_0^2}{N_{sp-sp}} = \frac{B_{elec}}{B_o} \frac{B_o^2}{B_c (2 B_o - B_c)} \quad (2.11.5)$$

$$ratio = \frac{1}{1 - \frac{B_{elec}}{4B_o}} = \frac{1}{1 - \frac{1}{4M}}. \quad (2.11.6)$$

This ratio is plotted against M in Fig. 2.11.1.

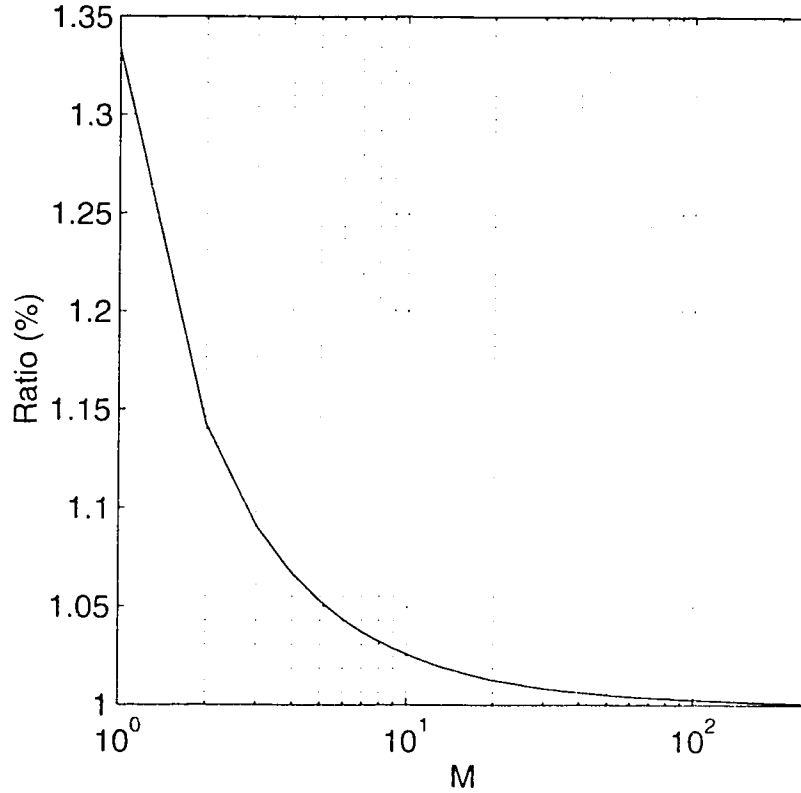


Fig. 2.11.1. The ratio of the sp-sp beat noise terms versus M .

It can be seen that the value of σ_0^2 is within 5% agreement of Olsson's when $M \geq 5$. Since the dominant noise term is sig-sp beat noise, the slight difference in sp-sp beat noise will not affect the accuracy of the analysis. Note that if we use $(M+1)$ components instead of M components in the derivation of the PDFs in section 2.8, the parameter M in (2.10.4.4) to (2.10.4.7) has to be replaced by $(M+1)$. The choice of using M components is just to show that the PDFs derived do match the previous noise theory in [11]. In the analysis of system performance, the value of M is at least ten.

Therefore whether using M or $(M+1)$ will not make significant difference.

2.12. The Probability of Error and the Bit Error Rate

The error due to noise for a logical one occurs when a logical one is transmitted and the decision is a logical zero. This error probability is given by the area of the PDF for logical ones in the interval $0 \leq y \leq I_d$, where I_d is the decision threshold, which does not have to be optimum in the following analysis. This area or the error probability for a logical one can be calculated by integrating the PDF over that interval:

$$P_1(I_d) = \int_0^{I_d} f_1(y) dy \quad (2.12.1)$$

$$= 1 - \int_{I_d}^{\infty} f_1(y) dy \quad (2.12.2)$$

$$= 1 - Q_M(a, b) \quad (2.12.3)$$

where $Q_M(a, b)$ is called the generalized Q-function for $M > 1$ and is called the Marcum-Q function for $M = 1$ [25, 26]. The proof of (2.12.3) can be found in Appendix A3. This function is analogous to the Q-function associated with Gaussian statistics. The arguments a, b are given by:

$$a = \sqrt{\frac{2MP_{sig}}{P_{ase}}} \quad (2.12.4)$$

$$b = \sqrt{\frac{2MI_d}{\Re P_{ase}}} \quad (2.12.5)$$

The integral representation of the generalized Q-function is given by:

$$Q_M(a, b) = \int_b^{\infty} x \left(\frac{x}{a} \right)^{M-1} \exp\left(-\frac{x^2 + a^2}{2}\right) I_{M-1}(ax) dx \quad (2.12.6)$$

where x is a dummy variable. If M is an integer, this function can be expressed as [25]:

$$Q_M(a, b) = Q(a, b) + \exp\left(-\frac{a^2 + b^2}{2}\right) \sum_{k=1}^{M-1} \left(\frac{b}{a}\right)^k I_k(ab) \quad (2.12.7)$$

where when $b > a$:

$$Q(a, b) = \exp\left(-\frac{a^2 + b^2}{2}\right) \sum_{k=0}^{\infty} \left(\frac{a}{b}\right)^k I_k(ab) \quad (2.12.8)$$

and when $a \geq b$:

$$Q(a, b) = 1 - \exp\left(-\frac{a^2 + b^2}{2}\right) \sum_{k=1}^{\infty} \left(\frac{b}{a}\right)^k I_k(ab). \quad (2.12.9)$$

The infinite summation term does not have a closed form and therefore it is necessary to truncate the series in order to calculate the probability of error. Denoting the truncated generalized Q-function as $\hat{Q}_M(a, b)$ and replacing ∞ by a finite integer L , the absolute truncation error can be expressed as:

$$Err(L) = |Q_M(a, b) - \hat{Q}_M(a, b)| \quad (2.12.10)$$

where for $a \geq b$, using equation (2.12.9) in equation (2.12.7), we have:

$$\hat{Q}_M(a, b) = 1 - \exp\left(-\frac{a^2 + b^2}{2}\right) \sum_{k=M}^L \left(\frac{b}{a}\right)^k I_k(ab) \quad (2.12.11)$$

and for $b > a$, using equation (2.12.8) in equation (2.12.7), we have:

$$\hat{Q}_M(a, b) = \exp\left(-\frac{a^2 + b^2}{2}\right) \sum_{k=1-M}^L \left(\frac{a}{b}\right)^k I_k(ab) \quad (2.12.12)$$

where the property $I_{-M}(x) = I_M(x)$ (M is an integer) has been used. The absolute truncation error has an upper bound given by:

$$Err(L) \leq \exp\left(-\frac{a^2 + b^2}{2}\right) \left(\frac{b}{a}\right)^L I_{L+1}(ab) \left(1 + \sqrt{\frac{\pi ab}{2}}\right) \quad (2.12.13)$$

for $(a \geq b)$, and

$$Err(L) < \exp\left(-\frac{a^2 + b^2}{2}\right) \left(\frac{a}{b}\right)^L I_{L+1}(ab) \left(1 + \sqrt{\frac{\pi ab}{2}}\right) \quad (2.12.14)$$

for $(b > a)$.

The derivation for the upper bound can be found in Appendix A4. The probability of error for a logical zero is determined by:

$$P_0(I_d) = \int_{I_d}^{\infty} f_0(y) dy \quad (2.12.15)$$

which has a closed form expression:

$$P_0(I_d) = \sum_{r=0}^{M-1} \left(\frac{I_d M}{\Re P_{ase}}\right)^r \frac{\exp\left(-\frac{I_d M}{\Re P_{ase}}\right)}{r!}. \quad (2.12.16)$$

The derivation of (2.12.16) can be found in Appendix A3. The average bit error rate is given by the expectation of P_0 and P_1 :

$$BER = \langle P_0(I_d) + P_1(I_d) \rangle. \quad (2.12.17)$$

If logical ones and logical zeros are equiprobable, then the bit error rate is given by:

$$BER = \frac{1}{2}[P_0(I_d) + P_1(I_d)]. \quad (2.12.18)$$

2.13. Gaussian Approximation

Gaussian statistics are widely used in the field of communications. The formulation of Gaussian statistics is relatively simple because it is sufficient to characterize the PDFs and the cumulative distribution functions (CDFs) by using the mean and the variance. For logical ones, the Gaussian PDF is given by:

$$f_{1g}(y) = \frac{1}{\sqrt{2\pi\sigma_1^2}} \exp\left(-\frac{(y - \bar{y}_1)^2}{2\sigma_1^2}\right). \quad (2.13.1)$$

Using equations (2.10.4.3) and (2.10.4.5) for the mean and variance, the PDF can be expressed as:

$$f_{1g}(y) = \frac{1}{\sqrt{\frac{2\pi}{M}[(\Re P_{ase})^2 + 2\Re^2 P_{ase} P_{sig}]}} \exp\left\{-\frac{\left[y - \Re(P_{ase} + P_{sig})\right]^2}{\frac{2}{M}[(\Re P_{ase})^2 + 2\Re^2 P_{ase} P_{sig}]}\right\} \quad (2.13.2)$$

Similarly, for logical zeros, using equations (2.10.4.2) and (2.10.4.4), the PDF is given by:

$$f_{0g}(y) = \frac{1}{\sqrt{2\pi\sigma_0^2}} \exp\left(-\frac{(y - \bar{y}_0)^2}{2\sigma_0^2}\right) \quad (2.13.3)$$

$$= \frac{1}{\sqrt{\frac{2\pi}{M}(\Re P_{ase})^2}} \exp \left\{ -\frac{[y - \Re P_{ase}]^2}{\frac{2}{M}[\Re P_{ase}]^2} \right\}. \quad (2.13.4)$$

The probability of errors can be expressed as:

$$P_{0g}(I_d) = Q \left(\frac{I_d - \bar{y}_0}{\sigma_0} \right) \quad (2.13.5)$$

$$= Q \left(\frac{I_d - \Re P_{ase}}{\sqrt{\frac{\Re P_{ase}}{M}}} \right) \quad (2.13.6)$$

$$P_{1g}(I_d) = Q \left(\frac{\bar{y}_1 - I_d}{\sigma_1} \right) \quad (2.13.7)$$

$$= Q \left(\frac{\Re(P_{ase} + P_{sig}) - I_d}{\sqrt{\frac{(\Re P_{ase})^2 + 2\Re^2 P_{ase} P_{sig}}{M}}} \right) \quad (2.13.8)$$

where $Q(\cdot)$ is the Q-function. When the extinction ratio is non-zero, equation (2.13.8) can be used for logical one with smaller P_{sig} .

2.14. Modification of Equations When Polarizer is Omitted

The derivations in the previous section assume the ASE is polarized spatially in the same state as the signal. Only minor modification to the equations is needed to accommodate the case when the polarizer is omitted. The proof of this can be found in Appendix A5.

Without the polarizer, M has to be replaced by $2M$. Also the polarization state parameter m_l has to be changed from one to two. In general, the parameter M should be replaced by $m_l M$ in order to account for the effect of the polarizer. When the polarizer is omitted

($m_l=2$), both M and P_{ase} are doubled. From equations (2.10.4.4) and (2.10.4.5), it can be seen that the sp-sp beat noise is doubled but the sig-sp beat noise remains the same. Removing the polarizer introduces additional ASE electric field which is spatially orthogonal to the signal electric field. The signal cannot beat with this additional ASE electric field and hence the sig-sp beat noise remains the same. The sp-sp beat noise however is doubled since the additional ASE electric field components beat among themselves.

2.15. The Optimum Threshold

When the threshold in equation (2.12.18) is set at its optimum value, the BER of the system is at its minimum. The optimum threshold is obtained by differentiating the BER with respect to I_d and setting the derivative to zero:

$$\frac{\partial BER}{\partial I_d} = \frac{1}{2} \frac{\partial}{\partial I_d} (P_0 + P_1) = 0. \quad (2.15.1)$$

Using equations (2.12.1) and (2.12.15), the optimum threshold I_{dopt} is determined from the condition:

$$f_0(I_{dopt}) = f_1(I_{dopt}). \quad (2.15.2)$$

Equation (2.15.2) can be solved numerically using methods such as the Bisection method [24]. For Gaussian distributions, the optimum threshold can be approximated by:

$$I_{doptgauss} = \frac{\sigma_0 \bar{y}_1 + \sigma_1 \bar{y}_0}{\sigma_0 + \sigma_1} \quad (2.15.3)$$

where y_0 and \bar{y}_1 are the means of logical zeros and logical ones given by (2.10.4.2) and (2.10.4.3), σ_0 and σ_1 are the standard deviations of logical zeros and logical ones given by the square root of (2.10.4.4) and (2.10.4.5).

2.16. The Coupling and Insertion Losses

In a real system, there are usually losses caused by the insertion of components such as isolators, optical filters, etc. Denoting the input coupling loss of the EDFA as μ_{in} , the output coupling loss as μ_{out} and the additional loss between the output of the EDFA and the photodiode as L , the signal and ASE power detected by the photodiode are calculated as:

$$\hat{P}_{ase} = \mu_{out} L P_{ase} \quad (2.16.1)$$

$$\hat{P}_{sig} = \mu_{in} G \mu_{out} L P_{in} \quad (2.16.2)$$

where P_{in} is the average power of a logical one or a logical zero at the input of the EDFA before input coupling loss. Therefore in order to simulate a real system, the powers P_{sig} and P_{ase} in the previous equations must be replaced by \hat{P}_{sig} and \hat{P}_{ase} respectively.

2.17. Comparison of Gaussian and Chi-Square PDFs

The PDFs for logical zeros and logical ones are shown in Fig. 2.17.1.(a-d). A polarizer is used for Fig. 2.17.1.(a-b) and therefore $m_i=1$. For Fig. 2.17.1.(c-d), the parameter $m_i=2$ because the polarizer is omitted. The values of the other parameters used are $\delta=0$, $P_{inI}=-36$ dBm, $P_{inav}=-39$ dBm, $P_{sat}=30$ mW, $G_o=30$ dB, $B_{elec}=20$ GHz, $B_o=1.4 \times 1.3$ nm (the factor 1.4 is for calculating the noise equivalent bandwidth of the optical BPF), $M=11$ for the case of using polarizer and $M=22$ for no polarizer, $N_{sp}=2$, $\mathfrak{R}=1$ A/W. The losses are neglected. Note the optical filter bandwidth B_o should be in hertz instead of nanometer. However for convenience, the value of B_o will be given in nanometer. In the actual calculations, the following conversion is applied to B_o to change its unit to hertz:

$$B_o(\text{Hz}) = \frac{c_o}{\lambda_c^2} B_o(\text{nm}) \quad (2.17.1)$$

where $c_o = 3 \times 10^8$ m/s is the speed of light in vacuum, λ_c is the wavelength of the light carrier. For example, at $\lambda_c = 1550$ nm, 1 nm of B_o corresponds to about 125 GHz.

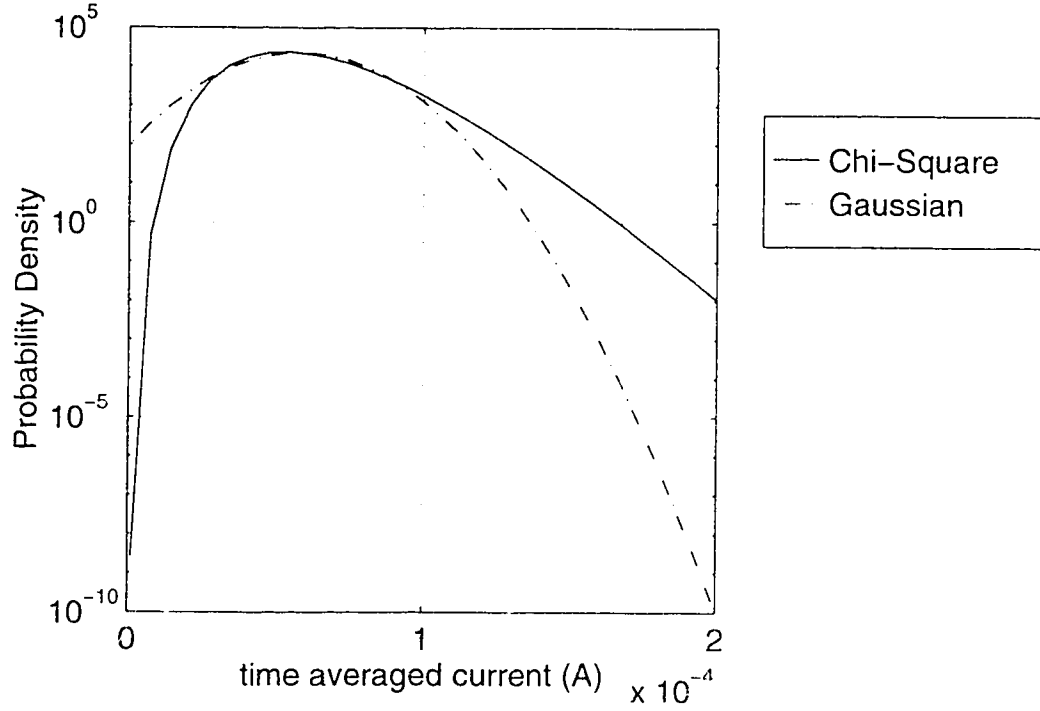


Fig. 2.17.1.a. PDFs of logical zeros with polarizer.

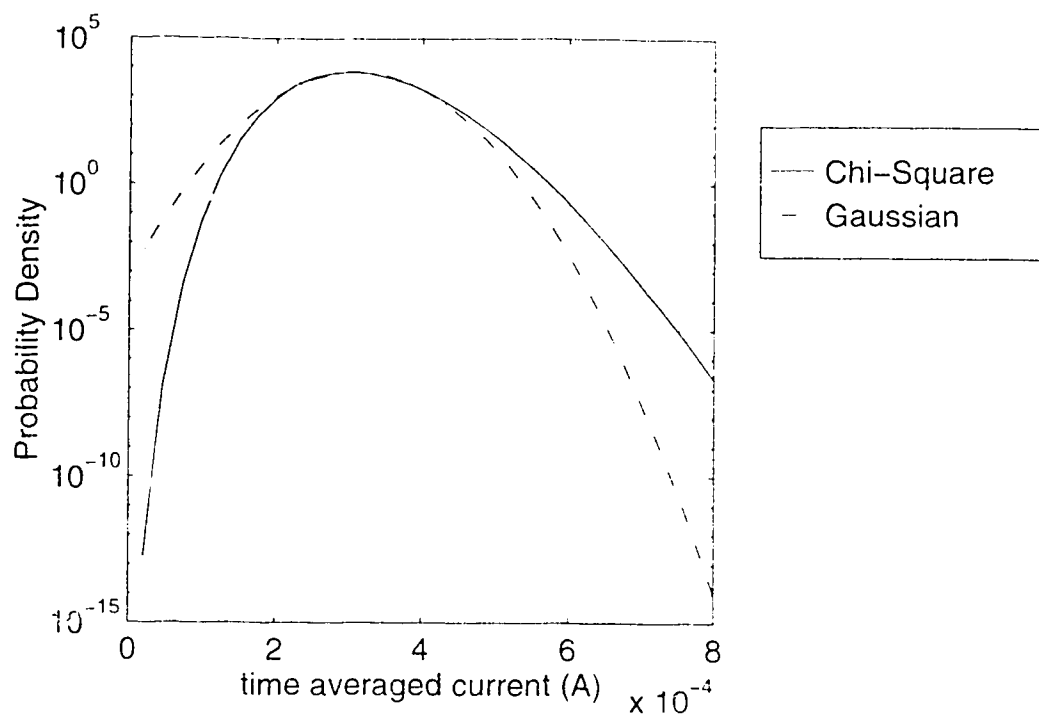


Fig. 2.17.1.b. PDFs of logical ones with polarizer.

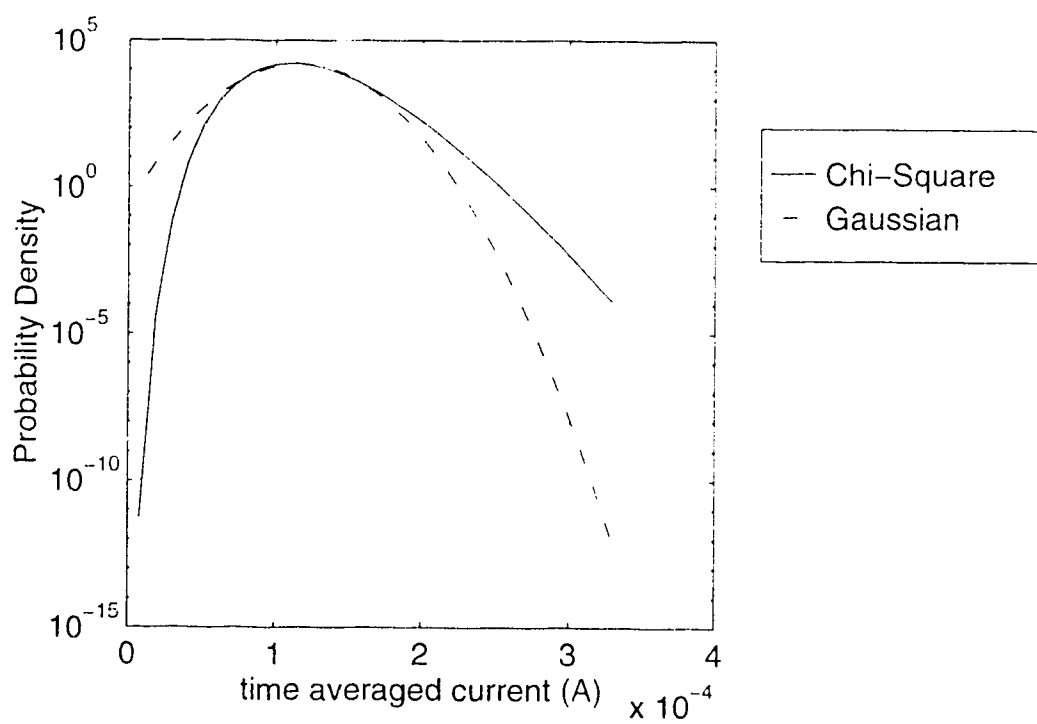


Fig. 2.17.1.c. PDFs of logical zeros without polarizer.

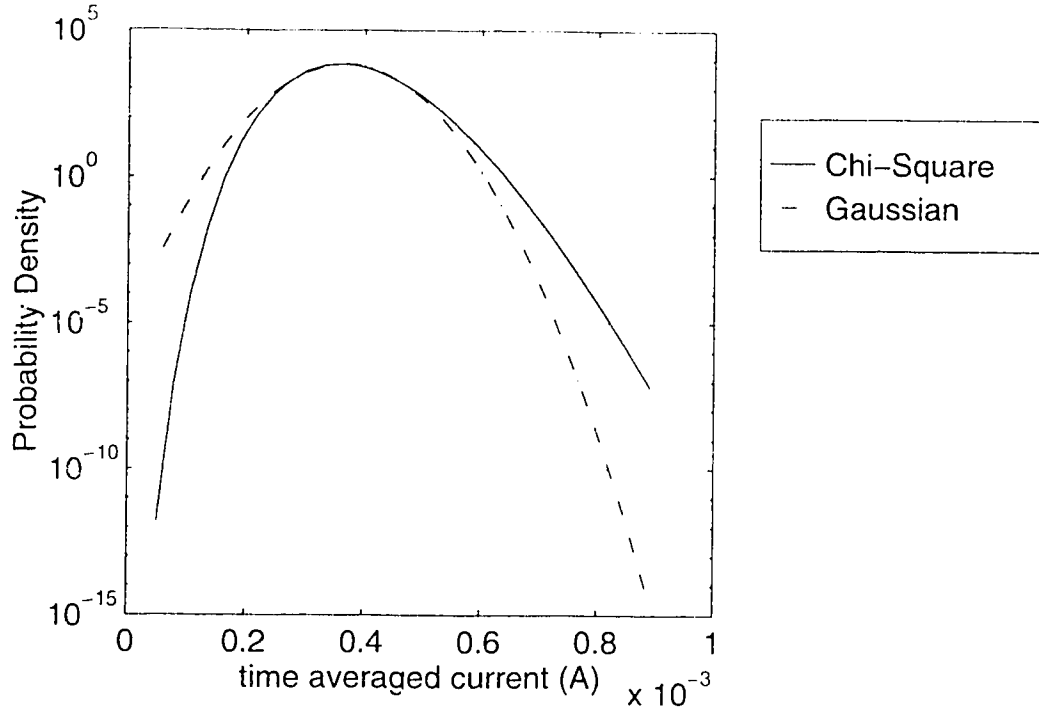


Fig. 2.17.1.d. PDFs of logical one . without polarizer.

As it can be seen, the Gaussian distribution is very different from the Chi-Square distribution. One of the tails of the Gaussian distribution extends to the negative side of the time averaged current axis. The tails of the Chi-Square are confined in the positive range of the time averaged current. The negative tail of the Gaussian distribution violates the condition that the photocurrent must be positive. However the impact of this is significant only under certain circumstances. If we are only interested in the sensitivity performance of the system, the Gaussian approximation will only give slightly different results from the Chi-Square distribution. Fig. 2.17.2.(a-b) illustrate the crossing points or the optimum thresholds of the Gaussian and the Chi-Square PDFs. The received power has been increased to $P_{inav}=-35$ dBm whereas the values of the other parameters are the same as the ones used for generating Fig. 2.17.1.(a-d).

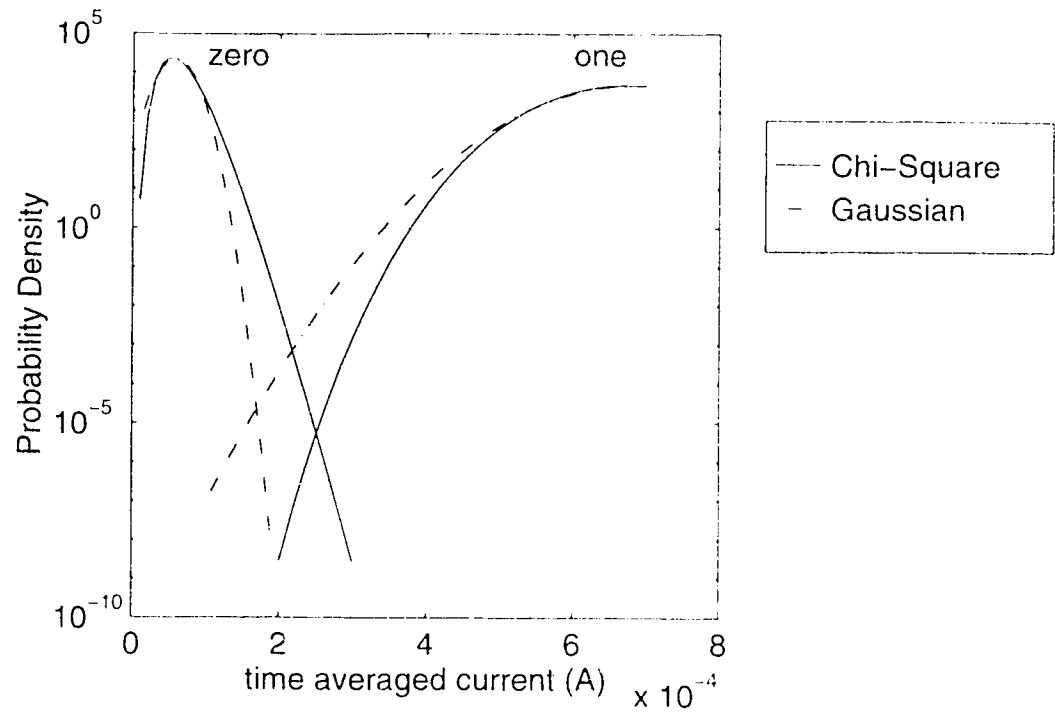


Fig. 2.17.2.a. Crossing points of PDFs with polarizer.

The mean values of the logical ones and logical zeros in Fig. 2.17.2.a are 6.82×10^{-4} A and 5.76×10^{-5} A respectively. The optimum thresholds of the Gaussian and Chi-Square PDFs are 1.7×10^{-4} A and 2.5×10^{-4} A respectively.

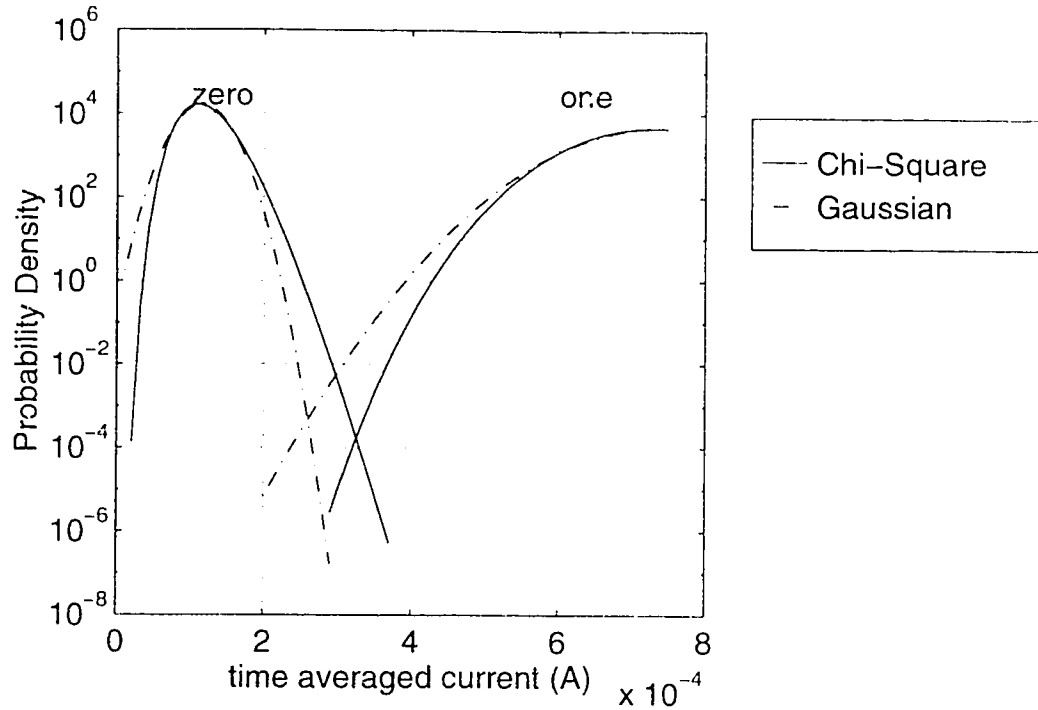


Fig. 2.17.2.b. Crossing points of PDFs without polarizer.

The mean values of the logical ones and logical zeros in Fig. 2.17.2.b are 7.39×10^{-4} A and 1.15×10^{-4} A respectively. The optimum thresholds of the Gaussian and Chi-Square PDFs are 2.6×10^{-4} A and 3.3×10^{-4} A respectively.

It can be seen from Fig. 2.17.2.(a-b) that the optimum thresholds predicted by Gaussian PDFs are very different from the ones predicted by the Chi-Square PDFs. Therefore in the analyses that involve the knowledge of the optimum threshold, using Gaussian approximation will not provide results that are adequately accurate. The different system performance analyses will be shown and discussed in chapter 4.

2.18. On The Computation of Functions

in the calculation of the probability of errors and the optimum threshold using the equations presented in this chapter, it is necessary to calculate the modified Bessel function of the first kind $I_M(z)$ with many different orders M and arguments z . The computing speed for $I_M(z)$ is very slow and the function can

sometimes return values which are too large for the computer to handle accurately because the argument is too large. However, the argument is not large enough and therefore the large argument approximation for the Bessel function cannot be used. In addition, there are also decaying exponential functions involved in the calculation, this function can sometimes return values which are too small to be handle accurately. These two functions limit the speed of computation and the range of values of parameter that can be used in the analysis because of accuracy.

In chapter 3, a method called the Steepest Descent Method will be introduced. This method will be used to approximate the inverse Laplace transform of the MGFs. It will be shown that this approximation is very accurate in chapter 3. In addition, no Bessel functions appear in the final equations and hence the computational speed is very fast. There is also no restriction on the values of parameters in the analysis. Moreover, it can be used to generate a wide variety of graphs in a short period of time. This method will be used to generate PDFs which will be compared with the ones generated by the Chi-Square distribution in chapter 3.

3. Non-Gaussian Noise Theory-Part II

The previous analysis has excluded the post-detection Gaussian noises such as thermal noise and shot noise. These post-detection noises will be significant if the optical filter bandwidth is sufficiently narrow or if the EDFA small signal gain is smaller than a certain value. In this chapter, a more complete MGF which includes the thermal and shot noises will be derived. The non-Gaussian PDFs for logical zeros and logical ones will be obtained by using the Steepest Descent Method (or the Saddle Point Method). The Steepest Descent Method will be briefly introduced in this chapter. More information about this method can be found in [28]. The derivations of the PDFs and the error probabilities are given in [8].

3.1. The MGF of Gaussian Noise

The MGF of the Gaussian PDF of a random variable y_g with zero mean and variance σ_g^2 is given by the bilateral Laplace transform of the PDF:

$$\langle \exp(-sy_g) \rangle = \frac{1}{\sqrt{2\pi\sigma_g^2}} \int_{-\infty}^{\infty} \exp\left(-\frac{y_g^2}{2\sigma_g^2} - sy_g\right) dy_g. \quad (3.1.1)$$

By completing the square in the exponential term and using the Gauss integral for complex argument from Appendix C, the MGF can be expressed as:

$$F_g(s) = \langle \exp(-sy_g) \rangle = \exp\left(-\frac{\sigma_g^2}{2}s^2\right). \quad (3.1.2)$$

3.2. The Variances of Thermal and Shot Noises

The distributions of the thermal and shot noises can be well approximated by the Gaussian PDF. The two sided PSDs for the thermal and shot noises are given by:

$$PSD_{th} = \frac{2kT_k}{R_{eq}} \quad (\text{thermal noise}) \quad (3.2.1)$$

$$PSD_{sh} = qI_{ph} \quad (\text{shot noise}) \quad (3.2.2)$$

where k is the Boltzmann's constant, T_k is the absolute temperature, R_{eq} is the equivalent noise resistance of the receiver, q is the electron charge and I_{ph} is the photocurrent. The variances are given by the noise powers:

$$\sigma_{th}^2 = \frac{2kT_k}{R_{eq}} B_{elec} \quad (3.2.3)$$

$$\sigma_{sh}^2 = qI_{ph} B_{elec} \quad (3.2.4)$$

where B_{elec} is the two-sided electrical bandwidth. Because of the presence of ASE, I_{ph} is a random variable. This means the PDF of shot noise is a conditional PDF and depends on the random variable I_{ph} . The MGF of the shot noise cannot be simply multiplied by the MGFs of the thermal, sig-sp beat and sp-sp beat noises. However, since shot noise is not a dominant noise term, in order to simplify the analysis, the current I_{ph} can be replaced by its mean value given by:

$$\langle I_{ph} \rangle = \bar{I}_{ph} = \Re(P_{sig} + P_{ase}) \quad (3.2.5)$$

where the signal power P_{sig} may or may not vanish for logical zeros. The variance for shot noise can then be written as:

$$\sigma_{sh}^2 = q\bar{I}_{ph} B_{elec} = q\Re(P_{sig} + P_{ase}) B_{elec} \quad (3.2.6)$$

and the shot noise PDF becomes an unconditional one.

3.3. The Overall MGF

Since the thermal noise is independent of the signal and the beat noises, its MGF can be multiplied by the MGF from (2.8.2). The PDF of the shot noise has been made unconditional and hence its MGF can also be multiplied by the MGFs of the beat noises and the thermal noise. The MGFs of the thermal and the shot noises can be obtained by substituting (3.2.3) and (3.2.6) in (3.1.2). Multiplying the MGFs of the thermal and the shot noise by (2.8.2), the overall MGF can be expressed as:

$$F(s) = \frac{1}{(1 + 2\sigma^2 Ks)^M} \exp\left(\frac{-sK \sum |E_n|^2}{1 + 2\sigma^2 Ks}\right) \exp\left(\frac{\sigma_{th}^2}{2} s^2\right) \exp\left(\frac{\sigma_{sh}^2}{2} s^2\right). \quad (3.3.1)$$

The PDF for logical ones is obtained from the inverse Laplace transform of $F(s)$. In order to simplify the expression, the following substitutions are made:

$$A = K \sum |E_n|^2 = \Re P_{sig} \quad (3.3.2)$$

$$B = 2\sigma^2 K = \frac{\Re P_{ase}}{M} \quad (3.3.3)$$

$$C = \frac{\sigma_{th}^2 + \sigma_{sh}^2}{2} \quad (3.3.4)$$

where equations (2.10.2.9) and (2.10.4.1) have been used. Using (3.3.2) to (3.3.4) in (3.3.1) and taking the inverse Laplace transform, the PDF for logical ones is then given by [29]:

$$f_1(y) = \frac{1}{2\pi j} \int_{\alpha-j\infty}^{\alpha+j\infty} \frac{1}{(1+Bs)^M} \exp\left(\frac{-As}{1+Bs}\right) \exp(Cs^2) \exp(ys) ds \quad (3.3.5)$$

where α is a constant so chosen that the contour of the integral in equation (3.3.5) lies to the right of the poles of the integrand. For example, the integrand in equation (3.3.5) has a pole at $s = -1/B$, therefore it is necessary to choose $\alpha > -1/B$. Notice that if C is set to zero, the analysis will be applying the Steepest Descent Method to the MGF of the Chi-Square distribution. Rewriting the first term in the integrand of (3.3.5) as:

$$\frac{1}{(1+Bs)^M} = \exp[-M \ln(1+Bs)] \quad (3.3.6)$$

and making a change of variable $u = 1 + Bs$, the PDF can be expressed as:

$$f_1(y) = \frac{1}{2\pi j B} \int_{1+B\alpha-j\infty}^{1+B\alpha+j\infty} \exp\left[\frac{-A(u-1)}{Bu} + \frac{C(u-1)^2}{B^2} + \frac{y(u-1)}{B} - M \ln u\right] du \quad (3.3.7)$$

$$= \frac{1}{2\pi j B} \int_{1+B\alpha-j\infty}^{1+B\alpha+j\infty} \exp[F(u)] du \quad (3.3.8)$$

where

$$F(u) = \frac{-A(u-1)}{Bu} + \frac{C(u-1)^2}{B^2} + \frac{y(u-1)}{B} - M \ln u. \quad (3.3.9)$$

The integral in equation (3.3.7) does not have a closed form expression. However a very good approximation can be made by

using the Method of Steepest Descent and the PDF can be expressed in closed form. Section 3.4 will give a brief introduction to this method and section 3.5 will apply this method to find the PDF.

3.4. The Steepest Descent Method

The materials in this section are mostly taken from [28]. This method can be found in many other physics textbooks such as [27]. The Steepest Descent Method was devised by P. Debye for evaluating the integrals of the form:

$$J(z) = \int_{C_1} \exp[zf(t)] dt \quad (3.4.1)$$

when $|z|$ is very large. In equation (3.4.1), $f(t)$ are analytic functions in some region containing the contour C_1 . The argument z can be real or complex. In the following analysis, the argument z will be assumed to be real, or equivalently its phase $\exp[i \arg(z)]$ is absorbed into $f(t)$. The method is based on the observation that the major contribution to the integral from the integrand comes from the regions along C_1 where $\text{Re}\{f(t)\}$ is largest or has a maximum. However, in these regions there would usually be very large oscillations and consequently important cancellations of the values of the integral due to the factor $\exp[j \text{Im}\{f(t)\}]$. These oscillations would make the evaluation of the integral very difficult. The idea of Debye is to deform the path C_1 in such a way that on a part C_o of C_1 , the following conditions are satisfied:

- (a) Along C_o , $\text{Im}\{f(t)\}$ is constant.
- (b) C_o goes through a point t_o where:

$$\left. \frac{df(t)}{dt} \right|_{t=t_o} = 0. \quad (3.4.2)$$

- (c) The path C_o is so chosen that at $t = t_o$, $\text{Re}\{f(t)\}$ goes through a relative maximum, and C_o is called the path of steepest descent.

The condition (a) will guarantee that there are no oscillations along C_o . Condition (a) and the fact that C_o goes through the point t_o determine the equation of the path C_o along which $\text{Im}\{f(t)\} = \text{Im}\{f(t_o)\}$. The condition (c) ensures that the integrand has a peak at $t = t_o$ so that the main contribution to the integral will come from an environment of the point t_o .

3.4.1. The paths of constant $\text{Im}\{f(t)\}$

We can expand the function $f(t)$ at $t = t_o$ as Taylor series:

$$f(t) = f(t_o) + (t - t_o) \left. \frac{df(t)}{dt} \right|_{t=t_o} + \frac{1}{2} (t - t_o)^2 \left. \frac{d^2 f(t)}{dt^2} \right|_{t=t_o} + \dots \quad (3.4.1.1)$$

Using (3.4.2) in (3.4.1.1) and observing that in the neighborhood of t_o , the terms higher than the second order can be ignored, the function becomes:

$$f(t) \cong f(t_o) + \frac{1}{2} (t - t_o)^2 \left. \frac{d^2 f(t)}{dt^2} \right|_{t=t_o} \quad (3.4.1.2)$$

where the second derivative of the function is assumed to be non-zero. Let

$$t - t_o = r \exp(j\varphi) \quad (3.4.1.3)$$

$$\text{and} \quad \frac{1}{2} \left. \frac{d^2 f(t)}{dt^2} \right|_{t=t_o} = R \exp(j\phi) \quad (3.4.1.4)$$

where the magnitude R and the angle ϕ are constants, the magnitude r and the angle φ are variables, then using (3.4.1.3) and (3.4.1.4) in (3.4.1.2), we have:

$$\text{Re}\{f(t) - f(t_o)\} \cong r^2 R \cos(2\varphi + \phi) \quad (3.4.1.5)$$

$$\text{and} \quad \text{Im}\{f(t) - f(t_o)\} \cong r^2 R \sin(2\varphi + \phi). \quad (3.4.1.6)$$

In order to find the path of constant $\text{Im}\{f(t)\}$, we need to enforce the condition $\text{Im}\{f(t)\} = \text{Im}\{f(t_o)\}$, then from (3.4.1.6), we have:

$$\sin(2\varphi + \phi) = 0 \quad (3.4.1.7)$$

$$\text{or} \quad 2\varphi + \phi = n\pi \quad (n = 0, 1, 2, 3) \quad (3.4.1.8)$$

$$\text{or} \quad \varphi = -\frac{\phi}{2} + \frac{n}{2}\pi. \quad (3.4.1.9)$$

Substituting equation (3.4.1.9) into equation (3.4.1.3), we have:

$$t - t_o = r \exp \left[j \left(-\frac{\phi}{2} + \frac{n}{2}\pi \right) \right] \quad (3.4.1.10)$$

$$\text{where} \quad t = t_o + r \exp \left(-j \frac{\phi}{2} \right) \quad \text{when } n = 0 \quad (3.4.1.11)$$

$$t = t_o + r \exp \left(-j \frac{\phi}{2} + \frac{\pi}{2} \right) \quad \text{when } n = 1 \quad (3.4.1.12)$$

$$t = t_o - r \exp \left(-j \frac{\phi}{2} \right) \quad \text{when } n = 2 \quad (3.4.1.13)$$

$$t = t_o - r \exp \left(-j \frac{\phi}{2} + \frac{\pi}{2} \right) \quad \text{when } n = 3. \quad (3.4.1.14)$$

Combining equations (3.4.1.11) and (3.4.1.13), we have:

$$t = t_o \pm r \exp \left(-j \frac{\phi}{2} \right). \quad (3.4.1.15)$$

Similarly, from equations (3.4.1.12) and (3.4.1.14), we have:

$$t = t_o \pm r \exp \left(-j \frac{\phi}{2} + \frac{\pi}{2} \right). \quad (3.4.1.16)$$

Since the angle ϕ is a constant, the equations (3.4.1.15) and (3.4.1.16) define two straight lines that passing through the point t_o and along which $\text{Im}\{f(t)\}$ is constant and equal to $\text{Im}\{f(t_o)\}$. Similarly it can be shown that there are two lines that pass through t_o and along which $\text{Re}\{f(t)\}$ is constant by enforcing the condition $\text{Re}\{f(t)\} = \text{Re}\{f(t_o)\}$. The lines are determined by the condition obtained from (3.4.1.5):

$$\cos(2\varphi + \phi) = 0 \quad (3.4.1.17)$$

and the equations of the lines are given by:

$$t = t_o \pm r \exp \left[j \left(-\frac{\phi}{2} + \frac{\pi}{4} \right) \right] \quad (3.4.1.18)$$

$$t = t_o \pm r \exp \left[j \left(-\frac{\phi}{2} + \frac{3\pi}{4} \right) \right]. \quad (3.4.1.19)$$

The lines in equations (3.4.1.18) and (3.4.1.19) divide any neighborhood of t_o into four sectors where alternatively:

$$\text{Re}\{f(t)\} > \text{Re}\{f(t_o)\} \quad (3.4.1.20)$$

for $\cos(2\varphi + \phi) > 0$ in (3.4.1.5), and

$$\text{Re}\{f(t)\} < \text{Re}\{f(t_o)\} \quad (3.4.1.21)$$

for $\cos(2\varphi + \phi) < 0$ in (3.4.1.5).

The shape of $\text{Re}\{f(t)\}$ in the neighborhood of t_o will then be governed by equations (3.4.1.20) and (3.4.1.21). Since between two zeros of the cosine function there is always one zero of the sine function, there is *in each of the four sectors, one and only one line of constant $\text{Im}\{f(t)\}$* . The constant $\text{Im}\{f(t)\}$ lines are given by (3.4.1.15) and (3.4.1.16).

3.4.2. The path of steepest descent

The directional derivative of the function $f(t)$ along any path in the complex plane is given by:

$$\frac{\partial f}{\partial l} = \nabla(\text{Re}\{f\} + j\text{Im}\{f\}) \cdot \vec{l} = \nabla(\text{Re}\{f\}) \cdot \vec{l} + j\nabla(\text{Im}\{f\}) \cdot \vec{l}. \quad (3.4.2.1)$$

and the modulus of the derivative in (3.4.2.1) is given by:

$$\left| \frac{\partial f}{\partial l} \right| = \left\{ \left[\nabla(\text{Re}\{f\}) \cdot \vec{l} \right]^2 + \left[\nabla(\text{Im}\{f\}) \cdot \vec{l} \right]^2 \right\}^{\frac{1}{2}} \quad (3.4.2.2)$$

where ∂l is an element of arc length and \vec{l} is the unit vector along the path, $\nabla(\cdot)$ is the gradient operator. Since at a given point t_0 , the modulus of the derivative in (3.4.2.2) has a certain constant value, so $\nabla(\text{Re}\{f\}) \cdot \vec{l}$ is the largest (either positive or negative) when $\nabla(\text{Im}\{f\}) \cdot \vec{l} = 0$ which is satisfied if $\text{Im}\{f\}$ is constant along the path. This means along a path of constant $\text{Im}\{f\}$, the rise and fall of $\text{Re}\{f\}$ is the fastest. Fig. 3.4.2.1 shows the paths of constant $\text{Im}\{f(t)\}$, 12 and 34.

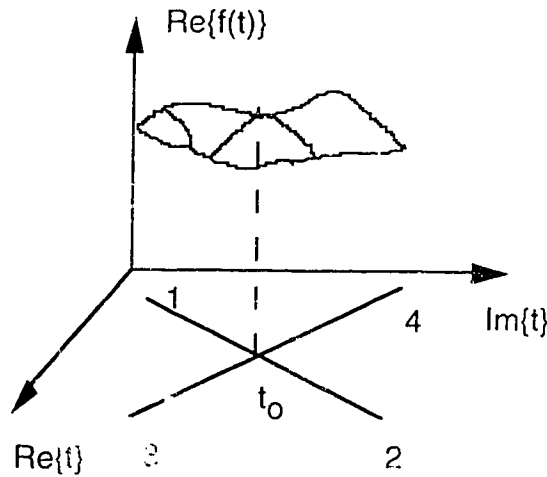


Fig. 3.4.2.1. Paths of constant $\text{Im}\{f(t)\}$.

Along path 12, $\text{Re}\{f(t)\}$ reaches a maximum at t_o and $\text{Re}\{f(t)\}$ decreases rapidly as we move away from t_o . Since $\text{Im}\{f(t)\}$ is also constant along path 12, according to the conditions stated in section 3.4, the path 12 is the path of steepest descent C_o . Along path 34, $\text{Re}\{f(t)\}$ reaches a minimum at t_o . Therefore $\text{Re}\{f(t)\}$ is neither a maximum nor a minimum at t_o . The environment in the neighborhood of t_o forms the shape of a saddle and hence the point t_o is called a saddle point and the method is also called the Saddle Point Method.

3.4.3. The evaluation of $J(z)$

The integral in equation (3.4.1) can be evaluated along the part C_o of the contour C_1 where Debye's conditions are satisfied. Let

$$f(t) = f(t_o) - w^2(t) \quad (3.4.3.1)$$

where $w(t)$ is assumed to be a real function along C_o because $\text{Im}\{f(t)\} = \text{Im}\{f(t_o)\}$ along C_o . The negative sign appears in front of $w^2(t)$ because C_o is a path of steepest descent and $\text{Re}\{f(t)\}$ should decrease rapidly as the point t moves away from t_o . Therefore the function $J(z)$ in (3.4.1) can be approximated as:

$$J(z) \cong \exp[zf(t_o)] \int_{C_o} \exp[-zw^2(t)] dt. \quad (3.4.3.2)$$

As t moves along C_o , $w(t)$ moves along the real axis since it has been assumed to be a real function, therefore the integral in (3.4.3.2) can be written as:

$$J(z) \cong \exp[zf(t_o)] \int_a^b \exp[-zw^2(t)] \frac{dt}{dw} dw \quad (3.4.3.3)$$

where a, b are arbitrary real constants. The dominant contribution to the integral in (3.4.3.3) comes from the regions along C_o where $w(t)$ is small and hence $\exp[-zw^2(t)]$ is large. Therefore negligible error will be made if the integral in (3.4.3.3) is replaced by an

integral from $-\infty$ to ∞ . By comparing (3.4.1.2) and (3.4.3.1), it can be seen that:

$$-w^2(t) = \frac{1}{2}(t-t_o)^2 f''(t_o) \quad (3.4.3.4)$$

or
$$t-t_o = \sqrt{\frac{-2w^2}{f''(t_o)}}. \quad (3.4.3.5)$$

Differentiating equation (3.4.3.5) with respect to w , we have:

$$\frac{dt}{dw} = \sqrt{\frac{-2}{f''(t_o)}}. \quad (3.4.3.6)$$

Substituting equation (3.4.3.6) into equation (3.4.3.3), we have:

$$J(z) \cong \exp[zf(t_o)] \int_{-\infty}^{\infty} \exp(-zw^2) \sqrt{\frac{-2}{f''(t_o)}} dw \quad (3.4.3.7)$$

$$= \exp[zf(t_o)] \sqrt{\frac{-2}{f''(t_o)}} \int_{-\infty}^{\infty} \exp(-zw^2) dw \quad (3.4.3.8)$$

$$= \exp[zf(t_o)] \sqrt{\frac{-2}{f''(t_o)}} \sqrt{2\pi} \frac{1}{2z} \quad (3.4.3.9)$$

$$= \exp[zf(t_o)] \sqrt{\frac{-2\pi}{zf''(t_o)}} \quad (3.4.3.10)$$

where the Gauss integral [30]:

$$\int_{-\infty}^{\infty} \exp\left(\frac{-w^2}{2x^2}\right) dw = \sqrt{2\pi} x^2 \quad (3.4.3.11)$$

has been used to obtain (3.4.3.9).

3.5. The Inverse Laplace Transform of the Overall MGF

The Steepest Descent Method can be applied to find a very good approximation to the inverse Laplace transform in (3.3.8) which is also the PDF of logical ones $f_1(y)$. The form of the integral in equation (3.4.1) is slightly different from the one in equation (3.3.8). The variable y is embedded in the function $F(u)$ given by (3.3.9). However the previous discussions can be generalized such that the Steepest Descent Method can be applied to (3.3.8). The integrand in (3.3.8) has a pole located at $u=0$. The contour of integration in equation (3.3.8) is a straight line as shown in Fig. 3.5.1.

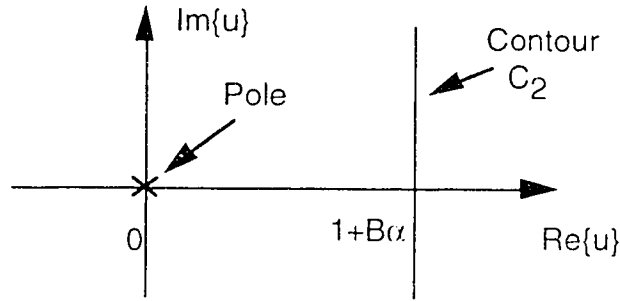


Fig. 3.5.1. The contour of integration.

3.5.1. The saddle point

The saddle point u_s is given by one of the roots of:

$$F'(u) = 0 \quad (3.5.1.1)$$

according to equation (3.4.2), assuming there is at least one saddle point. The saddle point must lie on the contour C_2 in Fig. 3.5.1 with $\text{Re}\{u_s\} = u_r = 1 + B\alpha$. Differentiating equation (3.3.9), rearranging terms and substituting in equation (3.5.1.1), we have:

$$u^3 + \left(\frac{yB}{2C} - 1\right)u^2 - \frac{MB^2}{2C}u - \frac{AB}{2C} = 0. \quad (3.5.1.2)$$

Let $u = u_r + ju_i$, the real part of equation (3.5.1.2) is given by:

$$u_r^3 - 3u_ru_i^2 + \left(\frac{yB}{2C} - 1\right)(u_r^2 - u_i^2) - \frac{MB^2}{2C}u_r - \frac{AB}{2C} = 0 \quad (3.5.1.3)$$

and the imaginary part is:

$$\left[3u_r^2 + \left(\frac{yB}{2C} - 1\right)(2u_r) - \frac{MB^2}{2C} - u_i^2 \right] u_i = 0. \quad (3.5.1.4)$$

The imaginary part implies that:

$$u_i = 0 \quad (3.5.1.5)$$

or
$$u_i^2 = 3u_r^2 + \left(\frac{yB}{2C} - 1\right)(2u_r) - \frac{MB^2}{2C}. \quad (3.5.1.6)$$

If equation (3.5.1.5) is true, the saddle point is real and is given by the positive real root of:

$$u_r^3 + \left(\frac{yB}{2C} - 1\right)u_r^2 - \frac{MB^2}{2C}u_r - \frac{AB}{2C} = 0. \quad (3.5.1.7)$$

The saddle point is positive because the contour of integration lies in the right hand plane ($1 + B\alpha > 0$) as it can be seen from Fig. 3.5.1. If equation (3.5.1.6) is true, the saddle point may be complex and could be obtained from solving equations (3.5.1.3) and (3.5.1.4). There may be several saddle points on the complex plane that will satisfy equation (3.5.1.2). However, it will be shown in the following sections that only one will enter the calculation.

3.5.2. The path of steepest descent

In order to find the path of steepest descent and the location of the saddle point, we need to expand the function $F(u)$ at the saddle point u_o using Taylor series expansion:

$$F(u) = F(u_o) + (u - u_o)F'(u_o) + \frac{(u - u_o)^2}{2}F''(u_o) + \dots \quad (3.5.2.1)$$

Ignoring the terms with order higher than the second order term and assuming that $F''(u_o) \neq 0$, and since $F'(u_o) = 0$ from (3.5.1.1), we have:

$$F(u) \cong F(u_o) + \frac{(u - u_o)^2}{2} F''(u_o). \quad (3.5.2.2)$$

Since the contour of integration is a straight line, the real part of an arbitrary point u on the contour C_2 in Fig. 3.5.1 is equal to the real part of the saddle point u_o . Therefore we have:

$$u - u_o = j(\text{Im}\{u\} - u_i) \quad (3.5.2.3)$$

where u_i is the imaginary part of the saddle point and

$$(u - u_o)^2 = -(\text{Im}\{u\} - u_i)^2 \quad (3.5.2.4)$$

which is a real and negative quantity. Since along a path of steepest descent C_o , the condition $\text{Im}\{F(u)\} = \text{Im}\{F(u_o)\}$ is satisfied, we shall let

$$F(u) = F(u_o) - w^2 \quad (3.5.2.5)$$

where w is a real function. Using the fact that the quantity in (3.5.2.4) is real and negative, and comparing (3.5.2.2) with (3.5.2.5), it implies that $F''(u_o)$ is real and positive. The second derivative of the function $F(u)$ is given by differentiating equation (3.3.9) with respect to u twice:

$$F''(u) = \frac{2A}{B} \frac{1}{u^3} + M \frac{1}{u^2} + \frac{2C}{B^2}. \quad (3.5.2.6)$$

Because of the inverse cubic function in the first term of (3.5.2.6), it is obvious that $F''(u_o)$ is real if and only if u_o is real. Now it has been shown that u_o is real, the saddle point will be given by the real

positive root of equation (3.5.1.7). It also follows that the function $F(u)$ is real at the saddle point. Using equations (3.4.1.15) and (3.4.1.16), the contours along which $\text{Im}\{F(u)\} = \text{Im}\{F(u_o)\}$ are the two straight lines given by:

$$u = u_o \pm r \exp\left(-j\frac{\phi}{2}\right) \quad (3.5.2.7)$$

and

$$u = u_o \pm r \exp\left[j\left(-\frac{\phi}{2} + \frac{\pi}{2}\right)\right] \quad (3.5.2.8)$$

where r is the magnitude of $(u - u_o)$ and ϕ is the phase of $F''(u_o)$ according to (3.4.1.3) and (3.4.1.4). Since $F''(u_o)$ is positive and real, its phase is given by:

$$\phi = 2n\pi \quad n = 0, \pm 1, \pm 2, \dots \quad (3.5.2.9)$$

Then equation (3.5.2.7) is just the real axis and equation (3.5.2.8) represents the contour C_2 shown in Fig. 3.5.1. The saddle point is located at the intersection of these two lines 12 and 34 as shown in Fig. 3.5.2.1.

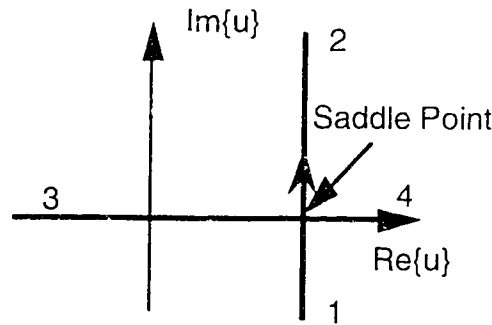


Fig. 3.5.2.1. Saddle point and constant $\text{Im}\{F(u)\}$ paths.

The path of steepest descent will be the part C_o of one of the paths 12 or 34, and C_o can be determined by analyzing the behavior of the

real part of the function $F(u)$ along each of the paths. Using equation (3.3.9) and substituting $u = u_r + ju_i$, the real part is obtained as:

$$\begin{aligned} \operatorname{Re}\{F(u)\} = & -\frac{A}{B} \left[\frac{(u_r - 1)u_r + u_i^2}{u_r^2 + u_i^2} \right] + \frac{C}{B^2} [(u_r - 1)^2 - u_i^2] \\ & + \frac{\gamma}{B} (u_r - 1) - M \ln \sqrt{u_r^2 + u_i^2}. \end{aligned} \quad (3.5.2.10)$$

Along path 34 in Fig. 3.5.2.1, $u_i = 0$, the first and second derivatives of $\operatorname{Re}\{F(u)\}$ with respect to u_r are given by:

$$\frac{\partial \operatorname{Re}\{F(u)\}}{\partial u_r} = -\frac{A}{B} \frac{1}{u_r^2} + \frac{2C}{B^2} (u_r - 1) + \frac{\gamma}{B} - \frac{M}{u_r} \quad (3.5.2.11)$$

$$\frac{\partial^2 \operatorname{Re}\{F(u)\}}{\partial u_r^2} = \frac{2A}{B} \frac{1}{u_r^3} + \frac{M}{u_r^2} + \frac{2C}{B^2}. \quad (3.5.2.12)$$

Since $u_r > 0$ at the saddle point, this implies that:

$$\frac{\partial^2 \operatorname{Re}\{F(u)\}}{\partial u_r^2} > 0 \quad (3.5.2.13)$$

and that $\operatorname{Re}\{F(u)\}$ is a minimum at the saddle point along the path 34. Therefore the path 12 in Fig. 3.5.2.1 must be such that $\operatorname{Re}\{F(u)\}$ goes through a maximum at the saddle point. It can then be concluded that the path of steepest descent C_o is the part of the path 12 that goes through the saddle point and contains some neighborhood of the saddle point. An example of the saddle point (marked by the cross), the path of steepest descent (the straight line) and the surface plot of $\operatorname{Re}\{F(u)\}$ is shown in Fig. 3.5.2.2.

Surface Plot of $\text{Re}\{F(u)\}$

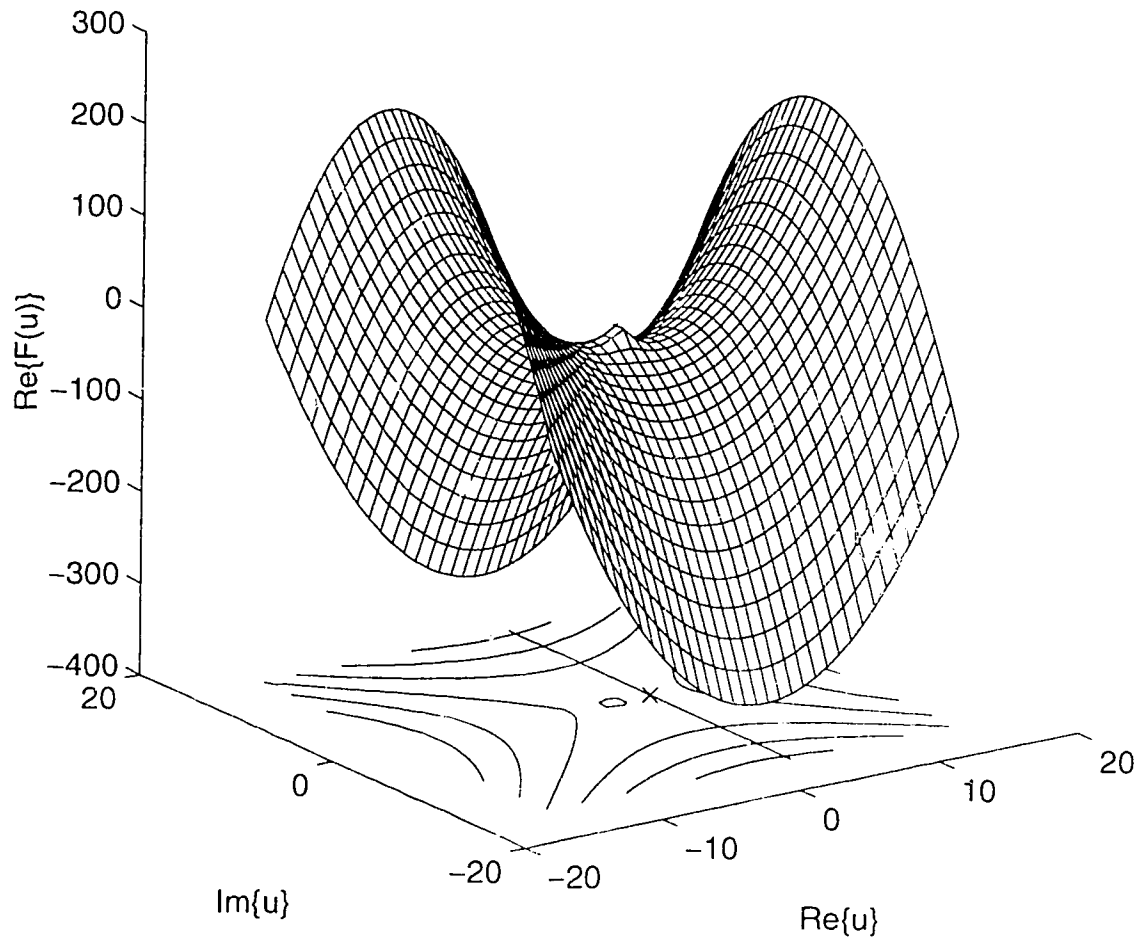


Fig. 3.5.2.2. Surface plot of $\text{Re}\{F(u)\}$, the path of steepest descent and the location of the saddle point.

The value of the saddle point in this example is $u_o = 2.9567 + j0$. The surface above the contour plot is of the shape of a saddle as predicted. Note that there is a pole at $u=0$ which is originally at $s = -1/B$ before the change of variable $u = 1 + Bs$. The pole in Fig. 3.5.2.2 has been suppressed so that the graph can be obtained.

3.5.3. The closed form expression of PDFs

Using (3.5.2.5) in (3.5.2.2) and rearranging the terms, we have:

$$u - u_o = \sqrt{\frac{-2w^2}{F''(u_o)}} \quad (3.5.3.1)$$

and
$$\frac{du}{dw} = \sqrt{\frac{-2}{F''(u_o)}}. \quad (3.5.3.2)$$

Using (3.5.2.5) and (3.5.3.2) in (3.3.8), we have:

$$f_1(y) = \frac{\exp[F(u_o)]}{2\pi jB} \int_{-\infty}^{\infty} \exp(-w^2) \frac{du}{dw} dw \quad (3.5.3.3)$$

$$= \frac{\exp[F(u_o)]}{2\pi jB} \int_{-\infty}^{\infty} \exp(-w^2) \sqrt{\frac{-2}{F''(u_o)}} dw \quad (3.5.3.4)$$

$$= \frac{\exp[F(u_o)]}{2\pi jB} \sqrt{\frac{-2}{F''(u_o)}} \sqrt{\pi} \quad (3.5.3.5)$$

$$= \frac{\exp[F(u_o)]}{B \sqrt{2\pi F''(u_o)}} \quad (3.5.3.6)$$

where the Gauss integral in (3.4.3.11) has been used to obtain (3.5.3.5). At each value of y , the saddle point u_o can be found from equation (3.5.1.7). Equation (3.5.3.6) can also represent the PDF of logical zeros by reducing the signal power P_{sig} . Therefore it is only necessary to change the constants A and C in (3.3.2) and (3.3.4) in order for (3.5.3.6) to represent the PDF of logical zeros. The signal power P_{sig} may or may not vanish for a logical zero depending on the extinction ratio specified. The means of logical zeros and logical ones are given by (2.10.4.2) and (2.10.4.3) respectively. The variances of logical zeros and logical ones are given by adding (3.2.3) and (3.2.6)

to (2.10.4.4) and (2.10.4.5). The optimum threshold can be obtained by using (3.5.3.6), (3.5.2.6) and (3.3.9) in (2.15.2) which can be solved numerically.

3.6. The Accuracy of the Steepest Descent Method

The Steepest Descent Method is very accurate and the error is within 1% as reported by Marcuse [8]. To test the accuracy, we can compare the PDFs generated by the Steepest Descent Method and the Chi-Square equations presented in chapter 2. The comparisons of the PDFs of logical zeros and logical ones are shown in Fig. 3.6.1.a. Fig. 3.6.1.b shows the relative error (in percentage) in the Steepest Descent Method, which is calculated by taking the ratio of the values of the PDFs. The values of the parameters used are $\delta=0$, $P_{in1}=-36$ dBm, $P_{inav}=-39$ dBm, $P_{sat}=30$ mW, $G_o=30$ dB, $B_{elec}=20$ GHz, $B_o=1.4 \times 1.3$ nm (the factor 1.4 is for calculating the noise equivalent bandwidth of the optical BPF), $m_f=1$, $M=11$, $N_{sp}=2$, $\mathfrak{R}=1$ A/W, $T_k=0$ K. The losses are neglected.

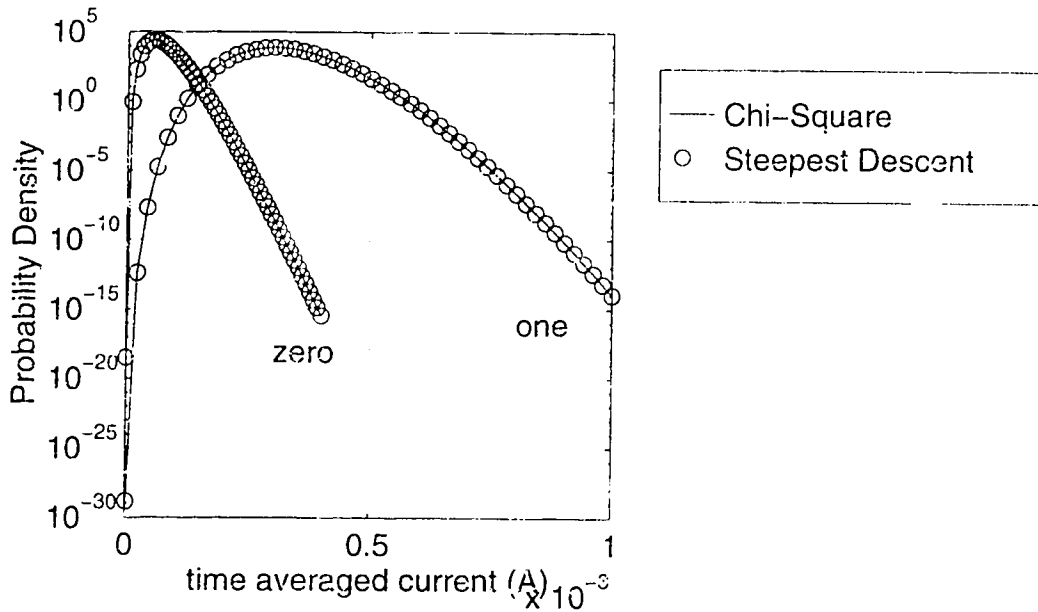


Fig. 3.6.1.a. Comparison of PDFs evaluated by Chi-Square distributions and Steepest Descent Method.

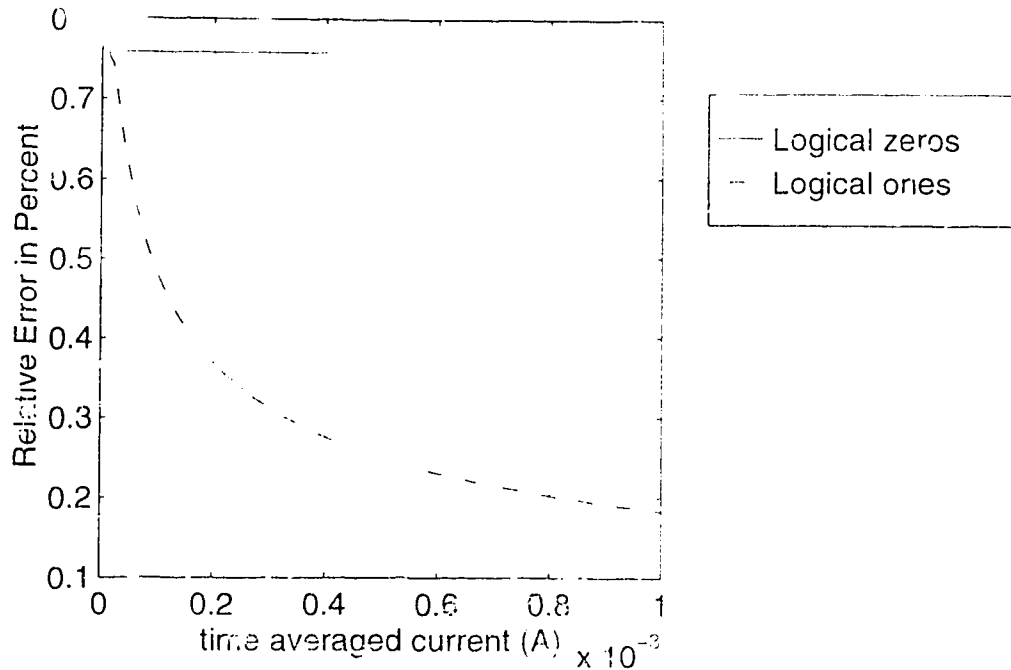


Fig. 3.6.1.b. Relative error in Steepest Descent Method.

As it can be seen, the difference between the PDFs of logical zeros and the difference between the PDFs of logical ones are very small within the range of interest. Therefore the Steepest Descent Method is indeed very accurate. The results that are obtained by using the Steepest Descent Method will be called 'non-Gaussian' in the following sections.

3.7. The Conversion of Current to Voltage

In a practical situation or experiment, the photocurrent sometimes is too small to be measured accurately because of the limitation of the resolution that can be provided by the equipment. The photocurrent however can be converted to voltage by using electrical amplifiers. After amplification, the voltage is much easier to measure and the influence of the resolution on accuracy can be minimized. In this section, the random variable y , which is the time averaged photocurrent, will be converted to a voltage random variable. The advantage of doing this is that the theoretical PDFs can be used to compare with the experimental PDFs. The conversion procedure is very simple. We can simply add an additional block into the receiver

of the theoretical model shown in Fig. 2.2.1. The new receiver is shown in Fig. 3.7.1.

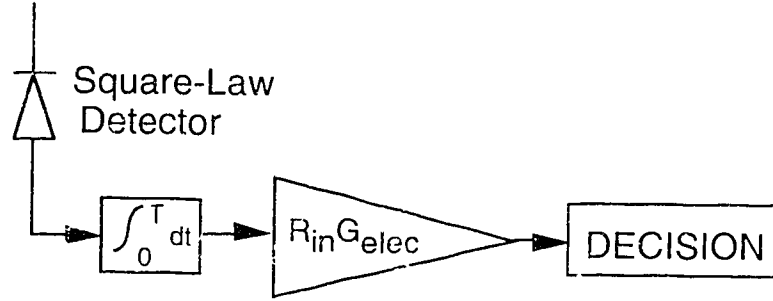


Fig. 3.7.1. Receiver with current to voltage conversion block.

The function of the block $R_{in}G_{elec}$ is to perform current to voltage conversion and provide electrical amplification. At the output of this block the random variable is voltage instead of current. The new equations of the PDFs can be easily obtained by multiplying the equations (3.2.3) and (3.3.3) by $R_{in}G_{elec}$ since the constants A and B have units of ampere A. The equation (3.3.4) has to be multiplied by $(R_{in}G_{elec})^2$ since the constant C has unit of A^2 . The time averaged current \bar{y} in (3.3.9) also needs to be multiplied by $R_{in}G_{elec}$. There is also a thermal noise factor F associated with the gain block shown in Fig. 3.7.1. The input resistance R_{in} is related to the thermal noise equivalent resistance R_{eq} as:

$$R_{eq} = \frac{R_{in}}{F}. \quad (3.7.1)$$

Therefore the thermal noise in (3.2.3) should be modified as:

$$\sigma_{th}^2 = \frac{2kT_k F}{R_{in}}. \quad (3.7.2)$$

The input resistance will be assumed to be $50 \, \Omega$ in the following analyses.

3.8. The Impact of Values of Parameters on PDFs

The non-Gaussian and the Gaussian PDFs are different in shape as shown earlier in Fig. 3.7.1.(a-d). However the difference is not often noticeable in the range of interest (e.g., PDF 10^{-4} to 10^{-12}) or the range in which experimental data can be taken. Therefore it is important to find out under what conditions that the difference is large enough to be experimentally measurable. As discussed in section 2.1, the only dominant noise in the system that has a non-Gaussian distribution is the sp-sp beat noise. Therefore in order to make the non-Gaussian distribution more apparent, the sp-sp beat noise power must be increased. We can examine the different ways of increasing the sp-sp beat noise power by rewriting equation (2.10.4.4) using equations (2.6.4) and (2.10.2.6), and replacing M by $m_t M$ (from section 2.14 of chapter 2) as:

$$\sigma_{sp-sp}^2 = \Re^2 m_t [N_{sp}(G-1)hf_c]^2 B_o B_{elec}. \quad (3.8.1)$$

For comparison, we can also use (2.6.4) and (2.10.2.6), and replace M by $m_t M$ to rewrite (2.10.4.5) as:

$$\sigma_{sig-sp}^2 = 2\Re^2 [N_{sp}(G-1)hf_c] GP_{in} B_{elec} \quad (3.8.2)$$

where P_{sig} has been replaced by GP_{in} . The power P_{in} is the received power and it can represent a logical one or a logical zero depending on its power level. As it can be seen from (3.8.1), the sp-sp beat noise power is directly proportional to the optical filter bandwidth B_o and the two-sided electrical bandwidth B_{elec} . In addition, the noise power is proportional the square of the EDFA small signal gain since $G \gg 1$. Therefore we can vary the values of the parameters B_o , B_{elec} and G in order to see the difference of the Gaussian and non-Gaussian PDFs. The PDFs of logical ones and logical zeros are plotted as functions of voltage random variable in Fig. 3.8.1.(a-b) by using two values of B_{elec} (1 and 20 GHz) are used. The values of other parameters used are $\delta=0$, $P_{in1}=-33$ dBm, $P_{inav}=-36$ dBm, $P_{sat}=30$

mW, $G_o=30$ dB, $B_o=1.4 \times 1.3$ nm (the factor 1.4 is for calculating the noise equivalent bandwidth of the optical BPF), $m_l=1$, $M=11$ (for $B_{elec}=20$ GHz) and 227 for ($B_{elec}=1$ GHz), $N_{sp}=2$, $\mathfrak{R}=1$ A/W, $R_{in}=50$ Ω , $G_{elec}=20$ dB, $T_k=298$ K, $F=5$. The losses are neglected.

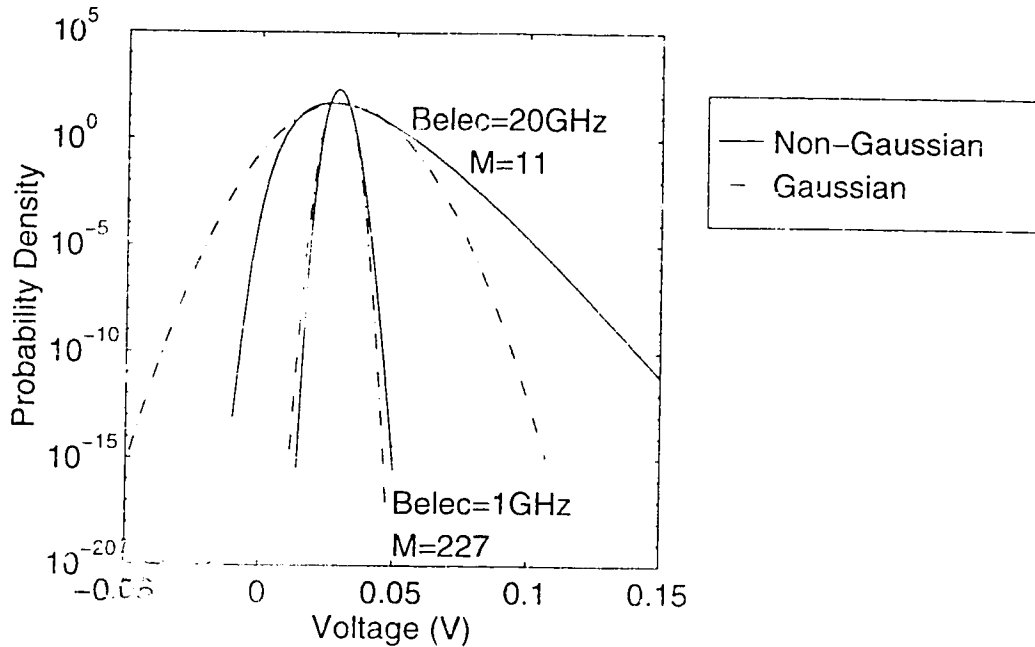


Fig. 3.8.1.a. PDFs of logical zeros with $B_{elec}=1-20$ GHz.

As it can be seen from Fig. 3.8.1.a, the difference between the Gaussian and the non-Gaussian distributions are small within the range of interest for $B_{elec}=1$ GHz. However when B_{elec} is increased to 20 GHz, the difference is quite significant and measurable. For example, at PDF= 10^{-10} , the voltage difference is about 50 mV. Similar situation is also observed for the PDFs of logical ones.

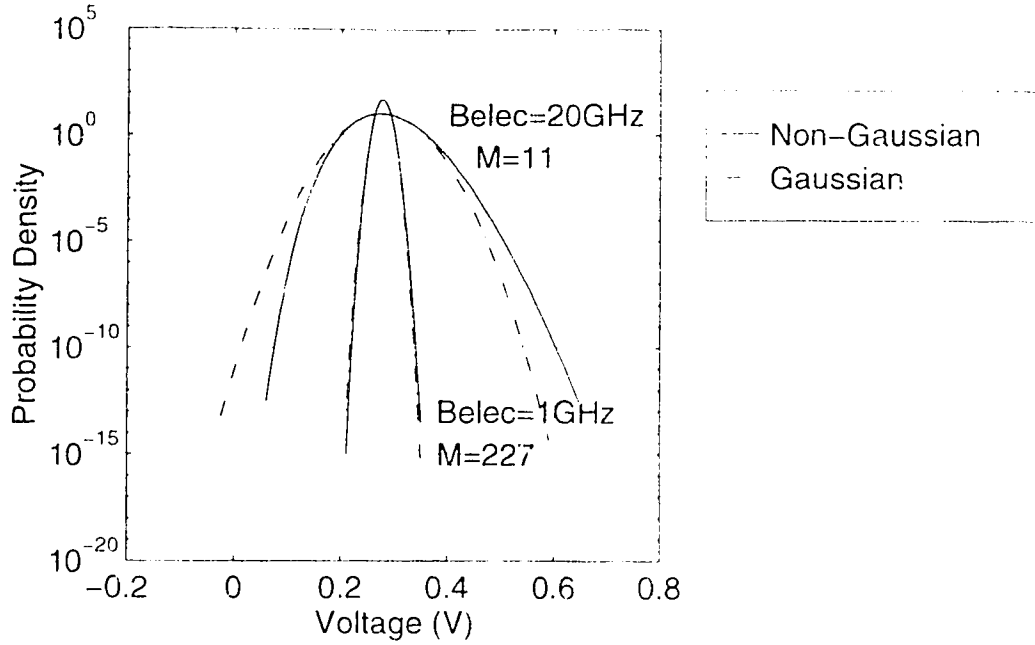


Fig. 3.8.1.b. PDFs of logical ones with $B_{elec}=1-20$ GHz.

The mean values of the PDFs do not increase with B_{elec} as it can be seen from equations (2.10.4.2) and (2.10.4.3). Only the variances of the PDFs increase with B_{elec} . When the variances are increased, the PDFs are broadened. However the PDF of the spurs beat noise cannot extend to the negative voltage region. Therefore the way that the non-Gaussian PDF is broadened is different from the one of the Gaussian PDF. The differences of the tails of the Gaussian and non-Gaussian PDFs are then more apparent. Note that in Fig. 3.8.1.a, the non-Gaussian PDF extends slightly into the negative voltage region. This is the result of including the thermal and shot noise in the analysis.

The PDFs of logical ones and logical zeros are also plotted in Fig. 3.8.2.(a-b) by using two values of B_o (1 and 3 nm). The values of other parameters used are $\delta=0$, $P_{in1}=-33$ dBm, $P_{inav}=-36$ dBm, $P_{sat}=30$ mW, $G_o=30$ dB, $B_{elec}=20$ GHz, $m_I=1$, $M=6$ (for $B_o=1$ nm) and 18 (for $B_o=3$ nm), $N_{sp}=2$, $\mathfrak{R}=1$ A/W, $R_{in}=50$ Ω , $G_{elec}=20$ dB, $T_k=298$ K, $F=5$. The losses are neglected. The choice of the value of $B_{elec}=20$ GHz is based on the results obtained from Fig. 3.8.1.(a-b).

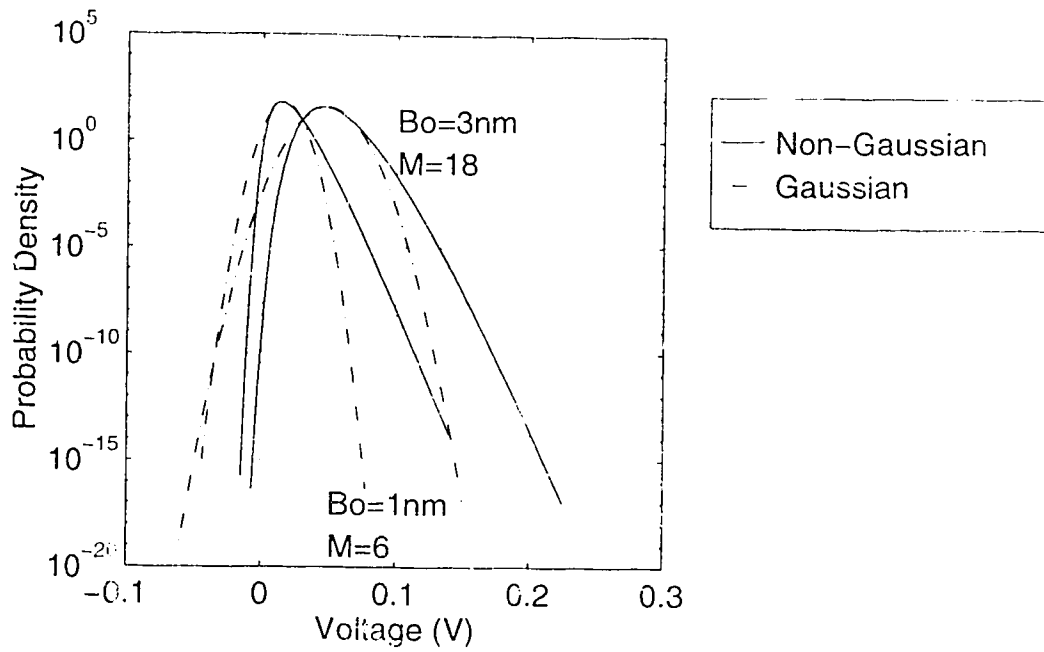


Fig. 3.8.2.a. PDFs of logical zeros with $B_o=1, 3$ nm.

The mean and the variances of the PDFs are both directly proportional to the optical bandwidth B_o as it can be seen from equations (2.6.4), (2.10.2.6) and (2.10.4.2) to (2.10.4.5). When B_o is increased, the PDFs are broadened and its peak is also shifted to the more positive voltage side. However when $B_{elec}=20$ GHz, the variation of B_o from 1 nm to 3 nm does not generate any more significant difference between the Gaussian and non-Gaussian PDFs. For the PDFs of logical ones, similar observation can also be made.

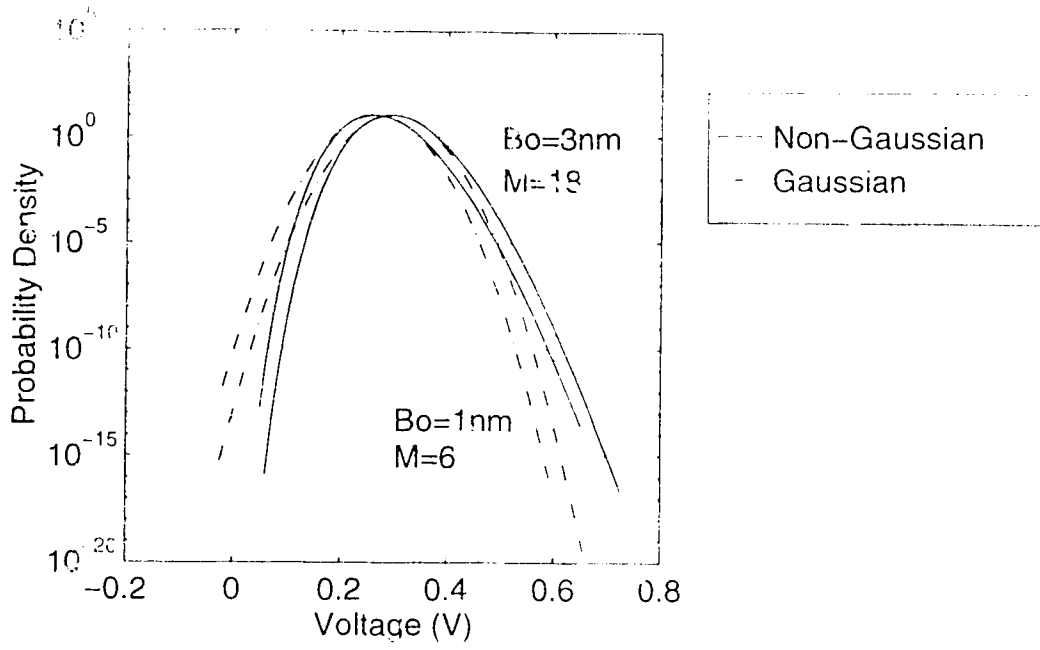


Fig. 3.8.2.b. PDFs of logical ones with $B_o=1, 3$ nm.

In Fig. 3.8.3.(a-b), two values of G_{clv} (20 and 30 dB) are used to plot the PDFs of logical zeros and logical ones. The values of other parameters used are $\delta=0$, $P_{in1}=-27$ dBm, $P_{inav}=-36$ dBm, $P_{sat}=3.0$ mW, $B_{elec}=20$ GHz, $B_o=1.4 \times 1.3$ nm (the factor 1.4 is for calculating the noise equivalent bandwidth of the optical BPF), $m_I=1$, $M=11$, $N_{sp}=2$, $\mathfrak{R}=1$ A/W, $R_{in}=50$ Ω , $G_{clv}=20$ dB, $T_k=298$ K, $F=5$. The losses are neglected. The choice of $B_o=1.4 \times 1.3$ nm is based on the actual value of the bandwidth of the optical BPF that is used in the laboratory.

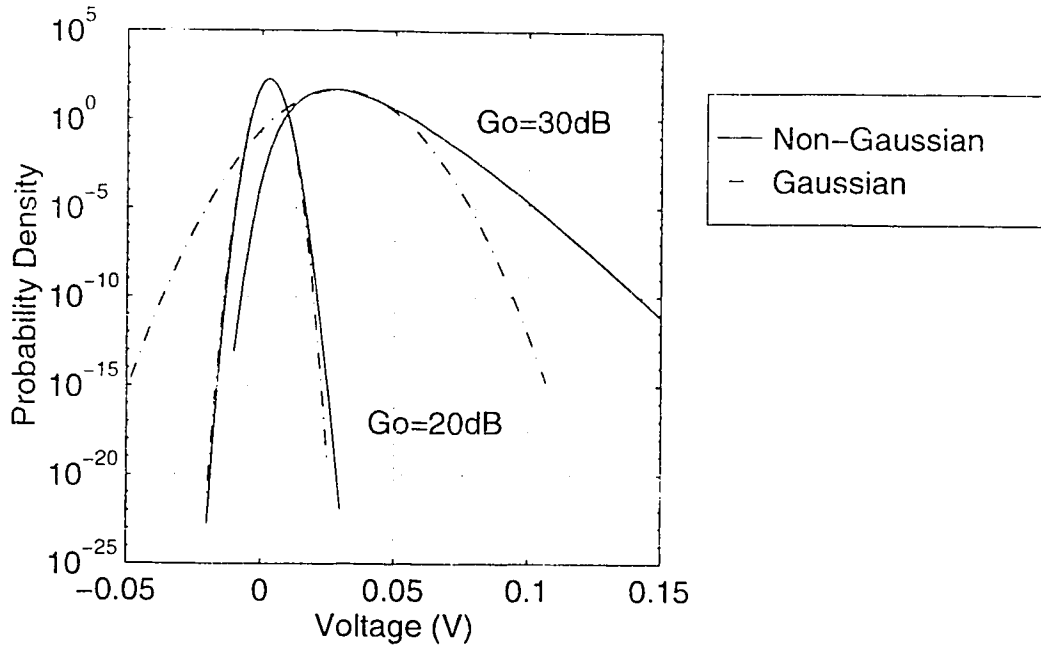


Fig. 3.8.3.a. PDFs of logical zeros with $G_o=20, 30$ dB.

According to equations (2.6.4), (2.10.2.6) and (2.10.4.2) to (2.10.4.5), and the fact that the signal power for a logical one at the photodiode P_{sig} is the product of the EDFA small signal gain G and the input power for the logical one at the EDFA input P_{in1} , the mean values of the PDFs are directly proportional to the EDFA small signal gain. The variances however are proportional to the square of the EDFA small signal gain. When the gain is increased, the peaks of the PDFs are shifted to the more positive voltage side and the PDFs are also broadened. Since the variances are proportional to the square of the gain, the broadening effect of the PDFs occurs faster than the shifting of the peaks. The difference between the Gaussian and non-Gaussian PDFs are more apparent when the EDFA small signal gain is sufficiently large.

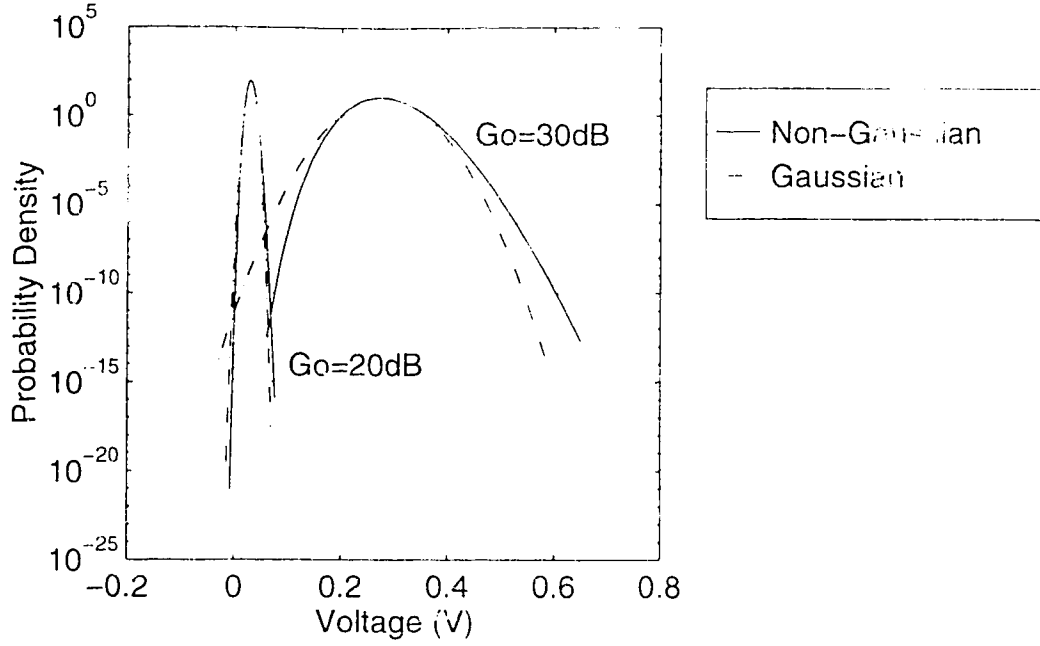


Fig. 3.8.3.b. PDFs of logical ones with $G_o=20, 30$ dB.

From the above results, it can be seen that the non-Gaussian PDFs are experimentally observable or measurable when EDFA small signal gain is sufficiently large and the electrical bandwidth is sufficiently wide. Since the effect of the optical filter bandwidth is not as great as G_o and B_{elec} , its value is not important.

3.9. The Probability of Error and the Bit Error Rate

The probabilities of errors for logical ones and logical zeros can be approximately derived by making use of the Taylor series expansion. The probability of error for logical ones can be derived as:

$$P_1 = \frac{\exp[G_1(u_{d1})]}{\sqrt{2\pi B}} \left[\frac{-1}{G'_1(u_{d1})} \right] \quad (\text{assuming } G'_1(u_{d1}) < 0) \quad (3.9.1)$$

$$\text{where} \quad G_1(u) = F_1(u) + \frac{1}{2} \ln \left(\frac{2A}{u^3} + \frac{2C}{B} + \frac{MB}{u^2} \right) \quad (3.9.2)$$

and

$$G'_1(u) = \frac{2A}{B} \left(\frac{1-u}{u^2} \right) + \frac{2C}{B^2} (1-u) + M \left(\frac{1-u}{u^2} \right) - \frac{(3AB + MB^2u)}{(2ABu + MB^2u^2 + 2Cu^4)} \quad (3.9.3)$$

where the constants A, B, C are given by (3.3.2), (3.3.3) and (3.3.4). The function $F_1(u)$ is given by (3.3.9). The variable u_{d1} is the saddle point at the decision threshold I_d for logical ones. In the system performance analyses in chapter 4, the decision threshold will be converted to percentage decision threshold and hence it does not matter whether the decision threshold is current or voltage. Note that the value of $G'_1(u_{d1})$ in (3.9.1) must be negative.

The probability of error for logical zeros can be derived as:

$$P_0 = \frac{\exp[G_0(u_{d0})]}{\sqrt{2\pi B}} \left\{ \frac{1 - \exp[-G'_0(u_{d0})u_{d0}]}{G'_0(u_{d0})} \right\} \quad (3.9.4)$$

where u_{d0} is the saddle point at decision threshold I_d for logical zeros. The value of u_{d0} is not necessarily equal to the value of u_{d1} because the signal powers (hence the constants A and C) are different for logical zeros and logical ones. The function $G_0(u)$ and $G'_0(u)$ are also given by (3.9.2) and (3.9.3) except with different values of A and C . The detailed derivations for the probabilities of errors of logical zeros and logical ones, and the accuracy of the Taylor series approximation are shown in Appendix B.

4. Simulation of System Performance

The performance of an EDFA preamplified digital transmission system can be evaluated based on the BER, the sensitivity and the optimum threshold, etc. It has been shown in chapter 3 that the non-Gaussian PDFs deviate the most from the Gaussian PDFs when the EDFA small signal gain is sufficiently large and the electrical bandwidth is sufficiently wide. We would expect that under these conditions, the system performance predicted by the non-Gaussian theory is significantly different from the one predicted by the Gaussian theory. However this is only true in certain analyses as it will be shown in the following sections.

4.1. The BER as a Function of the Received Power

A common way of assessing the performance of a particular communications system is to study the relation of the BER and the received signal power. For the case of an EDFA preamplified transmission system, the received power is the average signal power at the input of the EDFA. When the received power is increased, the BER is decreased because of the opening of the data eye in the receiver. The shot noise and the sig-sp beat noise are both signal dependent noises with the sig-sp beat noise being the dominant one. The sig-sp beat noise power is directly proportional to the optical signal power as it can be seen from equation (3.8.2). However the electrical signal power is proportional to the square of the optical signal power. Therefore the electrical signal-to-noise ratio (SNR) can be improved by increasing the optical signal power. Although the sig-sp beat noise is a signal dependent noise, it will not cause a BER floor.

The BER is plotted as a function of the received power in Fig. 4.1.1.(a-b). The descriptions of the parameters used and their values are listed in Table 4.1.1. The values of some of the parameters are kept constant throughout the following analyses. Some parameters will be used as variables and their values are not shown in the table. Their values will be specified before each the following graphs.

Symbol	Description	Value	Unit
h	Planck's constant	6.6262×10^{-34}	J-s
k	Boltzmann's constant	1.38×10^{-23}	J/K
q	electron charge	1.6022×10^{-19}	C
c_o	free space light speed	3×10^8	m/s
λ_c	light carrier wavelength	1.55×10^{-6}	m
T_k	temperature	298	K
F	noise figure of electrical amplifier	7	dB
R_{in}	input resistance of electrical amplifier	50	Ω
\mathcal{R}	responsivity of photodiode	1	A/W
P_{sat}	EDFA saturation power	30	mW
μ_{in}	EDFA input coupling loss	0	dB
μ_{out}	EDFA output coupling loss	0	dB
L	loss between EDFA and photodiode	0	dB
m_t	polarization parameter	variable	-
δ	extinction ratio	variable	dB
N_{sp}	spontaneous emission factor	variable	-
G_o	EDFA small signal gain	variable	dB
P_{in}	EDFA input power for logical ones	variable	dBm
	average EDFA input power (received power)	variable	dBm
B_{elec}	two-sided electrical bandwidth	variable	GHz
B_o	optical BPF bandwidth	variable	nm
M	ratio of optical to electrical bandwidths	variable	-

Table 4.1.1. Simulation parameters.

The values of the universal constants such as the Planck's constant, the Boltzmann's constant etc. are taken from [16]. As indicated in Table 4.1.1, the losses in the system will be neglected.

For Fig. 4.1.1.(a-b), the values of the parameters used are $\delta=-20$ dB, $G_o=30$ dB, $B_{elec}=1$ GHz (for Fig. 4.1.1.a) and 20 GHz (for Fig. 4.1.1.b), $B_o=1.4 \times 1.3$ nm (the factor 1.4 is for calculating the noise equivalent bandwidth of the optical BPF), $m_I=1$ (with polarizer) and 2 (without polarizer), $M=11$ (for $B_{elec}=20$ GHz) and 220 (for $B_{elec}=1$ GHz), $N_{sp}=2$.

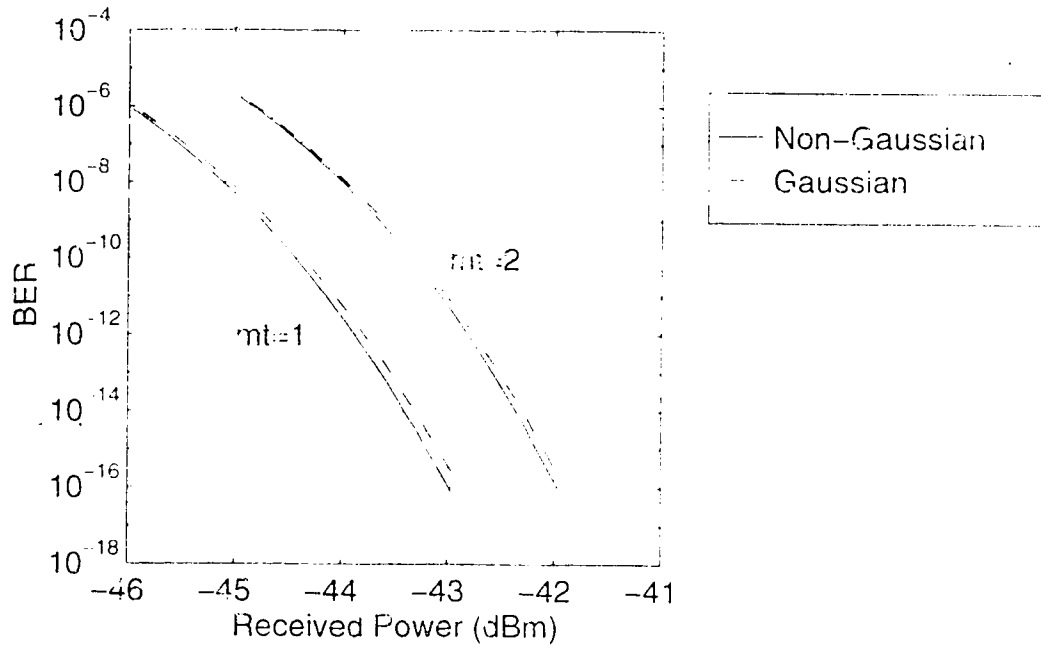


Fig. 4.1.1.a. BER versus Received Power with $B_{elec}=1$ GHz.

The sensitivity at $BER=10^{-9}$ is about -44.7 dBm for $m_I=1$. When the polarizer is not used or $m_I=2$, the sensitivity is degraded by about 1 dB. The degradation is due to the increase in sp-sp beat noise power. This additional noise power comes from the self-field-mixing effect of the ASE electric field component which is spatially orthogonal to the signal electric field. The sig-sp beat noise remains unchanged because of this spatial orthogonality. The difference between the Gaussian and the non-Gaussian curves are small since the two-sided electrical bandwidth is not sufficiently large. Therefore we would

expect that the difference will be more apparent when the electrical bandwidth is increased.

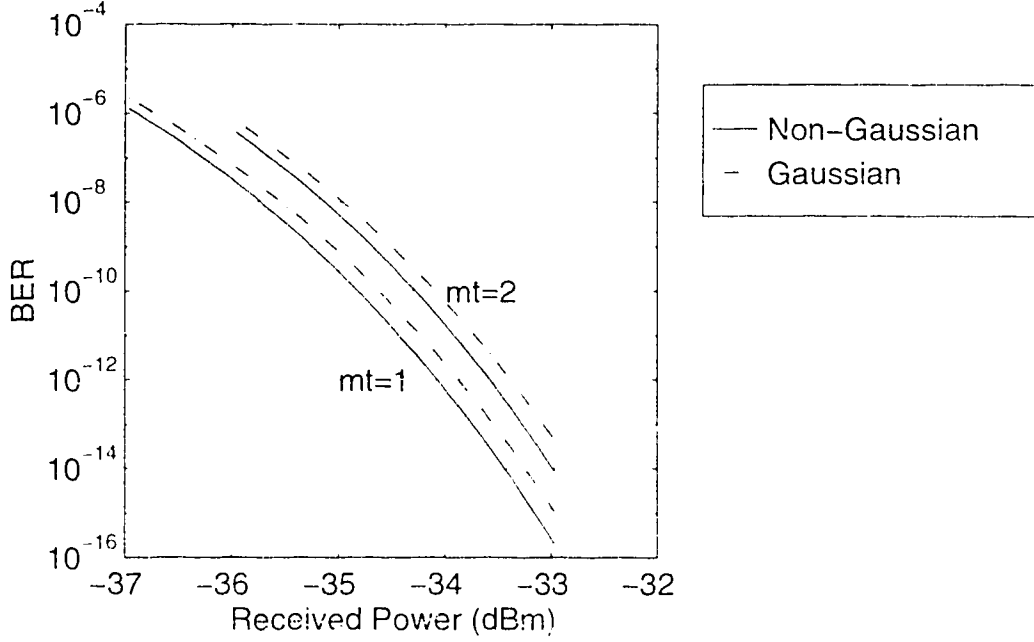


Fig. 4.1.1.b. BER versus Received Power with $B_{elec}=20$ GHz.

In Fig. 4.1.1.b, $B_{elec}=20$ GHz is used and the sensitivity for $BER=10^{-9}$ is about -35.2 dBm for $m_t=1$. A penalty of about 0.5 dB is observed when the polarizer is not used. The penalty is smaller than the one in Fig. 4.1.1.a because the signal power is larger and hence the sig-sp beat noise is more dominant. The effect of the increased sp-sp noise power when $m_t=2$ is less significant. The difference between the Gaussian and the non-Gaussian theories is indeed more apparent. It can be seen that the Gaussian theory overestimates the BER relative to the non-Gaussian theory. However the maximum difference in the BER is only about half a decade and in the received power is only about 0.2 to 0.3 dB. This result agrees quite well with the result obtained by Lee and Shim [9]. In practice, this difference is too small to be measurable.

Now that we have learned the Gaussian theory can be used to predict the BER versus received power curves with small amount of error,

we can use it together with the non-Gaussian theory to study the effect of the parameter M on the curves. Since M is the ratio of the optical bandwidth to the two-sided electrical bandwidth, there are two ways of changing its value. The first one is to keep the optical bandwidth constant and vary the electrical bandwidth. The second one is to keep the electrical bandwidth constant and vary the optical bandwidth. The BER versus received power using $B_{elec}=1$ GHz ($M=220$), $B_{elec}=10$ GHz ($M=22$), $B_{elec}=20$ GHz ($M=11$), are plotted in Fig. 4.1.2.a. The values of the parameters used are $\delta=-20$ dB, $G_o=30$ dB, $B_o=1.4 \times 1.3$ nm, $m_t=1$ (with polarizer), $N_{sp}=2$.

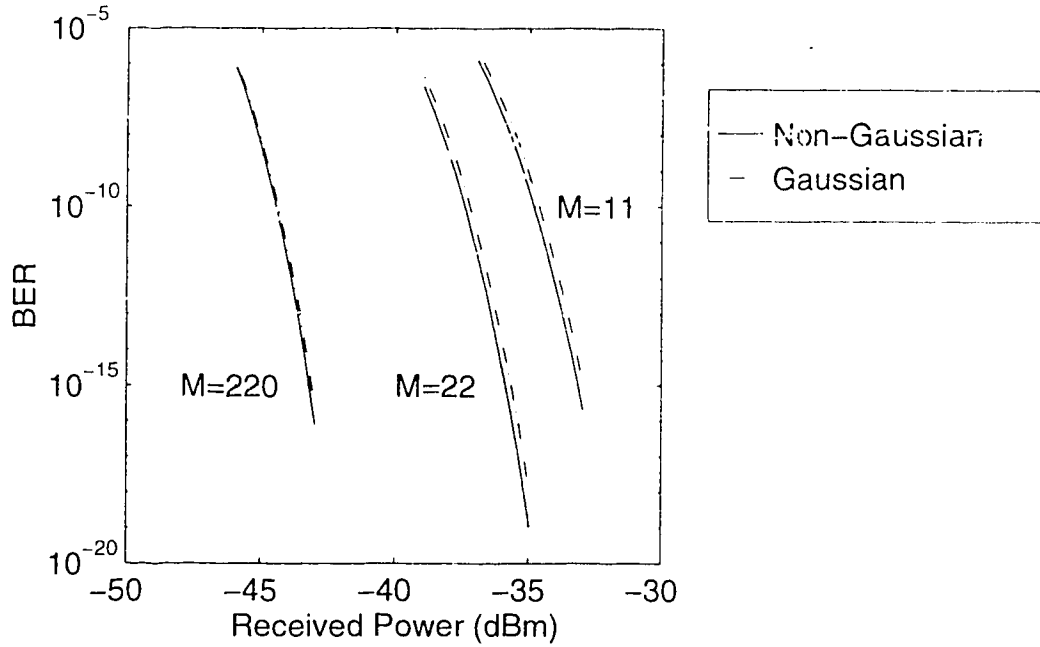


Fig. 4.1.2.a. BER versus Received Power with $B_{elec}=1, 10, 20$ GHz.

When the electrical bandwidth is increased from 1 GHz to 10 GHz, we observe a sensitivity penalty of about 7 dB which is due to the increase of all the noises. However when the bandwidth is further increased from 10 to 20 GHz, the penalty is only about 2 to 3 dB. The relation between the signal power required to achieve a certain BER and the electrical bandwidth is not linear. This can be seen from the argument of the Q -function in equation (2.13.8). This non-linearity is in part due to the sig-sp beat noise term. When the electrical

bandwidth is increased, the optical signal power has to be increased in order to achieve the same BER. However increasing the signal also increases the sig-sp beat noise power. This non-linear behavior will be shown later when we plot the sensitivity versus the electrical bandwidth.

Fig. 4.1.2.b shows the plot of BER versus received power with $B_o=1, 2, 4$ nm. The values of the parameters used are $\delta=-20$ dB, $G_o=30$ dB, $B_{elec}=20$ GHz, $m_I=1$ (with polarizer), $N_{sp}=2$.

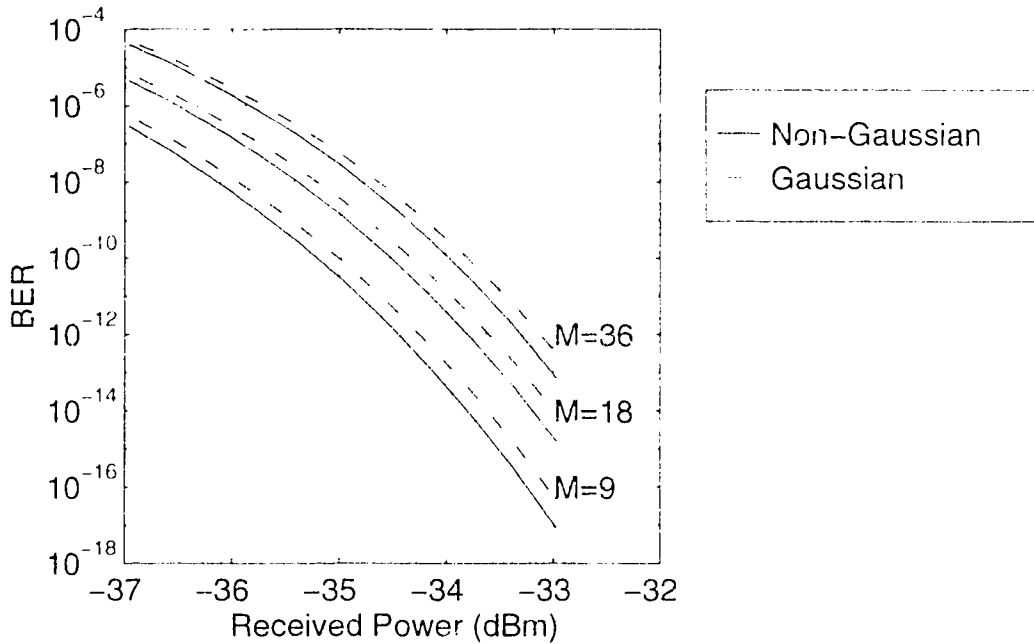


Fig. 4.1.2.b. BER versus Received Power with $B_o=1, 2, 4$ nm.

The penalty of the sensitivity at $\text{BER}=10^{-9}$ when the optical bandwidth is increased from 1 to 2 nm is about 0.7 dB. When the optical bandwidth is increased from 2 to 4 nm, the penalty is about 0.5 dB. In this case when the optical bandwidth is increased, only the sp-sp beat noise is increased. The sig-sp beat noise, the thermal noise and the shot noise are independent of the optical bandwidth. The sp-sp beat noise is increased by two and four times because the optical bandwidth is increased by two and four times. However in Fig. 4.1.2.a, the electrical bandwidth is increased by ten and twenty

times and so are the noises. Therefore the penalties in Fig. 4.1.2.b are less than the ones in Fig. 4.1.2.a.

In order to show the relative significance of each of the noise terms in the receiver, the noise power is plotted as a function of received power in Fig. 4.1.3. The values of the parameters used are $\delta=-20$ dB, $G_o=30$ dB, $B_{elec}=20$ GHz, $B_o=1.4 \times 1.3$ nm, $m_I=1$ (with polarizer), $N_{sp}=2$.

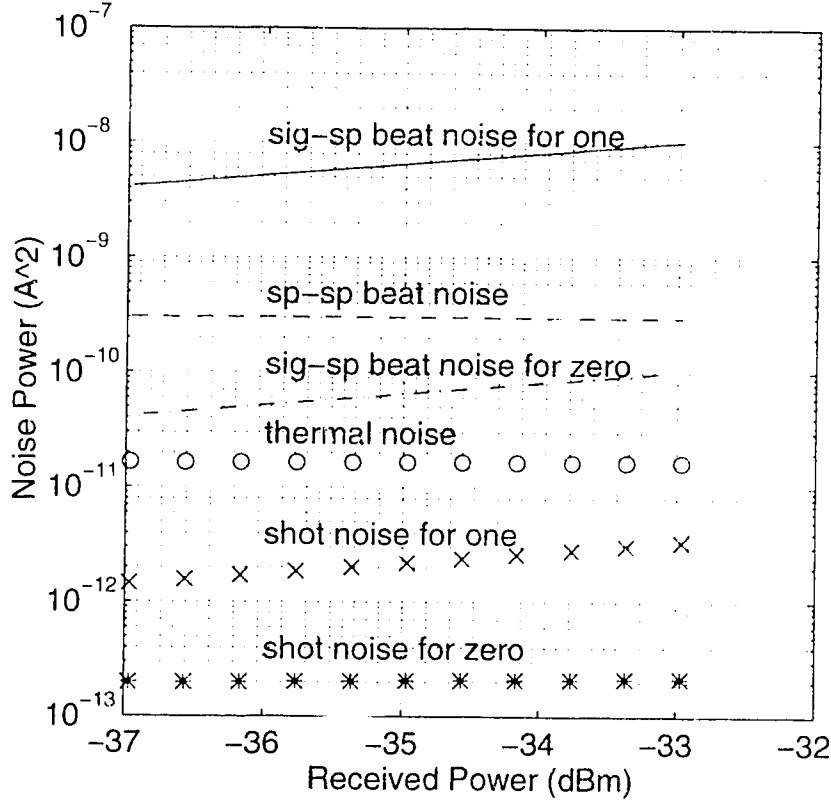


Fig. 4.1.3. Noise Power versus Received Power.

Clearly the dominant noise source for logical ones is the signal dependent sig-sp beat noise. When the received power is increased, the power of the sig-sp beat noise is also increased. The second dominant noise for both logical zeros and logical ones is the sp-sp beat noise which is signal independent. If the extinction ratio is poor or large enough, the sig-sp beat noise might be the dominant noise for logical zeros. The thermal noise will be significant if the EDFA small signal gain is not sufficiently large. The shot noise for logical zeros is negligible. However the shot noise for logical ones could be

important if the EDFA small signal gain is small and the signal power is large.

4.2. The Sensitivity of the System

The sensitivity of the EDFA preamplified system is the received power required to achieve a certain BER. In the following analyses, the sensitivities for $\text{BER}=10^{-9}$ and 10^{-14} will be considered. The sensitivity is plotted as functions of the two-sided electrical bandwidth and the optical filter bandwidth in Fig. 4.2.1.(a-b) respectively. The values of the parameters used are $\delta=-20$ dB, $G_o=30$ dB, $B_{elec}=20$ GHz (for Fig. 4.2.1.b), $B_o=1.4 \times 1.3$ nm (for Fig. 4.2.1.a), $m_l=1$ (with polarizer), $N_{sp}=2$.

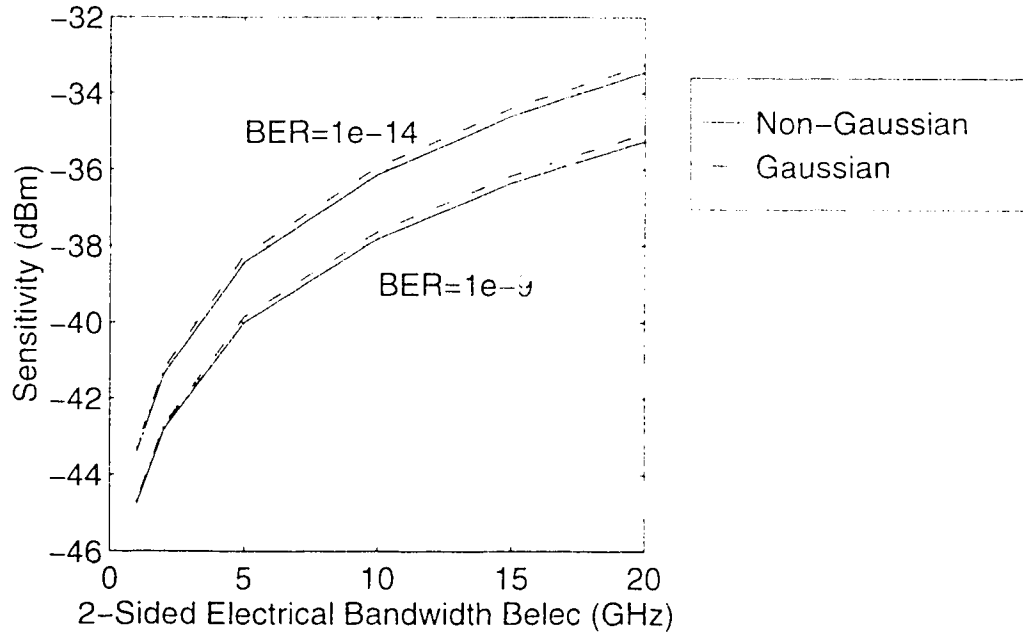


Fig. 4.2.1.a. Sensitivity versus Electrical Bandwidth.

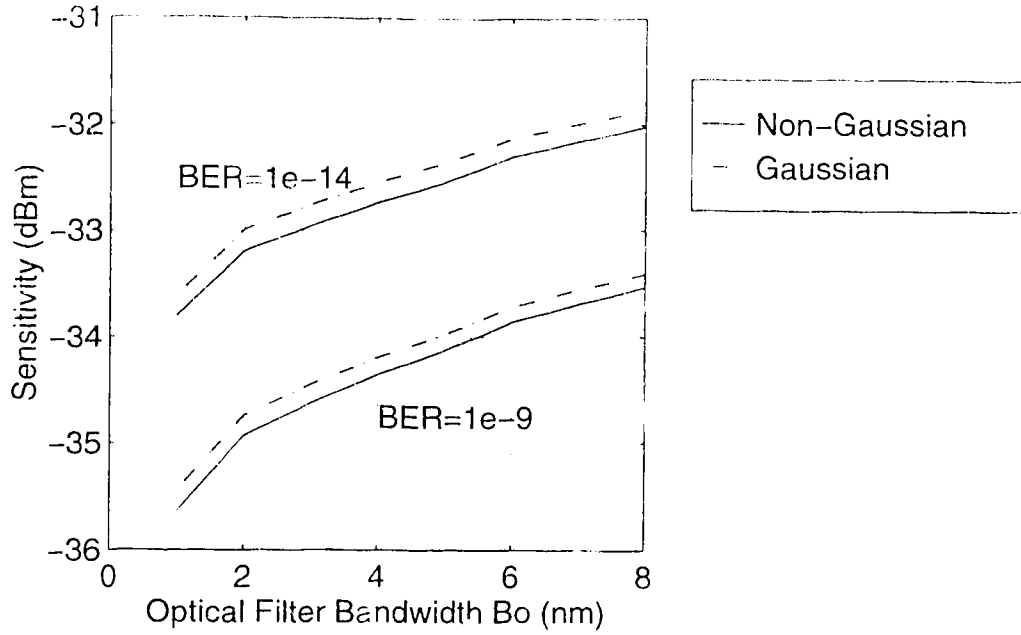


Fig. 4.2.1.b. Sensitivity versus Optical Bandwidth.

The curves in Fig. 4.2.1.(a-b) show the non-linear relation between the sensitivity and the electrical and optical bandwidth. This non-linearity has been observed earlier in Fig. 4.1.2.(a-b). Note that the $\text{BER}=10^{-14}$ curve is above the $\text{BER}=10^{-9}$ curve because it requires more power to achieve the lower BER.

It is also worthwhile to investigate the sensitivity penalty due to the increase in extinction ratio and the spontaneous emission factor of the EDFA. The sensitivity is plotted as functions of the extinction ratio and the spontaneous emission factor in Fig. 4.2.2.(a-b) respectively. The values of the parameters used are $\delta=-20$ dB (for Fig. 4.2.2.b), $G_o=30$ dB, $B_{elec}=20$ GHz, $B_o=1.4 \times 1.3$ nm, $m_f=1$ (with polarizer), $N_{sp}=2$ (for Fig. 4.2.2.a).

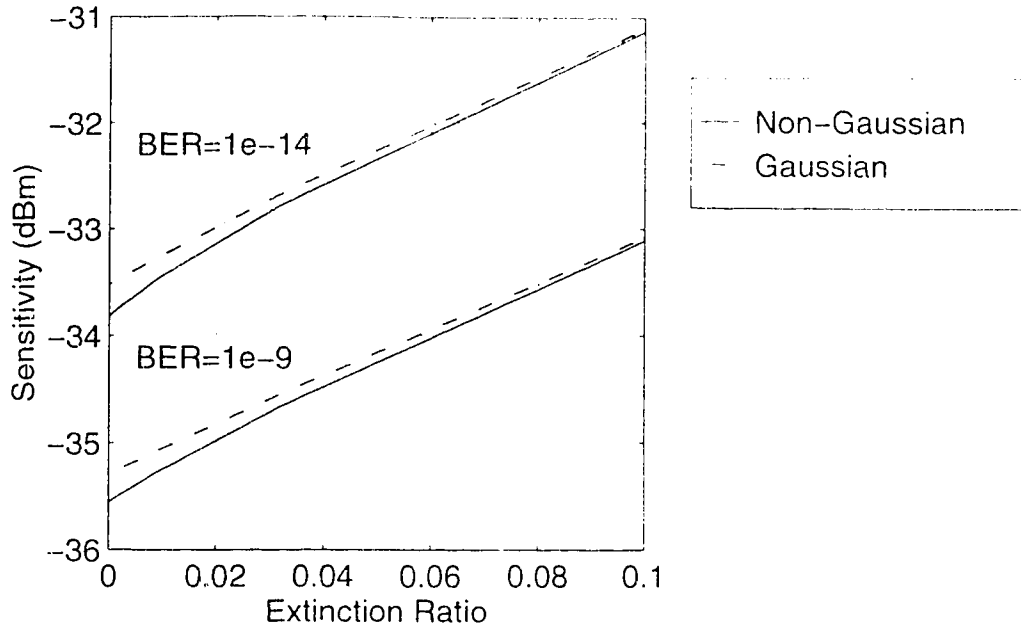


Fig. 4.2.2.a. Sensitivity versus Extinction Ratio.

From Fig. 4.2.2.a, it can be seen that the sensitivity degrades with the extinction ratio because the mean level of logical zeros is raised and the sig-sp beat noise for logical zeros is also increased. When the extinction ratio is increased from 0.01 to 0.1, which is 10 dB increment, the penalty is about 2 dB. Note that the Gaussian and the non-Gaussian curves deviate the most from each other at zero extinction ratio. This is because the sig-sp beat noise for logical zeros vanishes and the sp-sp beat noise, which has a non-Gaussian PDF, dominates. However this difference is still insignificant. The Gaussian theory can still be used with small errors.

Fig. 4.2.2.b shows the relation between the sensitivity and the spontaneous emission factor. The expression for sp-sp beat noise in (3.8.1) shows that the sp-sp beat noise power is proportional to the square of the spontaneous emission factor. Therefore if the spontaneous emission factor is doubled, the noise power is quadrupled. The expression for the sig-sp beat noise in (3.8.2) shows that the sig-sp noise power is linearly proportional to the spontaneous emission factor. Therefore when the spontaneous emission factor is doubled, the sig-sp beat noise is doubled. It is

clear then the sensitivity of the receiver will be very sensitive to the value of the spontaneous emission factor. From Fig. 4.2.2.b, it can be seen that the penalty is about 3 dB when the value of the spontaneous emission factor is increased from one to two. The value of the spontaneous emission factor varies from EDFA to EDFA depending on the design. The ideal theoretical value is one at which the best receiver sensitivity can be obtained.

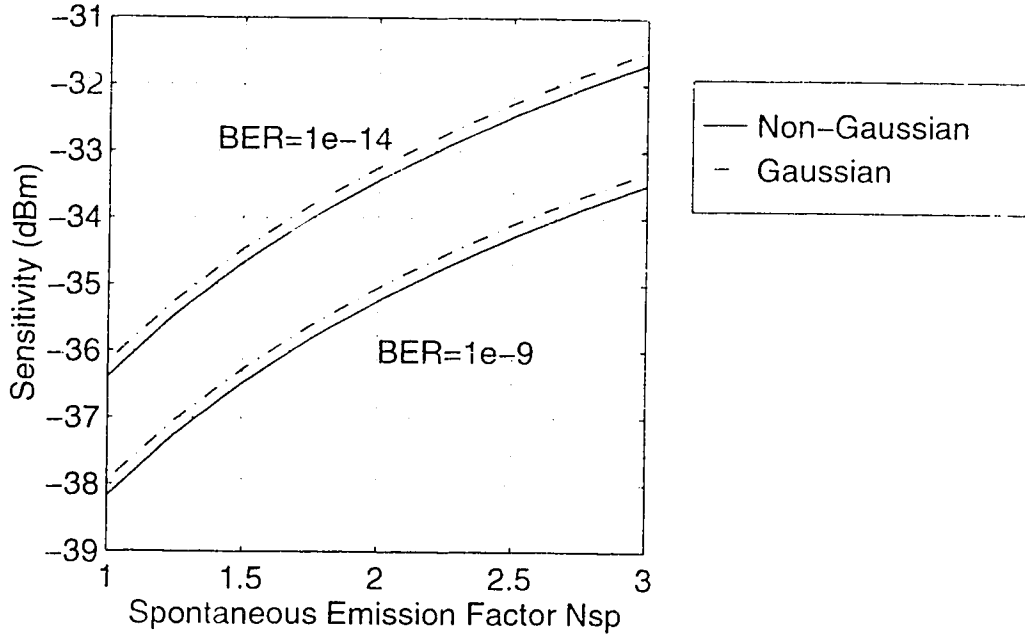


Fig. 4.2.2.b. Sensitivity versus Spontaneous Emission Factor.

4.2.1. The EDFA gain dependence of beat noises

When the EDFA small signal gain is much greater than one, the sp-sp and the sig-sp beat noises are both proportional to the square of the gain as it can be seen from equations (3.8.1) and (3.8.2). This gain dependence of the beat noises limits the performance of the system. The sensitivity is plotted as a function of the EDFA small signal gain in Fig. 4.2.1.1. The values of the parameters used are $\delta = -20$ dB, $B_{elec} = 20$ GHz, $B_o = 1.4 \times 1.3$ nm, $m_t = 1$ (with polarizer), $N_{sp} = 2$.

It can be seen from Fig. 4.2.1.1 that the sensitivity is improved drastically when the EDFA small signal gain is increased from 10 to 20 dB. This is because in the 10 to 20 dB range, the gain is not

sufficiently large for the beat noises to dominate. The thermal noise is the dominant noise. Since the thermal noise is independent of the signal or the gain, when the small signal gain is increased, the signal power at the photodiode is increased. The electrical SNR is increased and hence the BER is reduced. If the BER is kept constant (e.g., $\text{BER}=10^{-9}$ as shown in Fig. 4.2.1.1), we would need less received power to achieve the same BER and hence the sensitivity is improved. When the small signal gain is greater than 20 dB, the beat noises become dominant. The improvement of the sensitivity becomes less. When the small signal gain is greater than 25 dB, the sensitivity is essentially independent of the gain.

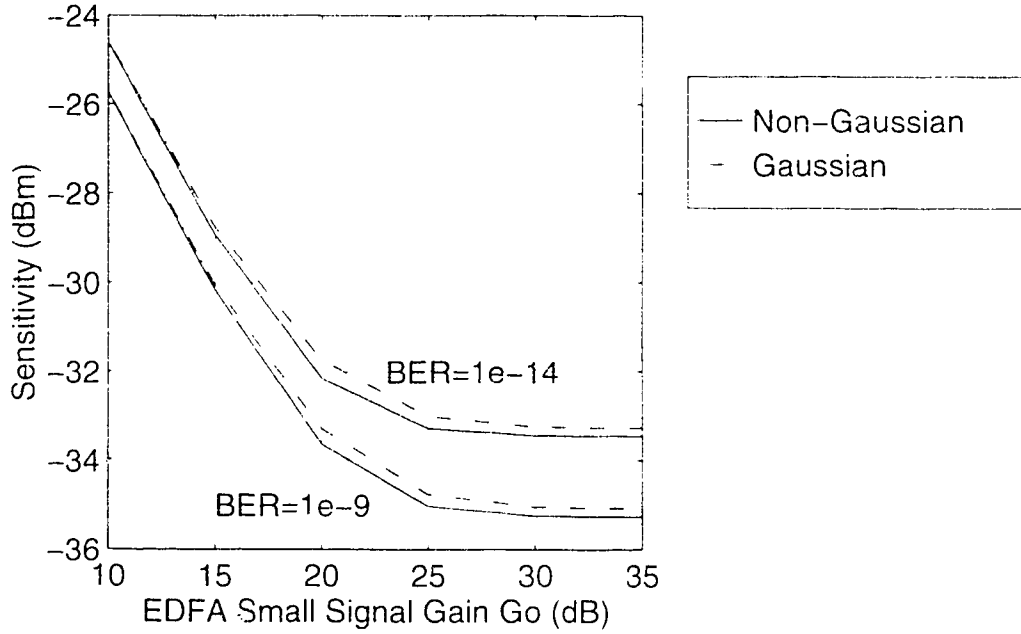


Fig. 4.2.1.1. Sensitivity versus EDFA Small Signal Gain.

This gain dependence and/or independence (when EDFA small signal gain is greater than 25 dB) of the sensitivity can be readily seen by forming the electrical SNR:

$$\text{SNR} = \frac{(\Re P_{sig})^2}{\sigma_{sp-sp}^2 + \sigma_{sig-sp}^2 + \sigma_{th}^2 + \sigma_{sh}^2}. \quad (4.2.1.1)$$

Using (3.2.3), (3.2.6), (3.8.1), (3.8.2) in (4.2.1.1), approximating $(G-1)$ by G , substituting $P_{sig}=GP_{in}$, and after rearranging terms, we have:

$$SNR = \frac{MP_{in}^2}{m_l(N_{sp}hf_cE_o)^2 + 2N_{sp}hf_cB_oP_{in} + \frac{(\sigma_{th}^2 + \sigma_{sh}^2)M}{\mathfrak{R}^2G^2}}. \quad (4.2.1.2)$$

The SNR in (4.2.1.2) applies to both logical ones and logical zeros except with different P_{in} . Note that when the small signal gain is sufficiently large, the third term in the denominator of (4.2.1.2) is small and the SNR is independent of the gain. Therefore the sensitivity reaches a floor as shown in Fig. 4.2.1.1. Note also the term in numerator of (4.2.1.2) is proportional to the square of P_{in} whereas the denominator is only linearly proportional to P_{in} . Therefore as P_{in} increases, the SNR increases and the BER is reduced. There is no BER floor as shown earlier in Fig. 4.1.1.(a-b) and Fig. 4.1.2.(a-b) even though the sig-sp beat noise is signal dependent. The sig-sp beat noise only depends on the optical signal but not the electrical signal.

4.3. The Impacts of Values of Parameters on BER

This section investigates the effect of the parameters such as the extinction ratio, the EDFA small signal gain, the electrical and the optical bandwidth on the BER. The BER is plotted as a function of the extinction ratio in Fig. 4.3.1. The values of the parameters used are $P_{in1}=-32$ dBm, $P_{inav}=-35$ dBm, $G_o=30$ dB, $B_{elec}=20$ GHz, $B_o=1.4 \times 1.3$ nm, $m_l=1$ (with polarizer), $M=11$, $N_{sp}=2$.

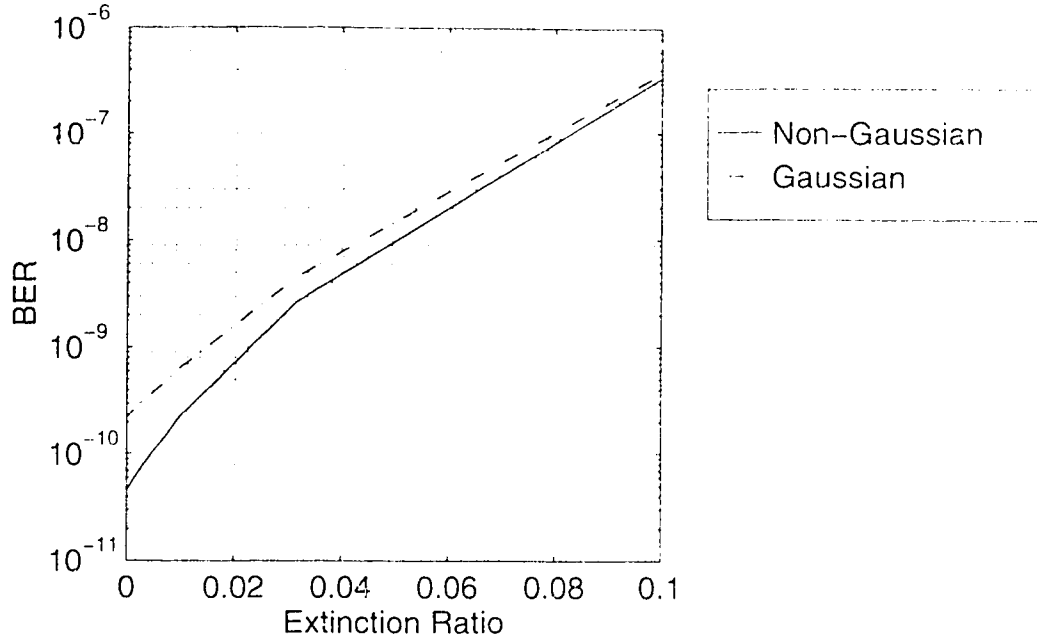


Fig. 4.3.1. BER versus Extinction Ratio.

As it can be seen from Fig. 4.3.1, the BER increases with the extinction ratio. This is because when the extinction ratio is increased, the mean level of logical zeros is raised and the sig-sp beat noise for logical zeros is increased. These two effects cause the closure of the data eye and hence the BER increases. Note that the maximum difference between the Gaussian and the non-Gaussian curves occur again at zero extinction ratio. However the difference in terms of the BER is less than a decade.

The BER is also plotted as a function of the EDFA small signal gain in Fig. 4.3.2. The values of the parameters used are $\delta = -20$ dB, $P_{in1} = -32$ dBm, $P_{inav} = -35$ dBm, $B_{elec} = 20$ GHz, $B_o = 1.4 \times 1.3$ nm, $m_l = 1$ (with polarizer), $M = 11$, $N_{sp} = 2$.

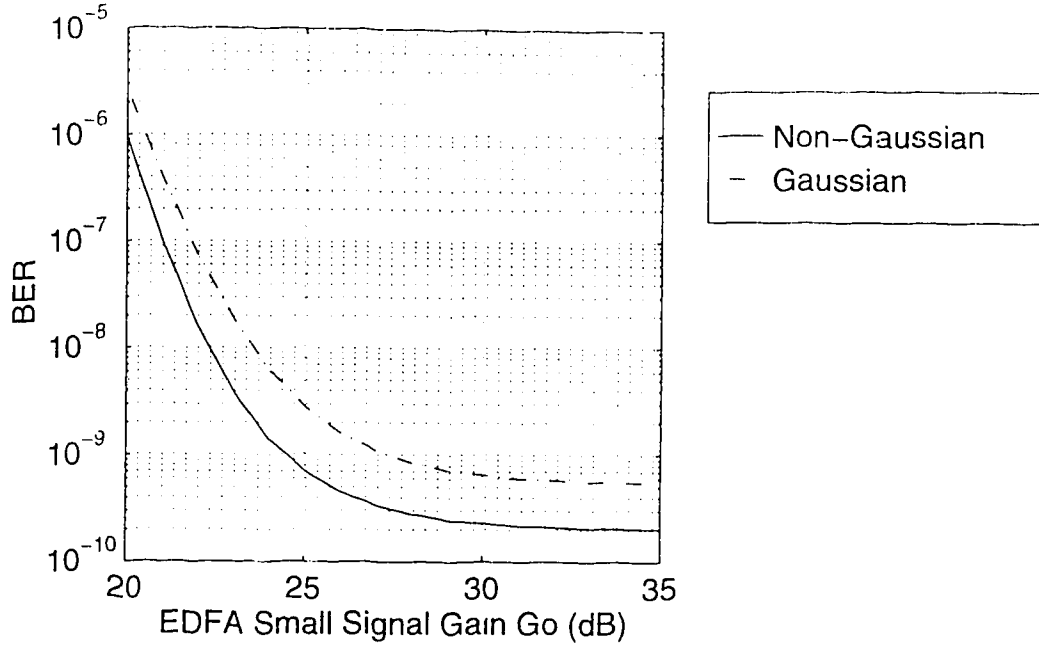


Fig. 4.3.2. BER versus EDFA Small Signal Gain.

It can be seen from Fig. 4.3.2 that a BER floor occurs when the EDFA small signal gain is greater than 25 dB. This again can be explained by the EDFA small signal gain dependence of the beat noises. When the gain is sufficiently large, the electrical SNR is almost independent of the gain as shown in equation (4.2.1.2). The argument of the Q -function in equation (2.13.8) has the form of the square root of the electrical SNR. Since the electrical SNR is independent of the gain when the gain is large, the Q -function is also independent of the gain and hence the BER is a constant at large EDFA small signal gain. This error floor can be reduced by increasing the received power as it can be clearly seen from equation (4.2.1.2). Note that the difference between the Gaussian and the non-Gaussian curves at $\text{BER}=10^{-9}$ in terms of the EDFA small signal gain is about 2.5 dB. However the maximum difference in BER is less than half a decade.

Fig. 4.3.3 and 4.3.4 show the plots of the BER as a function of the parameter M . The electrical bandwidth is varied in Fig. 4.3.3 and the optical bandwidth is kept constant at $B_o=1.4 \times 1.3$ nm. In Fig. 4.3.4, the optical bandwidth is varied and the electrical bandwidth is kept constant at $B_{elec}=20$ GHz. For both Fig. 4.3.3 and 4.3.4, the values of

the parameters used are $\delta=-20$ dB, $G_o=30$ dB, $P_{in1}=-32$ dBm, $P_{inav}=-35$ dBm, $m_i=1$ (with polarizer), $N_{sp}=2$.

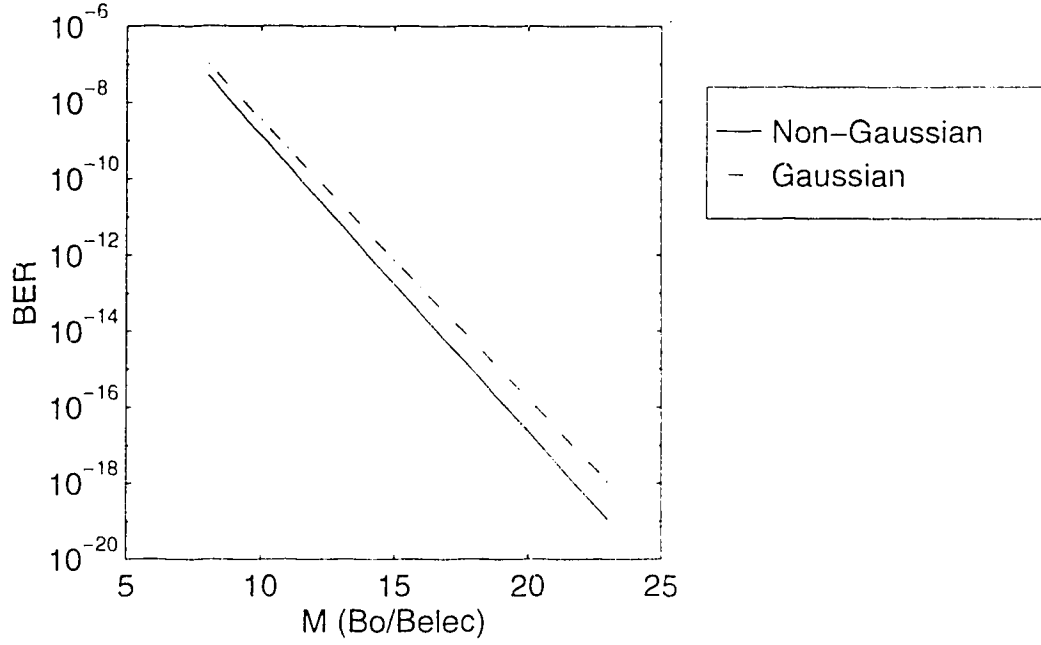


Fig. 4.3.3. BER versus M (by varying B_{elec}).

In Fig. 4.3.3, the improvement in BER when M increases is due to the reduction of the electrical bandwidth which reduces all the noises in the receiver. In Fig. 4.3.4, the degradation of the BER when M increases is due to the increase of the sp-sp beat noise which is directly proportional to the optical bandwidth.

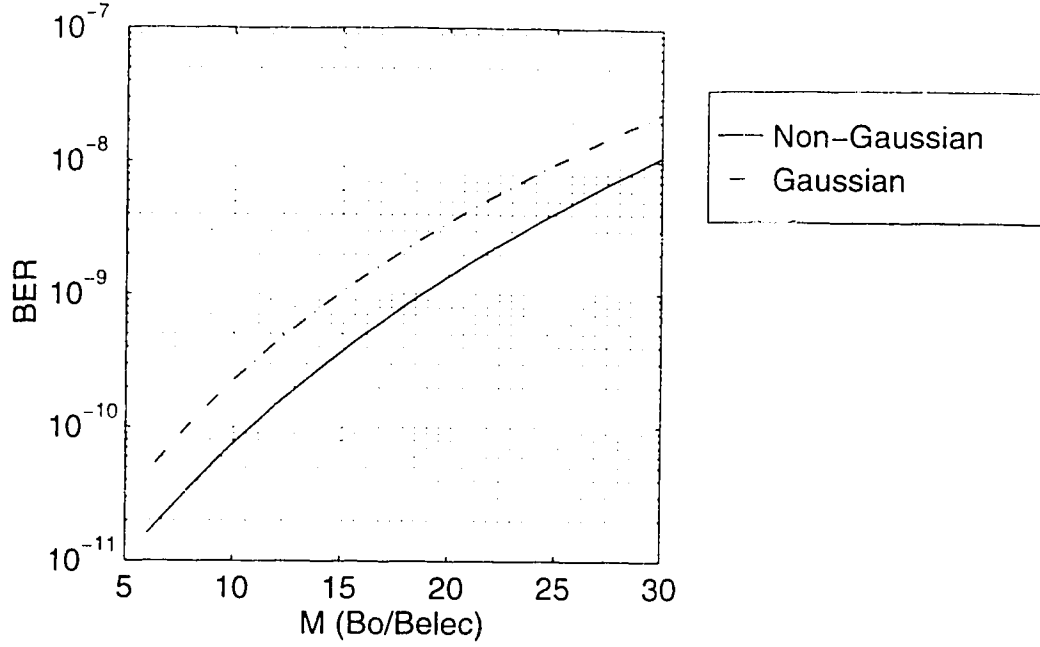


Fig. 4.3.4. BER versus M (by varying B_o).

4.4. The BER as a Function of the Decision Threshold

We have seen in the previous sections that the Gaussian theory is a very good approximation to the non-Gaussian theory in the analyses that involve the BER and the sensitivity of the system. It has also been shown earlier in chapter 3 that when the electrical bandwidth and the EDFA small signal gain are sufficiently large, the PDFs predicted by the non-Gaussian theory is very different from those predicted by the Gaussian theory. The impact of the non-Gaussian distributions on the system shows up not in the sensitivity related analyses but in the optimum threshold analyses.

The BER is plotted as a function of the percentage threshold in Fig. 4.4.1.(a-b) at different received power levels. The percentage threshold is given by:

$$\% \text{threshold} = \frac{I_d - \bar{y}_0}{\bar{y}_1 - \bar{y}_0} \times 100\% \quad (4.4.1)$$

where I_d is the decision threshold, \bar{y}_0 and \bar{y}_1 are the mean values of the logical ones and logical zeros given by equations (2.10.4.2) and (2.10.4.3) respectively. In Fig. 4.4.1.a, the electrical bandwidth is $B_{elec}=1$ GHz whereas $B_{elec}=20$ GHz is used for Fig. 4.4.1.b. The values of the parameters used are $B_o=1.4 \times 1.3$ nm, $m_l=1$ (with polarizer), $N_{sp}=2$.

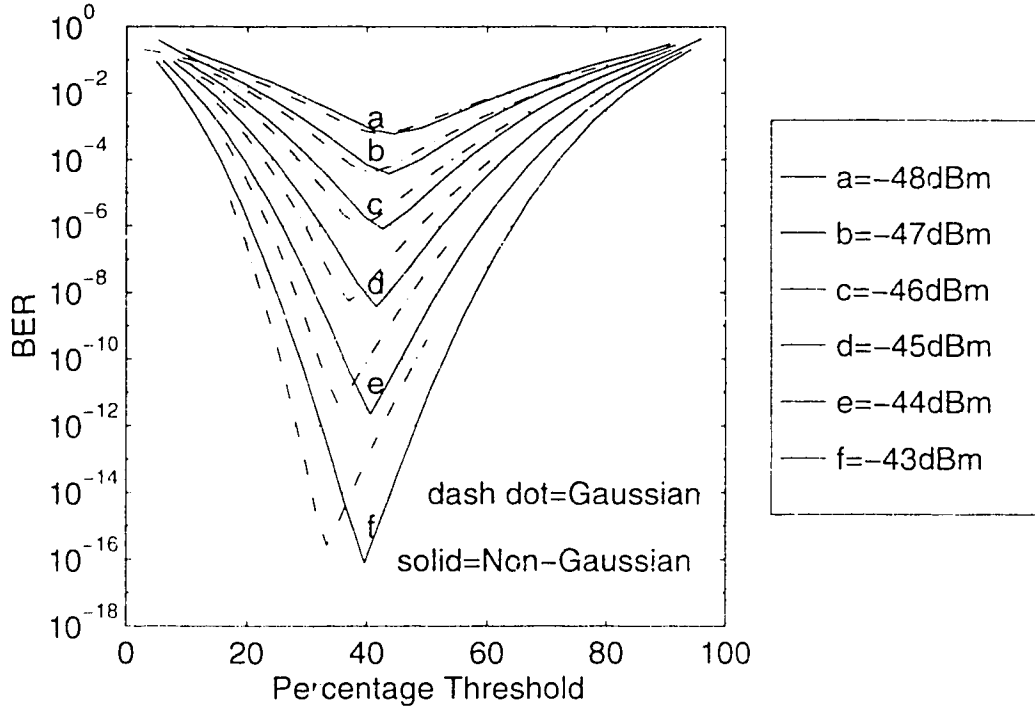


Fig. 4.4.1.a. BER versus Percentage Threshold, $B_{elec}=1$ GHz.

It can be seen from Fig. 4.4.1.a that the difference between the Gaussian and the non-Gaussian curves are small for $B_{elec}=1$ GHz. However when the electrical bandwidth is increased to $B_{elec}=20$ GHz as shown in Fig. 4.4.1.b, the percentage optimum threshold (the minimum point on the curve) predicted by the Gaussian theory is significantly different from that predicted by the non-Gaussian theory. When $BER=10^{-9}$ (or received power is about -35 dBm), the difference in the optimum threshold is more than ten percent. In a real system, the peak-to-peak voltage amplitude of the data at the input of the decision circuit is typically from 500 mV_{pp} to 1 V_{pp}.

The ten percent difference will correspond to 50 to 100 mV difference in actual voltage. Moreover if the optimum threshold predicted by the Gaussian theory is used in the real system, a penalty of about 2 dB will result. For example, from Fig. 4.4.1.b, when the received power is -35 dBm, we would expect to obtain a BER of 10^{-9} . However if we used the Gaussian optimum threshold, the actual achievable BER is only about 10^{-6} . In order to achieve $BER=10^{-9}$, the received power has to be increased by about 2 dB.

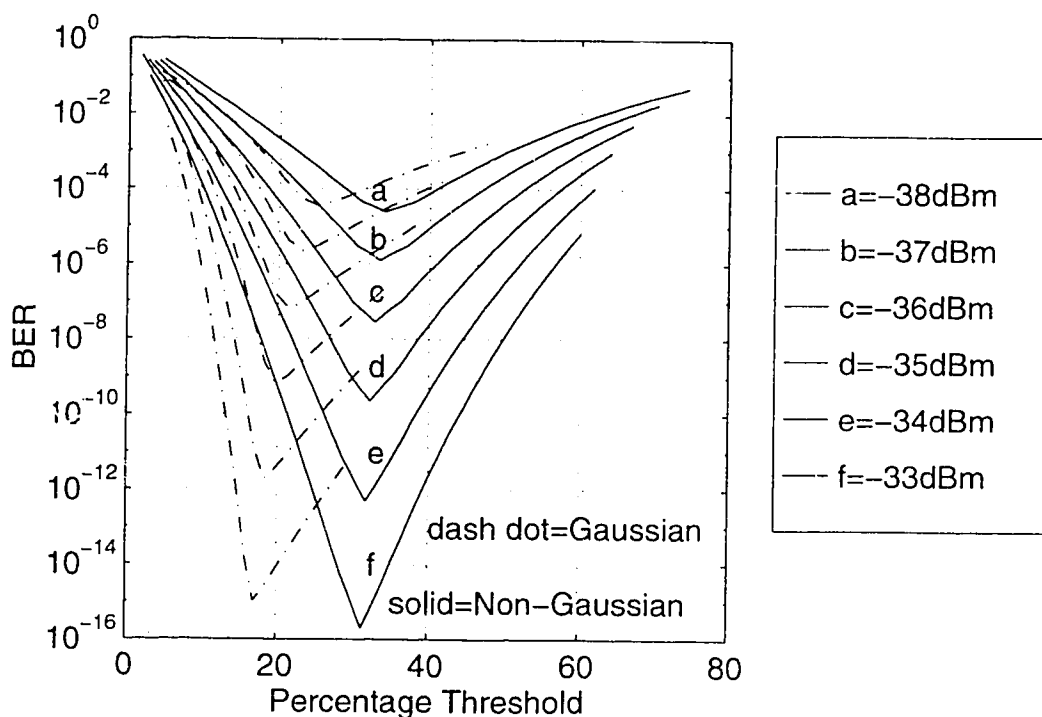


Fig. 4.4.1.b. BER versus Percentage Threshold, $B_{elec}=20$ GHz.

4.4.1. The loci of the percentage optimum threshold

The minimum points in Fig. 4.4.1.(a-b) can be traced out to form loci which can be plotted as functions of the received power as shown in Fig. 4.4.1.1 and 4.4.1.2.

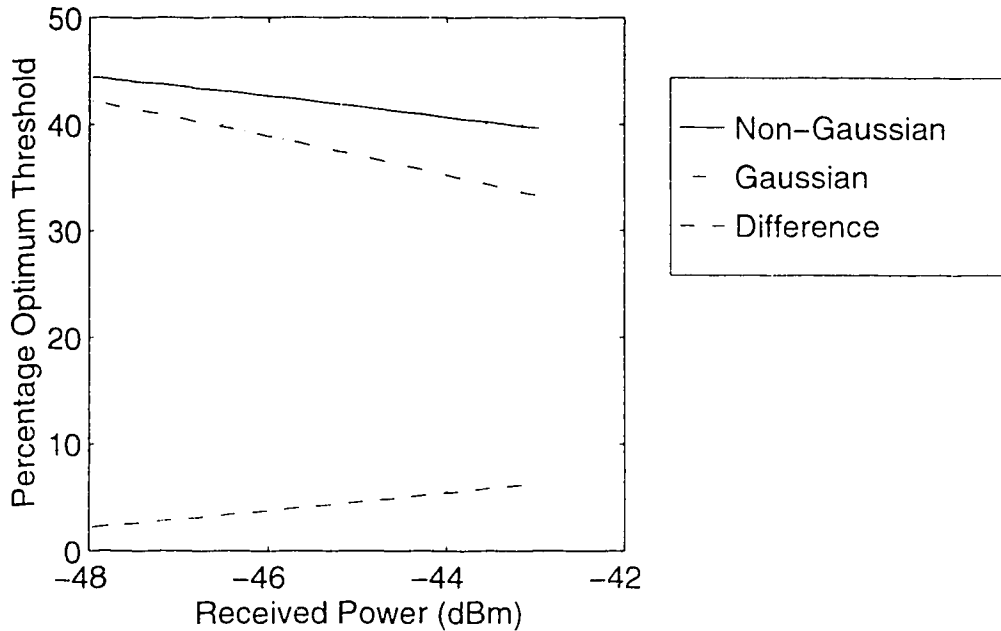


Fig. 4.4.1.1. Percentage Optimum Threshold versus Received Power, $B_{elc}=1$ GHz.

As it can be seen from Fig. 4.4.1.1, when the electrical bandwidth is $B_{elc}=1$ GHz, the maximum difference between the Gaussian and the non-Gaussian curves within the practically observable BER range (BER greater than 10^{-16}) is only about five percent. At large electrical bandwidth ($B_{elc}=20$ GHz) however, the maximum difference is almost fifteen percent as it can be seen from Fig. 4.4.1.2. Note that the Gaussian curve varies by about eight percent in the percentage optimum threshold when the received power is increased from -38 to -33 dBm. However the non-Gaussian curve varies by less than three percent. In other words, the actual percentage optimum threshold stays fairly constant when the power is changed.

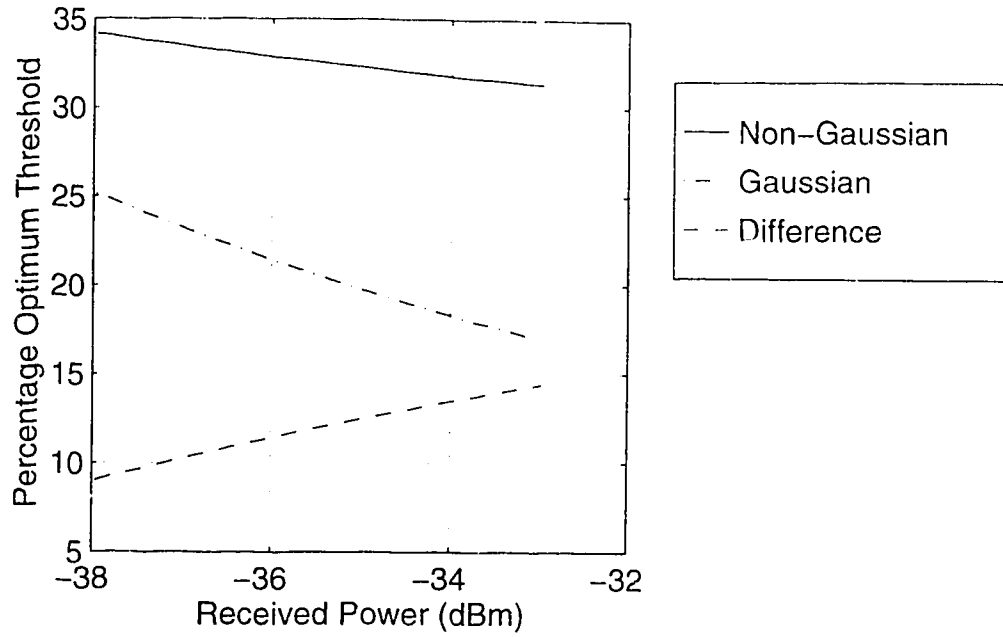


Fig. 4.4.1.2. Percentage Optimum Threshold versus Received Power, $B_{elec}=20$ GHz.

4.5. The Impacts of Values of Parameters on Threshold

We have seen that when the electrical bandwidth is wide enough, the impact of the non-Gaussian distributions on the optimum threshold is quite significant. It is therefore worthwhile to investigate the impacts of the values of the other parameters on the optimum threshold. Fig. 4.5.1 shows the plot of the percentage optimum threshold versus the extinction ratio. The values of the parameters used are $G_o=30$ dB, $P_{in1}=-32$ dBm, $P_{inav}=-35$ dBm, $B_{elec}=20$ GHz, $B_o=1.4 \times 1.3$ nm, $m_l=1$ (with polarizer), $M=11$, $N_{sp}=2$.

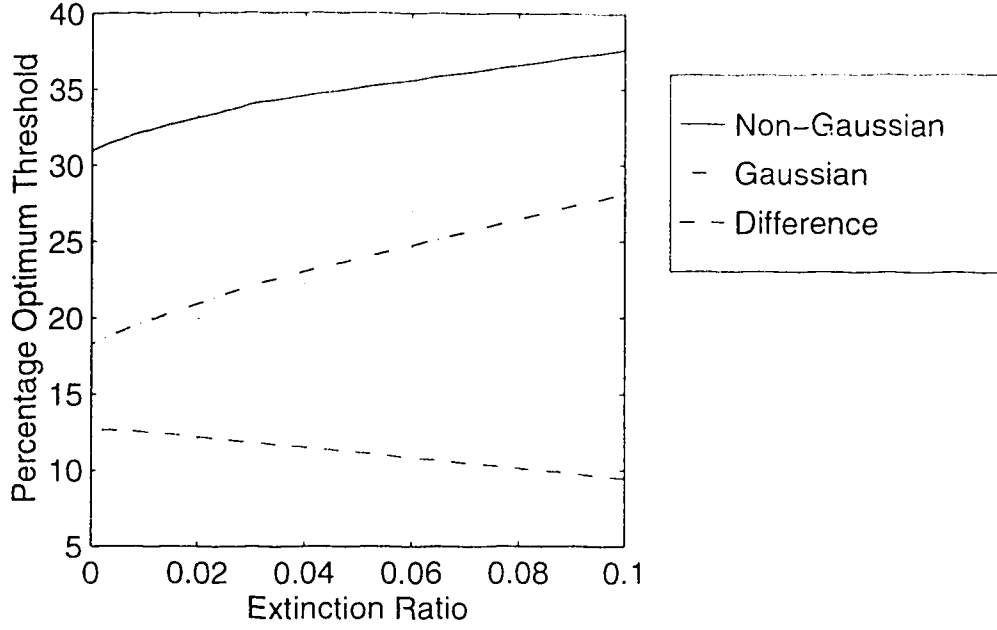


Fig. 4.5.1. Percentage Optimum Threshold versus Extinction Ratio.

It can be seen from Fig. 4.5.1 that when the extinction ratio is increased, the difference between the Gaussian and the non-Gaussian curves decreases. However the impact of the extinction ratio seems to be small because the difference is only decreased by about two percent when the extinction ratio is varied from 0 to 0.1.

Fig. 4.5.2 shows the plot of the percentage optimum threshold as a function of the EDFA small signal gain. The values of the parameters used are $\delta = -20$ dB, $P_{in1} = -32$ dBm, $P_{inav} = -35$ dBm, $B_{elec} = 20$ GHz, $B_o = 1.4 \times 1.3$ nm, $m_I = 1$ (with polarizer), $M = 11$, $N_{sp} = 2$. The shapes of the Gaussian and the non-Gaussian curves bear similarities to the curves in Fig. 4.3.2 and Fig. 4.2.1.1. Note that when the EDFA small signal gain is small, the Gaussian curve merges quickly with the non-Gaussian curve. This is because at small EDFA gain, the thermal noise is the dominant noise. When the gain is increased, the beat noises become dominant and the percentage optimum threshold is almost independent of the gain.

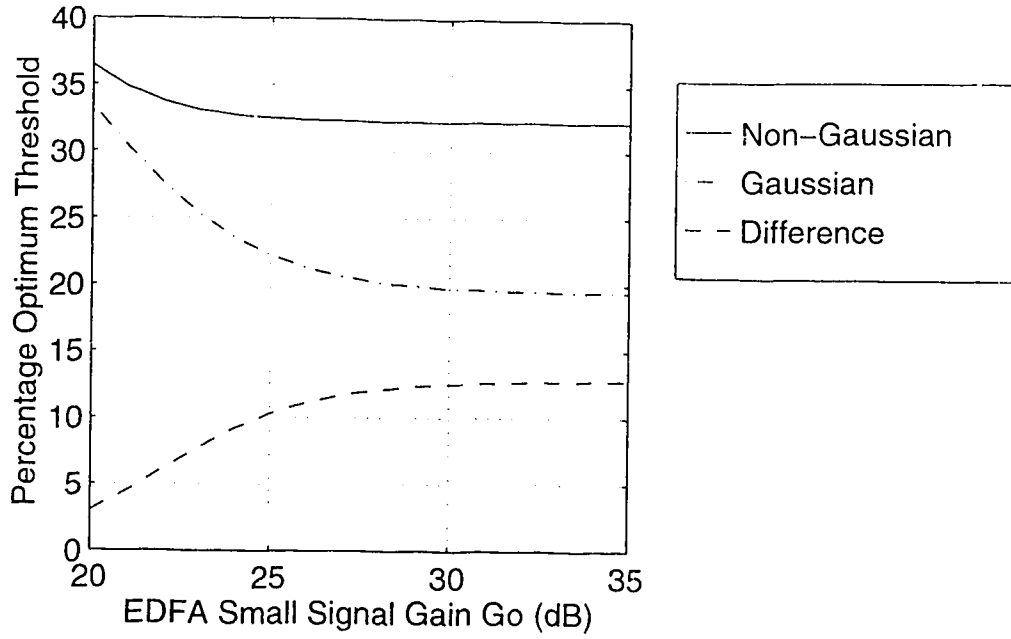


Fig. 4.5.2. Percentage Optimum Threshold versus EDFA Small Signal Gain.

The percentage optimum threshold is also plotted as a function of the parameter M in Fig. 4.5.3 and 4.5.4. The two-sided electrical bandwidth B_{elec} is varied in Fig. 4.5.3 and the optical bandwidth B_o is held constant. The optical bandwidth B_o is varied in Fig. 4.5.4 and the electrical bandwidth is held constant. The values of the parameters used are $\delta = -20$ dB, $G_o = 30$ dB, $P_{in1} = -32$ dBm (for Fig. 4.5.4), $P_{inav} = -35$ dBm (for Fig. 4.5.4), $B_{elec} = 20$ GHz (for Fig. 4.5.4), $B_o = 1.4 \times 1.3$ nm (for Fig. 4.5.3), $m_l = 1$ (with polarizer), $N_{sp} = 2$. For Fig. 4.5.3, in order to see the effect of varying of B_{elec} on the percentage optimum threshold, the BER is held constant at 10^{-9} and the received power is varied at each value of M such that $BER = 10^{-9}$ can be achieved.

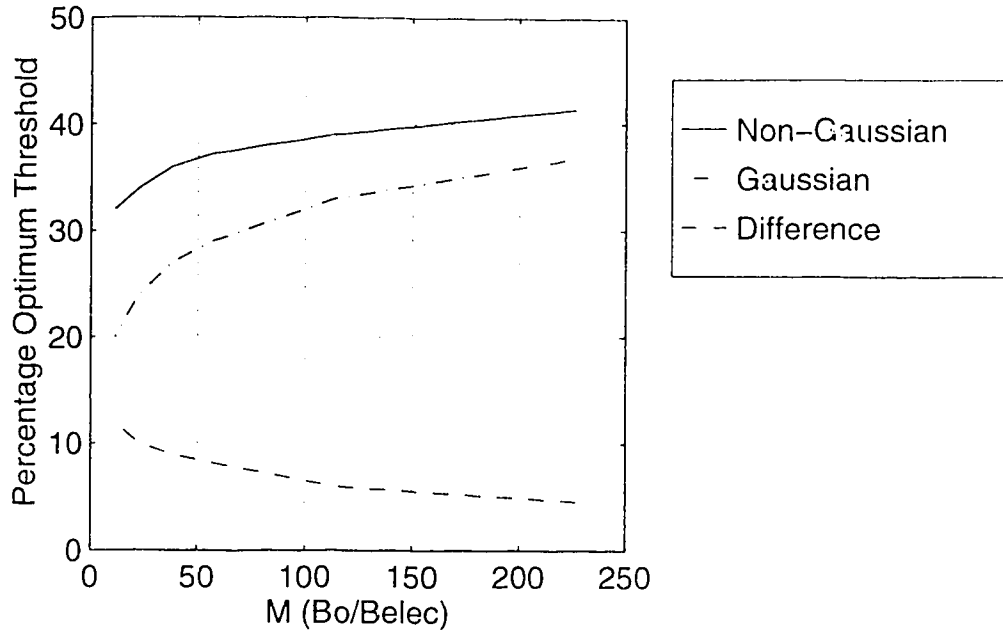


Fig. 4.5.3. Percentage Optimum Threshold versus M (varying B_{elec}).

The two-sided electrical bandwidth in Fig. 4.5.3 is varied from 1 (M large) to 20 (M small) GHz. When the electrical bandwidth is reduced, the difference between the Gaussian and the non-Gaussian curves becomes small. When the two-sided electrical bandwidth is increased to 20 GHz, the difference in percentage optimum threshold is as much as 10 % because the PDFs of logical ones and zeros are more non-Gaussian as shown earlier in chapter 3.

The optical bandwidth in Fig. 4.5.4 is varied from 0.7 to 3.4 nm. The optical bandwidth can affect both the mean values and the variances of logical ones and logical zeros as shown earlier in chapter 3. The difference is the largest when the optical bandwidth is small. Both Fig. 4.5.3 and Fig. 4.5.4 show that the percentage optimum threshold predicted by the non-Gaussian theory differs the most from that predicted by the Gaussian theory when the ratio of optical bandwidth to electrical bandwidth is small.

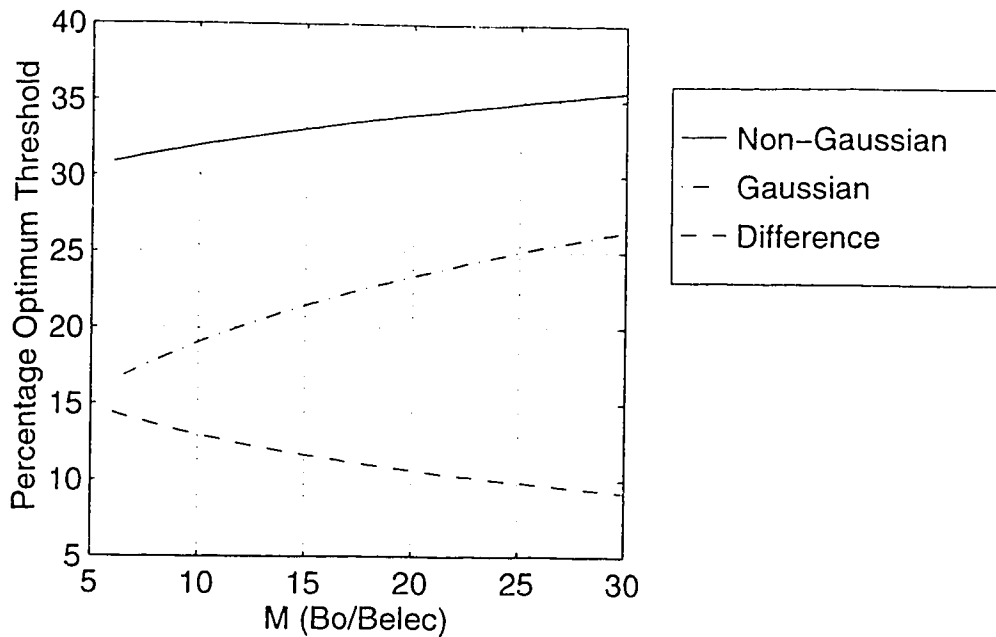


Fig. 4.5.4. Percentage Optimum Threshold versus M (varying B_o).

4.6. Implications of Simulation Results

If we are only interested in the BER versus received power curves or the sensitivity of the system, the Gaussian theory is sufficient to provide valuable information. However in searching for the optimum threshold for an EDFA preamplified digital transmission system with high EDFA small signal gain, wide electrical bandwidth and narrow optical bandwidth, the non-Gaussian theory must be used. In analyzing low bit rate system such as the OC-12 system, the Gaussian theory can be used in all the analyses of the system performance. For high bit rate system such as the OC-192 system, the non-Gaussian theory must be used if optimum threshold analysis is required. Furthermore the simulations show that the difference in the percentage optimum threshold is measurable in a practical system if the following conditions are met:

- a.) small extinction ratio,
- b.) large EDFA small signal gain,
- c.) wide electrical bandwidth,
- d.) narrow optical bandwidth.

5. Experimental Non-Gaussian PDFs

The non-Gaussian noise distributions of the binary digits in an EDFA preamplified lightwave system have been experimentally measured for the first time. The experimental setup, methods and results are presented and discussed in this chapter.

5.1. Experimental Setup and Methods

We have theoretically shown that the PDFs of logical ones and logical zeros in an EDFA preamplified optical transmission system are non-Gaussian. The non-Gaussian PDFs differ most from the Gaussian PDFs when the EDFA small signal gain is sufficiently large and the electrical bandwidth is sufficiently wide. The theoretical analysis has ignored ISI. Therefore it is necessary that the experimental method can eliminate the effect of ISI. It is also preferable that the method can separate the logical one from the logical zero such that the PDFs of logical ones and logical zeros can be measured independently. The experimental setup contains an optical source, an EDFA preamplifier and a direct detection receiver. The detailed experimental setup is shown in Fig. 5.1.1.(a-c). Fig. 5.1.1.a shows the optical signal source arrangement for the experiment.

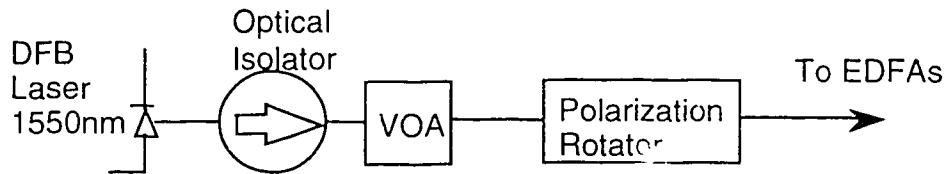


Fig. 5.1.1.a. The optical signal source for PDF experiment.

The light source is a Fujitsu DFB laser operating at 1550 nm. An optical isolator with about 2.3 dB insertion loss is used to protect the laser from reflected light. The output laser power is controlled by a variable optical attenuator (VOA). The polarization rotator is optional and its use is discussed later. Notice that the laser light is not modulated. The constant power from the laser can represent either logical ones or logical zeros depending on the power level. One advantage of using the unmodulated, constant laser power is that the

problem of ISI can be completely eliminated. The laser power is very stable. The fluctuation does not exceed ± 0.02 dBm. This stability is one of requirements for the PDFs to be measurable. Fig. 5.1.1.b shows the setup for the EDFA preamplifier.

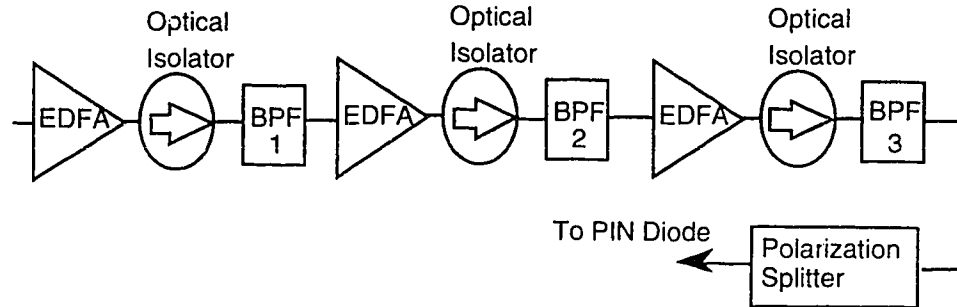


Fig. 5.1.1.b. The cascaded EDFAs for PDF experiment.

The EDFAs shown in Fig. 5.1.1.b are built by TRLabs. The Erbium Doped Fibers (EDFs) in the EDFAs have been partially cut for the purpose other studies and hence each EDFA can only provide a small signal gain of 10 to 15 dB at 1550 nm. However for the purpose of the PDF measurement, the optical preamplifier must provide small signal gain greater than 25 dB. In order to compensate for the low gain of each EDFA, the EDFAs can be cascaded. An optical isolator and an optical BPF are placed between two EDFAs. The isolator is to prevent the backscattering of the signal and the backward propagating ASE. The optical BPF is used to filter out part of the ASE such that the following EDFA will not be significantly saturated. The optical BPF at the output of the last EDFA is used to filter out part of the ASE. When two of the EDFAs are cascaded, we find that the net small signal gain is only about 23 dB and this is not enough for the beat noises to dominate. Therefore it is necessary to cascade three of the EDFAs in order to provide sufficient gain. When three of the EDFAs are cascaded, the net small signal gain is on the order of 32 dB which is about the value of the small signal gain that an EDFA preamplifier should have and the three cascaded EDFAs act as one single EDFA preamplifier. The optical BPFs 1, 2 and 3 have full-width-half-maximum (FWHM) bandwidths of 1.7, 1.3 and 1.3 nm

respectively. The noise equivalent bandwidths of the optical BPFs can be approximately obtained by multiplying the FWHM bandwidths by a factor of 1.4. The polarization splitter is optional. It is used to filter out the ASE electric field component which is spatially orthogonal to the signal electric field. It is used in conjunction with the polarization rotator in Fig. 5.1.1.a such that the PDFs for $m_I=1$ can be measured. It can be seen from equation (2.10.2.6) that the ASE power is independent of time. Practically the ASE power does vary with time, which may be due to the inadequate stabilization of the pump laser. However the variation is also small and this means the PDF of the sp-sp beat noise is experimentally measurable. Fig. 5.1.1.c shows the receiver for the experiment.

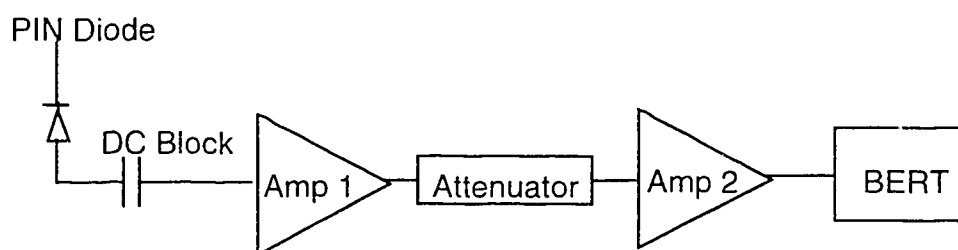


Fig. 5.1.1.c. The receiver for PDF experiment.

The signal and noise generated at the PIN diode are too small to be measurable at that point in the system. Therefore two ac-coupled microwave amplifiers were used in the receiver to amplify the signal and noise. The PIN diode is a BT&D PIN diode which has a responsivity of about 0.6 A/W at low frequencies. The frequency response of the BT&D PIN diode has been previously characterized in [31]. The single-sided noise equivalent bandwidth of the PIN diode is estimated to be about 6.5 GHz. The bit error rate tester (BERT) contains a Hewlett Packard (HP) 70322A synthesized signal generator, a HP 70841A pattern generator and a HP 70842A error detector. The detailed setup of the BERT is shown in Fig. 5.1.2.

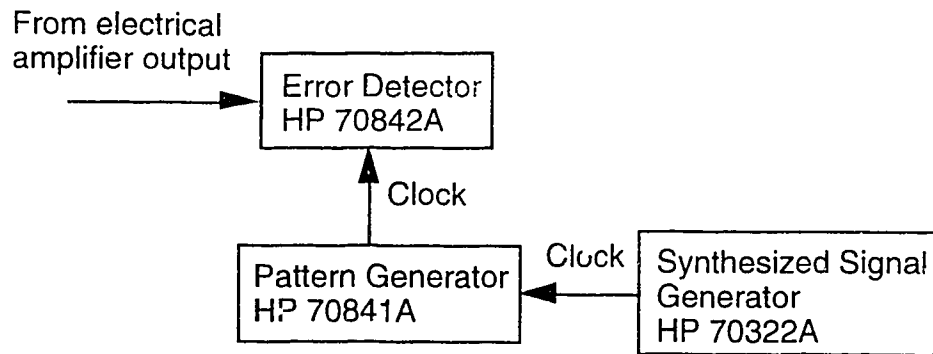


Fig. 5.1.2. The setup of the BERT.

Since the laser power is not modulated, there are no binary digits and the clock recovery circuit is not needed. Therefore the clock output from the pattern generator can be connected directly to the error detector. The clock frequency determines the sampling rate. We now use the above setup to describe the experimental procedure for measuring the PDFs of noises. When the EDFAs and the laser (with constant power) are turned on, the beat noises are generated at the PIN diode due to the mixing of the signal and ASE electric fields. The mean value or the dc component of the photocurrent generated by the total optical power is blocked by the capacitor (the dc block) such that only the ac components (the noises) are passed to the microwave amplifiers. The noises are then amplified and are sampled by the error detector. Fig. 5.1.3 illustrates how the PDF of the noise is measured. The noise in Fig. 5.1.3 rides on a dc voltage level and a voltage threshold is applied for detecting the noise. The dc voltage level and the voltage threshold will be discussed later.

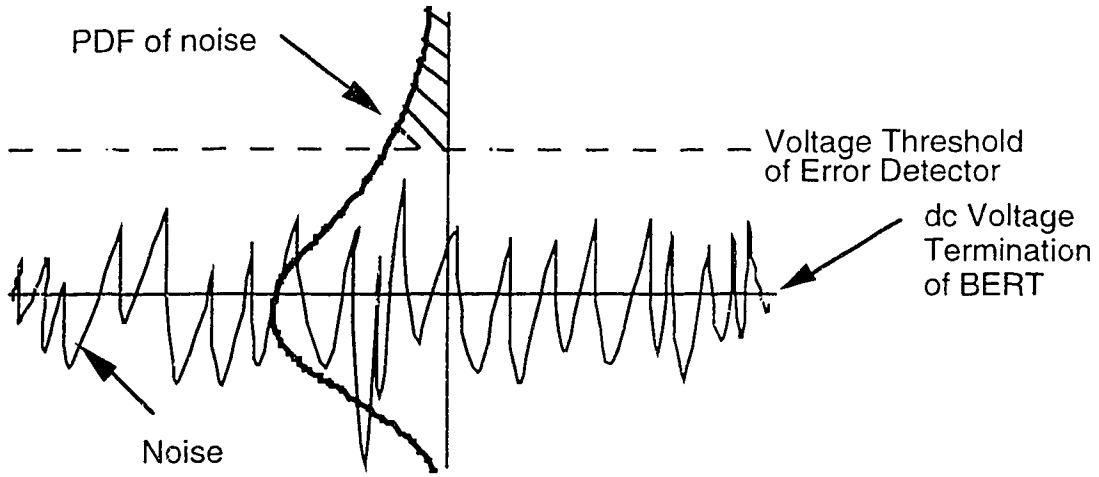


Fig. 5.1.3. The threshold detection of noise.

In Fig. 5.1.3, the voltage threshold is set above the dc voltage level. The shaded area in Fig. 5.1.3 represents the probability of the noise voltage exceeding the voltage threshold. If we are detecting all logical zeros, this probability will represent the probability of error for logical zeros. When we vary the voltage threshold, the shaded area will be different and it represents a new probability of error for logical zeros. The error probabilities P_e for logical zeros at the voltage threshold levels V can be used to determine the upper part of the PDF (the part that is above the dc voltage level) by using the following relation:

$$PDF = \left| \frac{\partial P_e}{\partial V} \right| \cong \left| \frac{\Delta P_e}{\Delta V} \right| \quad (5.1.1)$$

where
$$P_e = \int_V^{\infty} PDF dV. \quad (5.1.2)$$

Similarly when the voltage threshold is set below the dc voltage level, we can use the error probabilities of logical ones in equation (5.1.1) to determine the lower part of the PDF. The integration limits in (5.1.2) will be from $-\infty$ to V .

Before we describe how the PDFs can be measured by using the built-in decision circuit of the error detector, we will first describe the settings of the error detector. The dc voltage termination of the

error detector, which is the dc level that the incoming ac-coupled signal or noise rides on, is set at a certain level. For example, the termination could be -2 V or 0 V, which are the two dc voltage levels available from the BERT. The error detector is then set to detect either all logical ones or all logical zeros (depending on which side of the PDF we want to measure) by editing and selecting a user pattern. For example, the user selected pattern could be eight consecutive logical ones (or other length). This 8-bit long pattern is repeated such that the error detector is detecting all logical ones. If a logical zero is detected, then an error is made. The voltage threshold of the error detector is set to manual mode. Therefore it could be adjusted to detect the noise as shown in Fig. 5.1.3. When the error detector is detecting all logical zeros, the shaded area in Fig. 5.1.3 represents the probability of error for logical zeros. This probability of error corresponds to the error rate reading from the error detector.

We now describe how the error rate readings and hence the PDFs are obtained. The voltage threshold is first set far above the dc voltage level. The error rate reading is on the order of 10^{-11} since it is very unlikely that the noise voltage would exceed the threshold voltage level. Ideally if there is no noise, the error rate would be zero no matter where the threshold is set (except possibly at the dc voltage level). However, because of the presence of noise, errors would be made and captured by the error detector at the sampling or the decision time. Once the threshold is set, the gating function is enabled to start the error counting. The accumulated error count ratio (the error rate), which is the ratio of total errors to total samples, is recorded together with the voltage threshold reading. The threshold is then gradually decreased towards the dc voltage level at steps of 10 or 20 mV depending on what resolution is needed. The minimum resolution, which is the minimum voltage step, available from the BERT is 10 mV. After each threshold adjustment, the gating function is re-started such that a new error count can begin at the new threshold. As the threshold decreases towards the dc voltage level, the error rate begins to increase since it is more likely that the noise voltage would exceed the threshold voltage. When the threshold passes the dc voltage level, the error

detector is set to detect all logical ones by editing and selecting the user pattern. We are then measuring the other side of the PDF. The threshold is further reduced until 10^{-11} error rate is reached again. Since it is very time consuming to observe the errors when the error rate is on the order of 10^{-11} , a total of more than 20 errors observed is used as the criteria for recording the 10^{-11} error rate. This method works very well because the noise process seems to be quite stationary. The error count ratio at each threshold level only drifts slightly. The experimental results will be shown in section 5.2.

5.2. Experimental Results

There are three experiments that have been done. Two of the experiments are performed to measure the PDFs. The third one is to measure the optimum threshold. In one of the PDF measurement, microwave amplifiers with single-sided 3-dB bandwidths smaller than the noise equivalent bandwidth of the BT&D PIN diode (see section 5.1) were used. The second experiment for PDF measurement used microwave amplifiers with single-sided 3-dB bandwidth larger than the noise equivalent bandwidth of the PIN diode. For each PDF experiment, different laser powers were used to show how the PDFs evolve. In addition, the polarization splitter was used with the polarization rotator to measure the PDFs for $m_I=1$. The clock frequency of the BERT was set to its maximum rate 3 GHz. The error detector termination was set to -2 V such that the noise was riding at this dc voltage level (the error detector actually had about 20 mV internal offset so that the exact voltage should be -1.98 V). The reason of doing this was to prevent any distortion to the PDF since the maximum and minimum input voltages of the error detector were 1 V and -4 V respectively. The voltage -2 V was almost in between these two voltages.

The Mini-Circuits microwave amplifiers which have the same single-sided 3-dB bandwidth of 4.2 GHz and gain of about 30 to 31 dB are used in the first measurement. The attenuator was chosen to be 20 dB and it set the net cascaded gain at about 40 to 42 dB. The noise figure of the amplifiers was about 8 dB. The net cascaded small signal gain of the EDFAs was set to about 33 dB and the laser was

turned off. The polarization splitter was removed ($m_l=2$). The total ASE power at the PIN diode was about -9 dBm. The measurement was repeated with the laser turned on. The VOA was adjusted such that the input powers into the cascaded EDFAs were -40.6 dBm and -37.6 dBm, and the total powers at the PIN diode were about -5 dBm and -3 dBm. The receiver thermal noise was also measured by removing the 20 dB attenuator (such that the noise was measurable) and using the same technique described in section 5.1. The PDFs corresponding to the cases of no laser power (ASE only), thermal noise only, and -40.6 dBm and -37.6 dBm laser powers are shown in Fig. 5.2.1.

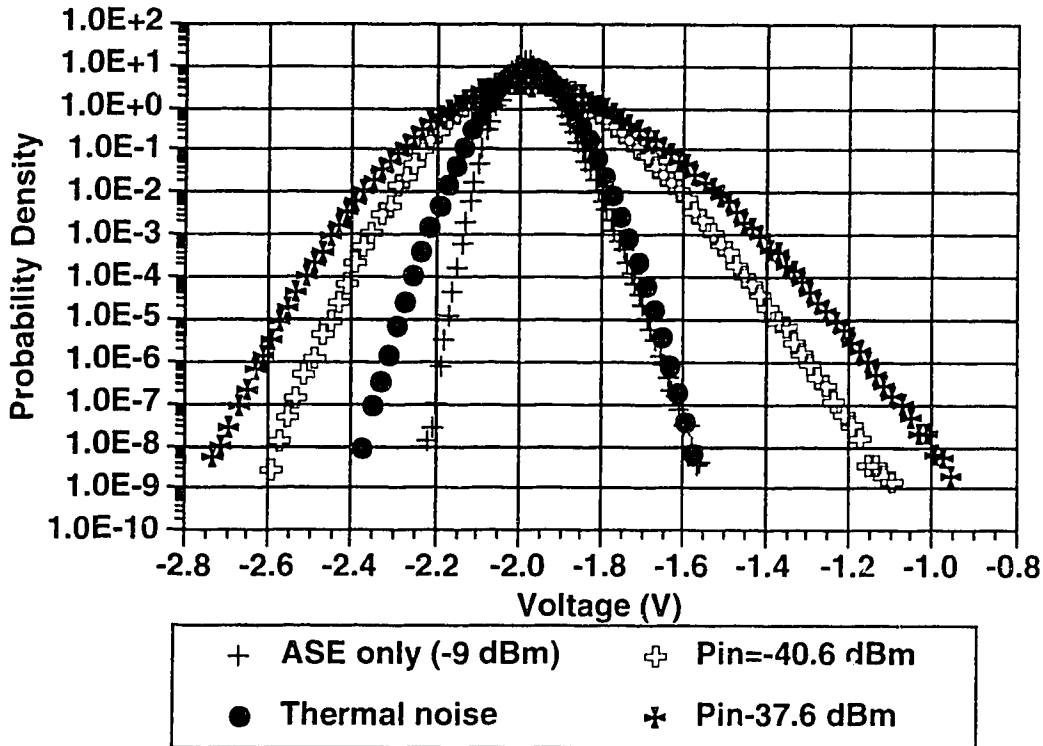


Fig. 5.2.1. Experimental PDFs of thermal and beat noises, $G=33$ dB, Mini-Circuits amplifiers.

It can be seen that the thermal noise PDF is symmetrical about the peak. However the beat noise PDFs are asymmetrical about the peak which means they are non-Gaussian. For purpose of comparison, the

experiment was repeated for the cases with reduced EDFA small signal gain and with polarization splitter.

From equation (3.8.1) and (3.8.2), it can be seen that the sig-sp beat noise will be more dominant than the sp-sp beat noise when the received power is increased. This means that the PDF will be more symmetrical about the peak. In order to investigate this, we increased the received power and reduced the EDFA small signal gain concurrently to protect the PIN diode from excess power. Since both the sig-sp and sp-sp beat noises are proportional to the square of the EDFA small signal gain, reducing the small signal gain will not change the relative powers of the beat noises. The net small signal gain of the EDFAs was reduced to about 29.5 dB. The total ASE power was about -12.2 dBm. The laser powers used were zero (no laser, ASE only), -40.6 dBm, -37.9 dBm and -33.1 dBm, and the total powers at the PIN diode were -12.2 dBm, -8.4 dBm, -6.5 dBm and -3 dBm respectively. The PDFs are shown in Fig. 5.2.2.

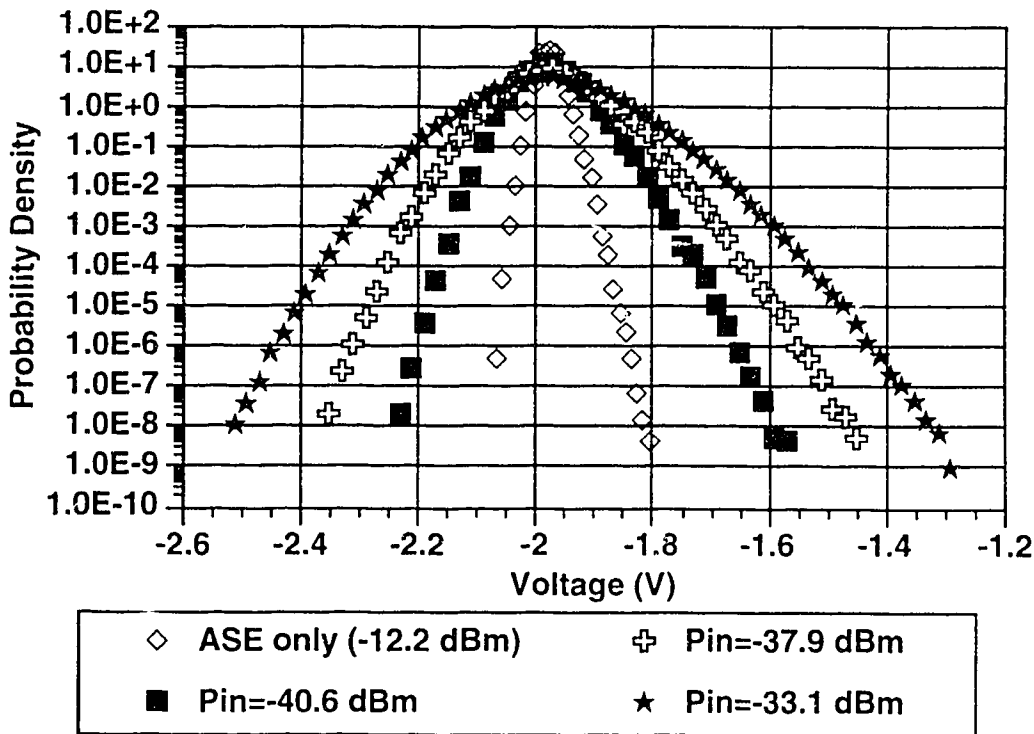


Fig. 5.2.2. Experimental PDFs of beat noises at different laser powers, $G=29.5$ dB, Mini-Circuits amplifiers.

We would expect that the PDFs at high laser powers (such as the case when the received power is -33.1 dBm) to be more symmetrical about the peaks. However the measurement does not show significant difference in terms of the symmetry within the range of observation.

The polarization splitter was then inserted ($m_I=1$) in the system to remove the ASE electric field component which is spatially orthogonal to the signal. The net small signal gain of the EDFAs was about 32.4 dB and the total ASE power was about -13.5 dBm. The laser powers used were zero (ASE only), -40.6 dBm and -36.3 dBm. The corresponding total powers at the PIN diode were -13.5 dBm, -7.5 dBm and -3.5 dBm respectively. The measured PDFs are shown in Fig. 5.2.3.

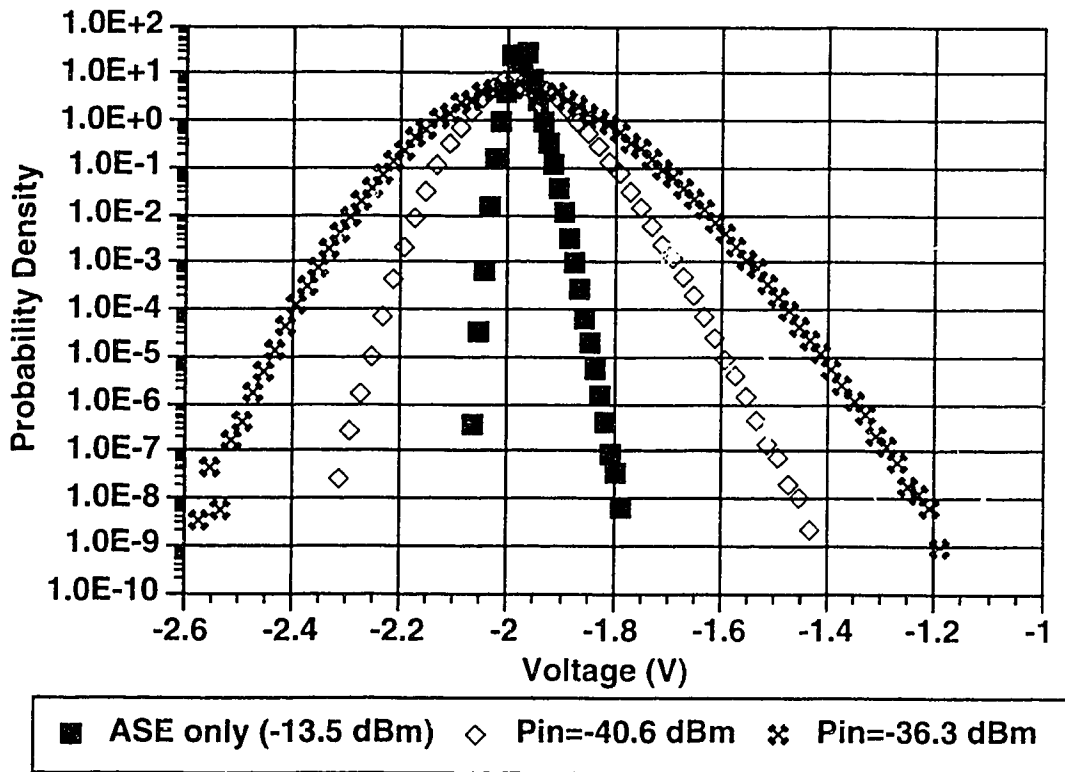


Fig. 5.2.3. Experimental PDFs of beat noises with polarizer, $G=32.4$ dB, $m_I=1$, Mini-Circuits amplifiers.

In this case, the net small signal gain of the EDFAs is about the same as the one used for Fig. 5.2.1. However the ASE power is much less than the one in Fig. 5.2.1. The sig-sp beat noise is more dominant at high laser powers. However there is no significant impact from inserting the polarization splitter on the asymmetry of the PDFs.

5.3. Comparison of Measured PDFs with Theories

We have chosen a few of the measured PDFs to be compared with the theoretical PDFs. The simulation parameters are summarized in Table 5.3.1.

Symbol	Description	Simulation Value	Experimental Value
λ_c	operating wavelength of laser	1550 nm	1550 \pm 1 nm
B_o	optical bandwidth	1.4x1.3 nm	1.4x1.3 \pm 0.1 nm
B_{elec}	two-sided electrical bandwidth	7 GHz	7 GHz (estimated)
R_{in}	input resistance of electrical amplifier	50 Ω	50 \pm 2 Ω
G_{elec}	net gain of electrical amplifiers	39.5-40.7 dB (for Figs. 5.3.1.b to 5.3.2.b) 49.5 dB (for Fig. 5.3.1.a)	41 \pm 1 dB (for Figs. 5.3.1.b to 5.3.2.b) 50 dB \pm 1 dB (for Fig. 5.3.1.a)
T_k	temperature	298 K	298 \pm 1 K
F	noise figure of electrical amplifier	8 dB	8 dB
\mathfrak{R}	responsivity of PIN diode	0.6 A/W	0.6 \pm 0.1 A/W

Table 5.3.1. Simulation and experimental parameters for PDF measurements using Mini-Circuits amplifiers.

The values of the simulation parameters in Table 5.3.1 are chosen to best fit the experimental data. For the purpose of shape comparison, the gain of the electrical amplifier is slightly varied in calculating the theoretical PDFs. The values of the electrical gain used are

reasonably close to the practical values. The discrepancies may due to experimental errors and the fact that the frequency dependent electrical gain is not included in the theoretical analyses. The discrepancies in the other parameters may result from the component tolerance (such as the input resistance of the electrical amplifier), and the limitation of measurement accuracy (such as the responsivity).

The shapes of the theoretical PDFs are in good agreement with the measured PDFs as it will be shown in Fig. 5.3.1 and Fig. 5.3.2. The two-sided electrical noise equivalent bandwidth is chosen to be 7 GHz because the single-sided bandwidth of the BERT is on the order of 3 GHz. The bandlimiting effect of the BERT will be shown in section 5.6. The PDF for the case of net small signal gain of EDFAs $G=32.4$ dB and $ASE=-13.5$ dBm was remeasured with the 20 dB attenuator between the two microwave amplifiers replaced by 10 dB such that the net electrical gain was about 50 ± 1 dB. This was done to increase the resolution of the PDF. The electrical gain used in the simulation for this case ($G=32.4$ dB, $ASE=-13.5$ dBm) was 49.5 dB. The measured ASE power and total power at the PIN diode were used in the equations in chapter 3 to evaluate the theoretical PDFs. The measured PDFs, the non-Gaussian theoretical PDFs and the Gaussian approximated PDFs are plotted in Fig. 5.3.1 to Fig. 5.3.2.

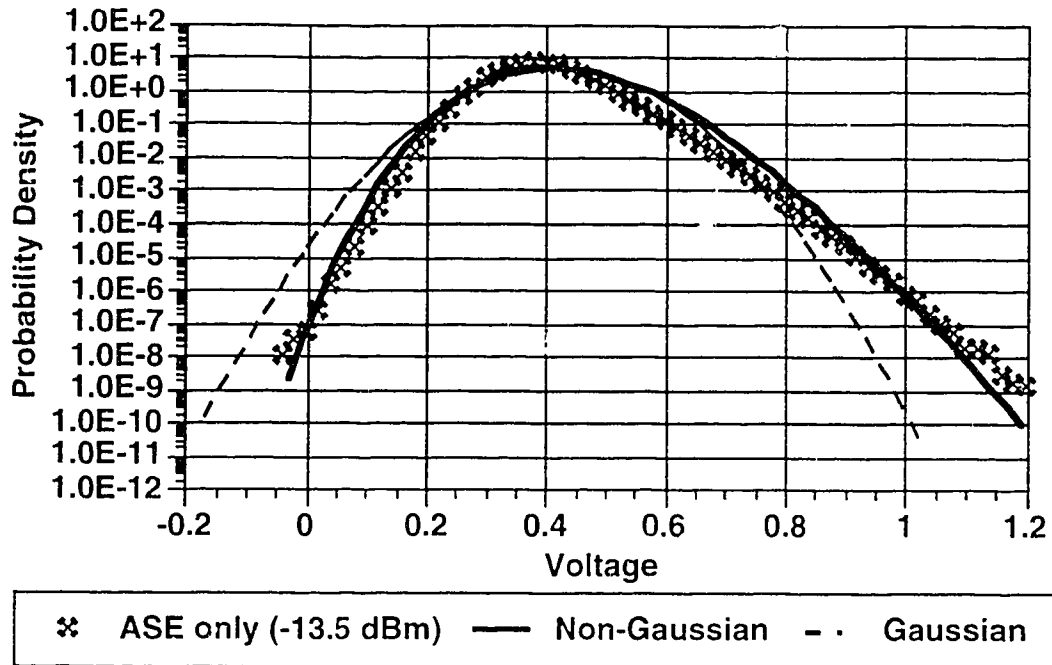


Fig. 5.3.1.a. Comparison of experimental PDF for ASE only with theories, $m_f=1$.

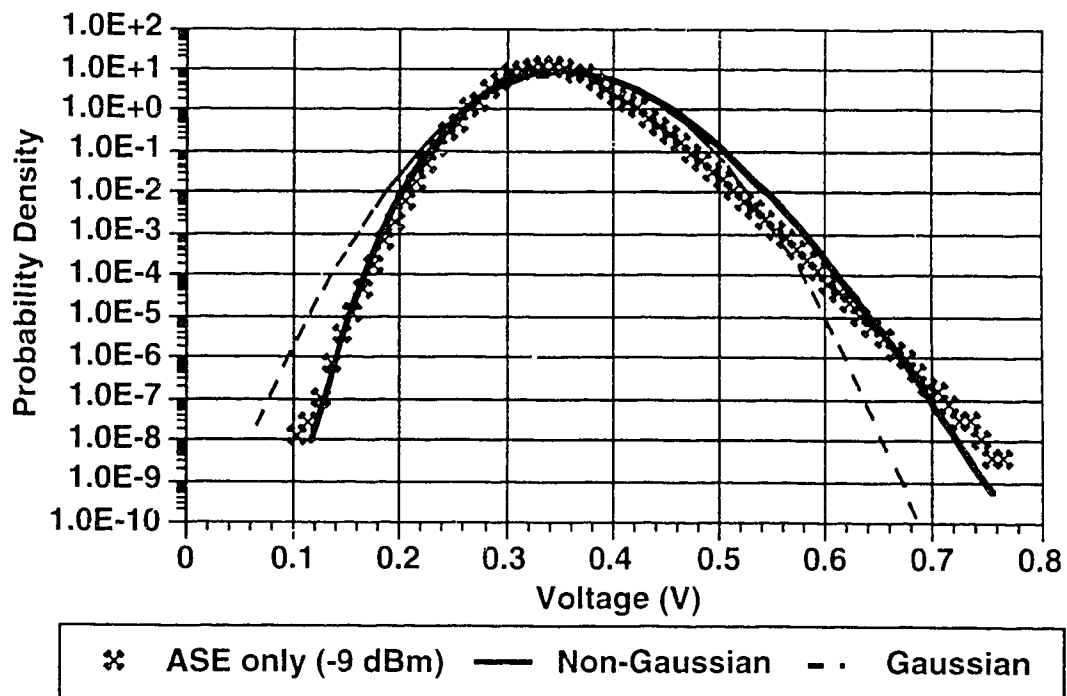


Fig. 5.3.1.b. Comparison of experimental PDF for ASE only with theories, $m_f=2$.

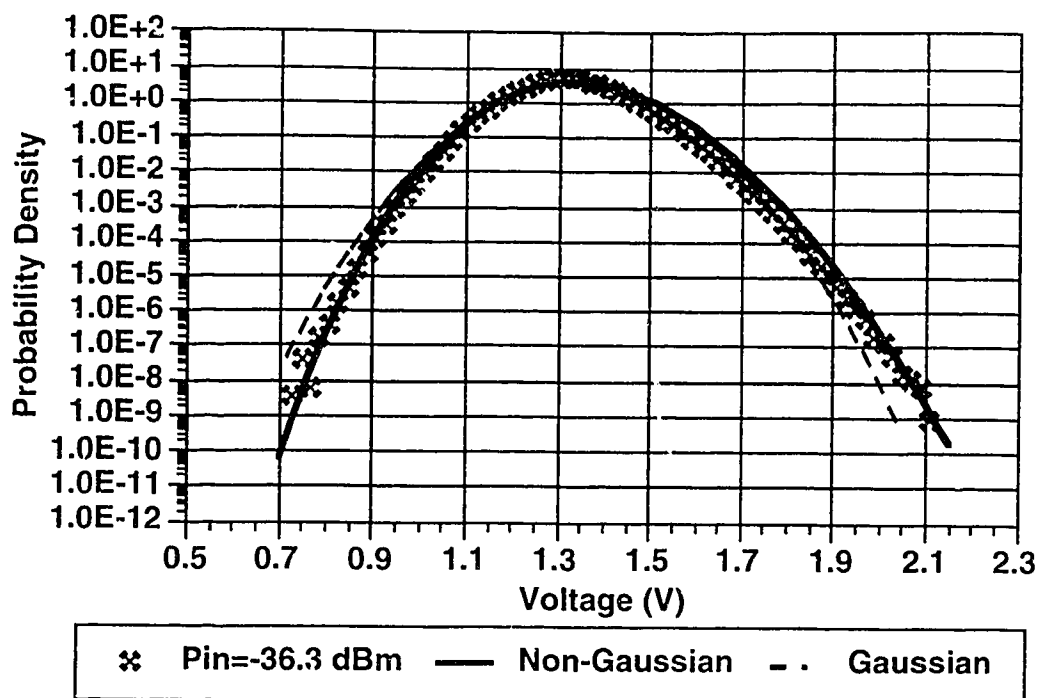


Fig. 5.3.2.a. Comparison of experimental PDF with theories, $m_l=1$, $P_{in}=-36.3$ dBm.

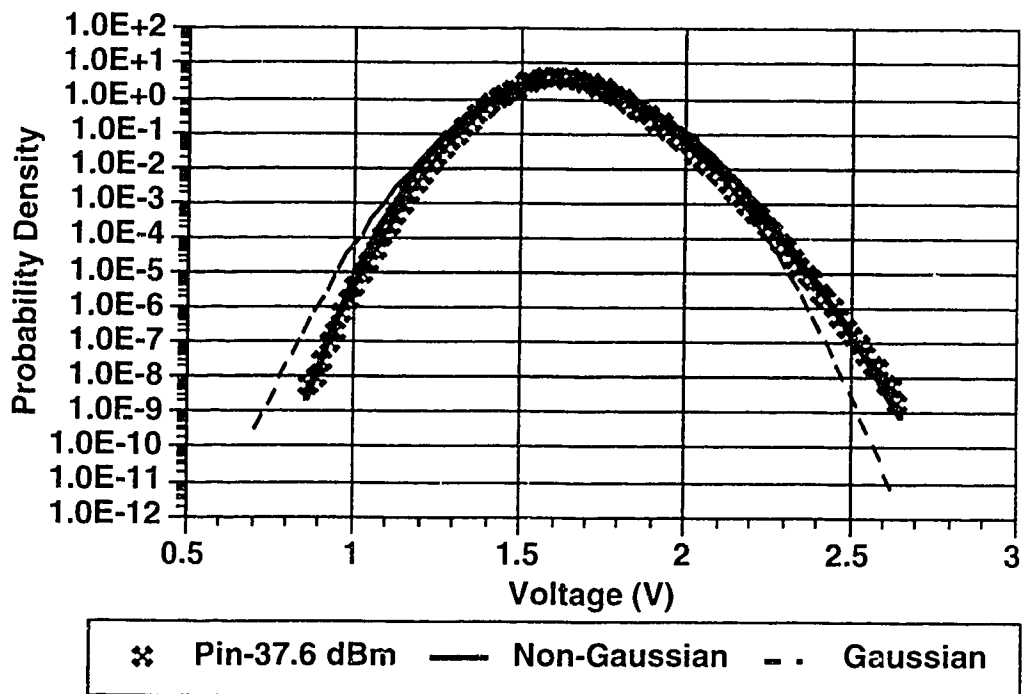


Fig. 5.3.2.b. Comparison of experimental PDF with theories, $m_l=2$, $P_{in}=-37.6$ dBm.

As it can be seen, the measured PDFs agree quite well with the non-Gaussian theory especially for the cases of ASE only. As the input laser power is increased, the differences between the non-Gaussian PDFs and the Gaussian PDFs within the range of observation become small to the point where any differences are negligible.

5.4. Measurement of PDFs with 10 GHz Electrical Amplifiers

In this experiment, two microwave amplifiers with single-sided 3-dB bandwidth of 10 GHz or wider are used such that the receiver electrical bandwidth is increased. The beat noises are handlimited by the BT&D PIN diode which has a single-sided noise equivalent bandwidth of about 6.5 GHz. The experimental setup is shown in Fig. 5.4.1.

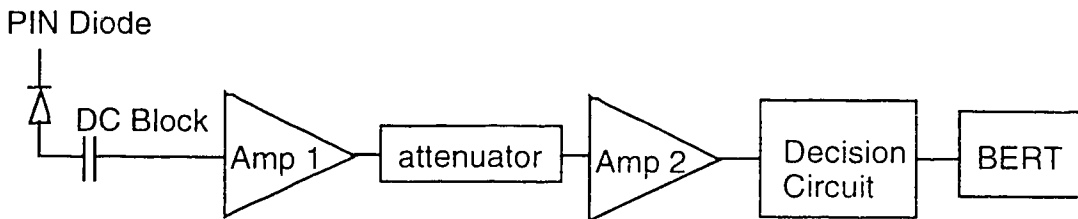


Fig. 5.4.1. Receiver for measuring PDFs with 10 GHz microwave amplifiers.

The receiver structure is basically the same as the one shown in Fig. 5.1.1.c except that a decision circuit is placed between the second amplifier and the BERT. The first amplifier is a SHF microwave amplifier which has a single-sided 3-dB bandwidth of about 15 GHz and gain of about 23 dB. The attenuator in Fig. 5.4.1 was set to 10 dB when the distribution of sp-sp beat noise was being measured and 20 dB for measuring the distribution of sig-sp plus sp-sp beat noise. The second amplifier is a Veritech microwave amplifier which has a single-sided 3-dB bandwidth of about 10 GHz and gain of about 34 dB. The noise figure of the amplifiers is about 7 dB. The decision circuit can function up to 10 Gb/s. The purpose of using the decision circuit will be discussed in section 5.5. The BERT can function up to 3 Gb/s.

5.5. The Function of the Decision Circuit

The probability of error P_e in equations (5.1.1) and (5.1.2) can be measured by using the BERT. However, because of the bandlimiting effect of the 3 Gb/s BERT, it cannot be directly connected to the output of the second electrical amplifier. If we were to use a BERT immediately after the second amplifier, the BERT would have to be functional for 10 Gb/s so that high frequency components of noise would not be attenuated. However, it is expensive to acquire a 10 Gb/s BERT. A simple solution to this has been obtained through two observations. First the noise process in the system is quite stationary which means the PDF can be measured by using any sampling rate (clock frequency). Second a digital decision circuit that functions up to 10 Gb/s will have minimal bandlimiting effect on the 10 GHz noise. Therefore the PDFs of the beat noises which are bandlimited by the PIN diode can be measured by placing a 10 Gb/s decision circuit in front of a low bit rate BERT (e.g., a 3 Gb/s BERT) as shown in Fig. 5.4.1.

The decision circuit can be modeled as a comparator followed by a digital flip flop as shown in Fig. 5.5.1.

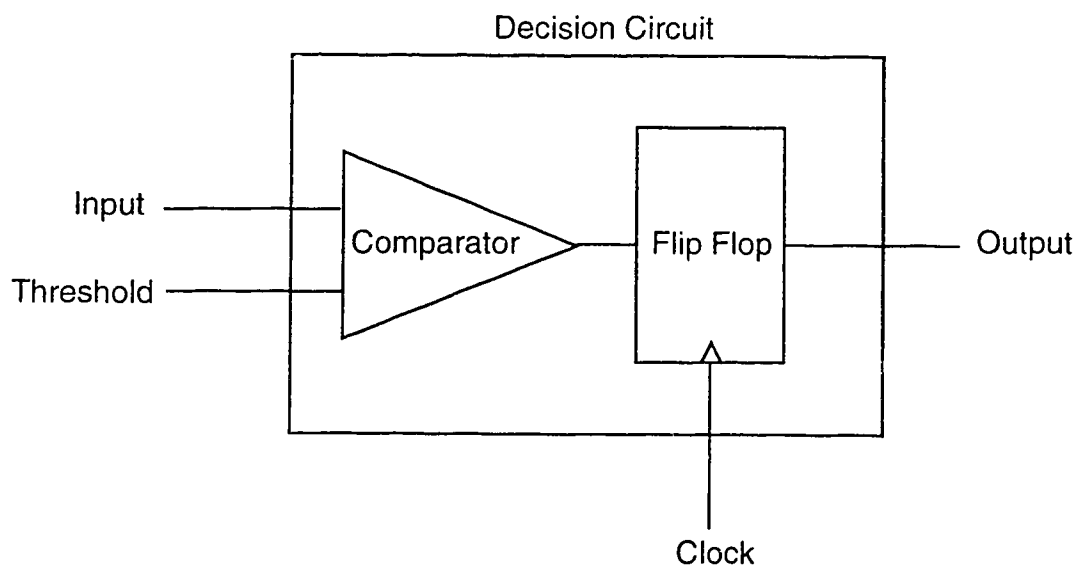


Fig. 5.5.1. Block diagram of the decision circuit.

Since the decision circuit is designed for decoding 10 Gb/s NRZ digital signal, it can preserve the high frequency noise components. The sampling rate is determined by the frequency of the clock applied to the flip flop. A faster clock will sample faster and hence is advantageous for measuring tails of PDF because it can save time. A slower clock will give the same results except that it is time consuming. The method for measuring the PDFs is the same as the one described in section 5.1. The only difference is that we are varying the voltage threshold applied to the decision circuit but not the threshold of the BERT. The input of the decision circuit was dc biased at -1 V and the noise rode on this level. The detection of the beat noises is similar to the diagram shown in Fig. 5.1.3 except the dc level is replaced by -1 V. The output of the decision circuit was a series of logical ones and logical zeros pulses which were triggered by the noise. The pulse amplitude was about 400 mV_{pp} and the dc level was -200 mV as shown in Fig. 5.5.2.a. The width of the pulse was determined by the sampling clock frequency. For example, the clock frequency used in Fig. 5.5.2.a was 3 GHz and hence the pulse width was about 336 ps. The built-in decision circuit of the BERT was used to detect the pulses triggered by the noise. The threshold of the BERT was set to -200 mV (middle of pulses) and the sampling time was set at the center of the pulses. The BERT was set to detect either all logical ones or all logical zeros. For example, when the threshold applied to the decision circuit was above -1 V, the BERT should be set to detect all logical zeros. Ideally if there was no noise, the output of the decision circuit would be at the logical zero level and the error rate would be zero as no pulses were triggered by noise. On the other hand if there was noise, pulses would be generated at the decision circuit output. Therefore errors would be made and captured by the BERT. Fig. 5.5.2.a and 5.5.2.b show the output of the decision circuit when the error rates were about 4×10^{-1} and 1×10^{-3} and the BERT was detecting all logical ones.

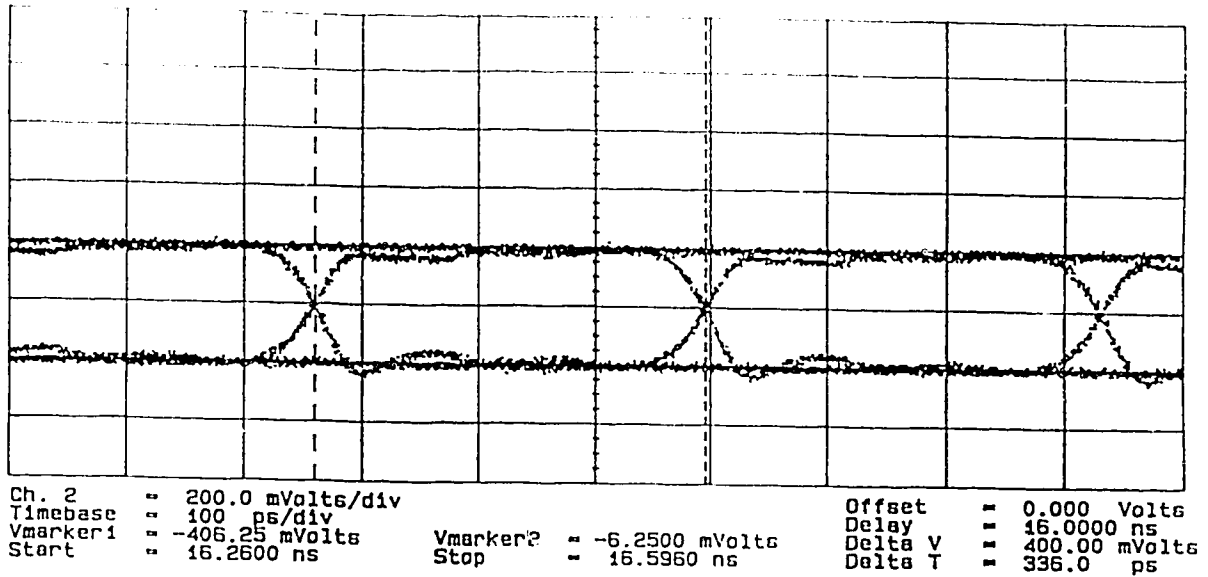


Fig. 5.5.2.a. Eye diagram of pulses at decision circuit output, $BER=4 \times 10^{-1}$.

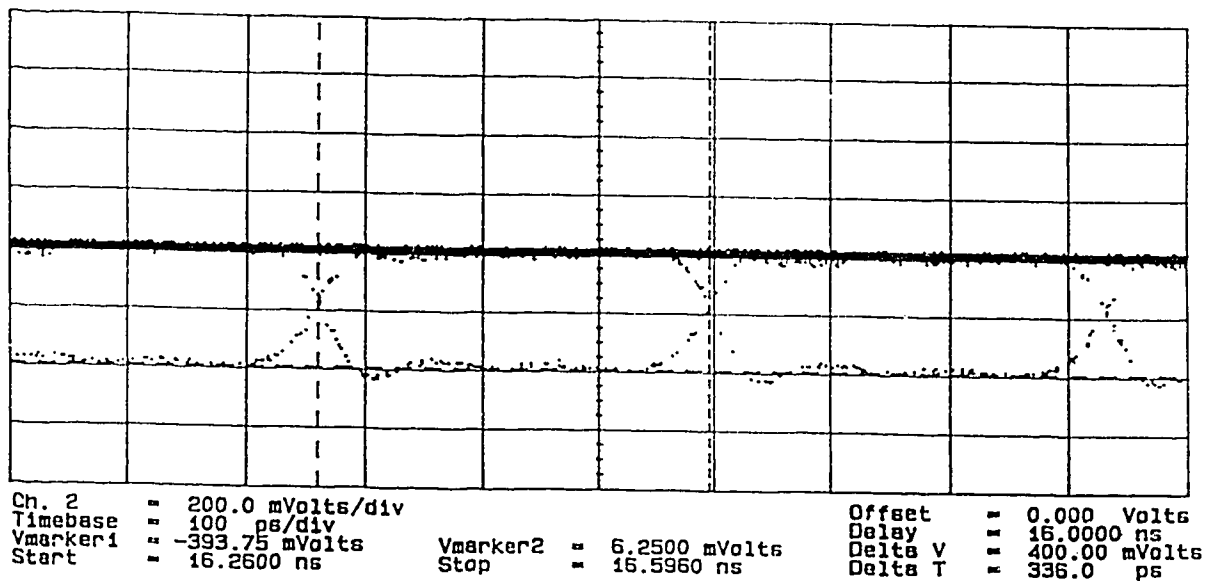


Fig. 5.5.2.b. Eye diagram of pulses at decision circuit output with $BER=1 \times 10^{-3}$.

As it can be seen from Fig. 5.5.2.b, the output of the decision circuit was most of the time at the logical one level. Occasionally, pulses at logical zeros level would be triggered by the noise and hence errors were made.

5.6. Results On PDFs Using 10 GHz Electrical Amplifiers

The first measurement was done with the net small signal gain of the EDFAs set to about 32 dB and the laser was turned off. The total ASE power at the PIN diode was about -10.7 dBm. The attenuator was chosen to be 10 dB so that the net electrical gain was about 47 ± 1 dB. The BERT was set to run at the maximum clock frequency 3 GHz. The measured PDF is shown in Fig. 5.6.1 and is compared with the non-Gaussian theory and the Gaussian theory. The simulation and experimental values of the parameters used are shown in Table 5.6.1. For the theoretical PDFs, the two-sided electrical bandwidths for the beat and shot noises are 13 GHz because of the bandlimiting effect of the PIN diode (see section 5.1). Since the thermal noise is not a dominant noise, the two-sided electrical bandwidth for the thermal noise is chosen to be 20 GHz. The measurement was repeated with a polarizer inserted. The ASE power at the PIN was -14 dBm and the result is shown in Fig. 5.6.2.

Symbol	Description	Simulation Value	Experimental Value
λ_c	operating wavelength of laser	1550 nm	1550 ± 1 nm
B_o	optical bandwidth	1.4x1.3 nm	$1.4 \times 1.3 \pm 0.1$ nm
B_{electh}	two-sided noise equivalent electrical bandwidth for thermal noise	20 GHz	> 20 GHz
B_{elec}	two-sided noise equivalent electrical bandwidth for beat and shot noises	13 GHz	13 ± 1 GHz
R_{in}	input resistance of electrical amplifier	50 Ω	50 ± 2 Ω
G_{elec}	net gain of electrical amplifiers	44-45.5 dB (for Figs. 5.6.1 to 5.6.2) 34.8-36 dB (for Figs. 5.6.4 to 5.6.7)	47 ± 1 dB (for Figs. 5.6.1 to 5.6.2) 37 ± 1 dB (for Figs. 5.6.4 to 5.6.7)
T_k	temperature	298 K	298 ± 1 K
F	noise figure of electrical amplifier	7 dB	7 dB
\Re	responsivity of PIN diode	0.6 A/W	0.6 ± 0.1 A/W

Table 5.6.1. Simulation and experimental parameters for PDF measurements using SHF and Veritech amplifiers.

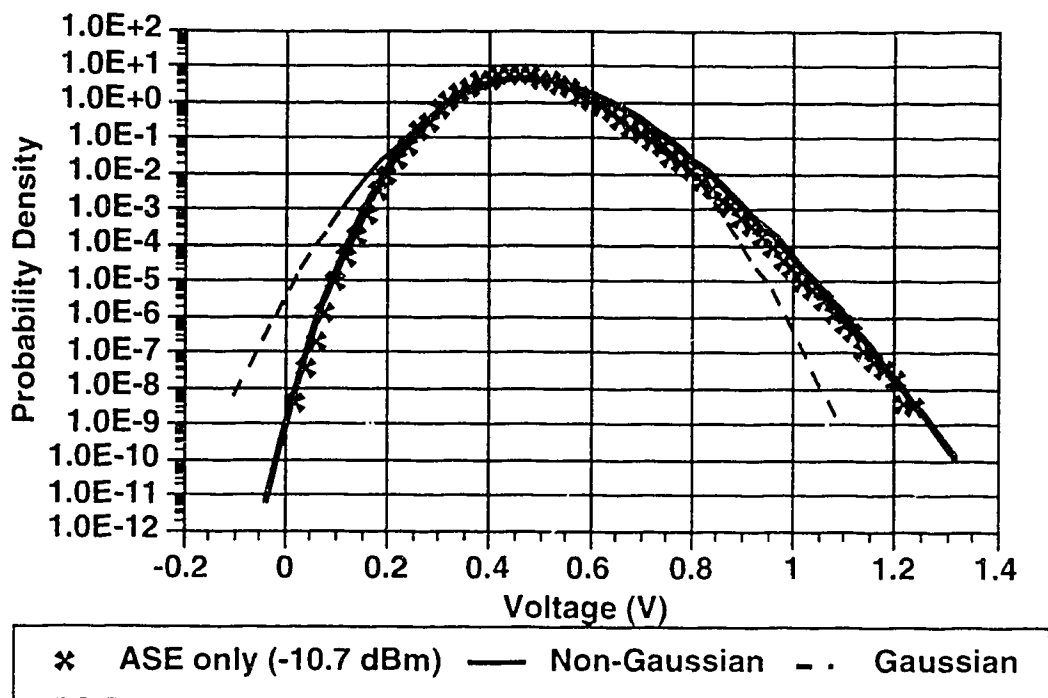


Fig. 5.6.1. Comparison of PDFs, $m_l=2$, ASE=-10.7 dBm.

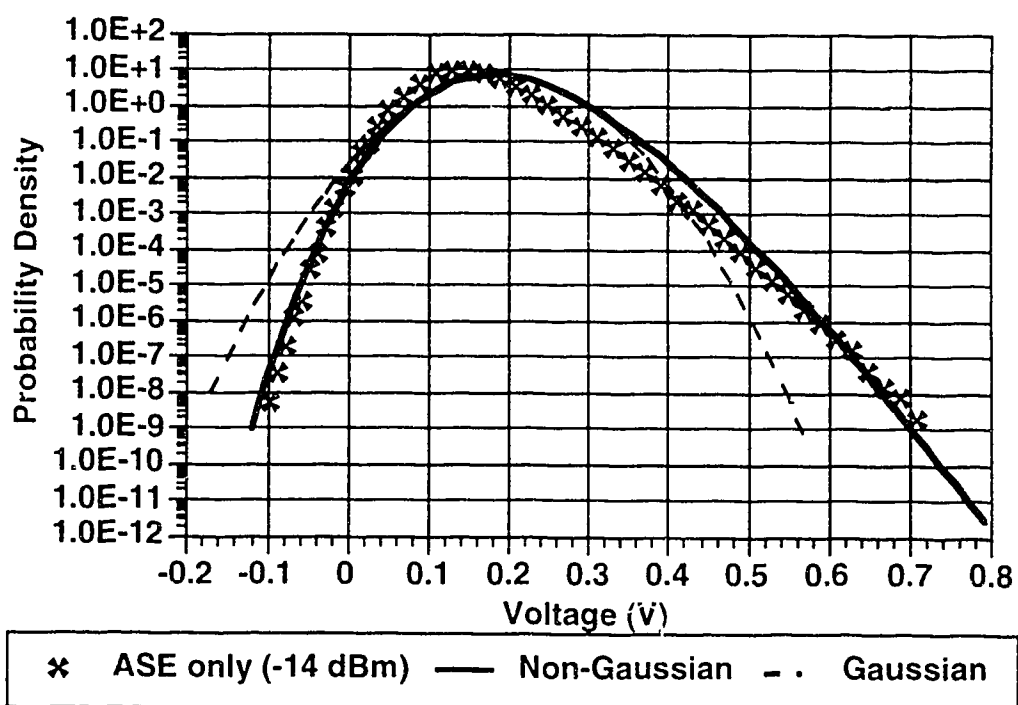


Fig. 5.6.2. Comparison of PDFs, $m_l=1$, ASE=-14 dBm.

As it can be seen from Fig. 5.6.1 and 5.6.2, the shapes of the measured PDFs agree very well with the non-Gaussian theory. In order to show that the measurement is independent of sampling rate, we measure the sp-sp beat noise PDF (for $m_I=2$ and $P_{ave}=-10.7$ dBm) using a 1 GHz clock. We also measured the PDF by removing the decision circuit and using the BERT directly to show that the decision circuit does preserve the high frequency components of the noise. The results are shown in Fig. 5.6.3. It can be seen that the PDF obtained from using the 1 GHz clock is reasonably close to the one using 3 GHz clock.

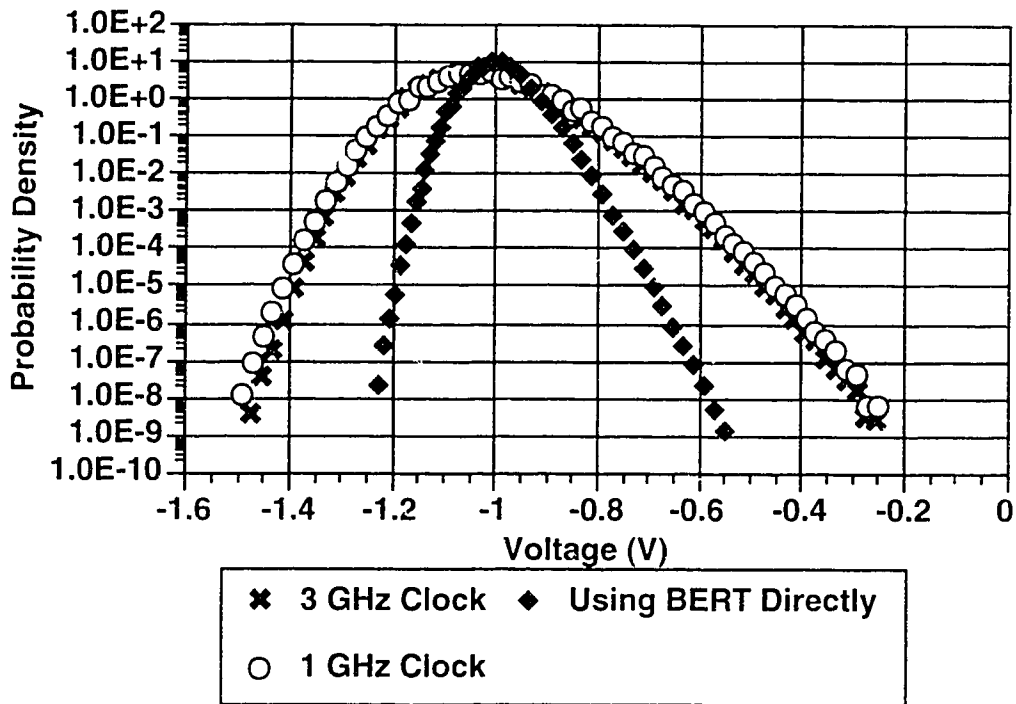


Fig. 5.6.3. Comparison of experimental PDFs obtained from using different clock frequency and from using the BERT directly.

In addition the PDF obtained from using the BERT directly is much narrower than the ones obtained from using the decision circuit. The narrowing of the PDF is due to the loss of noise power caused by bandlimiting effect of the BERT on high frequency components of noise.

The laser was then turned on in order to measure the distribution of sig-sp plus sp-sp beat noises. The attenuator was changed to 20 dB such that the overall gain was about 37 dB (34.8 to 36 dB was used for the theoretical PDFs). The VOA was adjusted such that the signal power at the input of the EDFAs was -39.7 dBm. The ASE power and the total power at the PIN were -10.8 and -6.0 dBm respectively. The net small signal gain of EDFAs can then be calculated to be about 32 dB. The measurement was also repeated with the polarizer inserted. The input power to the EDFAs, the ASE power and the total power at the PIN were -32.3, -14.3 and -6.0 dBm respectively. The net small signal gain of EDFAs is about 25.6 dB. The total power at the PIN is the same as the previous case but the input power to the EDFAs is higher because of the loss due to polarization misalignment between the signal electric field and the axis of the polarization splitter. However since only the signal power at the PIN diode is important, we can compensate the loss by increasing the signal power at the input of the EDFAs. The measured PDFs are shown in Fig. 5.6.4 and 5.6.5.

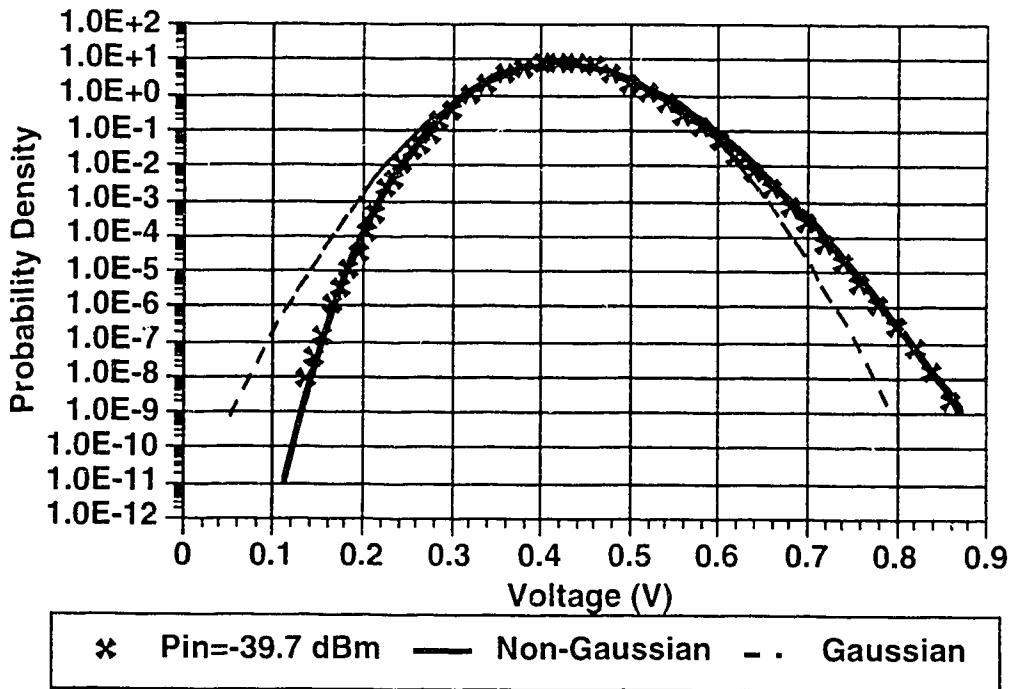


Fig. 5.6.4. Comparison of PDFs, $m_t=2$, $P_{in}=-39.7$ dBm.

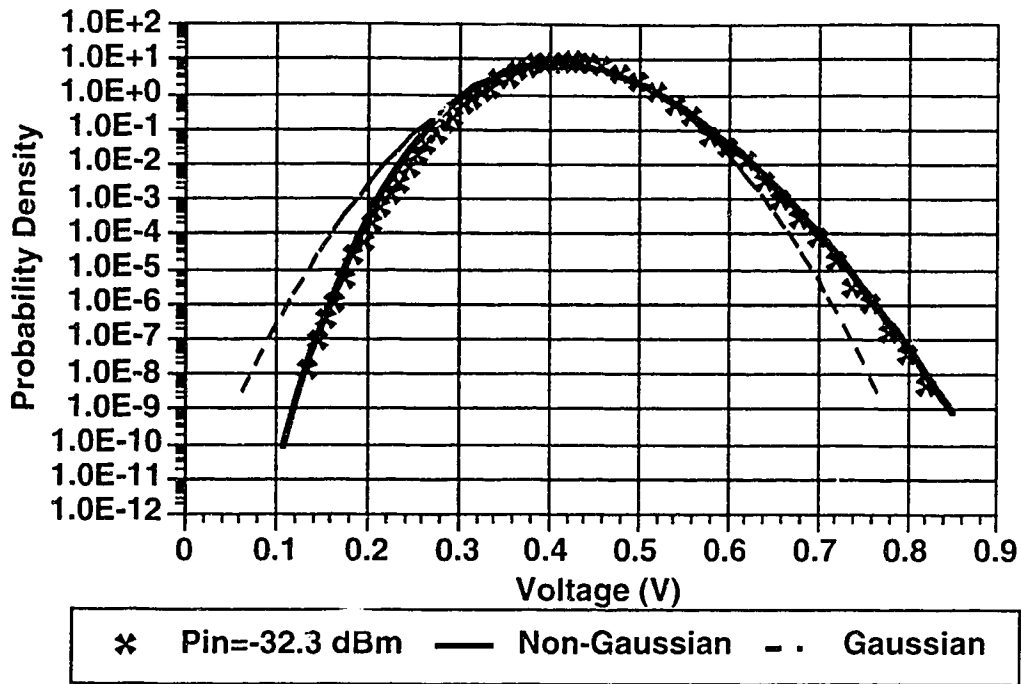


Fig. 5.6.5. Comparison of PDFs, $m_I=1$, $P_{in}=-32.3$ dBm.

The last measurement was done with a laser power level which could represent a logical one. The input power, the ASE power and the total power were -35, -10.5 and -2.5 dBm respectively. The net small signal gain of EDFAs was about 31.8 dB. For the case with the polarizer inserted, the input power, the ASE power and the total power were -30.3 dBm, -13.8 and -2.4 dBm respectively, and the net small signal gain of EDFAs was about 27.5 dB. High input power is needed again because of loss due to polarization misalignment. The results are shown in Fig. 5.6.6 and 5.6.7.

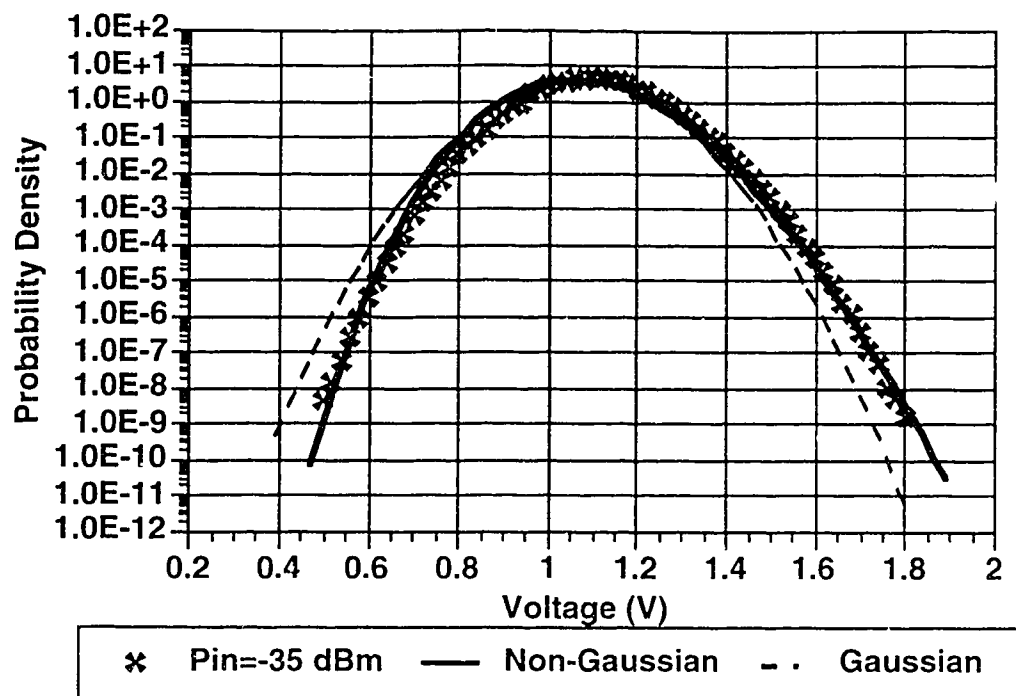


Fig. 5.6.6. Comparison of PDFs, $m_t=2$, $P_{in}=-35$ dBm.

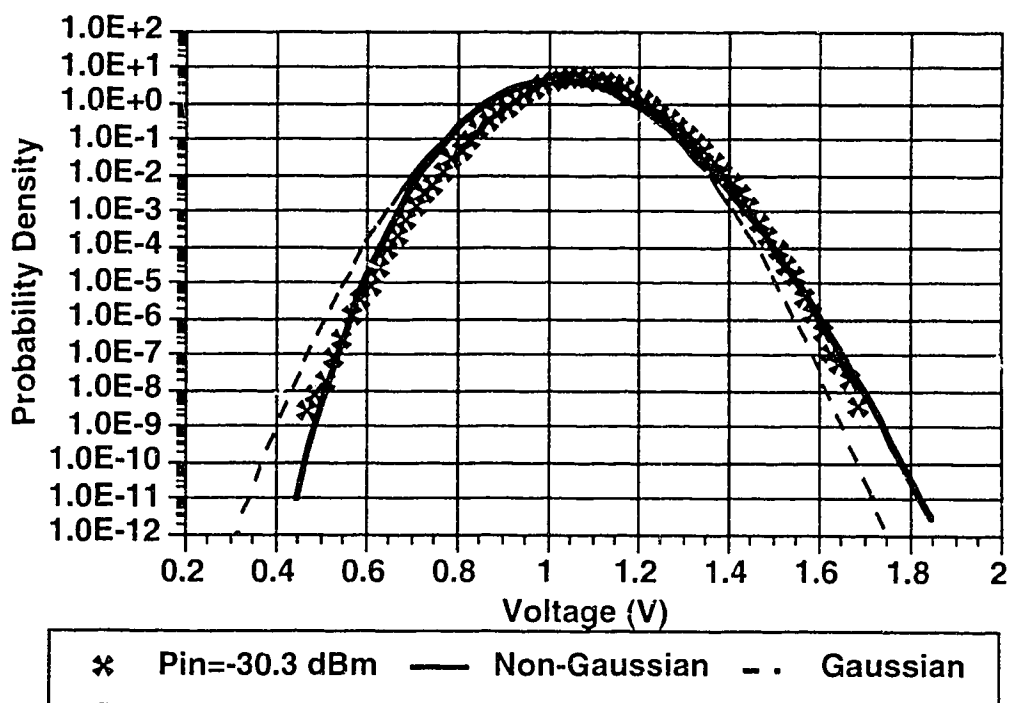


Fig. 5.6.7. Comparison of PDFs, $m_t=1$, $P_{in}=-30.3$ dBm.

As it can be seen from Fig. 5.6.6 and 5.6.7, at high laser power, it is difficult to distinguish the Gaussian PDF from the non-Gaussian PDF.

5.7. The Percentage Optimum Threshold Measurement

It has been shown in chapter 4 that the percentage optimum threshold predicted by the non-Gaussian PDFs is very different from the one predicted by the Gaussian PDFs when the electrical bandwidth is sufficiently wide and the EDFA small signal gain is sufficiently high. In order to experimentally verify the optimum threshold, the DFB laser in Fig. 5.1.1.a was directly modulated with digital pulses as shown in Fig. 5.7.1. The EDFAs and the receiver are the same as the ones in Fig. 5.1.1.b and Fig. 5.4.1 respectively.

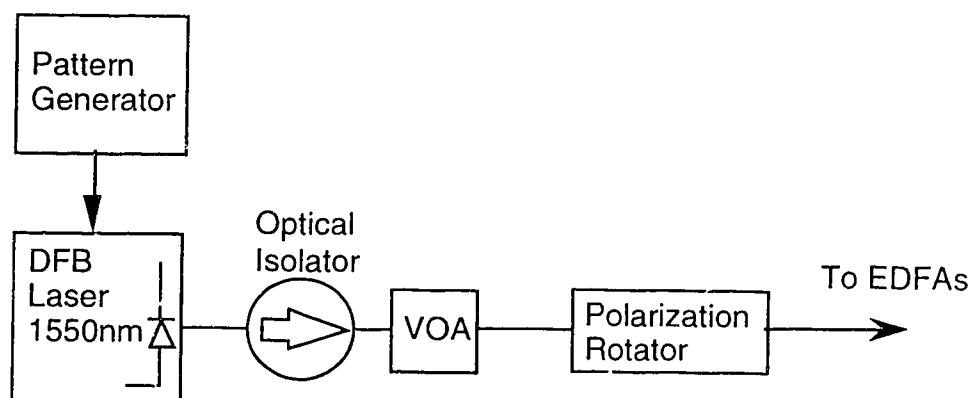


Fig. 5.7.1. Direct modulation of 1550 nm DFB laser.

The output light power versus drive current transfer characteristic of the DFB laser has been measured by varying the dc bias current and is shown in Fig. 5.7.2.

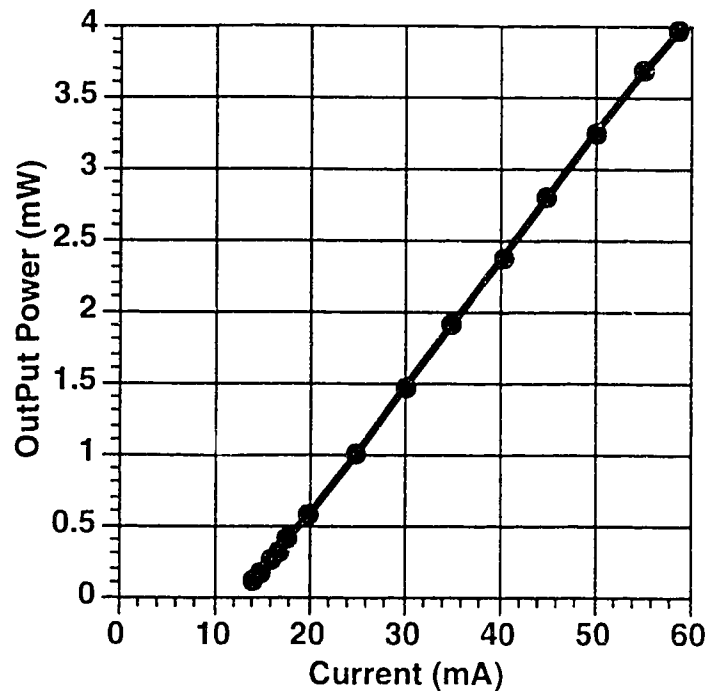


Fig. 5.7.2. The transfer characteristic of 1550 nm DFB laser.

The threshold current is about 15 mA at which the output power is about -7.8 dBm. The laser current driver can provide a maximum current of about 58.9 mA at which the output power is about 6 dBm. The electrical input port of the laser has an input impedance of 50 Ω . The bias current is set to 35 mA. The input data from the pattern generator has a peak-to-peak amplitude of 2 V_{pp} which corresponds to 40 mA_{pp}. Therefore the logical zero is at 15 mA or -7.8 dBm. The logical one is at 55 mA or 5.7 dBm. The extinction ratio is then about -13.5 dB. The single-sided 3-dB modulation bandwidth of the laser is about 1 GHz. In order to minimize ISI and obtain a nearly perfect square wave, the simple pattern 10101010 ... at 100 Mb/s is used. The square wave acts like a 'noise carrier'. Since there is minimum ISI, the BER is mainly due to the noise riding the square wave. The optimum threshold will be the crossing point of the tails of the PDFs of logical ones and logical zeros. The waveforms of the pulses used to drive the laser, the waveform of the received pulses and the received pulses with noise are shown in Fig. 5.7.3.(a-d).

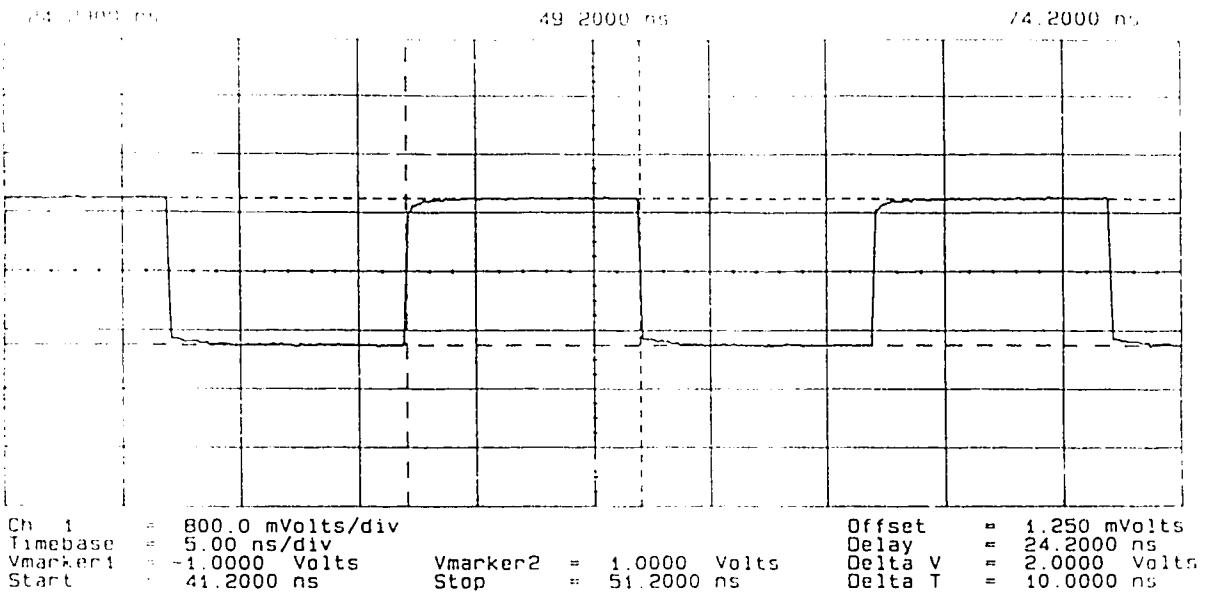


Fig. 5.7.3.a. Pulses used to drive the laser.

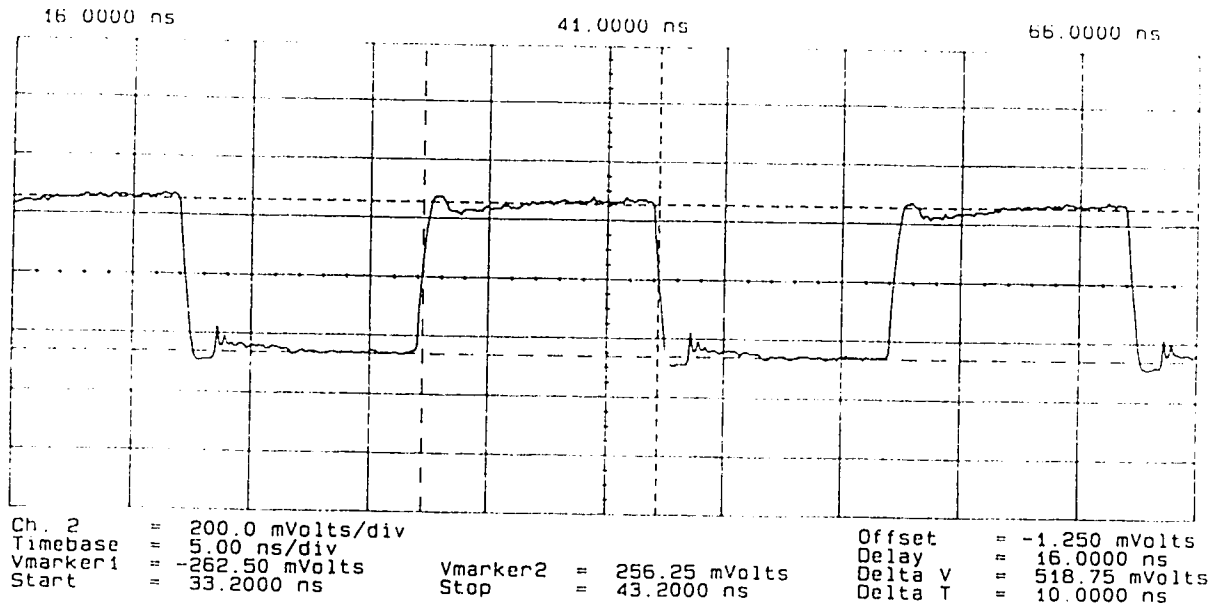


Fig. 5.7.3.b. Waveform of received pulses.

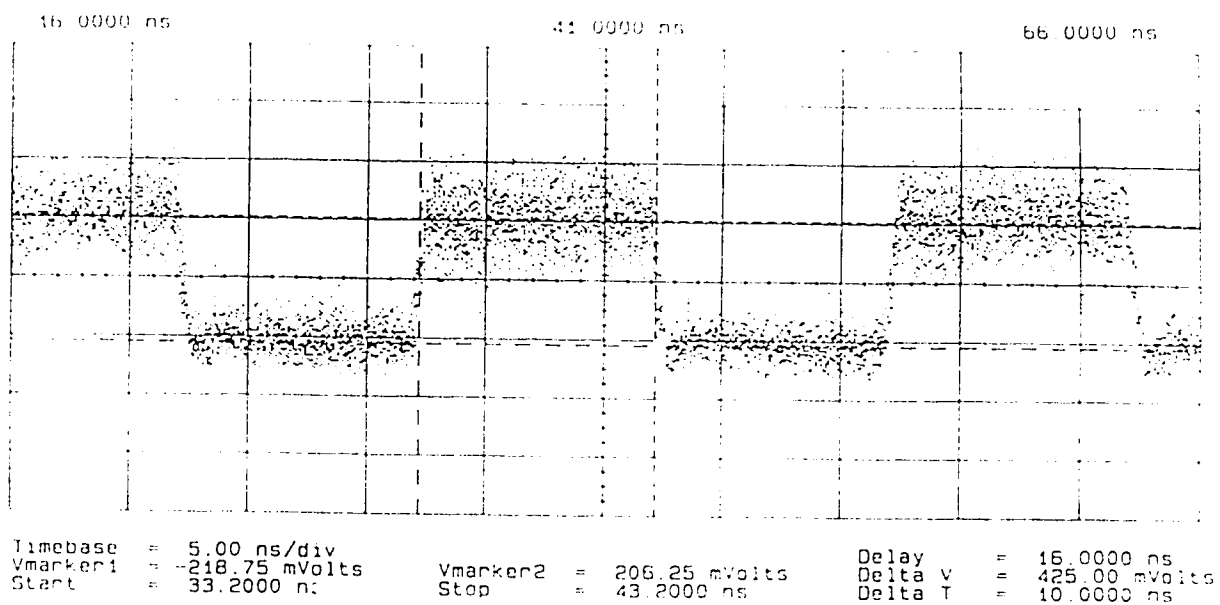


Fig. 5.7.3.c. Received pulses with noise, $G=32$ dB, $m_t=2$.

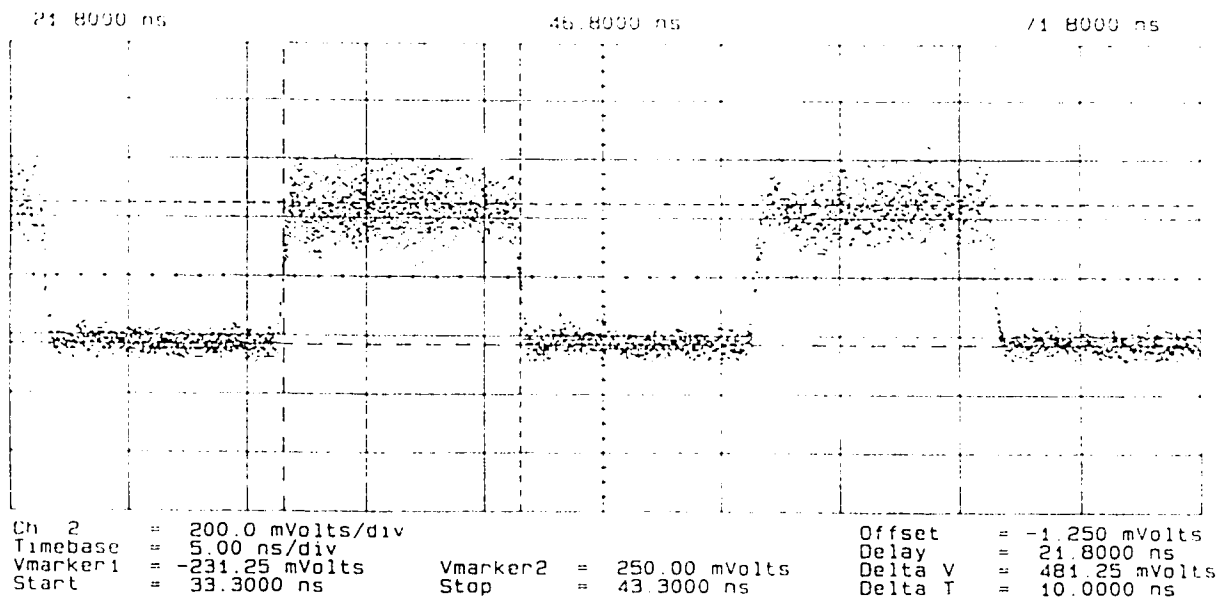


Fig. 5.7.3.d. Received pulses with noise, $G=31$ dB, $m_t=1$.

5.8. Experimental Results on Percentage Optimum Threshold

The first measurement was done with the net small signal gain of the EDFAs set to about 32 dB and the polarization splitter was removed ($m_t=2$). The measured optimum threshold was in terms of voltage and was converted to percentage optimum threshold by using the mean values of the logical ones and logical zeros. The mean values of logical ones and logical zeros were measured by using the digital sampling oscilloscope (HP 54120B) and the four-channel tester (54123A). The histogram function on the digital sampling oscilloscope was used to collect the voltage samples of the noise corrupted logical ones and logical zeros and hence determine the mean values. The measured BER is plotted against the received power and the experimental curve is compared with the theoretical curves as shown in Fig. 5.8.1.a. The simulation parameters used for the theoretical curves are shown Table 5.8.1. The input resistance and the gain of the electrical amplifiers are not important in this experiment since the decision thresholds are converted to percentage threshold. Therefore they are omitted from Table 5.8.1. The measured net small signal gains of EDFAs are used for calculating the theoretical curves that are shown in the following figures. The measured net small signal gain of EDFAs and the measured ASE power are used to calculate the spontaneous emission factor N_{sp} of the three cascaded EDFAs using equation (2.10.2.6) (recall that the three cascaded EDFAs are treated as a single EDFA preamplifier). The value of the spontaneous emission factor is about 1.3 and is also used in calculating the theoretical curves.

Symbol	Description	Simulation Value	Experimental Value
λ_c	operating wavelength of laser	1550 nm	1550 ± 1 nm
B_o	optical bandwidth	1.4x1.3 nm	$1.4 \times 1.3 \pm 0.1$ nm
B_{electh}	two-sided noise equivalent electrical bandwidth for thermal noise	20 GHz	> 20 GHz
δ	extinction ratio	-13.5 dB	-13.5 ± 0.1 dB
G_o	EDFA small signal gain	32 dB (for Figs. 5.8.1.(a-c)) 31 dB (for Figs. 5.8.2.(a-c))	32 ± 1 dB (for Figs. 5.8.1.(a-c)) 31 ± 1 dB (for Figs. 5.8.2.(a-c))
B_{elec}	two-sided noise equivalent electrical bandwidth for beat and shot noises	13 GHz	13 ± 1 GHz
N_{sp}	spontaneous emission factor of EDFA	1.3	1.3 ± 0.1
R_m	input resistance of electrical amplifiers	50 Ω	50 ± 2 Ω
T_k	temperature	298 K	298 ± 1 K
F	noise figure of electrical amplifier	7 dB	7 dB
\Re	responsivity of PIN diode	0.6 A/W	0.6 ± 0.1 A/W

Table 5.8.1. Simulation and experimental parameters for threshold measurements using SHF and Veritech amplifiers.

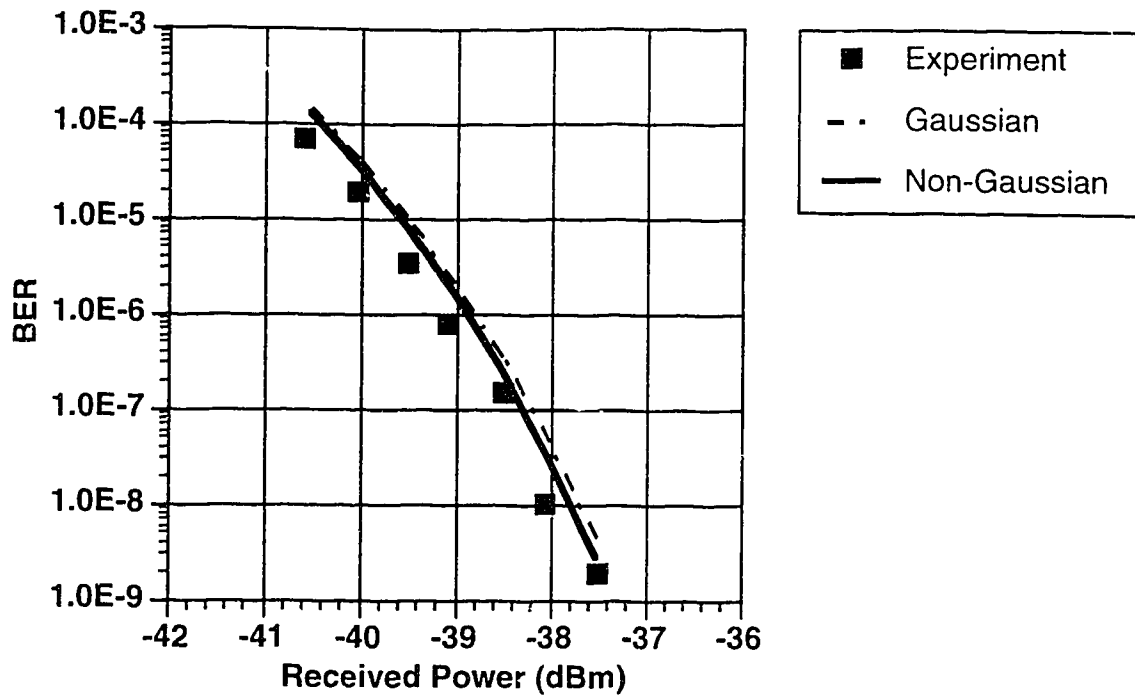


Fig. 5.8.1.a. BER versus Received Power, $G=32$ dB, $m_f=2$.

It can be seen from Fig. 5.8.1.a that the experimental curve agrees well with the theoretical curves. However from Fig. 5.8.1.(b-c), it can be seen that the experimental percentage optimum thresholds agree more with the non-Gaussian theory than the Gaussian theory. The Gaussian theory predicts a much lower percentage optimum threshold and a much faster decrease in the percentage optimum threshold than the non-Gaussian theory. The experimental percentage optimum thresholds carry about $\pm 1\%$ errors. However the errors are small compared with the separation between the non-Gaussian and the Gaussian curves which is ranged from about 6 to 9 %.

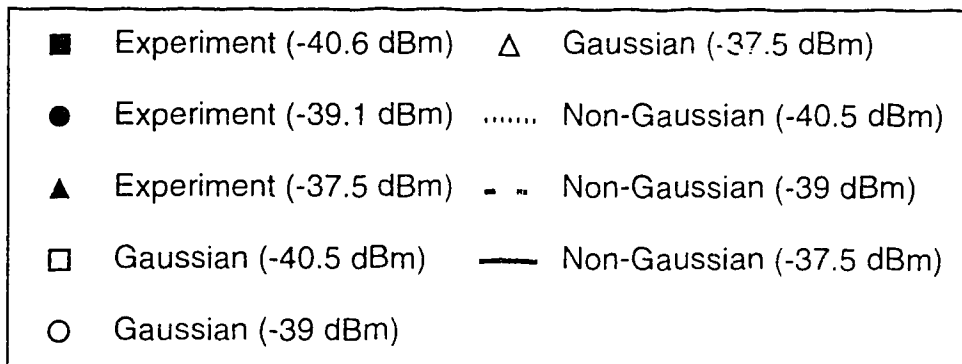
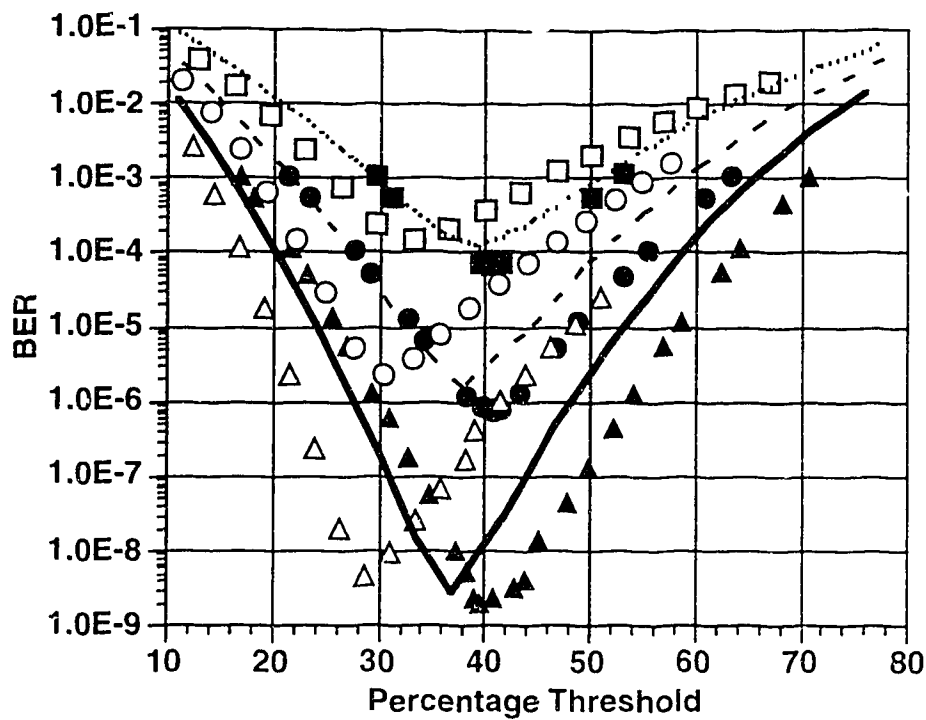


Fig. 5.8.1.b. BER versus Percentage Optimum Threshold, $G=32$ dB, $m_f=2$.

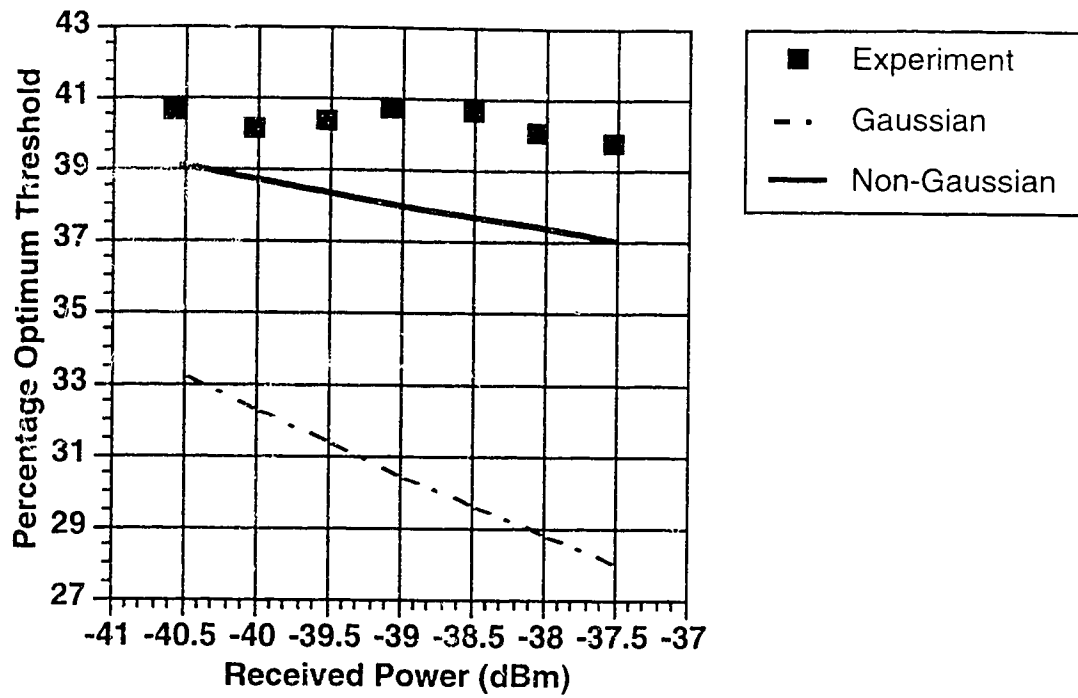


Fig. 5.8.1.c. Percentage Optimum Threshold versus Received Power, $G=32$ dB, $m_l=2$.

For the purpose of comparison, the measurement is repeated with the polarization splitter inserted. The BER versus received power curves, the BER versus percentage threshold curves, and the percentage optimum threshold versus received power curves are shown in Fig. 5.8.2.(a-c) respectively.

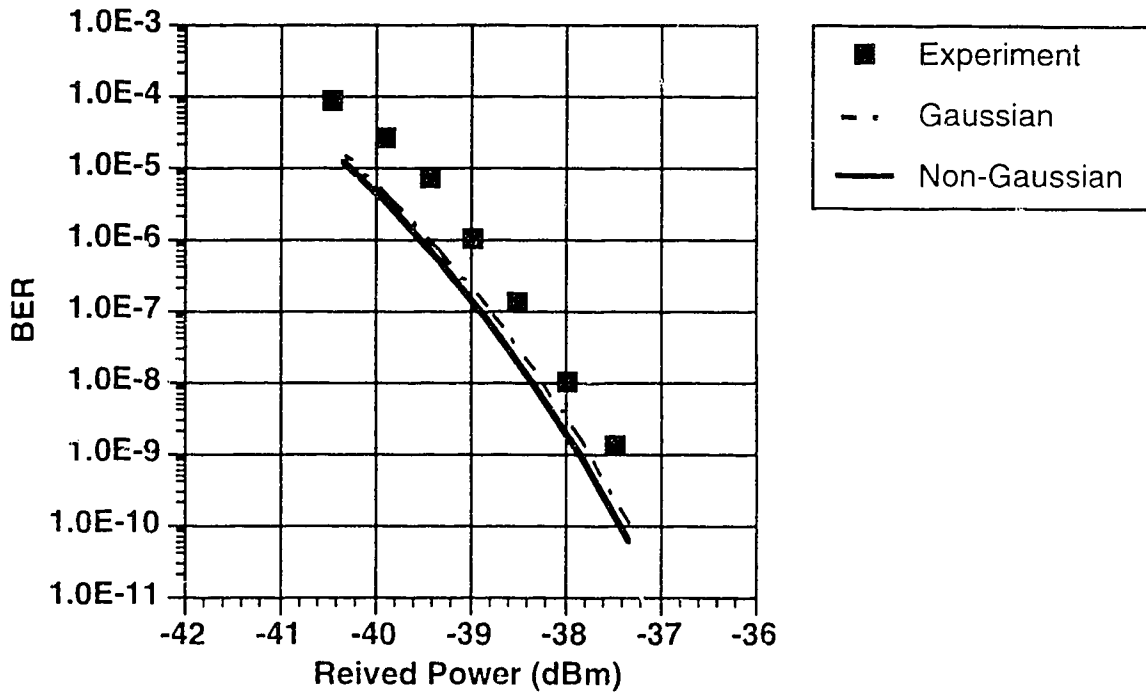


Fig. 5.8.2.a. BER versus Received Power, $G=31$ dB, $m_I=1$.

From Fig. 5.8.2.(b-c), it can be seen that the experimental percentage optimum thresholds again agree more with the non-Gaussian theory than the Gaussian theory. The percentage optimum thresholds are lower than the ones shown in Fig. 5.8.1.c. This is because the sp-sp beat noise, which is the dominant noise for the logical zeros, is reduced when the polarization splitter is used.

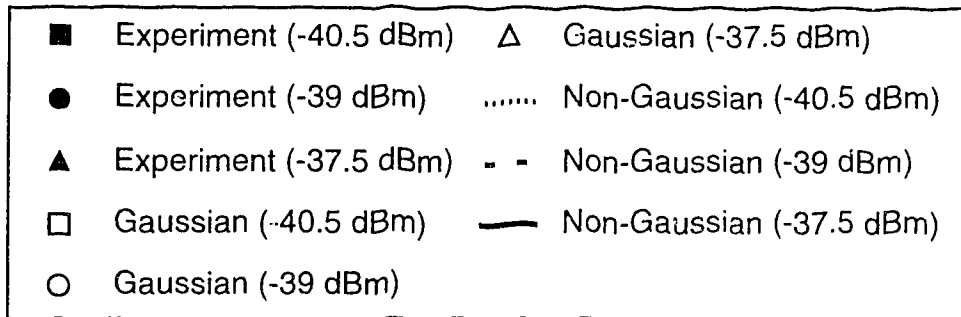
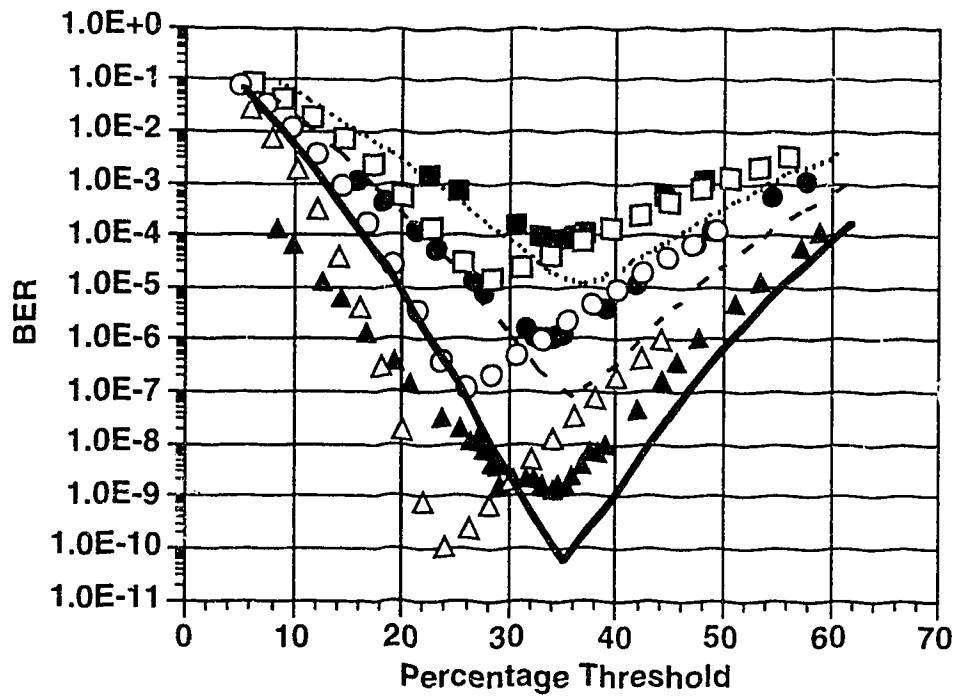


Fig. 5.8.2.b. BER versus Percentage Optimum Threshold, $G=31$ dB, $m_t=1$.

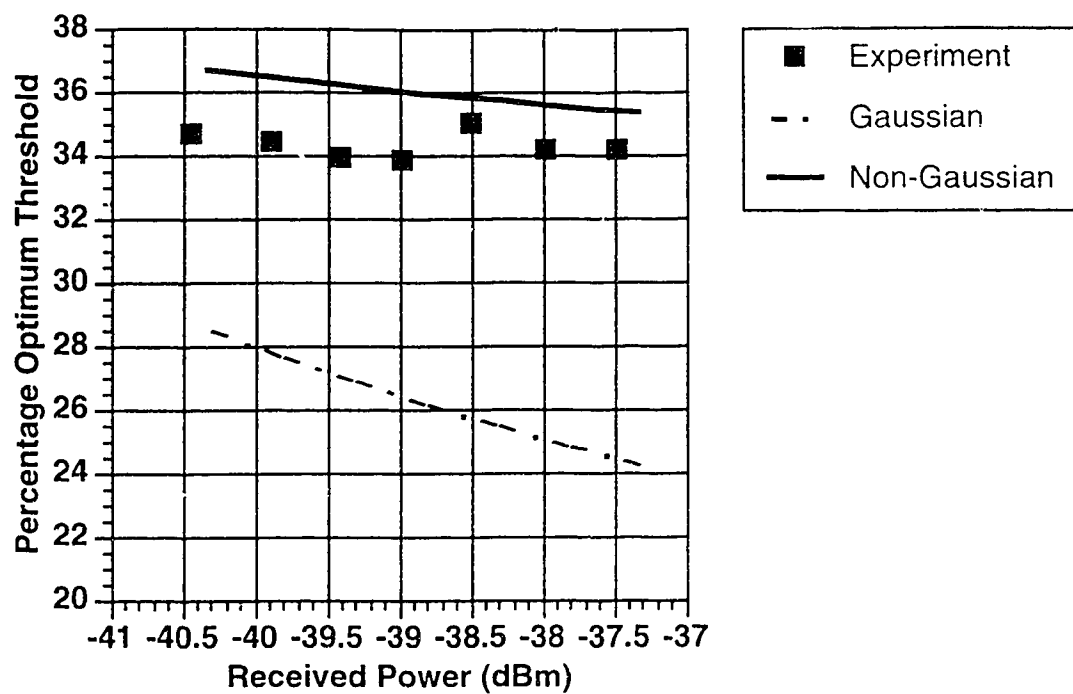


Fig. 5.8.2.c. Percentage Optimum Threshold versus Received Power, $G=31$ dB, $m_f=1$.

6. The OC-192 System

In this chapter, the performance of an OC-192 system will be studied and evaluated. The following measurements were done at division one of Bell Northern Research (BNR) where an OC-192 transmission system was designed and set up. The OC-192 system is a digital lightwave system which transmits data at a bit rate of approximately 10 Gb/s. Because of this high bit rate, the receiver has been designed with single-sided bandwidth of about 10 GHz. The investigations include using EDFAs as optical preamplifiers and using 81 km of fiber in the system.

In chapter 5, we have already looked at the non-Gaussian PDFs and the impact of the non-Gaussian PDFs on percentage optimum thresholds for an EDFA preamplified digital system with a wide-band receiver. We have also compared the results with the Gaussian and non-Gaussian theories and have found reasonably good agreements. However the ISI has been neglected in the theoretical analyses and in the earlier experiments. In a real system such as the OC-192 system, the ISI will play an important role in the system performance. When long fibers are used in the OC-192 system, fiber dispersion is also an important issue that has to be taken into account. Therefore this chapter is devoted to the experimental studies of these effects.

For the purpose of comparison, three different setups of the OC-192 system were studied. The first setup is a simple back to back system in which no EDFAs or fibers were used. The second setup has an EDFA preamplifier inserted such that the impact of the EDFA can be studied. The third setup has an EDFA preamplifier and 81 km of fibers inserted such that the impact of long fibers can be studied. The bit rate used for the following measurements was at the exact OC-192 bit rate of 9.953280 Gb/s. The length of the pseudo random bit sequence (PRBS) used was $2^{23}-1$ for all the measurements. The three setups of the OC-192 system are described in sections 6.1 and 6.2. Some characteristics of an EDFA preamplifier are shown in section 6.3. The sensitivity, the constant BER contours, and the

optimum thresholds of the OC-192 system will be presented and discussed in section 6.4.

6.1. Back to Back OC-192 System

In order to investigate the impact of inserting EDFA, optical BPF and long fibers on the OC-192 system, the measurement was done first with a back to back system with 0 km of fiber and no EDFA. The block diagram of the transmitter of the OC-192 system is shown in Fig. 6.1.1.

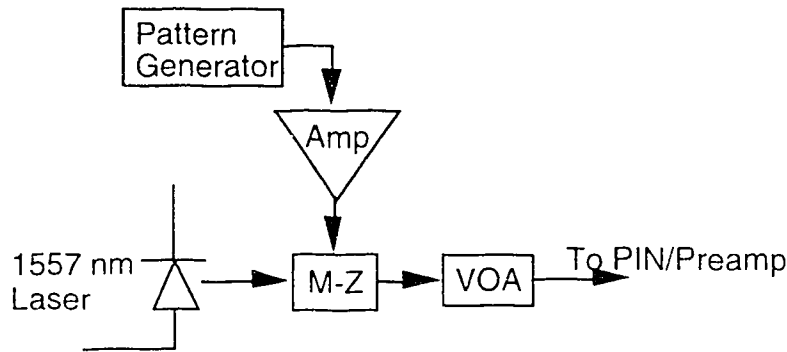


Fig. 6.1.1. Transmitter block diagram of OC-192 system.

The data amplitude was set at 1 V_{pp}. The data was amplified by an electrical amplifier with adjustable gain. The Mach-Zehnder modulator (MZ) is a LiNbO₃ device with a switching voltage $V_{\pi} \approx 3.3$ V. It is an external modulator designed for high bit rate modulation and transmission. The laser has a center wavelength of 1557 nm. The laser power and the MZ bias voltage were adjusted to give an optimal optical eye at the output of the MZ device. The achievable extinction ratio was between 15 and 17 dB. Fig. 6.1.2.a shows an optical eye diagram with an extinction ratio of about 15 dB. The eye is called an optical eye because the voltage amplitude of the eye is linearly proportional to the optical power. Fig. 6.1.2.b shows the histograms of logical ones and logical zeros of the optical eye. The eye diagrams in Fig. 6.1.2.(a-b) were obtained by using a HP Lightwave Converter with bandwidth greater than 20 GHz and a HP digital sampling oscilloscope.

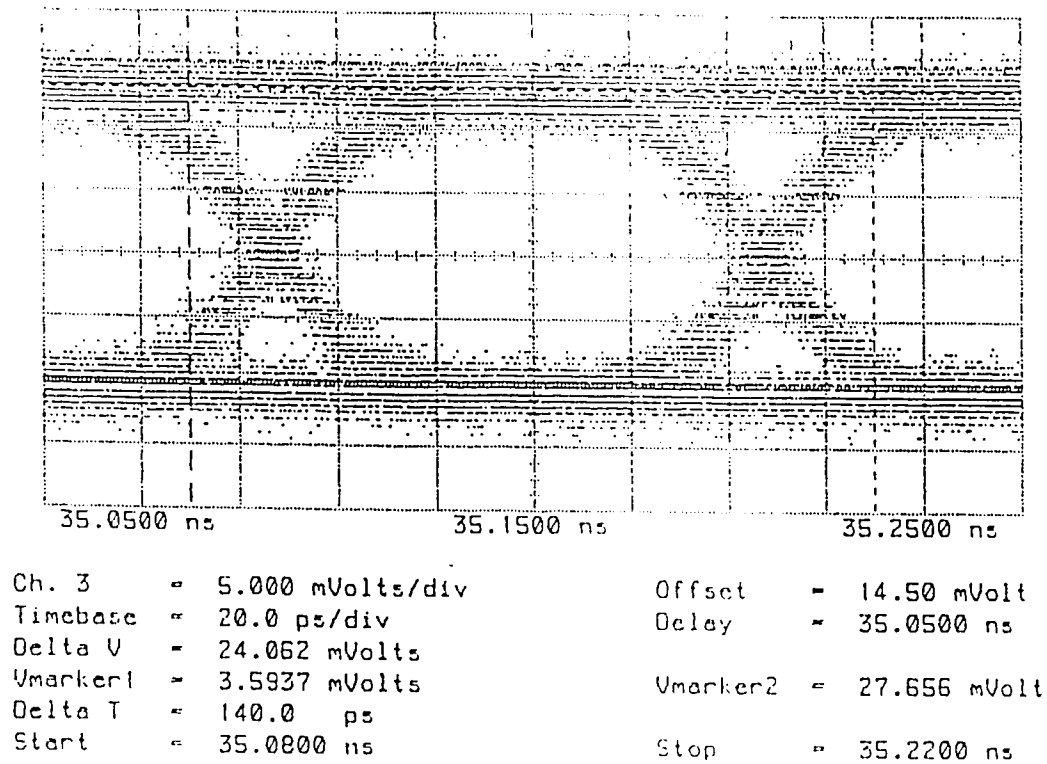


Fig. 6.1.2.a. Optical eye of MZ output.

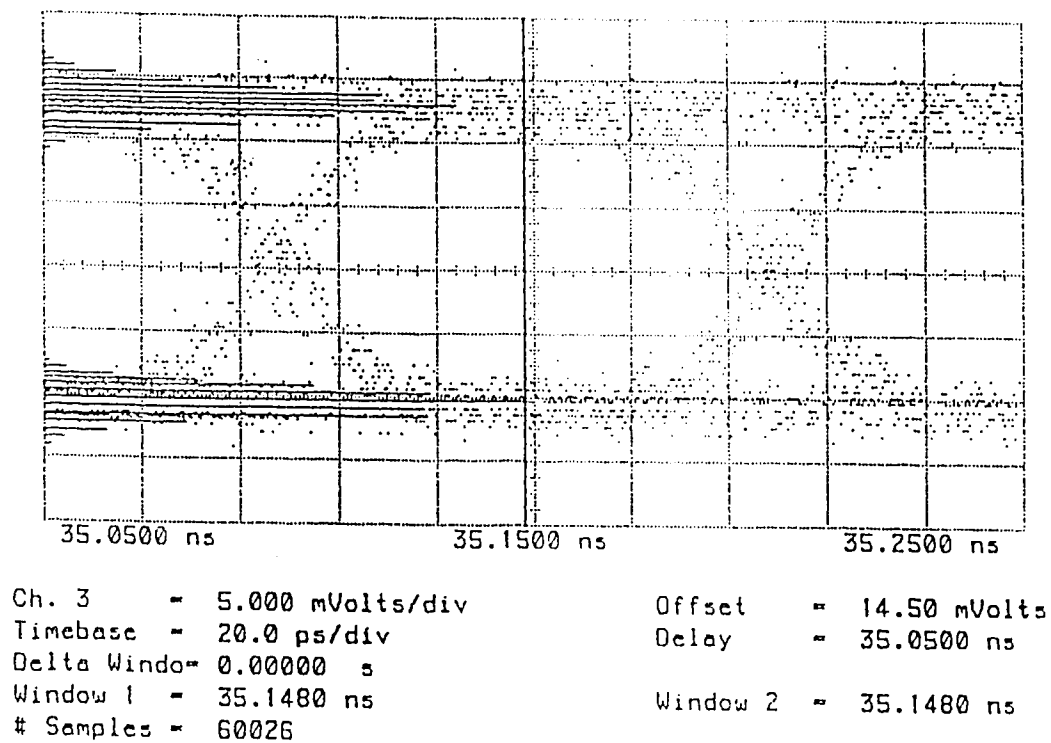


Fig. 6.1.2.b. Histograms of MZ optical eye.

The receiver of the OC-192 system is shown in Fig. 6.1.3. It contains a PIN/preamp module followed by a dc block and an electrical post-amplifier. The PIN diode has a responsivity of 0.8 A/W. The preamp is a transimpedance amplifier which has a single-sided 3-dB bandwidth of about 10 GHz and a gain of about 20 dB. The post-amplifier is a SHF 90P microwave amplifier which has a gain of 23 dB and a single-sided 3-dB bandwidth greater than 10 GHz (10 KHz to >10 GHz). The 3 dB microwave attenuator was used for reflection protection. The power splitter has a bandwidth from 0 to 26.5 GHz. After the power splitter, the data was amplified again to compensate the loss due to power splitting. The amplifier in the data path was another SHF 90P amplifier which has a single-sided 3-dB bandwidth of 15 GHz (10 KHz to 15 GHz). The detailed clock recovery block diagram is shown in Fig. 6.1.4. An adjustable delay box was used to control the phase relation between the recovered clock and the data. The delay box could provide a delay resolution of 0.5 ps.

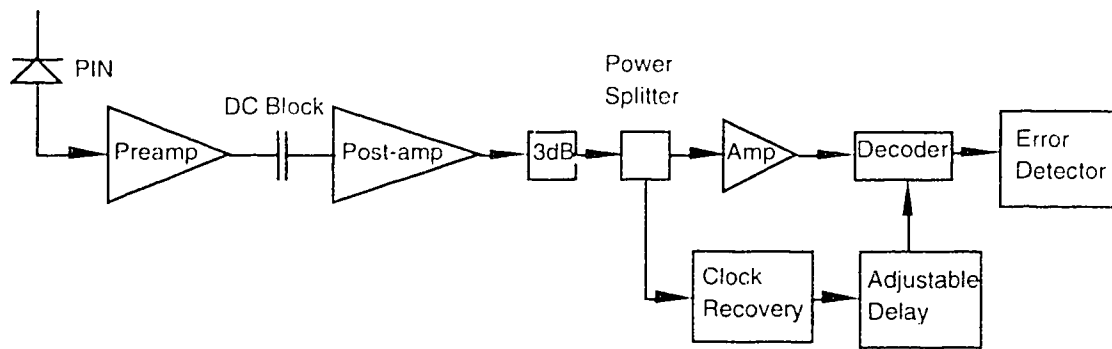


Fig. 6.1.3. Receiver block diagram of OC-192 system.

The clock recovery circuit was used to recover the clock at the OC-192 bit rate from the received non-return-zero (NRZ) polar signal. Because of the dc block, the signaling scheme was changed from on-off keying (OOK) to polar signaling. The NRZ polar signal was first amplified with a gain adjustable Veritech amplifier with a 3-dB single-sided bandwidth of about 10 GHz. The spectrum of the NRZ polar signal (and the NRZ OOK signal) does not contain clock tones which can be used for clock extraction. Therefore a frequency doubler (FD), which was a nonlinear device, was used to generate the

clock tones. A narrow-band filter centered at the OC-192 bit rate was used to extract the clock tone at the OC-192 bit rate in the spectrum of the signal at the output of the FD. The extracted clock was further amplified by a limiting amplifier which has a bandwidth from 7 to 12.4 GHz.

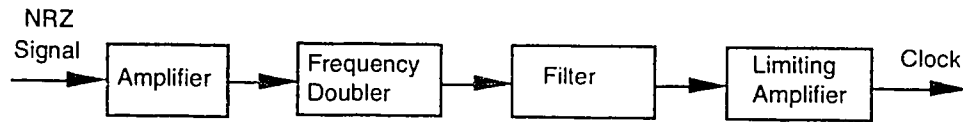


Fig. 6.1.4. Block diagram of clock recovery circuit.

An eye diagram, which corresponds to a BER of 4×10^{-9} , at the input of the decoder is shown in Fig. 6.1.5. The dominant noise in this case is the thermal noise. Since the thermal noise is signal independent, the logical ones and logical zeros carry the same amount of noise and the data eye looks symmetrical. It will be shown in section 6.2 that this will not be the case if an EDFA is inserted as an optical preamplifier.

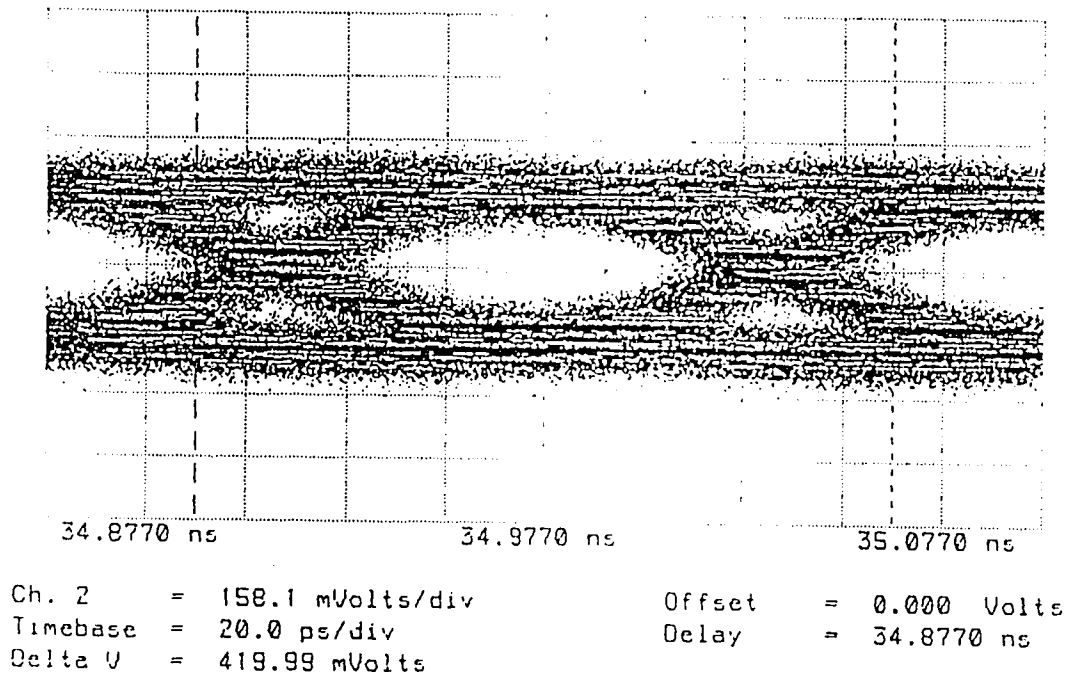


Fig. 6.1.5. A data eye at the input of decoder.

6.2. Back to Back OC-192 System With EDFA and Optical BPF

The measurement was repeated with an EDFA and an optical BPF inserted. The EDFA was used as an optical preamplifier which could significantly improve the sensitivity (in terms of the received optical power) of the receiver. The optical BPF was used to filter out part of the ASE generated by the EDFA. The block diagram of the system is shown in Fig. 6.2.1.

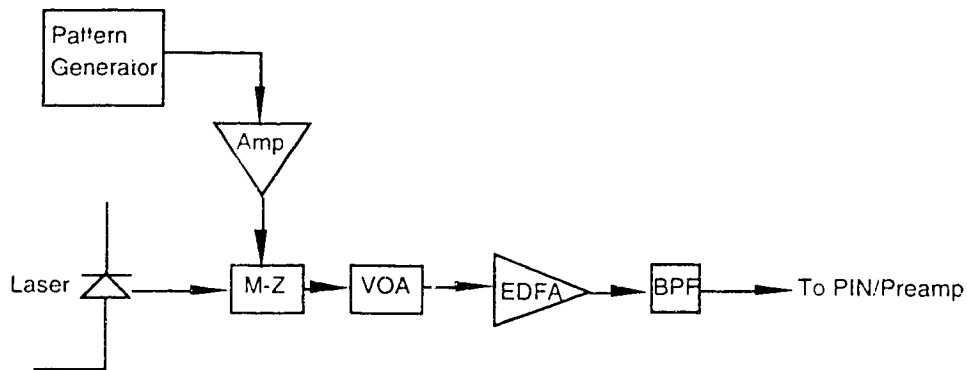


Fig. 6.2.1. Block diagram of back to back OC-192 system with EDFA and optical BPF.

Note that long optical fibers can be placed between the MZ and the EDFA for the study of impact of long fibers. Two different EDFAs were used to do the measurement. The first one was an EDFA with Tektronix packaging (which will be called Tek EDFA). The Tek EDFA has built-in isolator to prevent reflection. The second one is a northern telecom EDFA (nt EDFA). For the case when the nt EDFA was used, the optical BPF was omitted. Some of the characteristics of the Tek EDFA are shown and discussed in section 6.3. Eye diagrams (when the Tek EDFA was used) corresponding to BERs of 10^{-6} and 10^{-9} at the input of the decoder are shown in Fig. 6.2.2 and Fig. 6.2.3 respectively. As it can be seen, the logical ones are noisier than the logical zeros because the dominant noise in the logical ones is the sig-sp beat noise which is signal dependent. The sp-sp beat noise is the dominant noise in the logical zeros.

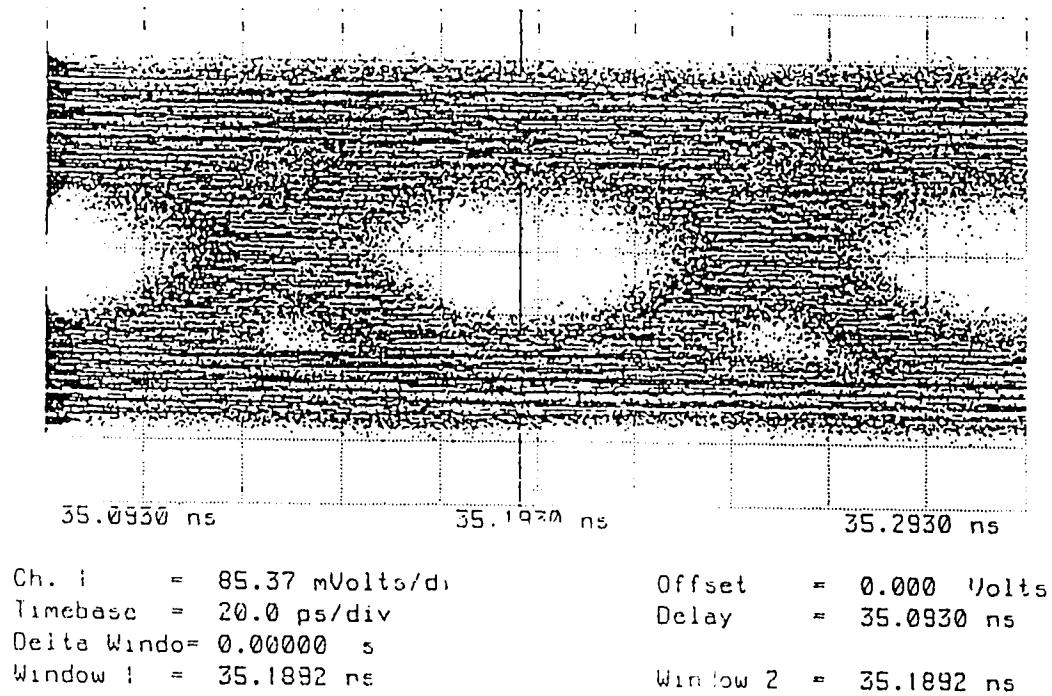


Fig. 6.2.2.a. Data eye diagram at the input of decoder (BER=10⁻⁶).

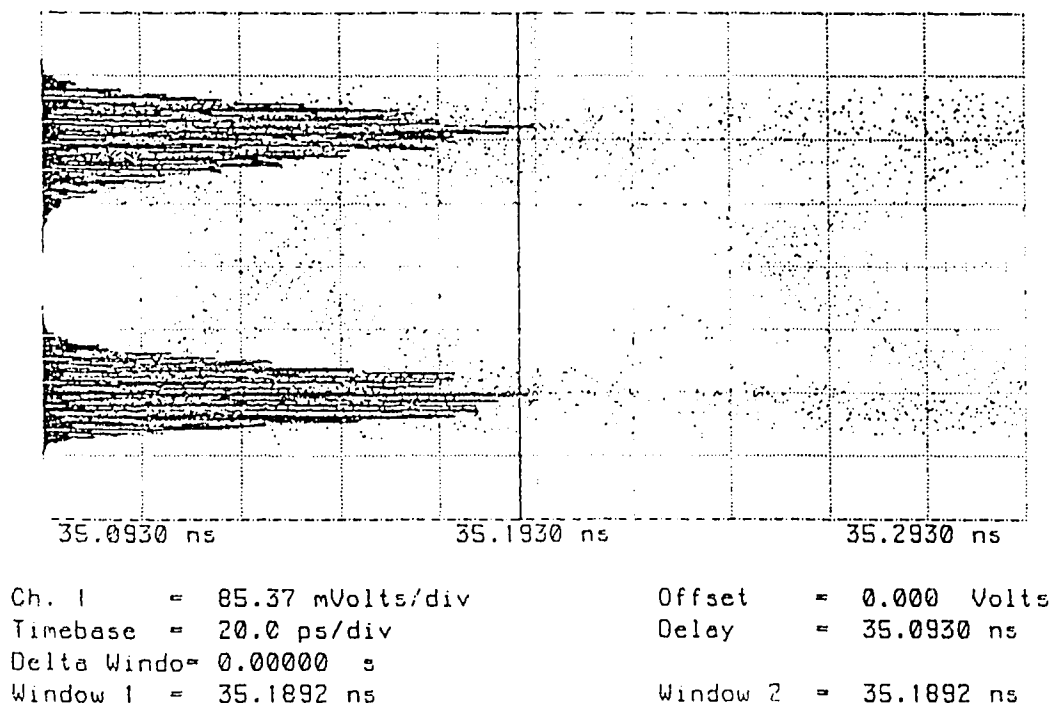


Fig. 6.2.2.b. Histograms of the data eye (BER=10⁻⁶).

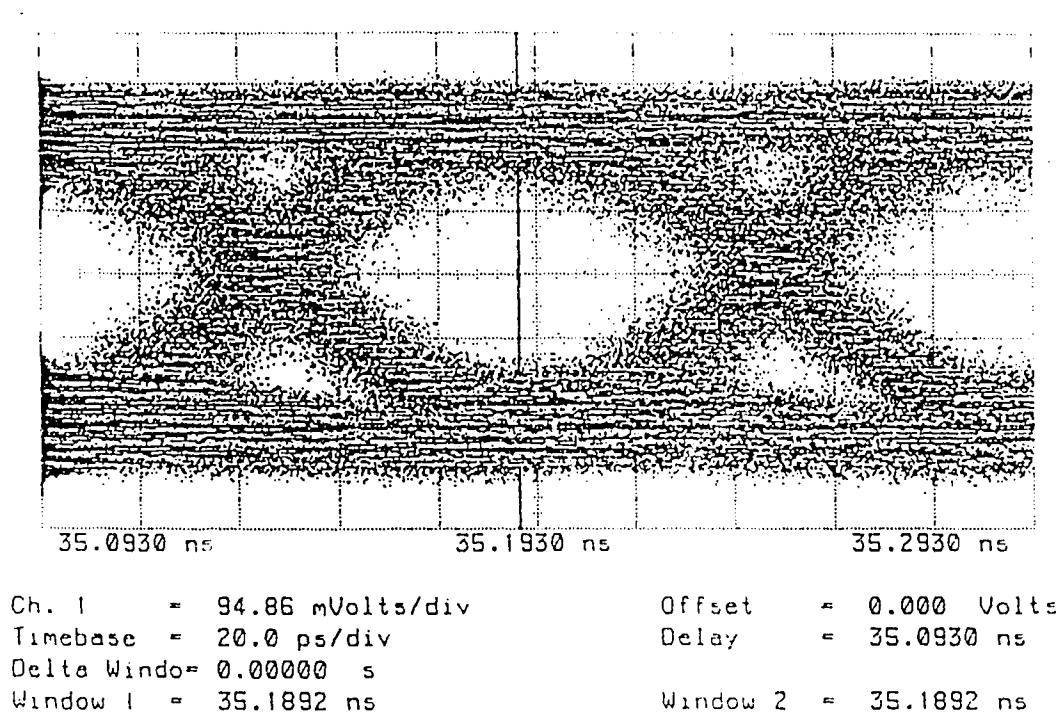


Fig. 6.2.3.a. Data eye diagram at the input of decoder (BER=10⁻⁹).

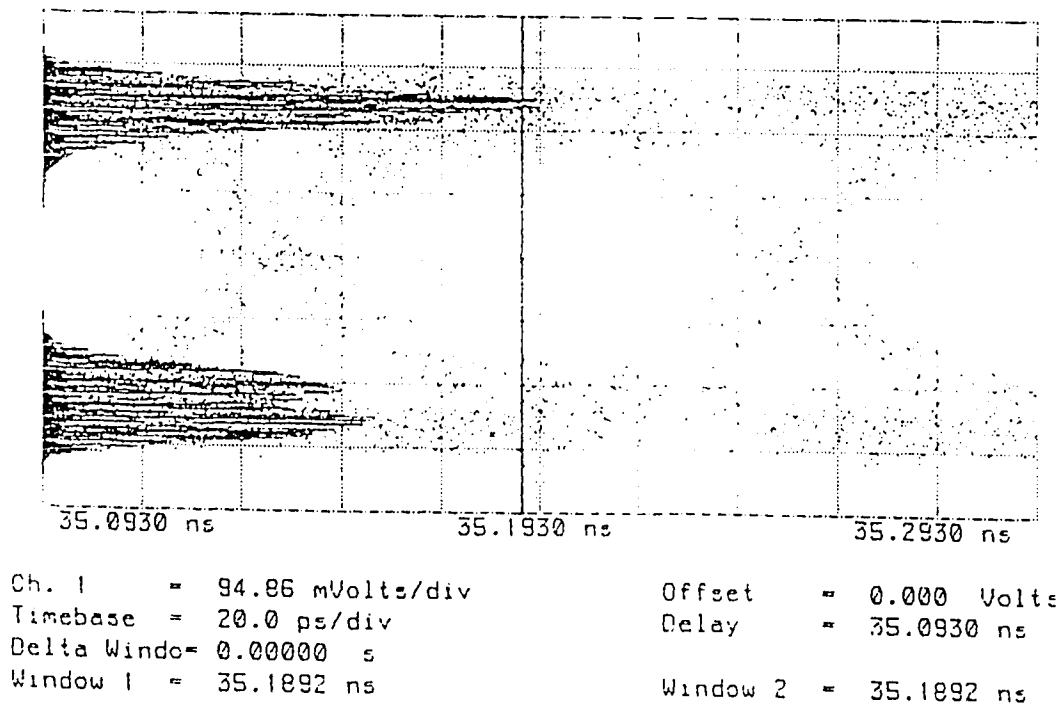


Fig. 6.2.3.b. Histograms of the data eye (BER=10⁻⁹).

Two interesting points can be observed from these eye diagrams. First for the logical zeros, double histograms are observed. However no observable double histograms appear for the logical ones. The effect is not observable from the optical eye in Fig. 6.1.2.b either. The two distinct histograms are possibly developed when the signal is electrically amplified. In other words, the double histograms may be caused by the responses of the electrical amplifiers. One is due to long logical ones and logical zeros and the other one is caused by other patterns as illustrated in Fig. 6.2.4. Long strings of logical ones and logical zeros have much longer time to settle down than the others and hence they can reach steady state levels. The other patterns have a shorter time to settle down and therefore they are not able to reach the steady state levels. Another possible explanation is that the double traces might have already existed in the optical domain perhaps due to the response of the MZ. However the separation of the two traces might be too small to be seen in Fig. 6.1.2.b because they are buried in the thermal noise of the HP Lightwave Converter. Increasing the optical signal power, which raises the logical zeros above the thermal noise level, might reveal the double histograms effect.

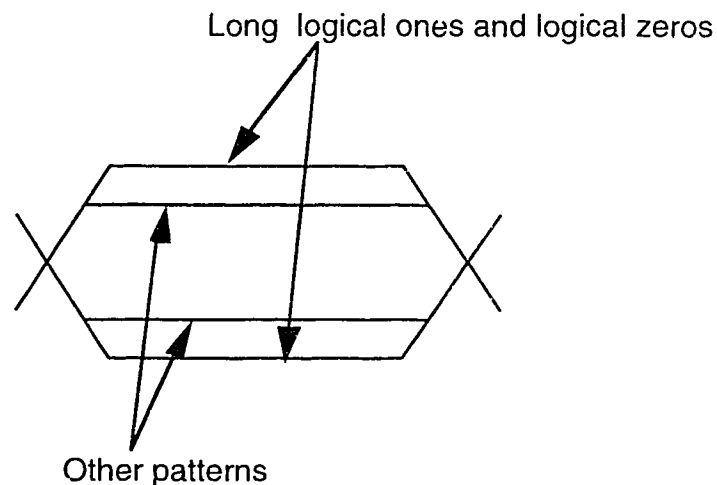


Fig. 6.2.4. Double traces in the data eye.

The second observation is that when the received optical power was increased, the double histograms in the logical zeros started to

separate further apart. A possible explanation to this is that the transfer function of the electrical post-amplifier is not very linear in the dynamic region. The effect of the nonlinearity of the transfer function is illustrated in Fig. 6.2.5.

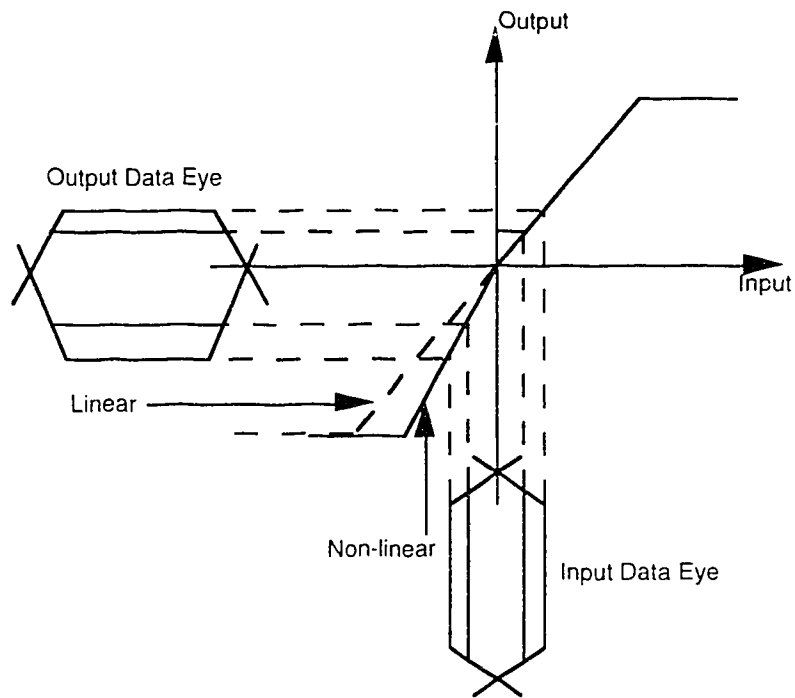


Fig. 6.2.5. Nonlinear transfer function of amplifier.

The slope of the transfer function in the dynamic region represents the gain of the amplifier. If the dynamic region is not linear, the logical ones and logical zeros will experience different gains. For the case shown in Fig. 6.2.5, the gain for the logical zeros is greater than the gain for the logical ones. Therefore the patterning effect for the logical zeros is amplified and relatively the patterning effect for the logical ones is suppressed. The diagram in Fig. 6.2.5 has been simplified for illustration purpose. In reality the gain spectrum of the amplifier is not flat and therefore different frequency components will experience different gains and hence different transfer functions.

6.3. Characteristics of the Tek EDFA

The Tek EDFA has a knob for adjusting the gain and a small display screen showing a number that is related to the gain. The relation between this EDFA number and the small signal gain has been investigated. The EDFA small signal gain was measured with the input signal power set at about -36.3 dBm. The results are shown in Fig. 6.3.1.

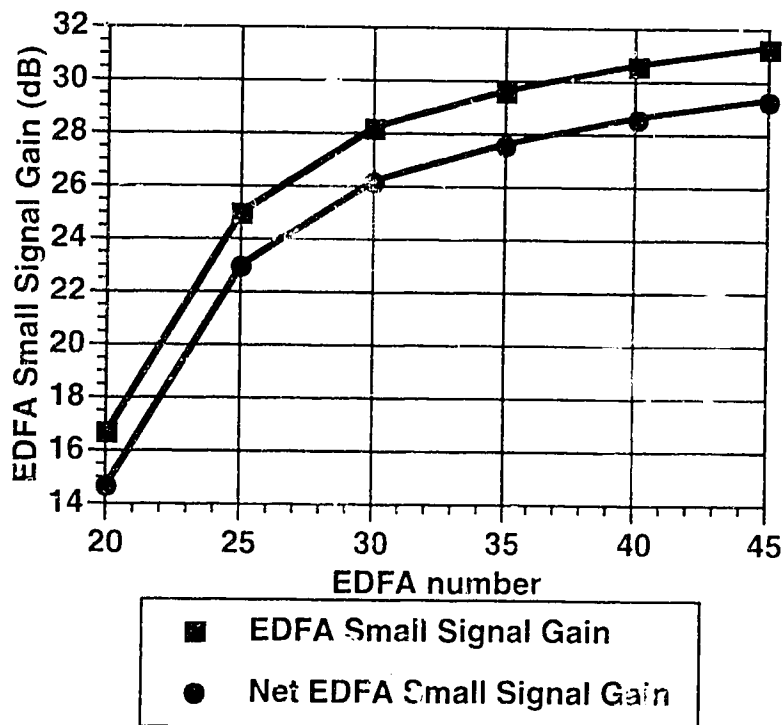


Fig. 6.3.1. Relation between EDFA small signal gain and EDFA number.

For example, when the displayed EDFA number is 30, it corresponds to EDFA gain of about 28 dB or net gain of about 26 dB (as the optical BPF has an insertion loss of about 2 dB).

The gain compression characteristics of the Tek EDFA are shown in Fig. 6.3.2. The measurement was taken with the EDFA number set at about 30. The EDFA gain is plotted against the input and output signal powers.

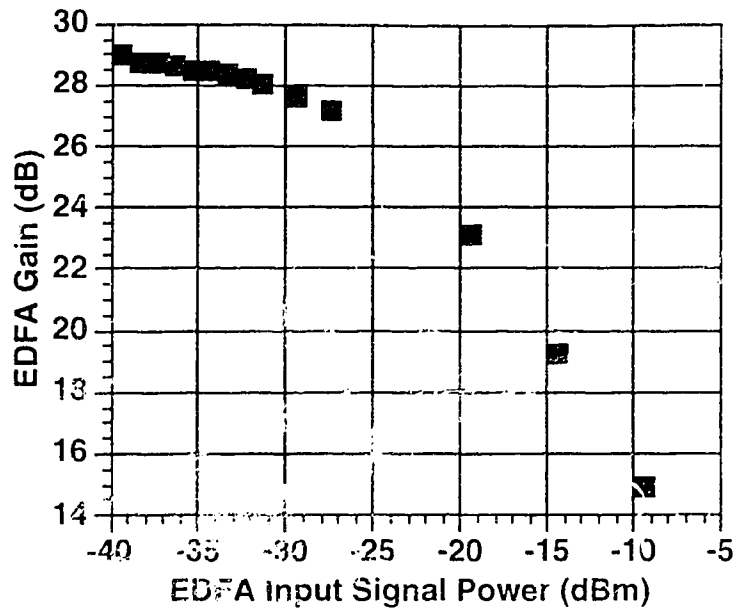


Fig. 6.3.2.a. EDFA gain as a function of input signal power.

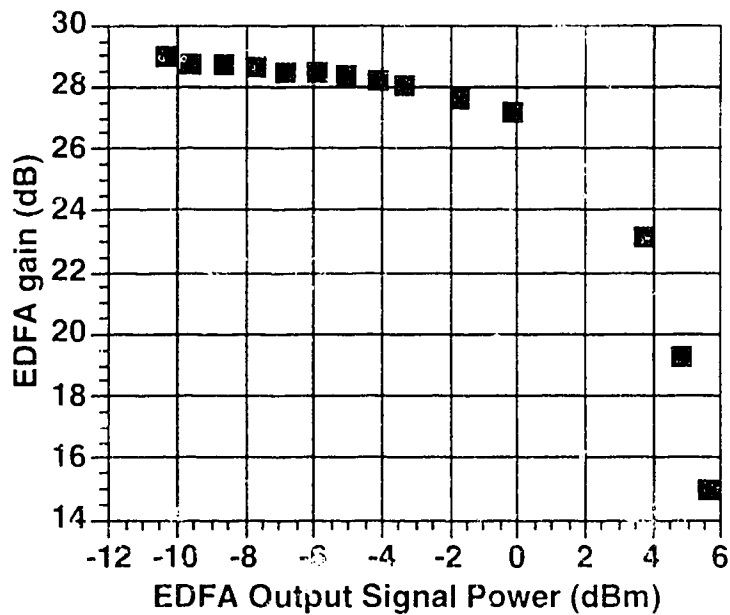


Fig. 6.3.2.b. EDFA gain as a function of output signal power.

The 3 dB gain compression point in terms of the output power (before the optical BPF) is about 2 dBm (or about -24 dBm in terms of the input power).

The measured N_{sp} of the EDFA is plotted as a function of EDFA small signal gain as shown in Fig. 6.3.3.

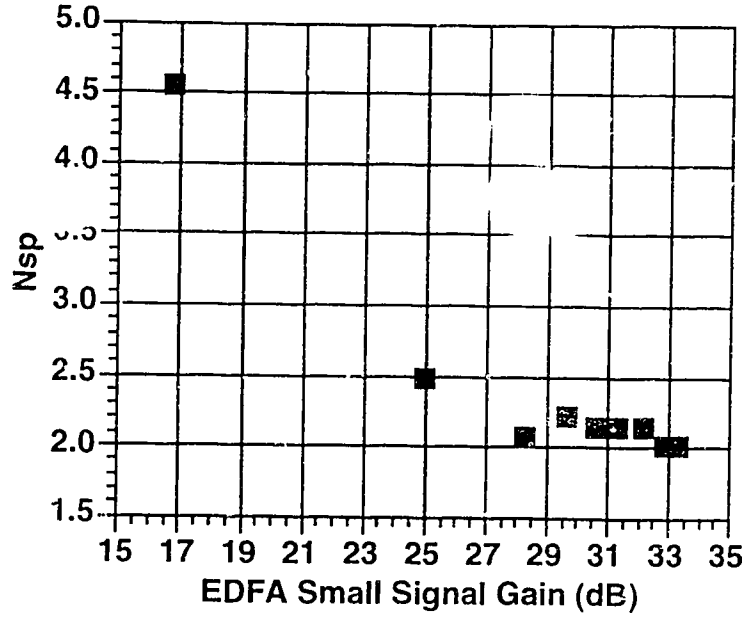


Fig. 6.3.3. N_{sp} as function of EDFA small signal gain.

The N_{sp} is calculated from the equation (2.10.2.6):

$$N_{sp} = \frac{P'_{ase}}{m_l(G-1)hf_c B_n} \quad (6.3.1)$$

where $P'_{ase} = P_{ase(measured)} + Filterloss$, $Filterloss$ is about 2 dB, and $B_n = 1.4 \cdot B_o$ is assumed to be the noise equivalent bandwidth of the optical BPF. The full-width-half-maximum (FWHM) bandwidth B_o of the optical BPF is about 1.3 nm. Since there is no optical polarizer, $m_l = 2$. The frequency f_c is given by:

$$f_c = \frac{c_o}{\lambda_c} \quad (6.3.2)$$

where $c_o = 3 \times 10^8$ m/s is the speed of light in vacuum, $\lambda_c = 1557$ nm is the laser operating wavelength. In equation (6.3.1), h is the Planck's constant and G is the EDFA small signal gain.

The sensitivity of the receiver as a function of the EDFA small signal gain (interpolated or extrapolated from Fig. 6.3.1) was also measured and is shown in Fig. 6.3.4. The sensitivity is defined as the optical power required at the input of the EDFA in order to achieve a BER of 10^{-9} .

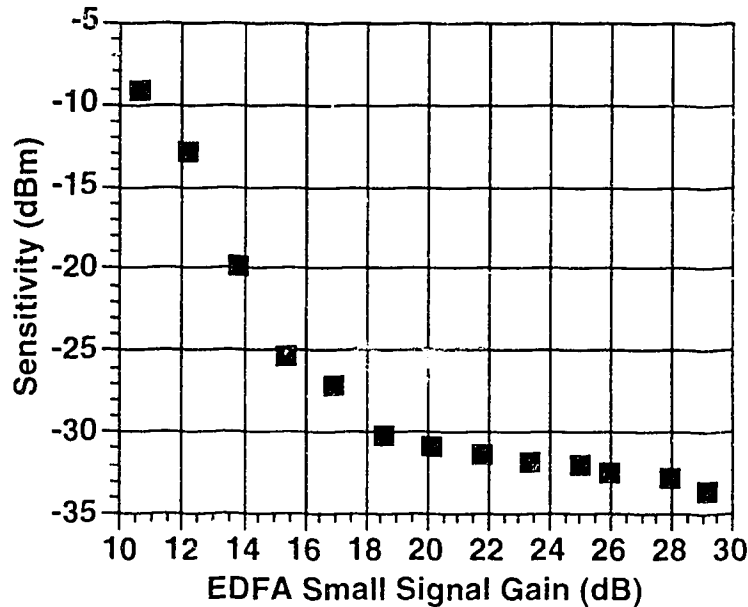


Fig. 6.3.4. Sensitivity of receiver as function of EDFA small signal gain.

Note that the experimental curve in Fig. 6.3.4 resembles the theoretical curves shown in Fig. 4.2.1.1 of chapter 4. When the EDFA small signal gain is below 20 dB, the sensitivity can be improved rapidly by increasing the EDFA small signal gain. The dominant noise in the region where the EDFA small signal gain is less than 20 dB is the thermal noise of the receiver circuit. When the gain is above 20 dB, increasing the gain can no longer improve the sensitivity drastically because the sig-sp and the sp-sp beat noises become the dominant noise terms. The floor of the curve in Fig. 6.3.4 is caused by the EDFA small signal gain dependence of the beat noises as discussed earlier in section 4.2.1 of chapter 4.

6.4. Experimental Results

6.4.1. Sensitivity of OC-192 Receiver

The Tek EDFA small signal gain was set to about 28 dB throughout the following measurements when it was used. The nt EDFA was used in such a way that its output power is always at 0 dBm. The sensitivity curves of the receiver are shown in Fig. 6.4.1.1. For the 0 km case without EDFA, the sensitivity (BER=10⁻⁹) is about -19.4 dBm. When the Tek EDFA and the optical BPF are inserted, the sensitivity is about -33.2 dBm which implies an improvement of about 13.8 dB. When the nt EDFA is in place and no optical BPF is used, the sensitivity is about -31.7 dBm which is about 1.5 dB worse than the one obtained from using the Tek EDFA and optical BPF.

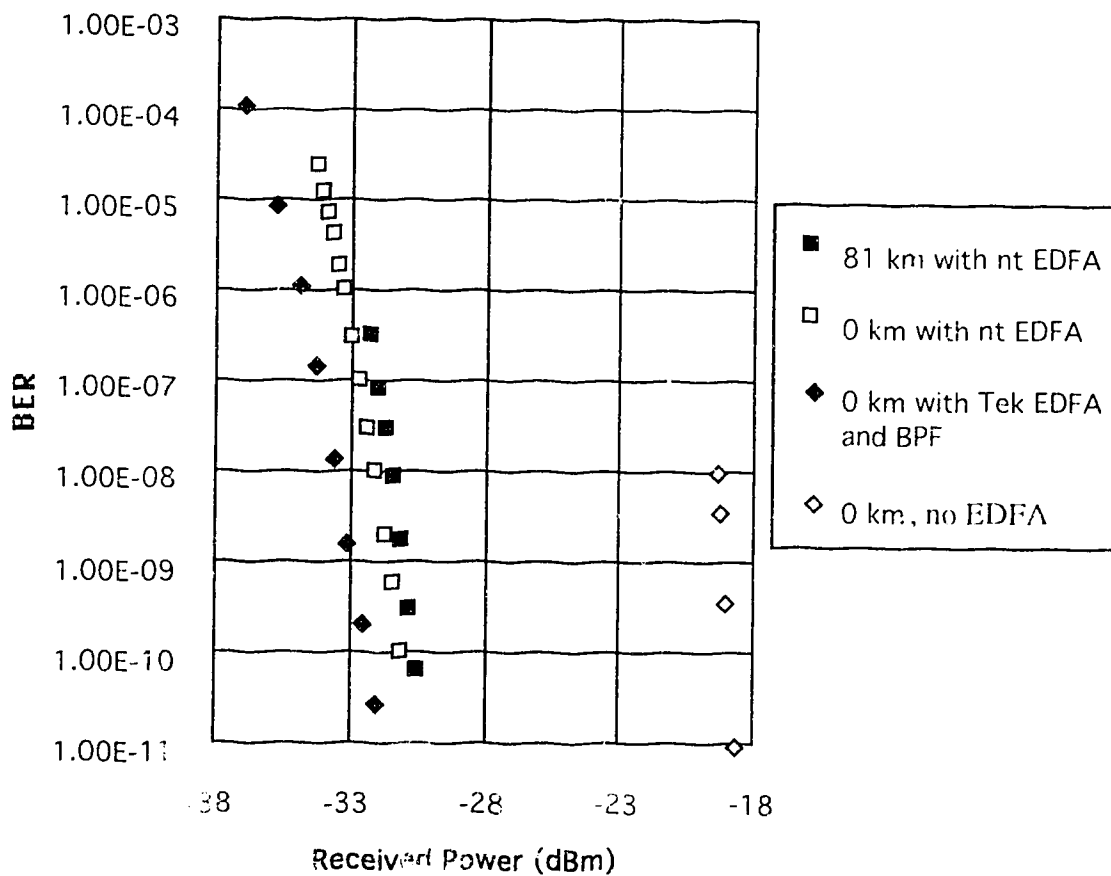


Fig. 6.4.1.1. Sensitivity curves of receiver.

With the nt EDFA in place, single mode fiber 81 km in length was inserted between the MZ and the EDFA. The sensitivity curve is plotted in Fig. 6.4.1.2 and is compared with the case when the fiber length is 0 km. The sensitivity for the 81 km case is about -31.1 dBm. It can be seen that the penalty is about 0.6 dB.

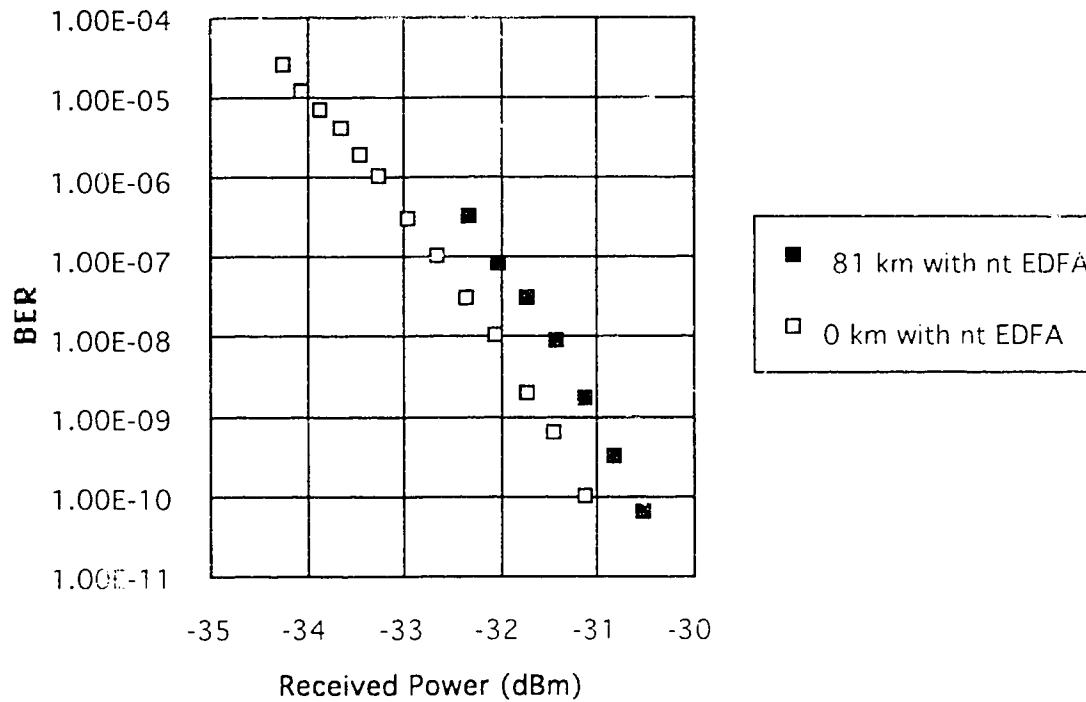


Fig. 6.4.1.2. Sensitivity curves for 0 and 81 km of fiber.

6.4.2. Constant BER contours of OC-192 system

In the previous analyses of the PDFs or the BER, we have only considered the statistics at the sampling time. In this section, we will extend the analyses to look at the statistics at several different instances in time across the data eye. The constant BER contours for the cases of 0 km and no EDFA, 0 km with Tek EDFA and optical BPF, and 81 km with nt EDFA are shown in Fig. 6.4.2.1.(a-c) respectively.

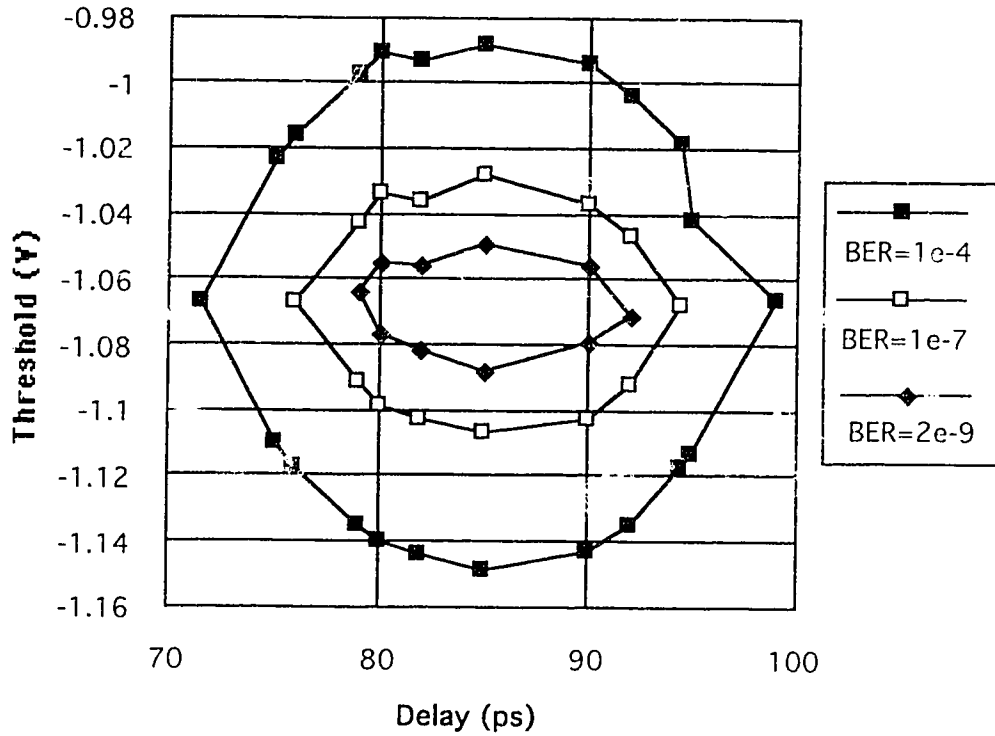


Fig. 6.4.2.1.a. Constant BER contour for 0 km, no EDFA.

For the contours in Fig. 6.4.2.1.a, the optical power at the PIN diode is about -18.8 dBm which corresponds to a minimum achievable BER of about 10^{-11} . Since thermal noise dominates in this case, the contours are fairly symmetrical about the optimum slicing level (-1.07 V) which stays fairly constant across the eye. Using the innermost contour ($\text{BER}=2 \times 10^{-9}$), the opening of the eye in time is about 13 ps and in amplitude is about 40 mV.

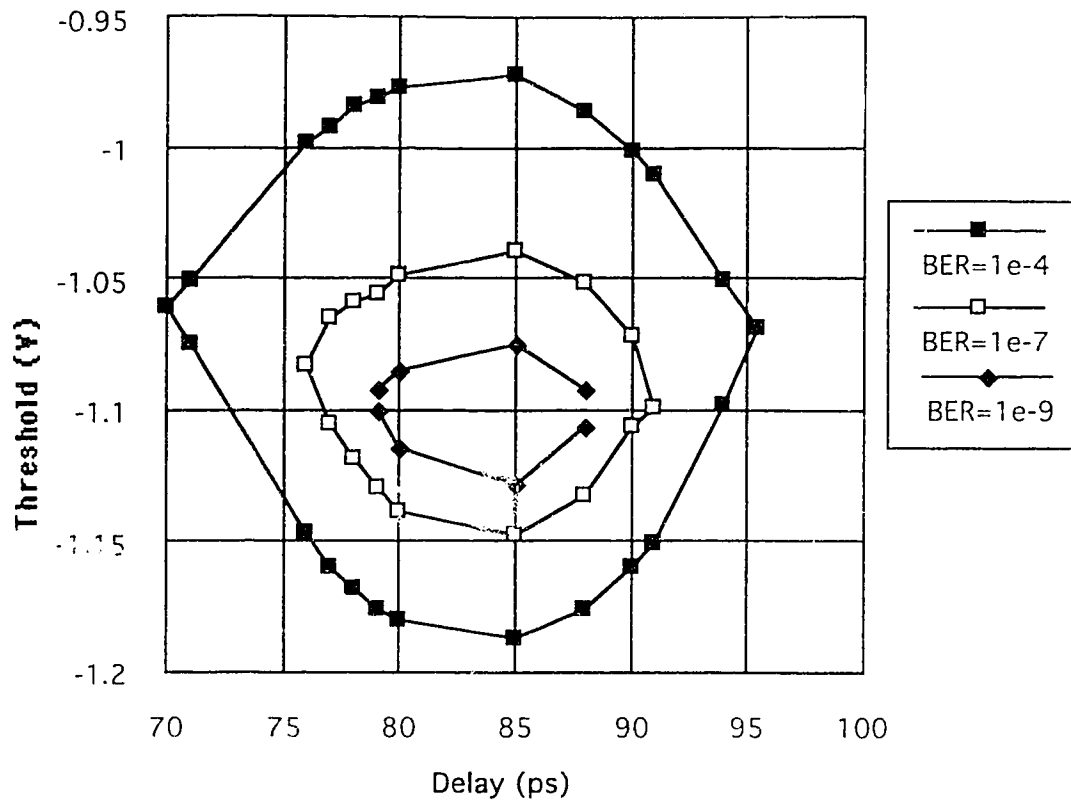


Fig. 6.4.2.1.b. Constant BER contour for 0 km with Tek EDFA and optical BPF.

The contours in Fig. 6.4.2.1.b are obtained with the Tek EDFA and optical BPF inserted. The received power at the EDFA input was about -32.2 dBm and the minimum achievable BER was about 10^{-11} . Using the innermost contour (BER= 10^{-9}), the eye opening in time is about 10 ps and in amplitude is about 53 mV. The logical ones carry more noise than the logical zeros because of the sig-sp beat noise. The optimum threshold for each contour stays fairly constant across the eye but it is different for each contour. This difference suggests that the statistics at the time edges of the eye are different from those close to the center of the eye. An explanation is that there is an increase in noise variance of the logical zeros at the edges of the eye. The ISI introduced at the edges of the eye increases the signal level of the logical zeros. This effect not only increases the mean value of the logical zeros but also the variance because of the sig-sp beat noise. Moreover the voltage level of the logical ones at the

edges of the eye is lower than that at the center of the eye. Hence there is a decrease in both the mean and the variance of the logical ones at the edges of the eye. These effects then shift the optimum threshold at the edges of the eye upward as shown in Fig. 6.4.2.1.b.

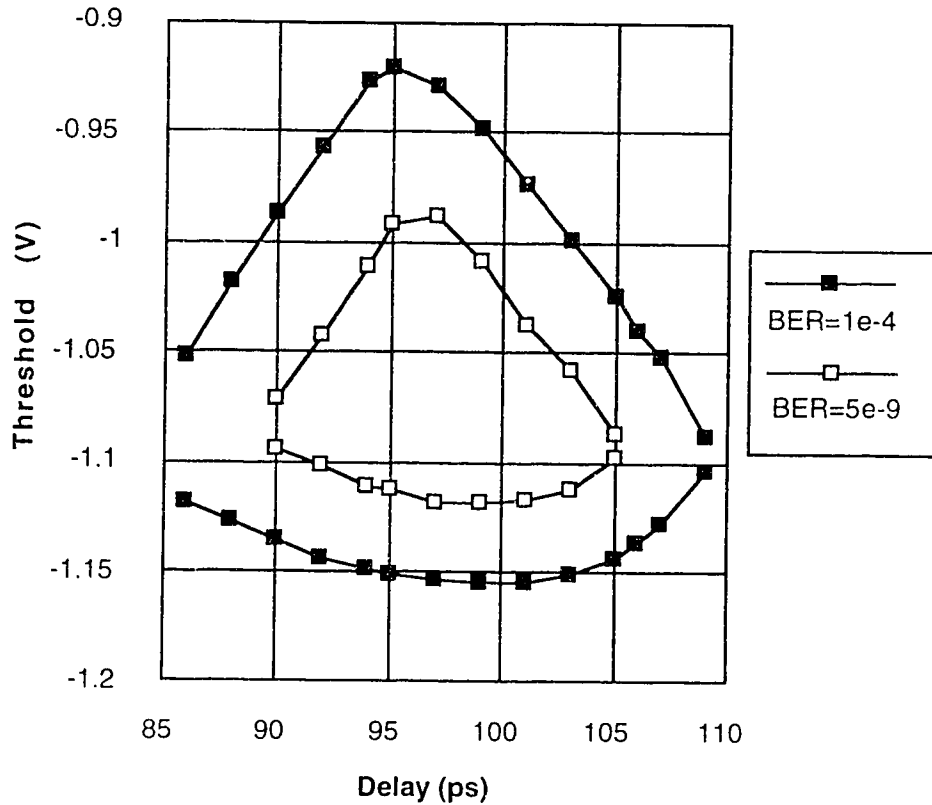


fig. 6.4.2.1.c. Constant BER contour for 81 km with nt EDFA.

Fig. 6.4.2.1.c shows the contours measured with nt EDFA and 81 km of single mode fibers inserted in front of the EDFA. The optical BPF was omitted. The received power was about -28 dBm which was about 3 dB above the sensitivity. The shape of the contour resembles the shape of the eye diagram shown in Fig. 6.4.2.2. The triangular shape of the contours is caused by fiber dispersion. The eye is neither symmetrical in time nor in amplitude. The asymmetry makes it difficult to search for the optimum decision time and threshold. Using the inner contour (BER=10⁻⁹), the eye opening in time is about 17 ps and in amplitude is about 130 mV.

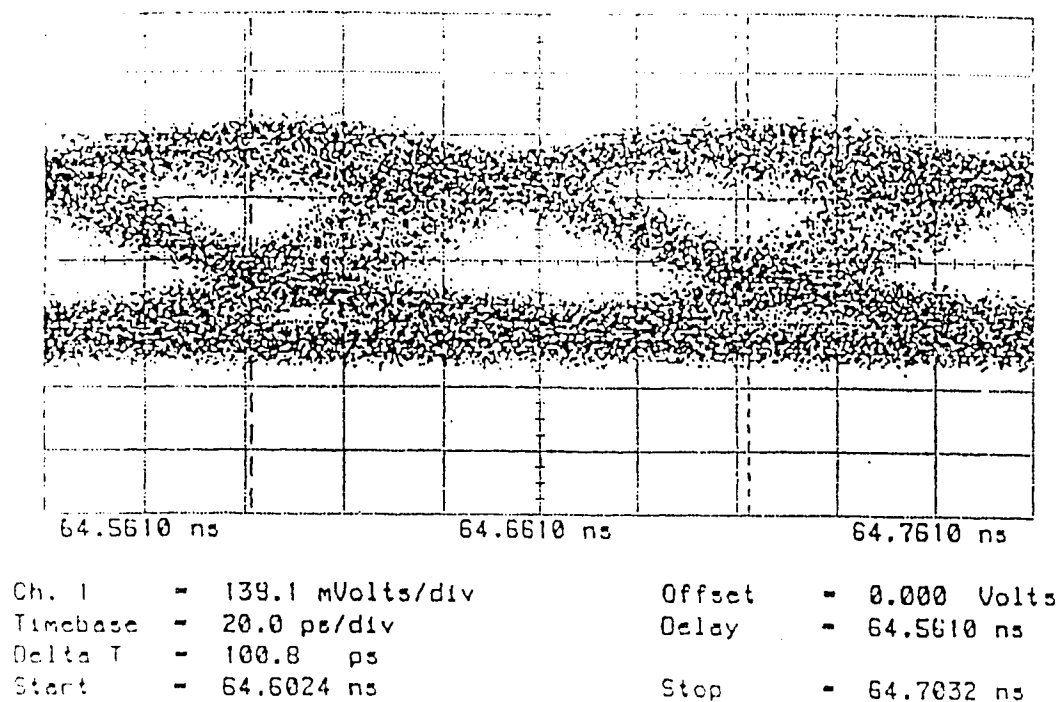


Fig. 6.4.2.2. Data eye at input of decoder with nt EDFA and 81 km of fibers.

6.4.3. Optimum Threshold versus Received Power

Fig. 6.4.3.1 shows the optimum threshold versus received power for the cases of 0 km with Tek EDFA and optical BPF, 0 km with nt EDFA and 81 km with nt EDFA. The optimum thresholds observed for the case when the Tek EDFA and the optical BPF are used shows a shift towards logical zeros as the signal power increases. This is again due to the increase in the sig-sp beat noise in the logical ones. A similar trend is observed for the case of using nt EDFA without optical BPF and fibers but the optimum threshold values are less negative. This may be due to the increase in the s-p noise power for the logical zeros when the optical BPF is omitted. For the case with 81 km of fibers, the threshold stays almost constant. In terms of percentage, the percentage optimum thresholds for the case of 0 km with Tek EDFA and optical BPF are estimated to be about 43 to 45 % across the range of received power. For the cases of 0 km and 81 km with nt EDFA, the percentage optimum thresholds are estimated to be about $50 \pm 2\%$.

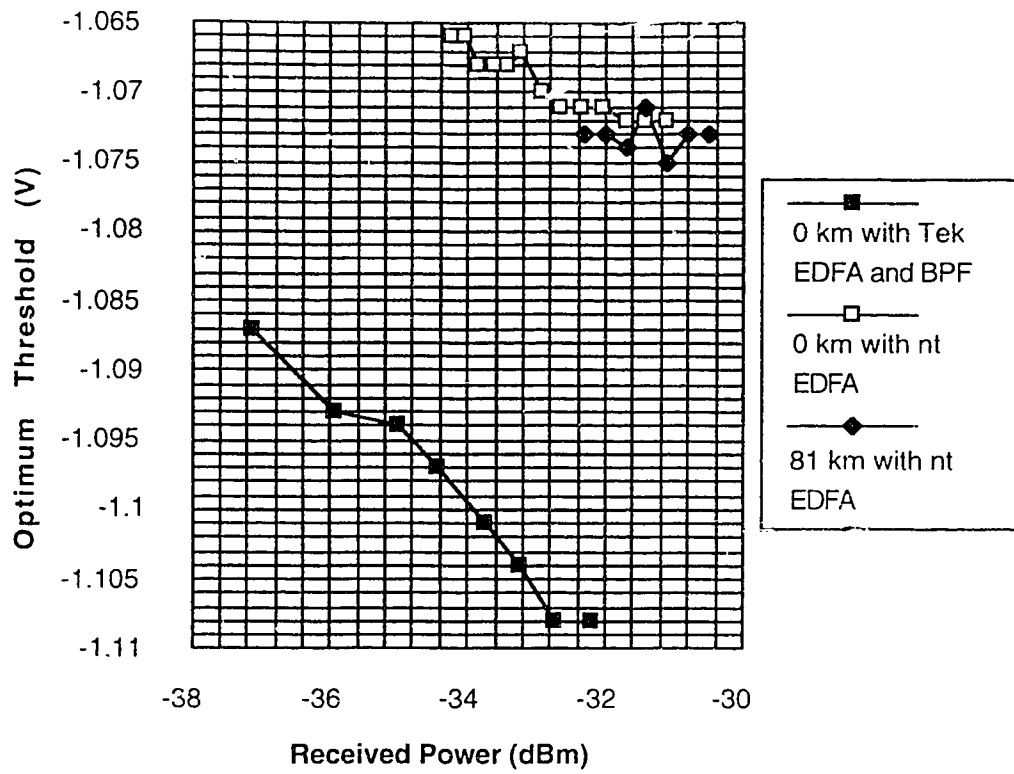


Fig. 6.4.3.1. Optimum threshold versus received power.

7. Conclusions

The non-Gaussian distributions of logical ones and logical zeros in an EDFA preamplified optical digital transmission system have been theoretically formulated in chapters 2 and 3. When the post-detection Gaussian noises (the thermal and shot noises) are neglected, the noise distribution for perfectly extinct logical zeros follows the Central Chi-Square PDF. For logical ones, the noise distribution follows the Non-Central Chi-Square PDF. When the thermal and the shot noises are included, the Steepest Descent Method can be used to find approximated PDFs for the logical ones and logical zeros with less than 1% of error. The difference between the non-Gaussian and Gaussian PDFs becomes apparent when the following conditions are satisfied:

- 1.) good extinction ratio,
- 2.) sufficiently large EDFA small signal gain,
- 3.) sufficiently wide electrical bandwidth,
- 4.) narrow optical bandwidth,
- 5.) conditions 3 and 4 imply that the optical bandwidth to electrical bandwidth ratio is small.

When the above conditions (especially 2 and 3) are satisfied, the dominant noise terms are the sp-sp beat noise for logical zeros and sig-sp beat noise for logical ones.

The theoretical performance of the EDFA preamplified digital system has been analyzed by making use of the PDFs generated by the Steepest Descent Method in chapter 4. It has been found that the Gaussian approximations of the PDFs of logical zeros and logical ones can be used to predict the receiver sensitivity performance with small error even when the above conditions are satisfied. However the Gaussian approximation is less accurate than the non-Gaussian theory in predicting the optimum threshold that should be used in the receiver decision circuit. When the above conditions are satisfied, the percentage optimum thresholds predicted by the

Gaussian and the non-Gaussian theories differ by as much as 10% depending on the received power level.

In chapter 5, a method has been devised to experimentally verify the non-Gaussian noise distributions of logical zeros and logical ones for the first time. The measured PDF of the ASE shows strong asymmetry about the peak of the PDF. This asymmetry clearly shows that the noise distribution is non-Gaussian. In addition the shape of the measured PDF of the ASE agrees reasonably well with the theoretical non-Gaussian shape. For the case of logical ones, there is no distinguishable difference between the experimental PDFs and the theoretical PDFs within the range of observation.

There is a slight mismatch in the widths of the experimental and theoretical PDFs. This slight mismatch may be due to the mathematical assumptions that have been made for the theoretical analyses such as using Fourier series expansion of the signal and ASE electric fields in the time interval $[0, T]$. Moreover, the mismatch may be due to the fact that the theories do not take into account the frequency dependent characteristics of the responsivity of the PIN diode and the gain of the electrical amplifiers. In addition, experimental errors are also factors for the mismatch.

The optimum thresholds of the PDFs of logical zeros and logical ones have also been experimentally measured. The measured percentage optimum thresholds agree more with the values predicted by the non-Gaussian theory than those by the Gaussian theory. This verifies the impact of the non-Gaussian distributions on the optimum thresholds.

7.1. Future works

We have seen in chapter 6 that in a real system such as the OC-192 system, the statistics are more complicated than just the non-Gaussian PDFs. The complication arises from the interactions of the non-Gaussian noise distributions, the ISI, the fiber dispersion, and possibly the patterning effect. It is preferable that the non-Gaussian noise theory can incorporate all the additional effects such as the ISI and the fiber dispersion. However, the analyses would require more sophisticated mathematical techniques if we were to pursue an

analytical solution (provided the solution exists). The ISI has been recently taken into account in [32]. For even more vigorous analyses, we can also incorporate the effects of laser line-width and phase noise [33, 34]. Alternative to analytical solutions, we could use computer simulation to analyze the behavior of the entire system using more realistic components. For example, we can replace the integrate-and-dump filter by a fourth order Butterworth low pass filter. We can also try to obtain a partial analytical solution and let the computer handle the rest.

Moreover we can also look into the techniques for reducing the beat noises in the receiver. One method which utilizes coherent detection has been proposed by Yamashita and Okoshi [6]. In addition it is also worthwhile to look into the possibility of combining the EDFA preamplifier with other kinds of photodetector such as the optoelectronic mixer (OEM). There are numerous combinations of EDFA preamplifier with photodetectors and it is possible that one of the many combinations would give optimal noise performance.

References

- [1] B. Mikkelsen, C. G. Jorgensen, N. Jensen, T. Durhuus, K. E. Stubkjaer, P. Doussiere, and B. Fournier, "High-Performance Semiconductor Optical Preamplifier Receiver at 10 Gb/s," *IEEE Photonics Technology Letters*, vol. 5, no. 9, pp. 1096-1097, 1993.
- [2] K. Bertilsson and P. A. Andrekson, "Modeling of Noise in Erbium-Doped Fiber Amplifiers in the Saturated Regime," *J. Lightwave Technol.*, vol. 12, no. 7, pp. 1198-1206, 1994.
- [3] C. R. Giles, E. Desurvire, J. L. Zyskind, and J. R. Simpson, "Noise Performance of Erbium-Doped Fiber Amplifier Pumped at 1.49 μ m, and Application to Signal Preamplification at 1.8 Gbit/s," *IEEE Photonics Technology Letters*, vol. 1, no. 11, pp. 367-369, 1989.
- [4] A. H. Gnauck and C. R. Giles, "2.5 and 10 Gb/s Transmission Experiments Using a 137 Photon/Bit Erbium-Fiber Preamplifier Receiver," *IEEE Photonics Technology Letters*, vol. 4, no. 1, pp. 80-82, 1992.
- [5] A. H. Gnauck and C. R. Giles, L. J. Cimini, Jr., J. Stone, L. W. Stulz, S. K. Korotky, and J. J. Veselka, "8-Gb/s-130 km Transmission Experiment Using Er-Doped Fiber Preamplifier and Optical Dispersion Equalization," *IEEE Photonics Technology Letters*, vol. 3, no. 12, pp. 1147-1149, 1991.
- [6] S. Yamashita and T. Okoshi, "Suppression of Beat Noise from Optical Amplifiers Using Coherent Receivers," *J. Lightwave Technol.*, vol. 12, no. 6, pp. 1029-1035, 1994.

- [7] D. Marcuse, "Derivation of Analytical Expressions for the Bit-Error Probability in Lightwave Systems with Optical Amplifiers," *J. Lightwave Technol.*, vol. 8, no. 12, pp. 1816-1823, 1990.
- [8] D. Marcuse, "Calculation of Bit-Error Probability for a Lightwave System with Optical Amplifiers and Post-Detection Gaussian Noise," *J. Lightwave Technol.*, vol. 9, no. 4, pp. 505-513, 1991.
- [9] J. S. Lee and C. S. Shim, "Bit-Error-Rate Analysis of Optically Preamplified Receivers Using an Eigenfunction Expansion Method in Optical Frequency Domain," *J. Lightwave Technol.*, vol. 12, no. 7, pp. 1224-1229, 1994.
- [10] P. A. Humblet and M. Azizoglu, "On the Bit-Error Rate of Lightwave Systems with Optical Amplifiers," *J. Lightwave Technol.*, vol. 9, no. 11, pp. 1576-1582, 1991.
- [11] N. A. Olsson, "Lightwave Systems With Optical Amplifier," *J. Lightwave Technol.*, vol. 7, no. 7, pp. 1071-1082, 1989.
- [12] M. Kae and A. J. F. Siegert, "On the theory of noise in radio receivers with square law detectors," *J. Appl. Phys.*, vol. 18, April, pp. 383-397, 1947.
- [13] E. Mazo and J. Salz, "Probability of error for quadratic detectors," *Bell Syst. Tech. J.*, vol. 44, pp. 2165-2186, 1965.
- [14] R. C. Emerson, "First probability densities for receivers with square law detectors," *J. Appl. Phys.*, vol. 24, pp. 1168-1176, 1953.
- [15] J. C. Cartledge and A. F. Elrefaie, "Effect of Chirping-Induced Waveform Distortion on the Performance of Direct Detection Receivers Using Traveling-Wave Semiconductor Optical Preamplifiers," *J. Lightwave Technol.*, vol. 9, no. 2, pp. 269-271, 1991.

- [16] Saleh and Teich, *Fundamentals of Photonics*, John Wiley & Sons, Inc., pp. 650-656, 1991.
- [17] Lathi, *Modern Digital And Analog Communication Systems*, The Dryden Press, Saunders College Publishing, 2nd Ed., pp. 32, pp. 424, 1989.
- [18] Proakis, *Digital Communications*, McGraw-Hill, 2nd Ed., pp. 25, pp. 39-40, pp. 149, 1989.
- [19] Papoulis, *Probability, Random Variables, and Stochastic Processes*, McGraw-Hill Inc., pp. 457, 1965.
- [20] H. J. Landau and H. O. Pollak, "Prolate Spheroidal Wave Equations, Fourier Analysis and Uncertainty: The Dimension of the Space of Essentially Time- and Band-Limited Signals," *Bell System Tech. J.*, vol. 41, P. 1295, 1962.
- [21] P. S. Henry, "Error-rate performance of optical amplifiers," *Opt. Fib. Commun. Conf*, paper THK3, 1989.
- [22] C. R. Giles and E. Desurvire, "Propagation of Signal and Noise in Concatenated Erbium-Doped Fiber Optical Amplifiers," *J. Lightwave Technol.*, vol. 9, no. 2, pp. 147-154, 1991.
- [23] J. Freeman and J. Conradi, "Gain Modulation Response of Erbium-Doped Fiber Amplifiers," *IEEE Photonics Technology Letters*, vol. 5, no. 2, pp. 224-226, 1993.
- [24] Jaluria, *Computer Methods For Engineering*, Allyn and Bacon, Inc., pp. 113-114, pp. 121-133, 1988.
- [25] S. Parl, "A New Method of Calculating the Generalized Q Function," *IEEE Transactions on Information Theory*, vol. IT-26, no. 1, January, 1980.

- [26] D. A. Shnidman, "The Calculation of the Probability of Detection and the Generalized Marcum Q-Function," *IEEE Transactions on Information Theory*, vol. 35, no. 2, March, 1989.
- [27] P. M. Morse and H. Feshbach, *Methods of Theoretical Physics Part I*, McGraw-Hill, New York, pp. 417-443, 1953.
- [28] Dennerly and Krzywicki, *Mathematics for Physicists*, Harper and Row Publishers, pp. 87-94, 1967.
- [29] Churchill and Brown, *Complex Variables and Applications*, McGraw-Hill, 5th Ed., pp. 200, 1990.
- [30] I. S. Gradshteyn and I. M. Ryzhik, *Tables of Integrals, Series and Products*, Academic, New York, pp. 354, 1980.
- [31] Benturud, *Fiber Optic Transmission Using OTDM*, M.Sc. Thesis, The University of Alberta, P. 112, 1993.
- [32] L. Ribeiro, J. Da Rocha, J. Pinto, "Performance Evaluation of EDFA Pre-amplified Receivers Taking into Account Intersymbol Interference," *J. Lightwave Technol.*, vol. 13, no. 2, pp. 225-232, 1995.
- [33] J. L. Gimlett and N. K. Cheung, "Effects of Phase-to-Intensity Noise Conversion by Multiple Reflections on Gigabit-per-Second DFB Laser Transmission Systems," *J. Lightwave Technol.*, vol. 7, no. 6, pp. 888-895, 1989.
- [34] O. K. Tonguz, "Theory of Direct-Detection Lightwave Receivers using Optical Amplifiers," *J. Lightwave Technol.*, vol. 9, no. 2, pp. 174-180, 1991.
- [35] F. Oberhettinger and L. Badii, *Tables of Laplace Transforms*, Springer-Verlag, New York, pp. 256, 1973.

Appendix A1

Derivations of MGFs, PDFs, Means and Variances

For simplicity the finite summation $\sum_{n=-\frac{M}{2}}^{\frac{M}{2}}$ is replaced by \sum .

Equation (1.2.1) can be expanded as:

$$K \left(\left| \hat{E}_s(t) \right|^2 + \hat{E}_s(t) \hat{e}_{sp}^*(t) + \hat{E}_s^* \hat{e}_{sp}(t) + \left| \hat{e}_{sp}(t) \right|^2 \right). \quad (\text{A1.1})$$

Using equations (2.5.11) and (2.5.12), we have:

$$\left| \hat{E}_s(t) \right|^2 = \sum |E_n|^2 + \sum \sum_{n \neq m} E_n E_m^* \exp[j(\omega_n - \omega_m)t] \quad (\text{A1.2})$$

$$\hat{E}_s(t) \hat{e}_{sp}^*(t) = \sum E_n c_n^* + \sum \sum_{n \neq m} E_n c_m^* \exp[-j(\omega_n - \omega_m)t] \quad (\text{A1.3})$$

$$\hat{E}_s^*(t) \hat{e}_{sp}(t) = \sum E_n^* c_n + \sum \sum_{n \neq m} E_n^* c_m \exp[-j(\omega_n - \omega_m)t] \quad (\text{A1.4})$$

$$\left| \hat{e}_{sp}(t) \right|^2 = \sum |c_n|^2 + \sum \sum_{n \neq m} c_n c_m^* \exp[j(\omega_n - \omega_m)t]. \quad (\text{A1.5})$$

The orthogonality property of the complex exponential function in the time interval $[0, T]$ is given by:

$$\int_0^T \exp[\pm j(\omega_n - \omega_m)t] dt = \begin{cases} 0 & (n \neq m) \\ T & (n = m) \end{cases}. \quad (\text{A1.6})$$

Using equations (A1.2) to (A1.6) in equation (2.8.1), the random variable y is calculated as:

$$y = K \sum |E_n|^2 + 2K \sum |E_n| (c_m \cos \theta_n - c_m^* \sin \theta_n) + K \sum |c_n|^2 \quad (\text{A1.7})$$

where the relation $Z + Z^* = 2\text{Re}\{Z\}$ has been used.

Since $y \geq 0$, the unilateral Laplace transform of the PDF or the MGF for logical ones is given by:

$$F_1(s) = \langle \exp(-sy) \rangle = \int_0^\infty f_1(y) \exp(-sy) dy \quad (\text{A1.8})$$

where $\langle \cdot \rangle$ is the expectation operator. Using equation (A1.7) in (A1.8), we have:

$$\begin{aligned} \langle \exp(-sy) \rangle &= \exp\left(-sK \sum |E_n|^2\right) \prod \langle \exp\left[-sK\left(2|E_n|\cos\theta_n c_m + c_m^2\right)\right] \rangle \\ &\quad \cdot \langle \exp\left[-sK\left(-2|E_n|\sin\theta_n c_m + c_m^2\right)\right] \rangle. \end{aligned} \quad (\text{A1.9})$$

Consider the c_m term:

$$\begin{aligned} &\langle \exp\left[-sK\left(2|E_n|\cos\theta_n c_m + c_m^2\right)\right] \rangle \\ &= \frac{1}{\sqrt{2\pi\sigma^2}} \int_{-\infty}^{\infty} \exp\left(-\frac{c_m^2}{2\sigma^2}\right) \exp\left[-sK\left(2|E_n|\cos\theta_n c_m + c_m^2\right)\right] dc_m \quad (\text{A1.10}) \end{aligned}$$

since c_m has been assumed to be a Gaussian random variable. Completing the square in equation (A1.10), we have:

$$\begin{aligned} &= \exp\left(\frac{2\sigma^2 K^2 |E_n|^2 \cos^2 \theta_n s^2}{1 + 2\sigma^2 K s}\right) \\ &\quad \frac{1}{\sqrt{2\pi\sigma^2}} \int_{-\infty}^{\infty} \exp\left[-\frac{(1 + 2\sigma^2 K s)}{2\sigma^2} \left(c_m + \frac{2\sigma^2 K s |E_n| \cos \theta_n}{1 + 2\sigma^2 K s}\right)^2\right] dc_m \quad (\text{A1.11}) \end{aligned}$$

$$= \frac{1}{\sqrt{1 + 2\sigma^2 K s}} \exp\left(\frac{2\sigma^2 K^2 |E_n|^2 \cos^2 \theta_n s^2}{1 + 2\sigma^2 K s}\right) \quad (\text{A1.12})$$

where the Gauss integral:

$$\frac{1}{\sqrt{2\pi\sigma^2}} \int_{-\infty}^{\infty} \exp \left[-\frac{(1+2\sigma^2 Ks)}{2\sigma^2} \left(c_m + \frac{2\sigma^2 Ks |\bar{E}_n| \cos \theta_n}{1+2\sigma^2 Ks} \right)^2 \right] dc_m = \frac{1}{\sqrt{1+2\sigma^2 Ks}} \quad (\text{A1.13})$$

has been used. The Gauss integral also applies to a function with complex coefficients. The proof of this is shown in Appendix C. Similarly for the c_{in} term, we have:

$$\begin{aligned} & \langle \exp \left[-sK \left(-2|E_n| \sin \theta_n c_{in} + c_{in}^2 \right) \right] \rangle \\ &= \frac{1}{\sqrt{2\pi Ks}} \exp \left(\frac{2\sigma^2 K^2 |E_n|^2 \sin^2 \theta_n s^2}{1+2\sigma^2 Ks} \right). \end{aligned} \quad (\text{A1.14})$$

Substituting equations (A1.12) and (A1.14) in equation (A1.9), and since there are M identical terms, we have:

$$F_1(s) = \frac{1}{(1+2\sigma^2 Ks)^M} \exp \left(\frac{-sK \sum |E_n|^2}{1+2\sigma^2 Ks} \right). \quad (\text{A1.15})$$

The PDF for logical ones is obtained by inverting the MGF $F_1(s)$ in equation (A1.15):

$$f_1(y) = \frac{1}{2\pi j} \int_{\alpha-j\infty}^{\alpha+j\infty} F_1(s) \exp(sy) ds. \quad (\text{A1.16})$$

Making a change of variable $u=1+2\sigma^2 Ks$, rearranging terms and using the table of Laplace transforms [35], the PDF for logical ones is given by:

$$f_1(y) = \frac{\exp\left(-\frac{K \sum |E_n|^2 + y}{2\sigma^2 K}\right)}{2\sigma^2 K} \left(\frac{y}{K \sum |E_n|^2}\right)^{\frac{M-1}{2}} I_{M-1}\left(\frac{\sqrt{yK \sum |E_n|^2}}{\sigma^2 K}\right) \quad (\text{A1.17})$$

where I_{M-1} is the modified Bessel function of the first kind with order $M-1$.

For logical zeros, assuming perfect extinction of signal, we have:

$$K \sum |E_n|^2 = 0. \quad (\text{A1.18})$$

Using (A1.18) in (A1.15), the MGF for logical zeros is given by:

$$F_0(s) = \frac{1}{(1 + 2\sigma^2 Ks)^M}. \quad (\text{A1.19})$$

Making the same change of variable $u = 1 + 2\sigma^2 Ks$, the PDF for logical zeros can be easily calculated as:

$$f_0(y) = \frac{1}{(2\sigma^2 K)^M} \frac{y^{M-1}}{(M-1)!} \exp\left(-\frac{y}{2\sigma^2 K}\right). \quad (\text{A1.20})$$

The mean of y for logical ones is given by:

$$\bar{y}_1 = \langle y \rangle_1 = -\frac{dF_1(s)}{ds} \Big|_{s=0} \quad (\text{A1.21})$$

$$= (2\sigma^2 K)M + K \sum |E_n|^2. \quad (\text{A1.22})$$

The variance of logical ones is given by:

$$\sigma_1^2 = \langle y^2 \rangle_1 - (\langle y \rangle_1)^2 \quad (\text{A1.23})$$

where the first term of (A1.23) is:

$$\langle y^2 \rangle_1 = \frac{d^2 F_1(s)}{ds^2} \Big|_{s=0}. \quad (\text{A1.24})$$

Using the results from equations (A1.24) and (A1.22) in (A1.23), the variance of logical ones can be calculated as:

$$\sigma_1^2 = M(2\sigma^2 K)^2 + 2(2\sigma^2 K)(K \sum_i |E_{\eta_i}'|^2). \quad (\text{A1.25})$$

The variance of logical zeros can be obtained by using (A1.18) in (A1.25) as:

$$\sigma_0^2 = M(2\sigma^2 K)^2. \quad (\text{A1.26})$$

Appendix A2

Derivation of equation (2.10.4.1)

The average signal power in the time interval $[0, T]$ is given by:

$$P_{sig} = \frac{K}{\Re T} \int_0^T \hat{E}_s(t) \hat{E}_s^*(t) dt. \quad (\text{A2.1})$$

Using (2.5.11) in (A2.1), we have:

$$P_{sig} = \frac{K}{\Re T} \int_0^T \sum E_n \exp(j\omega_n t) \sum E_n^* \exp(-j\omega_n t) dt \quad (\text{A2.2})$$

$$= \sum E_n \sum E_m^* \frac{K}{\Re T} \int_0^T \exp[j(\omega_n - \omega_m)t] dt. \quad (\text{A2.3})$$

Using the orthogonality property of the exponential function in $[0, T]$ or equation (A1.6), the average signal power becomes:

$$P_{sig} = \frac{K}{\Re} \sum |E_n|^2. \quad (\text{A2.4})$$

Multiplying both sides by the responsivity \Re of the photodiode, we have:

$$K \sum |E_n|^2 = \Re P_{sig}. \quad (\text{A2.5})$$

Appendix A3

Derivation of probability of error for logical ones

The probability of error for logical ones is given by:

$$P_1(I_d) = 1 - \int_{I_d}^{\infty} f_1(y) dy \quad (\text{A3.1})$$

$$= 1 - \int_{I_d}^{\infty} \left(\frac{M}{\Re P_{ase}} \right) \left(\frac{y}{\Re P_{sig}} \right)^{\frac{M-1}{2}} \exp \left(-\frac{M(y + \Re P_{sig})}{\Re P_{ase}} \right) I_{M-1} \left(\frac{2M\sqrt{y\Re P_{ase}}}{\Re P_{ase}} \right) dy. \quad (\text{A3.2})$$

$$\text{Let} \quad a = \sqrt{\frac{2MP_{sig}}{P_{ase}}} \quad (\text{A3.3})$$

$$\text{then} \quad 2M \frac{\sqrt{y\Re P_{sig}}}{\Re P_{ase}} = \sqrt{\frac{2My}{\Re P_{ase}}} \cdot \sqrt{\frac{2MP_{sig}}{P_{ase}}} \quad (\text{A3.4})$$

$$= \sqrt{\frac{2My}{\Re P_{ase}}} \cdot a. \quad (\text{A3.5})$$

$$\text{Let} \quad u = \sqrt{\frac{2My}{\Re P_{ase}}} \quad (\text{A3.6})$$

$$\text{then} \quad y = \frac{\Re P_{ase} u^2}{2M} \quad (\text{A3.7})$$

$$\text{and} \quad dy = \frac{\Re P_{ase}}{M} u du. \quad (\text{A3.8})$$

When $y \rightarrow \infty$, $u \rightarrow \infty$, and when $y = I_d$, (A3.6) becomes:

$$u = \sqrt{\frac{2MI_d}{\Re P_{ase}}} = b. \quad (\text{A3.9})$$

Substituting (A3.7) to (A3.9) in (A3.2), and rearranging terms, the error probability of logical ones can be expressed as:

$$1 - \int_b^\infty u \left(\frac{u}{\sqrt{2MP_{sig}/P_{ase}}} \right)^{M-1} \exp \left[- \left(\frac{u^2}{2} + \frac{MP_{sig}}{P_{ase}} \right) \right] I_{M-1} \left(\sqrt{\frac{2MP_{sig}}{P_{ase}}} u \right) du \quad (A3.10)$$

$$= 1 - \int_b^\infty u \left(\frac{u}{a} \right)^{M-1} \exp \left(- \frac{u^2 + a^2}{2} \right) I_{M-1}(au) du. \quad (A3.11)$$

The integral in (A3.11) is the integral representation of the generalized Q-function, therefore the error probability for logical ones is:

$$P_1(I_d) = 1 - Q_M(a, b) \quad (A3.12)$$

where a and b are given by (A3.3) and (A3.9) respectively.

Derivation of probability of error for logical zeros

The probability of error for logical zeros is given by:

$$P_0(I_d) = \int_{I_d}^\infty f_0(y) dy \quad (A3.13)$$

$$= \int_{I_d}^\infty \left(\frac{M}{\Re P_{ase}} \right)^M \frac{y^{M-1}}{(M-1)!} \exp \left(- \frac{yM}{\Re P_{ase}} \right) dy. \quad (A3.14)$$

$$\text{Let } y = \frac{\Re P_{ase}}{M} u \quad (A3.15)$$

$$\text{then } dy = \frac{\Re P_{ase}}{M} du. \quad (A3.16)$$

When $y \rightarrow \infty$, $u \rightarrow \infty$ and when $y = I_d$, (A3.15) becomes:

$$u = \frac{M}{\Re P_{ase}} I_d = c. \quad (\text{A3.17})$$

Using (A3.15) to (A3.17) in (A3.14), the error probability can be expressed as:

$$P_0(I_d) = \frac{1}{(M-1)!} \int_c^\infty u^{M-1} \exp(-u) du. \quad (\text{A3.18})$$

The integral in (A3.18) can be solved by integration by parts. After applying integration by parts $(M-1)$ times, we have M similar terms added together and the error probability for logical zeros is:

$$P_0(I_d) = \sum_{r=0}^{M-1} \left(\frac{I_d M}{\Re P_{ase}} \right)^r \frac{\exp\left(-\frac{I_d M}{\Re P_{ase}}\right)}{r!}. \quad (\text{A3.19})$$

Appendix A4

Derivation of error upper bound

The truncation error is given by:

$$Err(L) = |Q_M(a, b) - \hat{Q}_M(a, b)|. \quad (A4.1)$$

Consider the case when $a \geq b$, using (2.12.7), (2.12.9) and (2.12.11) in (A4.1), we have:

$$Err(L) = \exp\left(-\frac{a^2 + b^2}{2}\right) \sum_{k=L+1}^{\infty} \left(\frac{b}{a}\right)^k I_k(ab) \quad (A4.2)$$

$$\leq \exp\left(-\frac{a^2 + b^2}{2}\right) \left(\frac{b}{a}\right)^L \sum_{k=L+1}^{\infty} I_k(ab) \quad (\text{since } a \geq b) \quad (A4.3)$$

$$\leq \exp\left(-\frac{a^2 + b^2}{2}\right) \left(\frac{b}{a}\right)^L I_{L+1}(ab) \left(1 + \sqrt{\frac{\pi ab}{2}}\right) \quad (A4.4)$$

where the inequality [25]:

$$\sum_{k=L+1}^{\infty} I_k(ab) \leq I_{L+1}(ab) \left(1 + \sqrt{\frac{\pi ab}{2}}\right) \quad (A4.5)$$

has been used for (A4.4).

Consider the case when $b > a$, the function $\hat{Q}_M(a, b)$ in (2.12.12) can be rewritten as:

$$\hat{Q}_M(a, b) = \exp\left(-\frac{a^2 + b^2}{2}\right) \left[\sum_{k=0}^L \left(\frac{a}{b}\right)^k I_k(ab) + \sum_{k=1}^{M-1} \left(\frac{b}{a}\right)^k I_k(ab) \right] \quad (A4.6)$$

where the property $I_{-M}(x) = I_M(x)$ (M is an integer) has been used.

Using (2.12.7), (2.12.8) and (A4.6) in (A4.1), we have:

$$Err(L) = \exp\left(-\frac{a^2 + b^2}{2}\right) \sum_{k=L+1}^{\infty} \left(\frac{a}{b}\right)^k I_k(ab) \quad (\text{A4.7})$$

$$< \exp\left(-\frac{a^2 + b^2}{2}\right) \left(\frac{a}{b}\right)^L \sum_{k=L+1}^{\infty} I_k(ab) \quad (\text{since } b > a) \quad (\text{A4.8})$$

$$\leq \exp\left(-\frac{a^2 + b^2}{2}\right) \left(\frac{a}{b}\right)^L I_{L+1}(ab) \left(1 + \sqrt{\frac{\pi ab}{2}}\right) \quad (\text{A4.9})$$

where the inequality in (A4.5) has been used.

Appendix A5

Equations of PDFs When Polarizer is Omitted

Without the polarizer, the filtered signal and ASE electric fields can be expressed as complex spatial vectors:

$$\vec{\tilde{E}}_s(t) = \sum E_n \exp(j\omega_n t) \vec{a}_x \quad (\text{A5.1})$$

$$\vec{\tilde{e}}_{sp}(t) = \sum c_n \exp(j\omega_n t) \vec{a}_x + \sum d_n \exp(j\omega_n t) \vec{a}_y \quad (\text{A5.2})$$

where the signal is assumed to be linearly polarized in the x-direction and the ASE electric field has components in both x and y-direction. The real and imaginary parts of the complex expansion coefficients d_n are assumed to be independent identically distributed Gaussian random variables with zero means and the same variance σ^2 which is also the variance for the real and imaginary parts of c_n . The total electric field is then given by:

$$\vec{\tilde{E}}_s(t) + \vec{\tilde{e}}_{sp}(t) = [\sum E_n \exp(j\omega_n t) + \sum c_n \exp(j\omega_n t)] \vec{a}_x + \sum d_n \exp(j\omega_n t) \vec{a}_y \quad (\text{A5.3})$$

The time averaged photocurrent is:

$$y = \frac{K}{T} \int_0^T \left| \vec{\tilde{E}}_s(t) + \vec{\tilde{e}}_{sp}(t) \right|^2 dt. \quad (\text{A5.4})$$

The integrand in (A5.4) can be expanded as:

$$\left| \vec{\tilde{E}}_s(t) + \vec{\tilde{e}}_{sp}(t) \right|^2 = [\vec{\tilde{E}}_s(t) + \vec{\tilde{e}}_{sp}(t)] [\vec{\tilde{E}}_s^*(t) + \vec{\tilde{e}}_{sp}^*(t)]. \quad (\text{A5.5})$$

Using $\vec{a}_x \cdot \vec{a}_y = 0$ and following the similar procedures shown in Appendix A1, we have:

$$y = K \sum |E_n|^2 + 2K \sum |E_n| (c_m \cos \theta_n - c_m \sin \theta_n) + K \sum |c_n|^2 + K \sum |d_n|^2 \quad (\text{A5.6})$$

The MGF of the PDF for logical ones can also be calculated using Appendix A1 and it can be written as:

$$F_1(s) = \langle \exp(-sy) \rangle = \frac{1}{(1 + 2\sigma^2 Ks)^M} \exp\left(\frac{-sK \sum |E_n|^2}{1 + 2\sigma^2 Ks}\right) \cdot \frac{1}{(1 + 2\sigma^2 Ks)^M}. \quad (\text{A5.7})$$

Equation (A5.7) differs from equation (A1.15) by an extra term $\frac{1}{(1 + 2\sigma^2 Ks)^M}$ which is the result of the term $K \sum |d_n|^2$ in equation (A5.6). Therefore the MGF of logical ones is:

$$F_1(s) = \langle \exp(-sy) \rangle = \frac{1}{(1 + 2\sigma^2 Ks)^{2M}} \exp\left(\frac{-sK \sum |E_n|^2}{1 + 2\sigma^2 Ks}\right). \quad (\text{A5.8})$$

For logical zeros, $K \sum |E_n|^2 = 0$ and hence the MGF is:

$$F_0(s) = \langle \exp(-sy) \rangle = \frac{1}{(1 + 2\sigma^2 Ks)^{2M}}. \quad (\text{A5.9})$$

The MGFs in (A5.8) and (A5.9) differ from the ones in (A1.15) and (A1.19) by the parameter M . It is obvious that if we take the inverse Laplace transform of (A5.8) and (A5.9), the PDFs will be identical to the ones in (A1.17) and (A1.20) except that the parameter M is replaced by $2M$. In general when the polarizer is omitted, all the appearances of M in the equations of PDFs, means and variances must be replaced by $2M$.

Appendix B

Derivations of The Probabilities of Errors

The probability of error for logical ones is given by:

$$P_1 = \int_{-\infty}^{I_d} f_1(y) dy \quad (\text{B.1})$$

where I_d is the threshold current. Using equation (3.5.3.6), the probability of error is:

$$P_1 = \frac{1}{B} \int_{-\infty}^{I_d} \frac{\exp[F_1(u_o)]}{\sqrt{2\pi F_1''(u_o)}} dy \quad (\text{B.2})$$

where subscripts are used for denoting logical ones. By rearranging equation (3.5.1.2), the time averaged current y can be expressed in terms of the saddle point u_o :

$$y = \frac{A}{u_o^2} + \frac{MB}{u_o} - \frac{2C(u_o - 1)}{B} \quad (\text{B.3})$$

$$\text{and} \quad \frac{dy}{du_o} = -\frac{2A}{u_o^3} - \frac{MB}{u_o^2} - \frac{2C}{B}. \quad (\text{B.4})$$

From (B.3), when $y = I_d$, $u_o = u_o(I_d)$, and when $y \rightarrow -\infty$, $u_o \rightarrow \infty$, therefore the probability of error can be expressed as:

$$P_1 = \frac{1}{B\sqrt{2\pi}} \int_{\infty}^{u_o(I_d)} \frac{\exp[F_1(u_o)]}{\sqrt{F_1''(u_o)}} \frac{dy}{du_o} du_o. \quad (\text{B.5})$$

From equations (3.5.2.6) and (B.4), we can obtain the following relation:

$$-\frac{dy}{du_o} \frac{1}{\sqrt{F_1''(u_o)}} = \sqrt{B} \sqrt{\frac{2A}{u_o^3} + \frac{MB}{u_o^2} + \frac{2C}{B}}. \quad (\text{B.6})$$

Using equations (B.6) in (B.5), we have:

$$P_1 = \frac{1}{\sqrt{2\pi B}} \int_{u_o(I_d)}^{\infty} \exp \left[F_1(u_o) + \frac{1}{2} \ln \left(\frac{2A}{u_o^3} + \frac{2C}{B} + \frac{MB}{u_o^2} \right) \right] du_o. \quad (\text{B.7})$$

Equation (B.7) can be simplified by making the substitutions:

$$G_1(u_o) = F_1(u_o) + \frac{1}{2} \ln \left(\frac{2A}{u_o^3} + \frac{2C}{B} + \frac{MB}{u_o^2} \right) \quad (\text{B.8})$$

and $u_{d1} = u_o(I_d)$ be the saddle point at the decision threshold I_d for logical ones, and $u = u_o$, we have:

$$P_1 = \frac{1}{\sqrt{2\pi B}} \int_{u_{d1}}^{\infty} \exp[G_1(u)] du \quad (\text{B.9})$$

$$\text{where} \quad G_1(u) = F_1(u) + \frac{1}{2} \ln \left(\frac{2A}{u^3} + \frac{2C}{B} + \frac{MB}{u^2} \right). \quad (\text{B.10})$$

The integral in (B.9) can be evaluated using the Taylor series expansion. Expanding $G_1(u)$ as Taylor series at u_{d1} and ignoring high order terms, we have:

$$G_1(u) \cong G_1(u_{d1}) + (u - u_{d1})G_1'(u_{d1}). \quad (\text{B.11})$$

Substituting (B.11) into (B.9), the probability of error can be approximated as:

$$P_1 \cong \frac{\exp[G_1(u_{d1})]}{\sqrt{2\pi B}} \int_{u_{d1}}^{\infty} \exp[G_1'(u_{d1})(u - u_{d1})] du \quad (\text{B.12})$$

$$= \frac{\exp[G_1(u_{d1})]}{\sqrt{2\pi B}} \left[\frac{-1}{G_1'(u_{d1})} \right] \quad (\text{assume } G_1'(u_{d1}) < 0). \quad (\text{B.13})$$

The Taylor series expansion is a very good approximation. Fig. B.1 shows an example of the original function and the approximated function. Note that the functions plotted are actually the exponential of the function $G_1(u)$ or the integrand of the integral in (B.9). The value of u_{d1} in this example is 1.39.

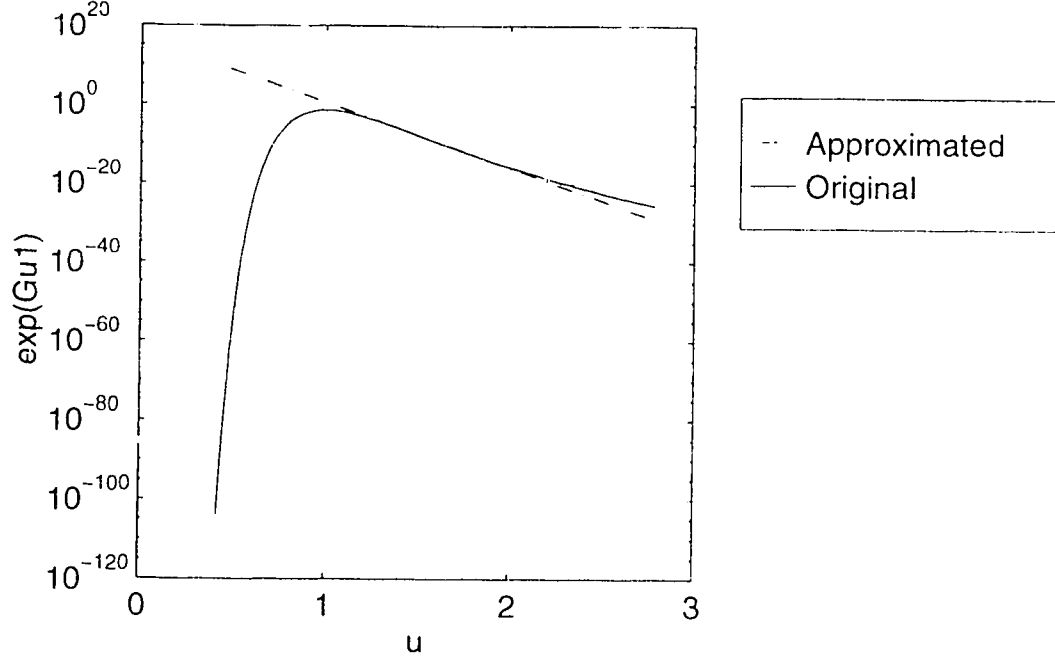


Fig. B.1. Taylor series approximation to $G_1(u)$.

The original function is integrated by using numerical integration (trapezoidal rule) and the result is compared with the one obtained by using the approximated equation. Denoting the exact probability of error for logical ones (obtained by numerical integration) as P_{lexact} and the approximated probability of error (obtained by Taylor series expansion) as P_{lapp} , the absolute percentage error can be calculated as:

$$\%Error = \left| 1 - \frac{P_{lapp}}{P_{lexact}} \right|. \quad (B.14)$$

The absolute percentage error is plotted as a function of the probability of error in Fig. B.2.

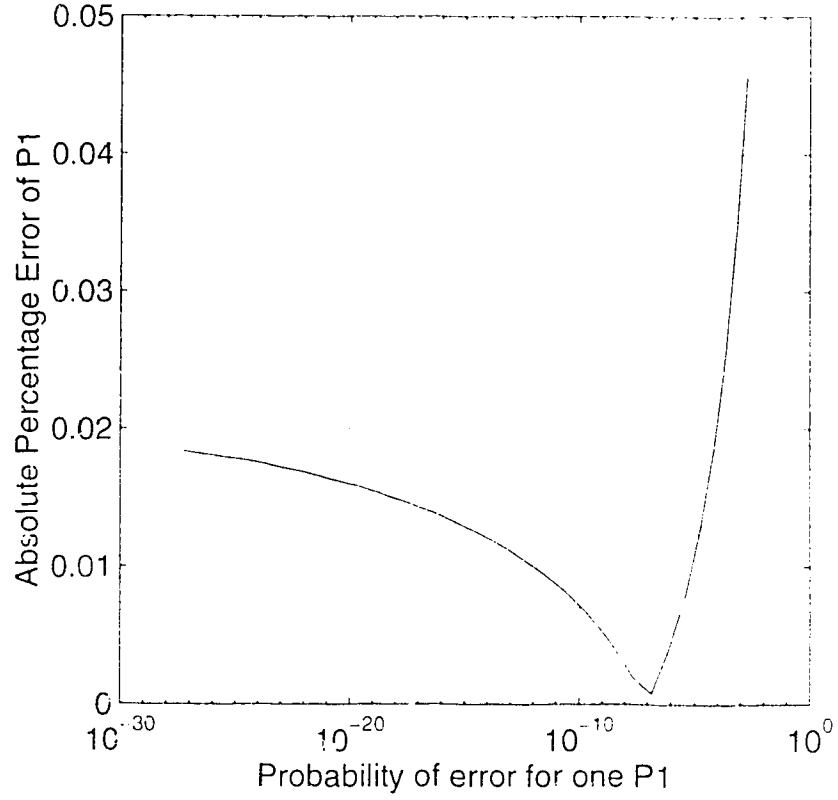


Fig. B.2. Absolute percentage error of P_1 .

As it can be seen from Fig. B.2, the approximation is very good, the error starts to increase when the probability of error is large.

The probability of error for logical zeros is given by:

$$P_0 = \int_{I_d}^{\infty} f_0(y) dy. \quad (\text{B.15})$$

Using (3.5.3.6) and subscripts to denote logical zeros, we have:

$$P_0 = \frac{1}{B} \int_{I_d}^{\infty} \frac{\exp[F_0(u_o)]}{\sqrt{2\pi F_0''(u_o)}} dy. \quad (\text{B.16})$$

Using (B.3) and making a change of variable, we have:

$$= \frac{1}{B\sqrt{2\pi}} \int_0^{u_0(I_d)} \frac{\exp[F_0(u_0)]}{\sqrt{F_0''(u_0)}} \left(-\frac{dy}{du_0} \right) du_0. \quad (\text{B.17})$$

Using (B.6) and (B.8), and change the subscript to logical zeros, we have:

$$P_0 = \frac{1}{\sqrt{2\pi B}} \int_0^{u_{d0}} \exp[G_0(u)] du \quad (\text{B.18})$$

where $u_{d0} = u_o(I_d)$ and $G_0(u)$ is given by the expression in equation (B.8) with different values of constants A and C . Using Taylor series expansion for $G_0(u)$ at u_{d0} and integrating, we have:

$$P_0 = \frac{\exp[G_0(u_{d0})]}{\sqrt{2\pi B}} \left\{ \frac{1 - \exp[-G_0'(u_{d0})u_{d0}]}{G_0'(u_{d0})} \right\} \quad (\text{B.19})$$

where u_{d0} is the saddle point at decision threshold for logical zeros. Fig. B.3 shows the original function and the approximated function.

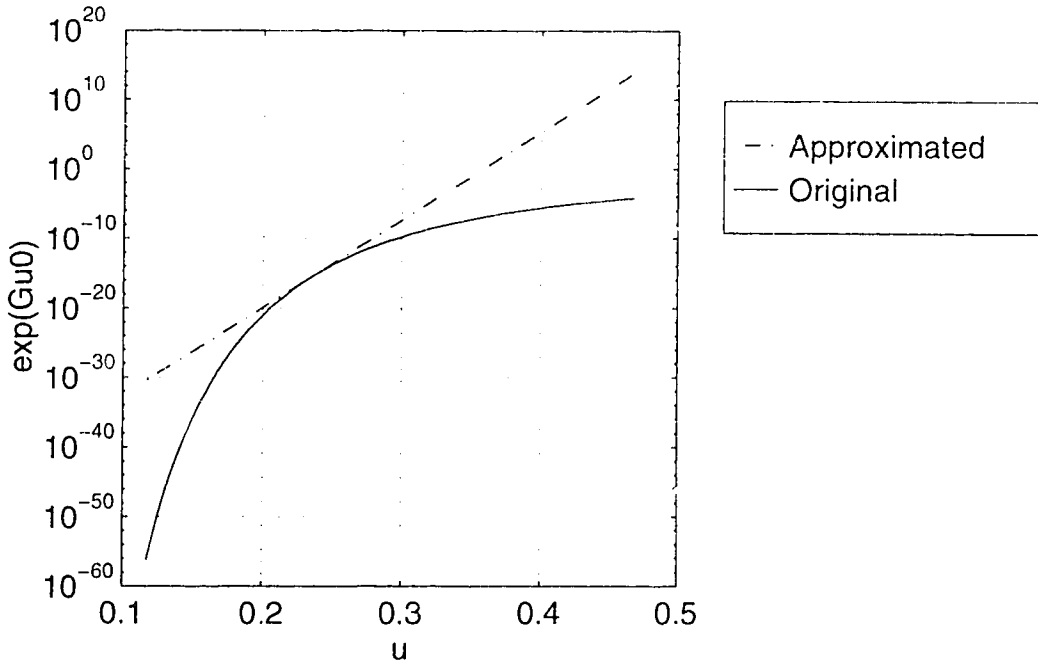


Fig. B.3. Taylor series approximation to $G_0(u)$.

The value of u_{d0} in Fig. B.3 is 0.23. The absolute percentage error is plotted as a function of the probability of error in Fig. B.4.

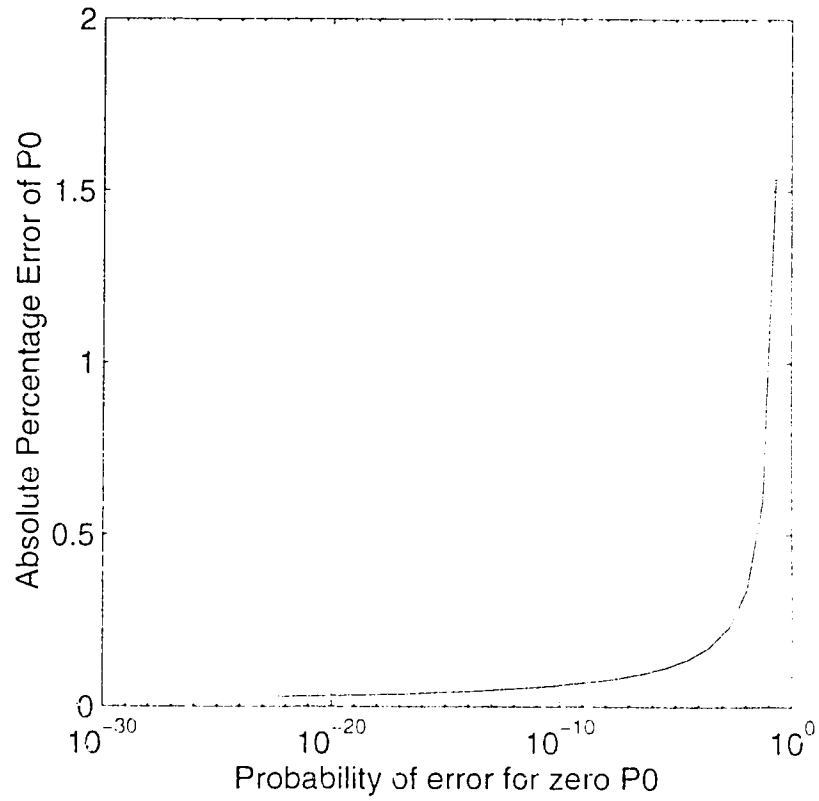


Fig. B.4. Absolute percentage error of P_0 .

The error for the probability of error for logical zeros is larger than that for logical ones. However the error in the range of interest ($P_0 < 10^{-5}$) is less than 10% which is still tolerable.

Appendix C

Derivation of the Value of Gauss Integral With Complex Argument

Consider a Gauss integral with complex argument s :

$$\int_{-\infty}^{\infty} \exp\left[-\frac{(y + \sigma^2 s)^2}{2\sigma^2}\right] dy \quad (C1)$$

where σ^2 is a constant and y is the variable. Let

$$z = \frac{y + \sigma^2 s}{\sqrt{2}\sigma} \quad (C2)$$

$$= \frac{y + \sigma^2 \operatorname{Re}\{s\} + j\sigma^2 \operatorname{Im}\{s\}}{\sqrt{2}\sigma} \quad (C3)$$

so that (C1) can be written as:

$$\sqrt{2}\sigma \int_{-\infty + j\frac{\sigma \operatorname{Im}\{s\}}{\sqrt{2}}}^{\infty + j\frac{\sigma \operatorname{Im}\{s\}}{\sqrt{2}}} \exp(-z^2) dz. \quad (C4)$$

Now consider the integral:

$$\int_C \exp(-z^2) dz \quad (C5)$$

where C is a closed contour as shown in Fig. C1.

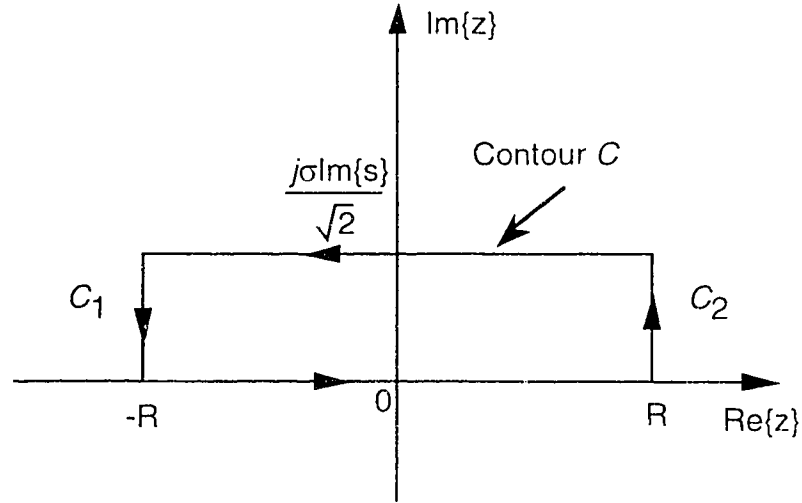


Fig. C1 Closed contour of (C5).

Since there is no pole inside and on the contour C (as the integrand in (C5) is analytic everywhere), the integral in (C5) is equal to zero by the Cauchy-Gourmat theorem [29]:

$$\int_C \exp(-z^2) dz = 0. \quad (C6)$$

The integral in (C6) can be written as the sum of four integrals along the contour C :

$$\int_{R+j\frac{\sigma \text{Im}\{s\}}{\sqrt{2}}}^{-R+j\frac{\sigma \text{Im}\{s\}}{\sqrt{2}}} \exp(-z^2) dz + \int_{C_1} \exp(-z^2) dz + \int_{-R}^R \exp(-z^2) dz + \int_{C_2} \exp(-z^2) dz = 0 \quad (C7)$$

where R is a constant.

Consider the last integral in (C7), it can be written as:

$$\int_{C_2} \exp(-z^2) dz = \int_R^{R+j\frac{\sigma \text{Im}\{s\}}{\sqrt{2}}} \exp(-z^2) dz. \quad (C8)$$

Since

$$z = z_r + jz_i \quad (C9)$$

where z_r and z_i are the real and imaginary parts of z , along path C_2 , the real part of z is equal to the constant R , hence:

$$dz = jdz_i. \quad (C10)$$

Using (C9) and (C10), the integral in (C8) can be written as:

$$j \exp(-z_r^2) \int_0^{\frac{\sigma \text{Im}\{s\}}{\sqrt{2}}} \exp(z_i^2 - j2z_r z_i) dz_i. \quad (C11)$$

Taking the modulus of (C11), we have:

$$0 \leq \exp(-z_r^2) \left| \int_0^{\frac{\sigma \text{Im}\{s\}}{\sqrt{2}}} \exp(z_i^2 - j2z_r z_i) dz_i \right| \leq \exp(-z_r^2) \int_0^{\frac{\sigma \text{Im}\{s\}}{\sqrt{2}}} \left| \exp(z_i^2 - j2z_r z_i) \right| dz_i \quad (C12)$$

$$= \exp(-z_r^2) V \quad (C13)$$

$$= \frac{V}{\exp(R^2)}. \quad (C14)$$

where the integral in (C12) has been replaced by V . As $R \rightarrow \infty$, (C14) approaches zero and hence the integral in (C8) approaches zero. Similarly the second integral in (C7) also approaches zero as $R \rightarrow \infty$. Therefore as R approaches infinity, (C7) becomes:

$$\int_{-\infty + j\frac{\sigma \text{Im}\{s\}}{\sqrt{2}}}^{\infty + j\frac{\sigma \text{Im}\{s\}}{\sqrt{2}}} \exp(-z^2) dz = \int_{-\infty}^{\infty} \exp(-z^2) dz = \int_{-\infty}^{\infty} \exp(-z_r^2) dz_r \quad (C15)$$

$$= \sqrt{\pi}. \quad (C16)$$

Therefore (C1) and (C4) are equal to $\sqrt{2\pi}\sigma$.

Appendix D

Matlab Programs

Parameters

% The following values of parameters are common to all the programs and will not be repeated.

% Values of Common Parameters

```
h=6.6262e-34;      % Planck's constant (J-s)
q=1.6022e-19;      % electron charge (C)
c=3e8;             % free space light speed (m/s)
lambda=1.55e-6;     % operating wavelength (m)
f=c/lambda;         % operating frequency (Hz)
prob1=0.5;          % probability of receiving a logical one
prob0=0.5;          % probability of receiving a logical zero
muin=10^(0/10);     % EDFA input coupling loss
muout=10^(0/10);    % EDFA output coupling loss
L=10^(0/10);        % additional loss after EDFA
```

Program 1

% This program calculates and plots the PDFs of the logical ones and logical zeros in an EDFA preamplified optical digital transmission system. The calculation neglects the thermal and the shot noises. The equations for the PDFs of logical ones and logical zeros are the Central and Non-central Chi-Square distributions respectively. The random variable is the time averaged photocurrent. Note that for non-zero extinction ratio, the Non-Central Chi-Square distribution can be used for the logical zeros.

```
clear, clg
delta=0;            % extinction ratio (ratio of powers of logical ones to logical zeros)
Pin1b=10^(-32/10)*1e-3; % input power for logical ones to EDFA before loss (W)
Pin0b=delta*Pin1b;   % input power for logical zeros to EDFA before loss (W)
Pinavb=prob1*Pin1b+prob0*Pin0b; % average input power to EDFA before loss (W)
PinavdBmb=10*log10(Pinavb/1e-3); % average input power before loss (dBm)
Pin1=muin*Pin1b;     % input power for logical ones to EDFA after loss (W)
Pin0=delta*Pin1;     % input power for logical zeros to EDFA after loss (W)
Pinav=prob1*Pin1+prob0*Pin0; % average input power to EDFA after loss (W)
PinavdBm=10*log10(Pinav/1e-3); % average input power after loss (dBm)
Psat=30e-3;          % EDFA saturation power (W)
Go=10^(30/10);        % EDFA small signal power gain
% Use Newton Raphson Method to solve for the EDFA gain
G=Go;                % starting point
g=G-Go*exp((1-G)*Pinav/Psat); % function to be solved
gp=1+(Go*Pinav/Psat)*exp((1-G)*Pinav/Psat); % first derivative of g(G)
eps=1e-10;           % error limit
while abs(g)>eps
    G=G-g/gp;
    g=G-Go*exp((1-G)*Pinav/Psat); % g(G)
    gp=1+(Go*Pinav/Psat)*exp((1-G)*Pinav/Psat); % g'(G)
end
Belec=20e9;           % electrical bandwidth (2-sided) (Hz)
Bopt=(c/lambda^2)*(1.4*1.3e-9); % optical bandwidth (Hz)
M=round(Bopt/Belec); % ratio of filter bandwidths
mt=1;                 % polarization state parameter (1,2=w/w/o polarizer)
M=mt*M;               % correction to M
Nsp=2;                % spontaneous emission factor of EDFA
```

```

eff=0.8; % detector quantum efficiency
R=eff*q/(h*f); % responsivity of PIN diode (A/W)
Pase=L*muout*mt*Nsp*(G-1)*h*f*Bopt; % ASE power (W)
% Probability density functions of the time averaged photocurrent
npdf=30; % number of points in PDF curves minus one
% For logical zeros - Central Chi-Square distribution
stimo=0.1e-4; % starting point of time averaged current (A)
endimo=3e-4; % end point of time averaged current (A)
stepimo=(endimo-stimo)/npdf; % step of time averaged current (A)
imo=stimo:stepimo:endimo; % time averaged current for logical zeros (A)
fac=gamma(M); % calculate (M-1)!
pdfchi0=(M/(R*Pase))^M*(imo.^(M-1)/fac).*exp(-(imo*M)/(R*Pase));
meanchi0=R*Pase; % mean of PDF (A)
varchi0=(R*Pase)^2/M; % variance of PDF (A^2)
% For non-perfectly extinct logical zeros only
% Non-central Chi-Square
Psig0=L*muout*G*Pin0; % output signal power of EDFA after loss (W)
%imo=stimo:stepimo:endimo; % time averaged current for logical zeros (A)
%argbessel0=2*M*sqrt(imo*R*Psig0)/(R*Pase); % argument of modified Bessel functions
%pdfchi0a=(M/(R*Pase))*(imo/(R*Psig0)).^((M-1)/2).*exp(-
M*(imo+R*Psig0)/(R*Pase));
%pdfchi0=pdfchi0a.*besseli(M-1,argbessel0);
%meanchi0=R*(Pase+Psig0); % mean of PDF (A)
%varchi0=(2*R^2*Pase*Psig0+(R*Pase)^2)/M; % variance of PDF (A^2)
% For logical ones - Non-central Chi-Square distribution
Psig1=L*muout*G*Pin1; % output signal power of EDFA (W)
stim1=2e-4; % starting point of time averaged current (A)
endim1=7e-4; % end point of time averaged current (A)
stepim1=(endim1-stim1)/npdf; % step of time averaged current (A)
im1=stim1:stepim1:endim1; % time averaged current for logical ones (A)
argbessel1=2*M*sqrt(im1*R*Psig1)/(R*Pase); % argument of modified Bessel functions
pdfchi1a=(M/(R*Pase))*(im1/(R*Psig1)).^((M-1)/2).*exp(-M*(im1+R*Psig1)/(R*Pase));
pdfchi1=pdfchi1a.*besseli(M-1,argbessel1);
meanchi1=R*(Pase+Psig1); % mean of PDF (A)
varchi1=(2*R^2*Pase*Psig1+(R*Pase)^2)/M; % variance of PDF (A^2)
% Gaussian approximation
% PDF for logical zeros
stimog=0.1e-4; % starting point of time average current (A)
endimog=1.9e-4; % end point of time averaged current (A)
stepimog=(endimog-stimog)/npdf; % step of time averaged current (A)
imog=stimog:stepimog:endimog; % time averaged current for logical zeros (A)
Imo=R*(Pase+Psig0); % mean current (A)
varo=(2*R^2*Pase*Psig0+(R*Pase)^2)/M; % variance of current (A^2)
pgauss0=(1/sqrt(2*pi*varo))*exp(-(imog-Imo).^2/(2*varo));
% PDF for logical ones
stim1g=1e-4; % starting point of time averaged current (A)
endim1g=7e-4; % end point of time averaged current (A)
stepim1g=(endim1g-stim1g)/npdf; % step of time averaged current (A)
im1g=stim1g:stepim1g:endim1g; % time averaged current for logical ones (A)
Im1=R*(Pase+Psig1); % mean current (A)
var1=(2*R^2*Pase*Psig1+(R*Pase)^2)/M; % variance of current (A^2)
pgauss1=(1/sqrt(2*pi*var1))*exp(-(im1g-Im1).^2/(2*var1));

```


Program 2

```

% This program calculates the PDFs of the logical ones and logical zeros in an EDFA
% preamplified optical digital transmission system. The calculation uses the equations
% derived from the Steepest Descent Method which can incorporate the thermal and the
% shot noises. The logical zeros does not need to be perfectly extinct. The random
% variable will be the voltage after the electrical amplifiers.
clear, clg
delta=0; % extinction ratio
Pin1b=10^(-33/10)*1e-3; % input power for logical ones to EDFA before loss (W)
Pin0b=delta*Pin1b; % input power for logical zeros to EDFA before loss (W)
Pinavb=prob1*Pin1b+prob0*Pin0b; % average input power to EDFA before loss (W)
PinavdBmb=10*log10(Pinavb/1e-3); % average input power before loss (dBm)
Pin1=muin*Pin1b; % input power for logical ones to EDFA after loss (W)
Pin0=delta*Pin1; % input power for logical zeros to EDFA after loss (W)
Pinav=prob1*Pin1+prob0*Pin0; % average input power to EDFA after loss (W)
PinavdBm=10*log10(Pinav/1e-3); % average input power (dBm)
Psat=30e-3; % EDFA saturation power (W)
Go=10^(30/10); % EDFA small signal power gain
% Use Newton Raphson Method to solve for the EDFA gain
G=Go; % starting point
g=G-Go*exp((1-G)*Pinav/Psat); % function to be solved
gp=1+(Go*Pinav/Psat)*exp((1-G)*Pinav/Psat); % first derivative of g(G)
eps=1e-10; % error limit
while abs(g)>eps
    G=G-g/gp;
    g=G-Go*exp((1-G)*Pinav/Psat); % g(G)
    gp=1+(Go*Pinav/Psat)*exp((1-G)*Pinav/Psat); % g'(G)
end
Belec=20e9; % electrical bandwidth (2-sided) (Hz)
Bopt=(c/lambda^2)*(1.4*1.3e-9); % optical bandwidth (Hz)
M=round(Bopt/Belec); % ratio of filter bandwidths
mt=1; % polarization state parameter (1.2=w/w, w/o polarizer)
M=mt*M; % correction to M
Rin=50; % input resistance of electrical amplifier (Ohm)
% net voltage gain of electrical amplifiers
Gainelec0=10^(20/20); % for logical zeros
Gainelec1=10^(20/20); % for logical ones
Tk=273+25; % temperature (Kelvin)
F=10^(7/10); % noise figure of electrical amplifier
varthermal=(2*k*Tk*F/Rin)*Belec; % variance of thermal noise (A^2)
Nsp=2; % spontaneous emission factor of EDFA
eff=0.8; % detector quantum efficiency
R=eff*q/(h*f); % responsivity of PIN diode (A/W)
Pase=L*muout*mt*Nsp*(G-1)*h*f*Bopt; % ASE power (W)
% Theoretical PDFs Using Steepest Descent Method With Voltage Random Variable
npdf=50; % number of points in PDF minus one
% For logical zeros
Psig0=L*muout*G*Pin0; % output signal power of EDFA (W)
varshot0=q*R*(Pase+Psig0)*Belec; % variance of shot noise for logical zeros (A^2)
stimpdf0=-20e-6; % starting point of time averaged current (A)
endimpdf0=300e-6; % end point of time averaged current (A)
stvmpdf0=stimpdf0*Rin*Gainelec0; % convert to voltage
endvmpdf0=endimpdf0*Rin*Gainelec0;

```

```

stepvmpdf0=(endvmpdf0-stvmpdf0)/npdf; % step of voltage (V)
A=R*Psig0*Rin*Gainelec0;
B=(R*Pase)*Rin*Gainelec0/M;
C=((varthermal+varshot0)*(Rin*Gainelec0)^2)/2;
Fp1=1; % coefficients for the polynomial F'(u)=0
Fp3=-M*B^2/(2*C);
Fp4=-A*B/(2*C);
for vm0=stvmpdf0:stepvmpdf0:endvmpdf0
    Fp2=B*vm0/(2*C)-1;
    Fp=[Fp1 Fp2 Fp3 Fp4];
    rootFp=roots(Fp); % solve for the roots of F'(u)=0
    u=rootFp(find(rootFp>0)); % take positive root
    Fdp=(2*A/B)/u^3+M/u^2+2*C/B^2; % second derivative of F(u)
    Fu=-A*(u-1)/(B*u)+(C/B^2)*(u-1)^2+(vm0/B)*(u-1)-M*log(u);
    pdf0((vm0-stvmpdf0)/stepvmpdf0+1)=exp(Fu)/(B*sqrt(2*pi*Fdp));
end
Vm0=R*(Pase+Psig0)*Rin*Gainelec0; % mean of PDF (V)
% variance of PDF (V^2)
var0=(Rin*Gainelec0)^2*((R*Pase)^2/M+2*R^2*Pase*Psig0/M+varthermal+varshot0);
vm0=stvmpdf0:stepvmpdf0:endvmpdf0;
% For logical ones
Psig1=L*muout*G*Pin1; % output signal power of EDFA (W)
varshot1=q*R*(Pase+Psig1)*Belec; % variance of shot noise for logical ones (A^2)
stimpdf1=120e-6; % starting point of time average current (A)
endimpdf1=1300e-6; % end point of time average current (A)
stvmpdf1=stimpdf1*Rin*Gainelec1; % convert to voltage
endvmpdf1=endimpdf1*Rin*Gainelec1;
stepvmpdf1=(endvmpdf1-stvmpdf1)/npdf; % step of voltage (V)
A=R*Psig1*Rin*Gainelec1;
B=(R*Pase)*Rin*Gainelec1/M;
C=((varthermal+varshot1)*(Rin*Gainelec1)^2)/2;
Fp1=1; % coefficients for the polynomial F'(u)=0
Fp3=-M*B^2/(2*C);
Fp4=-A*B/(2*C);
for vm1=stvmpdf1:stepvmpdf1:endvmpdf1
    Fp2=B*vm1/(2*C)-1;
    Fp=[Fp1 Fp2 Fp3 Fp4];
    rootFp=roots(Fp); % solve for the roots of F'(u)=0
    u=rootFp(find(rootFp>0)); % take positive root
    Fdp=(2*A/B)/u^3+M/u^2+2*C/B^2; % second derivative of F(u)
    Fu=-A*(u-1)/(B*u)+(C/B^2)*(u-1)^2+(vm1/B)*(u-1)-M*log(u);
    pdf1((vm1-stvmpdf1)/stepvmpdf1+1)=exp(Fu)/(B*sqrt(2*pi*Fdp));
end
Vm1=R*(Pase+Psig1)*Rin*Gainelec1; % mean of PDF (V)
% variance of PDF (V^2)
var1=(Rin*Gainelec1)^2*((R*Pase)^2/M+2*R^2*Pase*Psig1/M+varthermal+varshot1);
vm1=stvmpdf1:stepvmpdf1:endvmpdf1;
% Gaussian approximation
% For logical zeros
stvmg0=5*stvmpdf0; % start point (V)
endvmg0=endvmpdf0/1.4; % end point (V)
stepvmg0=(endvmg0-stvmg0)/npdf; % step (V)
vmg0=stvmg0:stepvmg0:endvmg0;
Vm0=R*(Pase+Psig0)*Rin*Gainelec0; % mean of PDF (V)

```

```

% variance of PDF (V^2)
varg0=(Rin*Gainelec0)^2*((2*R^2*Pase*Psig0+(R*Pase)^2)/M+varthermal+varshot0);
pdfgauss0=(1/sqrt(2*pi*varg0))*exp(-(vmg0-Vmg0).^2/(2*varg0));
% For logical ones
stvmg1=-0.5*stvmpdf1; % start point (V)
endvmg1=endvmpdf1/1.1; % end point (V)
stepvmg1=(endvmg1-stvmg1)/npdf; % step (V)
vmg1=stvmg1:stepvmg1:endvmg1;
Vmg1=R*(Pase+Psig1)*Rin*Gainelec1;
varg1=(Rin*Gainelec1)^2*((2*R^2*Pase*Psig1+(R*Pase)^2)/M+varthermal+varshot1);
pdfgauss1=(1/sqrt(2*pi*varg1))*exp(-(vmg1-Vmg1).^2/(2*varg1));

Program 3
% This program uses the Taylor series expansion approximation to calculate the probability
% of error and BER as a function of received power.
clear, clg
delta=10^(-20/10); % extinction ratio
Belec=20e9; % electrical bandwidth (2-sided) (Hz)
Bopt=(c/lambda^2)*(1.4*1.3e-9); % optical bandwidth (Hz)
M=round(Bopt/Belec); % ratio of filter bandwidths
mt=2; % polarization state parameter (1,2=w/w/o polarizer)
M=mt*M; % correction to M
Rin=50; % input resistance of electrical amplifier (Ohm)
Tk=273+25; % temperature (Kelvin)
F=10^(7/10); % noise figure of electrical amplifier
varthermal=(2*k*Tk*F/Rin)*Belec; % variance of thermal noise (A^2)
Psat=30e-3; % EDFA saturation power (W)
Go=10^(30/10); % EDFA small signal power gain
Nsp=2; % spontaneous emission factor
eff=0.8; % detector quantum efficiency
R=eff*q/(h*f); % responsivity of PIN diode (A/W)
stPinldBm=-33; % starting point of input power to EDFA for logical ones (dBm)
endPinldBm=-30; % end point of input power (dBm)
nBER=10; % number of points in the BER curve minus one
stePinldBm=(endPinldBm-stPinldBm)/nBER; % step of input power (dBm)
for PinldBm=stPinldBm:stePinldBm:endPinldBm
    index=(PinldBm-stPinldBm)/stePinldBm+1;
    Pinl=muin*10^(PinldBm/10)*1e-3; % input power to EDFA for logical ones (W)
    Pin0=delta*Pinl; % input power to EDFA for logical zeros (W)
    Pinav=prob1*Pinl+prob0*Pin0; % average input power to EDFA (W)
    PinavdBm=10*log10(Pinav/1e-3); % average input power (dBm)
    % Use Newton Raphson Method to solve for the EDFA gain
    G=Go; % starting point
    g=G-Go*exp((1-G)*Pinav/Psat); % function to be solved
    gp=1+(Go*Pinav/Psat)*exp((1-G)*Pinav/Psat); % first derivative of g(G)
    eps=1e-10; % error limit
    while abs(g)>eps
        G=G-g/gp;
        g=G-Go*exp((1-G)*Pinav/Psat); % g(G)
        gp=1+(Go*Pinav/Psat)*exp((1-G)*Pinav/Psat); % g'(G)
    end
    Psig1=L*muout*G*Pinl; % input power to detector for logical ones (W)
    Psig0=L*muout*G*Pin0; % input power to detector for logical zeros (W)
    Pase=L*muout*mt*Nsp*(G-1)*h*f*Bopt; % ASE power to detector (W)

```

```

varshot0=q*R*(Pasc+Psig0)*Belec; % variance of shot noise (A^2)
varshot1=q*R*(Pasc+Psig1)*Belec; % variance of shot noise (A^2)
% Solve for the optimum threshold using Bisection Method
Id1=R*(Psig0+Pasc); % Id1 and Id2 traps the root Idopt
Id2=R*(Psig1+Pasc);
eps=1e-20; % maximum absolute error
I0=Id2-Id1; % interval contains the root
N=round(log10(I0/eps)/log10(2)-1); % number of iterations
A0=R*Psig0;
B0=(R*Pasc)/M;
C0=(varthermal+varshot0)/2;
F0p1=1; % coefficients for the polynomial F'(u)=0
F0p3=-M*B0^2/(2*C0);
F0p4=-A0*B0/(2*C0);
A1=R*Psig1;
B1=(R*Pasc)/M;
C1=(varthermal+varshot1)/2;
F1p1=1; % coefficients for the polynomial F'(u)=0
F1p3=-M*B1^2/(2*C1);
F1p4=-A1*B1/(2*C1);
for n=1:N
    Id0=(Id1+Id2)/2;
    F0p2=B0*Id0/(2*C0)-1;
    F0p=[F0p1 F0p2 F0p3 F0p4];
    rootF0p=roots(F0p); % solve for the roots of F'(u)=0
    u0=rootF0p(find(rootF0p>0)); % the saddle point
    F0dp=(2*A0/B0)/u0^3+M/u0^2+2*C0/B0^2; % second derivative of F(u)
    Fu0=-A0*(u0-1)/(B0*u0)+(C0/B0^2)*(u0-1)^2+(Id0/B0)*(u0-1)-
M*log(u0);
    F1p2=B1*Id0/(2*C1)-1;
    F1p=[F1p1 F1p2 F1p3 F1p4];
    rootF1p=roots(F1p);
    u1=rootF1p(find(rootF1p>0));
    F1dp=(2*A1/B1)/u1^3+M/u1^2+2*C1/B1^2;
    Fu1=-A1*(u1-1)/(B1*u1)+(C1/B1^2)*(u1-1)^2+(Id0/B1)*(u1-1)-
M*log(u1);
    % Find the intersection of the PDFs at Id0
    FId0=1-(sqrt(F0dp)/exp(Fu0))*(exp(Fu1)/sqrt(F1dp))*(prob1/prob0);
    F0p2=B0*Id1/(2*C0)-1;
    F0p=[F0p1 F0p2 F0p3 F0p4];
    rootF0p=roots(F0p); % solve for the roots of F'(u)=0
    u0=rootF0p(find(rootF0p>0)); % take positive root
    F0dp=(2*A0/B0)/u0^3+M/u0^2+2*C0/B0^2; % second derivative of
F(u)
    Fu0=-A0*(u0-1)/(B0*u0)+(C0/B0^2)*(u0-1)^2+(Id1/B0)*(u0-1)-
M*log(u0);
    F1p2=B1*Id1/(2*C1)-1;
    F1p=[F1p1 F1p2 F1p3 F1p4];
    rootF1p=roots(F1p);
    u1=rootF1p(find(rootF1p>0));
    F1dp=(2*A1/B1)/u1^3+M/u1^2+2*C1/B1^2;
    Fu1=-A1*(u1-1)/(B1*u1)+(C1/B1^2)*(u1-1)^2+(Id1/B1)*(u1-1)-
M*log(u1);
    % Find the intersection of the PDFs at Id1

```

```

        Fld1=1-(sqrt(F0dp)/exp(Fu0))*(exp(Fu1)/sqrt(F1dp))*(prob1/prob0);
        if Fld1*Fld0<0
            Id2=Id0;
        else
            Id1=Id0;
        end
    end
end
% Store the optimum threshold
Id=Id1;
Idopt(index)=Id1;
% Probability of error for logical zeros
F0p2=B0*Id/(2*C0)-1;
F0p=[F0p1 F0p2 F0p3 F0p4];
rootF0p=roots(F0p);
u0=rootF0p(find(rootF0p>0));
%Fu0=-A0*(u0-1)/(B0*u0)+(C0/B0^2)*(u0-1)^2+(Id/B0)*(u0-1)-M*log(u0);
Fu0=-A0*(u0-1)^2/(B0*u0^2)-(C0/B0^2)*(u0-1)^2+M*(u0-1)/u0-M*log(u0);
Gu0=Fu0+0.5*log(2*A0/u0^3+M*B0/u0^2+2*C0/B0);
Gu0p1=(2*A0/B0)*((1-u0)/u0^3);
Gu0p2=(2*C0/B0^2)*(1-u0);
Gu0p3=M*((1-u0)/u0^2);
Gu0p4=(-(3*A0+M*B0*u0)/(2*A0*u0+M*B0*u0^2+2*C0*u0^4/B0));
Gu0p=Gu0p1+Gu0p2+Gu0p3+Gu0p4; % G'(u)
P0(index)=exp(Gu0)*(1-exp(-Gu0p*u0))/(sqrt(2*pi*B0)*Gu0p);
% Probability of error for logical ones
F1p2=B1*Id/(2*C1)-1;
F1p=[F1p1 F1p2 F1p3 F1p4];
rootF1p=roots(F1p);
u1=rootF1p(find(rootF1p>0));
%Fu1=-A1*(u1-1)/(B1*u1)+(C1/B1^2)*(u1-1)^2+(Id/B1)*(u1-1)-M*log(u1);
Fu1=-A1*(u1-1)^2/(B1*u1^2)-(C1/B1^2)*(u1-1)^2+M*(u1-1)/u1-M*log(u1);
Gu1=Fu1+0.5*log(2*A1/u1^3+M*B1/u1^2+2*C1/B1);
Gu1p1=(2*A1/B1)*((1-u1)/u1^3);
Gu1p2=(2*C1/B1^2)*(1-u1);
Gu1p3=M*((1-u1)/u1^2);
Gu1p4=(-(3*A1+M*B1*u1)/(2*A1*u1+M*B1*u1^2+2*C1*u1^4/B1));
Gu1p=Gu1p1+Gu1p2+Gu1p3+Gu1p4; % G'(u)
P1(index)=exp(Gu1)/(sqrt(2*pi*B1)*(-Gu1p));
% Gaussian approximation
Imo=R*(Psig0+Pase); % mean current for logical zeros (A)
% variance of current for logical zeros (A^2)
varo=(2*R^2*Pase*Psig0+(R*Pase)^2)/M+varthermal+varshot0;
Im1=R*(Psig1+Pase); % mean current for logical ones (A)
% variance of current for logical ones (A^2)
var1=(2*R^2*Pase*Psig1+(R*Pase)^2)/M+varthermal+varshot1;
% Solving for the optimum threshold of Gaussian PDFs
A=var1-varo;
B=2*(Im1*varo-Imo*var1);
C=var1*Imo^2-varo*Im1^2-var1*varo*log(prob0^2*var1/(prob1^2*varo));
Idg=roots([A B C]);
Idgauss=Idg(find(Idg>0));
%Idgauss=(Im1*varo+Imo*var1)/(varo+var1); % approximated equation
Idoptg(index)=Idgauss;
% For logical zeros

```

```

    argerfc0=(Idgauss-Imo)/sqrt(2*varo);
    P0g(index)=0.5*erfc(argerfc0);
    % For logical ones
    argerfc1=(Im1-Idgauss)/sqrt(2*var1);
    P1g(index)=0.5*erfc(argerfc1);
    % Noises
    varsh0(index)=varshot0;
    varsh1(index)=varshot1;
    varth(index)=varthermal;
    varspsp(index)=(R*Pase)^2/M;
    varsigsp0(index)=2*R^2*Psig0*Pase/M;
    varsigsp1(index)=2*R^2*Psig1*Pase/M;
    % Calculate percentage threshold
    Idoptper(index)=(Id-Imo)/(Im1-Imo);
    Idoptgper(index)=(Idgauss-Imo)/(Im1-Imo);
end
% Determine the BER
BER=prob0*P0+prob1*P1;
BERg=prob0*P0g+prob1*P1g;
Program 4
% This program uses the Taylor series expansion approximation to calculate the probability
% of error and the BER as a function of the percentage threshold.
clear, clg
delta=10^(-20/10); % extinction ratio
% Input power to EDFA for logical ones before loss (dBm)
Pin1dBmvec=[-35 -34 -33 -32 -31 -30];
Pin1=10.^(Pin1dBmvec/10)*1e-3; % input power to EDFA for logical ones (W)
Pin0=delta*Pin1; % input power to EDFA for logical zeros (W)
Pinav=prob0*Pin0+prob1*Pin1; % average input power to EDFA before loss (W)
PinavdBm=10*log10(Pinav/1e-3); % average input power to EDFA before loss (dBm)
for Pin1dBmindex=1:length(Pin1dBmvec);
    Pin1dBm=Pin1dBmvec(Pin1dBmindex);
    Pin1=muin*10^(Pin1dBm/10)*1e-3; % input power to EDFA for logical ones (W)
    Pin0=delta*Pin1; % input power to EDFA for logical zeros (W)
    Pinav=prob1*Pin1+prob0*Pin0; % average input power to EDFA after loss (W)
    Psat=30e-3; % EDFA saturation power (W)
    Go=10^(30/10); % EDFA small signal power gain
    % Use Newton Raphson Method to solve for the EDFA gain
    G=Go; % starting point
    g=G-Go*exp((1-G)*Pinav/Psat); % function to be solved
    gp=1+(Go*Pinav/Psat)*exp((1-G)*Pinav/Psat); % first derivative of g(G)
    eps=1e-10; % error limit
    while abs(g)>eps
        G=G-g/gp;
        g=G-Go*exp((1-G)*Pinav/Psat); % g(G)
        gp=1+(Go*Pinav/Psat)*exp((1-G)*Pinav/Psat); % g'(G)
    end
    Belec=20e9; % electrical bandwidth (2-sided) (Hz)
    Bopt=(c/lambda^2)*(1.4*1.3e-9); % optical bandwidth (Hz)
    M=round(Bopt/Belec); % ratio of filter bandwidths
    mt=1; % polarization state parameter (1,2=w/,w/o polarizer)
    M=mt*M; % correction to M
    Rin=50; % input resistance of electrical amplifier (Ohm)

```

```

Tk=273+25; % temperature (Kelvin)
F=10^(7/10); % noise figure of electrical amplifier
varthermal=(2*k*Tk*F/Rin)*Belec; % variance of thermal noise (A^2)
Nsp=2; % spontaneous emission factor
eff=0.8; % detector quantum efficiency
R=eff*q/(h*f); % responsivity of PIN diode (A/W)
Pase=L*muout*mt*Nsp*(G-1)*h*f*Bopt; % ASE power (W)
% Solve for the optimum threshold
Psig0=L*muout*G*Pin0;
varshot0=q*R*(Pase+Psig0)*Belec; % variance of shot noise for logical zeros (A^2)
Psig1=L*muout*G*Pin1;
varshot1=q*R*(Pase+Psig1)*Belec; % variance of shot noise for logical ones (A^2)
Id1=R*(Pase+Psig0);
Id2=R*(Psig1+Pase);
eps=1e-20; % maximum absolute error
I0=Id2-Id1;
N=round(log10(I0/eps)/log10(2)-1);
A0=R*Psig0;
B0=(R*Pase)/M;
C0=(varthermal+varshot0)/2;
F0p1=1; % coefficients for the polynomial F'(u)=0
F0p3=-M*B0^2/(2*C0);
F0p4=-A0*B0/(2*C0);
A1=R*Psig1;
B1=(R*Pase)/M;
C1=(varthermal+varshot1)/2;
F1p1=1;
F1p3=-M*B1^2/(2*C1);
F1p4=-A1*B1/(2*C1);
for n=1:N
    Id0=(Id1+Id2)/2;
    F0p2=B0*Id0/(2*C0)-1;
    F0p=[F0p1 F0p2 F0p3 F0p4];
    rootF0p=roots(F0p); % solve for the roots of F'(u)=0
    u0=rootF0p(find(rootF0p>0)); % take positive root
    F0dp=(2*A0/B0)/u0^3+M/u0^2+2*C0/B0^2; % second derivative of F(u)
    Fu0=-A0*(u0-1)/(B0*u0)+(C0/B0^2)*(u0-1)^2+(Id0/B0)*(u0-1)-M*log(u0);
    F1p2=B1*Id0/(2*C1)-1;
    F1p=[F1p1 F1p2 F1p3 F1p4];
    rootF1p=roots(F1p);
    u1=rootF1p(find(rootF1p>0));
    F1dp=(2*A1/B1)/u1^3+M/u1^2+2*C1/B1^2;
    Fu1=-A1*(u1-1)/(B1*u1)+(C1/B1^2)*(u1-1)^2+(Id0/B1)*(u1-1)-M*log(u1);
    Fld0=1-(sqrt(F0dp)/exp(Fu0))*(exp(Fu1)/sqrt(F1dp))*(prob1/prob0);
    F0p2=B0*Id1/(2*C0)-1;
    F0p=[F0p1 F0p2 F0p3 F0p4];
    rootF0p=roots(F0p); % solve for the roots of F'(u)=0
    u0=rootF0p(find(rootF0p>0)); % take positive root
    F0dp=(2*A0/B0)/u0^3+M/u0^2+2*C0/B0^2; % second derivative of F(u)
    Fu0=-A0*(u0-1)/(B0*u0)+(C0/B0^2)*(u0-1)^2+(Id1/B0)*(u0-1)-M*log(u0);
    F1p2=B1*Id1/(2*C1)-1;
    F1p=[F1p1 F1p2 F1p3 F1p4];
    rootF1p=roots(F1p);
    u1=rootF1p(find(rootF1p>0));

```

```

F1dp=(2*A1/B1)/u1^3+M/u1^2+2*C1/B1^2;
Fu1=-A1*(u1-1)/(B1*u1)+(C1/B1^2)*(u1-1)^2+(Id1/B1)*(u1-1)-M*log(u1);
F1d1=1-(sqrt(F0dp)/exp(Fu0))*(exp(Fu1)/sqrt(F1dp))*(prob1/prob0);
if F1d1*F1d0<0
    Id2=Id0;
else
    Id1=Id0;
end
end
Idopt=Id1;
% Probability of error of the mean currents into the decision circuit
nPe=30; % number of points in Pe curve minus one (even integer)
dev=0.05; % deviation from Idopt
stepId=dev*Idopt; % step size of threshold current (A)
stId=Idopt-(nPe/2)*stepId; % starting point of threshold current (A)
endId=Idopt+(nPe/2)*stepId; % end point of threshold current (A)
% Determine the range of current to plot
Id=stId;
[P0,Gu0p]=P0P1(A0,B0,C0,F0p1,F0p3,F0p4,Id,M,0);
while P0>1
    stId=stId+stepId;
    Id=stId;
    [P0,Gu0p]=P0P1(A0,B0,C0,F0p1,F0p3,F0p4,Id,M,0);
end
Id=endId;
[P1,Gu1p]=P0P1(A1,B1,C1,F1p1,F1p3,F1p4,Id,M,1);
while Gu1p>0 | P1>1
    endId=endId-stepId;
    Id=endId;
    [P1,Gu1p]=P0P1(A1,B1,C1,F1p1,F1p3,F1p4,Id,M,1);
end
% Probability of error
nPe=20; % number of points in Pe curve minus one (even integer)
stepId1=(Idopt-stId)/(nPe/2); % step size of threshold current (A)
Id1=stId:stepId1:Idopt-stepId1;
stepId2=(endId-Idopt)/(nPe/2); % step size of threshold current (A)
Id2=Idopt:stepId2:endId;
Idvec=[Id1 Id2];
col=PinIdBmindex;
Idmat(:,col)=Idvec';
Imo=R*(Pase+Psig0); % mean current for logical zeros (A)
Im1=R*(Pase+Psig1); % mean current for logical ones (A)
Idmatper(:,col)=(Idvec-Imo)/(Im1-Imo)';
for Idindex=1:length(Idvec)
    Id=Idvec(Idindex);
    % Probability of error for logical zeros
    [P0vec(Idindex),Gu0p]=P0P1(A0,B0,C0,F0p1,F0p3,F0p4,Id,M,0);
    % Probability of error for logical ones
    [P1vec(Idindex),Gu1p]=P0P1(A1,B1,C1,F1p1,F1p3,F1p4,Id,M,1);
end
P0mat(:,col)=P0vec';
P1mat(:,col)=P1vec';
% Gaussian approximation
% Solve for optimum Id of Gaussian

```



```

Imo=R*(Pase+Psig0); % mean current for logical zeros (A)
varo=(2*R^2*Pase*Psig0+(R*Pase)^2)/M+varthermal+varshot0; % variance for logical
zeros (A^2)
Im1=R*(Pase+Psig1); % mean current for logical ones (A)
var1=(2*R^2*Pase*Psig1+(R*Pase)^2)/M+varthermal+varshot1; % variance for logical
ones (A^2)
A=var1-varo;
B=2*(Im1*varo-Imo*var1);
C=var1*Imo^2-varo*Im1^2-var1*varo*log(prob0^2*var1/(prob1^2*varo));
Idg=roots([A B C]);
Idoptg=Idg(find(Idg>0));
nPc=20; % number of points in Pc curve minus one (even integer)
devg=0.05; % deviation from Idopt
stepIdg=devg*Idoptg; % step size of threshold current (A)
stIdg=Idoptg-(nPc/2)*stepIdg; % starting point of threshold current (A)
endIdg=Idoptg+(nPc/2)*stepIdg; % end point of threshold current (A)
while stIdg<0
    stIdg=stIdg+stepIdg;
    endIdg=endIdg-stepIdg;
end
Idg=stIdg:stepIdg:endIdg; % threshold current for Gaussian (A)
Idmatg(:,col)=Idg';
% Calculate percentage optimum threshold
Idperg=(Idg-Imo)/(Im1-Imo);
Idmatper(:,col)=Idperg';
% For logical zeros
argerfc0=(Idg-Imo)/sqrt(2*varo);
P0g(:,col)=(0.5*erfc(argerfc0));
% For logical ones
argerfc1=(Im1-Idg)/sqrt(2*var1);
P1g(:,col)=(0.5*erfc(argerfc1));
end
% Determine the BER
BER=prob0*P0mat+prob1*P1mat;
BERg=prob0*P0g+prob1*P1g;
% Form the locus
for col=1:length(PinIdBmvec);
    BERIdper=[BER(:,col) Idmatper(:,col)];
    BERmin(col)=min(BER(:,col));
    Idminper(col)=Idmatper(find(BER(:,col)==BERmin(col)),col);
    BERIdperg=[BERg(:,col) Idmatperg(:,col)];
    BERming(col)=min(BERg(:,col));
    Idmingper(col)=Idmatperg(find(BERg(:,col)==BERming(col)),col);
end

```

Program 5

% This sub-routine program calculates the probability of error using the Steepest descent
 % Method and the Taylor series expansion.

```

function[P,Gup]=P0P1(A,B,C,Fp1,Fp3,Fp4,Id,M,status)
Fp2=B*Id/(2*C)-1;
Fp=[Fp1 Fp2 Fp3 Fp4];
rootFp=roots(Fp);
u=rootFp(find(rootFp>0));

```

```

%Fu=-A*(u-1)/(B*u)+(C/B^2)*(u-1)^2+(Id/B)*(u-1)-M*log(u);
Fu=-A*(u-1)^2/(B*u^2)-(C/B^2)*(u-1)^2+M*(u-1)/u-M*log(u);
Gu=Fu+0.5*log(2*A/u^3+M*B/u^2+2*C/B);
Gup1=(2*A/B)*((1-u)/u^3);
Gup2=(2*C/B^2)*(1-u);
Gup3=M*((1-u)/u^2);
Gup4=-(3*A+M*B*u)/(2*A*u+M*B*u^2+2*C*u^4/B);
Gup=Gup1+Gup2+Gup3+Gup4;
if status==0
    P=exp(Gu)*(1-exp(-Gup*u))/(sqrt(2*pi*B)*Gup); % P0
else
    P=exp(Gu)/(sqrt(2*pi*B)*(-Gup)); % P1
end

```

Program 6

% This program calculates the sensitivity versus EDFA small signal gain curve. The % sensitivity can also be calculated as a function of the parameters such as the extinction % ratio, the spontaneous emission factor etc. by simply modifying this program and % varying the values of the parameters.

```

clear, clg
delta=10^(-20/10); % extinction ratio
Belec=20e9; % electrical bandwidth (2-sided) (Hz)
Bopt=(c/lambda^2)*(1.4*1.3e-9); % optical bandwidth (Hz)
M=round(Bopt/Belec); % ratio of filter bandwidths
mt=1; % polarization state parameter (1,2=w/,w/o polarizer)
M=mt*M; % correction to M
Nsp=2; % spontaneous emission factor
BERgoal1=1e-9; % BER needed
BERgoal2=1e-14; % BER needed
epsBER1=1e-15; % tolerable errors
epsBER2=1e-20;
Gop=10.^([10 15 20 25 30 35]/10); % EDFA small signal gain Go
stgo=1; % starting point of Go
endgo=length(Gop); % end point
stepgo=1; % step
for go=stgo:stepgo:endgo
    Go=Gop(go);
    Pin1dBmb=-50; % initial guess of input power to EDFA for logical ones (dBm)
    Pin1b=10^(Pin1dBmb/10)*1e-3; % input power to EDFA for logical ones (W)
    Pin0b=delta*Pin1b; % input signal power to EDFA for logical zeros (W)
    Pinavb=prob1*Pin1b+prob0*Pin0b; % initial average input power to EDFA (W)
    PinavdBmb=10*log10(Pinavb/1e-3); % Pinav in dBm
    BER=BERchi(Bopt,Belec,mt,Nsp,Go,Pin1b,delta,prob1,prob0)
    BERg=BERgauss(Bopt,Belec,mt,Nsp,Go,Pin1b,delta,prob1,prob0)
    absdiff1=BER-BERgoal1; % compare with the BER needed
    absdiff1g=BERg-BERgoal1;
    while abs(absdiff1)>epsBER1
        delPinavdBmb=(1/2)*log10(BER/BERgoal1);
        PinavdBmb=PinavdBmb+delPinavdBmb;
        Pinavb=10^(PinavdBmb/10)*1e-3;
        Pin1b=Pinavb/(prob0*delta+prob1);
        Pin0b=delta*Pin1b;
        BER=BERchi(Bopt,Belec,mt,Nsp,Go,Pin1b,delta,prob1,prob0)
        absdiff1=BER-BERgoal1;
    end
end

```

```

end
sen1(go)=PinavdBmb
while abs(absdiff1g)>epsBER1
    delPinavdBmgb=(1/2)*log10(BERg/BERgoal1);
    PinavdBmb=PinavdBmb+delPinavdBmgb;
    Pinavb=10^(PinavdBmb/10)*1e-3;
    Pin1b=Pinavb/(prob0*delta+prob1);
    Pin0b=delta*Pin1b;
    BERg=BERgauss(Bopt,Belec,mt,Nsp,Go,Pin1b,delta,prob1,prob0)
    absdiff1g=BERg-BERgoal1;
end
sen1g(go)=PinavdBmb
absdiff2=BER-BERgoal2;
absdiff2g=BERg-BERgoal2;
while abs(absdiff2)>epsBER2
    delPinavdBmb=(1/4)*log10(BER/BERgoal2);
    PinavdBmb=PinavdBmb+delPinavdBmb;
    Pinavb=10^(PinavdBmb/10)*1e-3;
    Pin1b=Pinavb/(prob0*delta+prob1);
    Pin0b=delta*Pin1b;
    BER=BERchi(Bopt,Belec,mt,Nsp,Go,Pin1b,delta,prob1,prob0)
    absdiff2=BER-BERgoal2;
end
sen2(go)=PinavdBmb
while abs(absdiff2g)>epsBER2
    delPinavdBmgb=(1/4)*log10(BERg/BERgoal2);
    PinavdBmb=PinavdBmb+delPinavdBmgb;
    Pinavb=10^(PinavdBmb/10)*1e-3;
    Pin1b=Pinavb/(prob0*delta+prob1);
    Pin0b=delta*Pin1b;
    BERg=BERgauss(Bopt,Belec,mt,Nsp,Go,Pin1b,delta,prob1,prob0)
    absdiff2g=BERg-BERgoal2;
end
sen2g(go)=PinavdBmb
end
GodB=10*log10(Gop);

```

Program 7

% This program uses the Taylor series expansion approximation to calculate the probability
 % of error and the BER as a function of the EDFA small signal gain. The BER can also be
 % calculated as a function of the parameters such as the extinction ratio, the spontaneous
 % emission factor etc. by simply modifying this program and varying the values of the
 % parameters.

```

clear, clg
delta=10^(-20/10); % extinction ratio
Pin1dBm=-32; % input power to EDFA for logical ones (dBm)
% EDFA small signal gain (dB)
Govec=[20 21 22 23 24 25 26 27 28 29 30 31 32 33 34 35];
for Goindex=1:length(Govec);
    Pin1b=10^(Pin1dBm/10)*1e-3; % input power to EDFA for logical ones (W)
    Pin0b=delta*Pin1b; % input power to EDFA for logical zeros (W)
    Pinavb=prob0*Pin0b+prob1*Pin1b;
    PinavdBmb=10*log10(Pinavb/1e-3);
    Pin1=muin*10^(Pin1dBm/10)*1e-3; % input power to EDFA for logical ones (W)

```

```

Pin0=delta*Pin1; % input power to EDFA for logical zeros (W)
Pinav=prob1*Pin1+prob0*Pin0; % average input power to EDFA (W)
Go=10^(Govec(Goindex)/10); % EDFA small signal power gain
Psat=30e-3; % EDFA saturation power (W)
% Use Newton Raphson Method to solve for the EDFA gain
G=Go; % starting point
g=G-Go*exp((1-G)*Pinav/Psat); % function to be solved
gp=1+(Go*Pinav/Psat)*exp((1-G)*Pinav/Psat); % first derivative of g(G)
eps=1e-10; % error limit
while abs(g)>eps
    G=G-g/gp;
    g=G-Go*exp((1-G)*Pinav/Psat); % g(G)
    gp=1+(Go*Pinav/Psat)*exp((1-G)*Pinav/Psat); % g'(G)
end
Belec=20e9; % electrical bandwidth (2-sided) (Hz)
Bopt=(c/lambda^2)*(1.4*1.3e-9); % optical bandwidth (Hz)
M=round(Bopt/Belec); % ratio of filter bandwidths
mt=1; % polarization state parameter (1,2=w/,w/o polarizer)
M=mt*M; % correction to M
Rin=50; % input resistance of electrical amplifier (Ohm)
Tk=273+25; % temperature (Kelvin)
F=10^(7/10); % noise figure of electrical amplifier
varthermal=(2*k*Tk*F/Rin)*Belec; % variance of thermal noise (A^2)
Nsp=2; % spontaneous emission factor
eff=0.8; % detector quantum efficiency
R=eff*q/(h*f); % responsivity of PIN diode (A/W)
Pase=L*muout*mt*Nsp*(G-1)*h*f*Bopt; % ASE power (W)
% Solve for the optimum threshold
Psig0=L*muout*G*Pin0;
varshot0=q*R*(Pase+Psig0)*Belec; % variance of shot noise for logical zeros (A^2)
Psig1=L*muout*G*Pin1;
varshot1=q*R*(Pase+Psig1)*Belec; % variance of shot noise for logical ones (A^2)
Id1=R*(Pase+Psig0);
Id2=R*(Psig1+Pase);
eps=1e-20; % maximum absolute error
I0=Id2-Id1;
N=round(log10(I0/eps)/log10(2)-1);
A0=R*Psig0;
B0=(R*Pase)/M;
C0=(varthermal+varshot0)/2;
F0p1=1; % coefficients for the polynomial F'(u)=0
F0p3=-M*B0^2/(2*C0);
F0p4=-A0*B0/(2*C0);
A1=R*Psig1;
B1=(R*Pase)/M;
C1=(varthermal+varshot1)/2;
F1p1=1;
F1p3=-M*B1^2/(2*C1);
F1p4=-A1*B1/(2*C1);
for n=1:N
    Id0=(Id1+Id2)/2;
    F0p2=B0*Id0/(2*C0)-1;
    F0p=[F0p1 F0p2 F0p3 F0p4];
    rootF0p=roots(F0p); % solve for the roots of F'(u)=0

```

```

u0=rootF0p(find(rootF0p>0)); % take positive root
F0dp=(2*A0/B0)/u0^3+M/u0^2+2*C0/B0^2; % second derivative of F(u)
Fu0=-A0*(u0-1)/(B0*u0)+(C0/B0^2)*(u0-1)^2+(Id0/B0)*(u0-1)-M*log(u0);
F1p2=B1*Id0/(2*C1)-1;
F1p=[F1p1 F1p2 F1p3 F1p4];
rootF1p=roots(F1p);
u1=rootF1p(find(rootF1p>0));
F1dp=(2*A1/B1)/u1^3+M/u1^2+2*C1/B1^2;
Fu1=-A1*(u1-1)/(B1*u1)+(C1/B1^2)*(u1-1)^2+(Id0/B1)*(u1-1)-M*log(u1);
F1d0=1-(sqrt(F0dp)/exp(Fu0))*(exp(Fu1)/sqrt(F1dp))*(prob1/prob0);
F0p2=B0*Id1/(2*C0)-1;
F0p=[F0p1 F0p2 F0p3 F0p4];
rootF0p=roots(F0p); % solve for the roots of F'(u)=0
u0=rootF0p(find(rootF0p>0)); % take positive root
F0dp=(2*A0/B0)/u0^3+M/u0^2+2*C0/B0^2; % second derivative of F(u)
Fu0=-A0*(u0-1)/(B0*u0)+(C0/B0^2)*(u0-1)^2+(Id1/B0)*(u0-1)-M*log(u0);
F1p2=B1*Id1/(2*C1)-1;
F1p=[F1p1 F1p2 F1p3 F1p4];
rootF1p=roots(F1p);
u1=rootF1p(find(rootF1p>0));
F1dp=(2*A1/B1)/u1^3+M/u1^2+2*C1/B1^2;
Fu1=-A1*(u1-1)/(B1*u1)+(C1/B1^2)*(u1-1)^2+(Id1/B1)*(u1-1)-M*log(u1);
F1d1=1-(sqrt(F0dp)/exp(Fu0))*(exp(Fu1)/sqrt(F1dp))*(prob1/prob0);
if F1d1*F1d0<0
    Id2=Id0;
else
    Id1=Id0;
end
end
Idopt=Id1;
% Probability of error of the mean currents into the decision circuit
nPe=30; % number of points in Pe curve minus one (even integer)
dev=0.05; % deviation from Idopt
stepId=dev*Idopt; % step size of threshold current (A)
stId=Idopt-(nPe/2)*stepId; % starting point of threshold current (A)
endId=Idopt+(nPe/2)*stepId; % end point of threshold current (A)
% Determine the range of current to plot
Id=stId;
[P0,Gu0p]=P0P1(A0,B0,C0,F0p1,F0p3,F0p4,Id,M,0);
while P0>1
    stId=stId+stepId;
    Id=stId;
    [P0,Gu0p]=P0P1(A0,B0,C0,F0p1,F0p3,F0p4,Id,M,0);
end
Id=endId;
[P1,Gu1p]=P0P1(A1,B1,C1,F1p1,F1p3,F1p4,Id,M,1);
while Gu1p>0 | P1>1
    endId=endId-stepId;
    Id=endId;
    [P1,Gu1p]=P0P1(A1,B1,C1,F1p1,F1p3,F1p4,Id,M,1);
end
% Probability of error
nPe=20; % number of points in Pe curve minus one (even integer)
stepId1=(Idopt-stId)/(nPe/2); % step size of threshold current (A)

```

```

Id1=stId:stepId1:Idopt-stepId1;
stepId2=(endId-Idopt)/(nPe/2); % step size of threshold current (A)
Id2=Idopt:stepId2:endId;
Idvec=[Id1 Id2];
col=Goindex;
Idmat(:,col)=Idvec';
Imo=R*(Pase+Psig0); % mean current for logical zeros (A)
Im1=R*(Pase+Psig1); % mean current for logical ones (A)
Idmatper(:,col)=((Idvec-Imo)/(Im1-Imo))';
for Idindex=1:length(Idvec)
    Id=Idvec(Idindex);
    % Probability of error for logical zeros
    [P0vec(Idindex),Gu0p]=P0P1(A0,B0,C0,F0p1,F0p3,F0p4,Id,M,0);
    % Probability of error for logical ones
    [P1vec(Idindex),Gu1p]=P0P1(A1,B1,C1,F1p1,F1p3,F1p4,Id,M,1);
end
P0mat(:,col)=P0vec';
P1mat(:,col)=P1vec';
% Gaussian approximation
% Solve for optimum Id of Gaussian
Imo=R*(Pase+Psig0); % mean current for logical zeros (A)
varo=(2*R^2*Pase*Psig0+(R*Pase)^2)/M+varthermal+varshot0; % variance (A^2)
Im1=R*(Pase+Psig1); % mean current for logical ones (A)
var1=(2*R^2*Pase*Psig1+(R*Pase)^2)/M+varthermal+varshot1; % variance (A^2)
A=var1-varo;
B=2*(Im1*varo-Imo*var1);
C=var1*Imo^2-varo*Im1^2-var1*varo*log(prob0^2*var1/(prob1^2*varo));
Idg=roots([A B C]);
Idoptg=Idg(find(Idg>0));
nPe=20; % number of points in Pe curve minus one (even integer)
devg=0.018; % deviation from Idopt
stepIdg=devg*Idoptg; % step size of threshold current (A)
stIdg=Idoptg-(nPe/2)*stepIdg; % starting point of threshold current (A)
endIdg=Idoptg+(nPe/2)*stepIdg; % end point of threshold current (A)
while stIdg<0
    stIdg=stIdg+stepIdg;
    endIdg=endIdg-stepIdg;
end
Idg=stIdg:stepIdg:endIdg; % threshold current for Gaussian (A)
Idmatg(:,col)=Idg';
% Calculate percentage optimum threshold
Idperg=(Idg-Imo)/(Im1-Imo);
Idmatperg(:,col)=Idperg';
% For logical zeros
argerfc0=(Idg-Imo)/sqrt(2*varo);
P0g(:,col)=(0.5*erfc(argerfc0))';
% For logical ones
argerfc1=(Im1-Idg)/sqrt(2*var1);
P1g(:,col)=(0.5*erfc(argerfc1))';

end

% Determine the BER
BER=prob0*P0mat+prob1*P1mat;

```

```

BERg=prob0*P0g+prob1*P1g;
% Form the locus
for col=1:length(Govec);
    BERldper=[BER(:,col) Idmatper(:,col)];
    BERmin(col)=min(BER(:,col));
    Idminper(col)=Idmatper(find(BER(:,col)==BERmin(col)),col);
    BERldperg=[BERg(:,col) Idmatperg(:,col)];
    BERming(col)=min(BERg(:,col));
    Idmingper(col)=Idmatperg(find(BERg(:,col)==BERming(col)),col);
end

```

Program 8

```

% This sub-routine program uses the Taylor series expansion approximation to calculate
% the probability of error and the BER.
function[BER]=BERchi(Bopt,Belec,mt,Nsp,Go,Pin1b,delta,prob1,prob0)
M=round(Bopt/Belec); % ratio of filter bandwidths
M=mt*M; % correction to M
Rin=50; % input resistance of electrical amplifier (Ohm)
Tk=273+25; % temperature (Kelvin)
F=10^(7/10); % noise figure of electrical amplifier
varthermal=(2*k*Tk*F/Rin)*Belec; % variance of thermal noise (A^2)
Psat=30e-3; % EDFA saturation power (W)
eff=0.8; % detector quantum efficiency
R=eff*q/(h*f); % responsivity of PIN diode (A/W)
Pin1=Pin1b*muin; % input power to EDFA for logical ones after loss (W)
Pin0=delta*Pin1; % input power to EDFA for logical zeros after loss (W)
Pinav=prob0*Pin0+prob1*Pin1; % average input power to EDFA after loss (W)
% Use Newton Raphson Method to solve for the EDFA gain
G=Go; % starting point
g=G-Go*exp((1-G)*Pinav/Psat); % function to be solved
gp=1+(Go*Pinav/Psat)*exp((1-G)*Pinav/Psat); % first derivative of g(G)
eps=1e-10; % error limit
while abs(g)>eps
    G=G-g/gp;
    g=G-Go*exp((1-G)*Pinav/Psat); % g(G)
    gp=1+(Go*Pinav/Psat)*exp((1-G)*Pinav/Psat); % g'(G)
end
Psig1=L*muout*G*Pin1; % output power of EDFA for logical ones (W)
Psig0=L*muout*G*Pin0; % output signal power of EDFA for logical zeros (W)
Pase=L*muout*mt*Nsp*(G-1)*h*f*Bopt; % ASE power (W)
% Solve for the optimum threshold using Bisection Method
varshot0=q*R*(Pase+Psig0)*Belec; % variance of shot noise for logical zeros (A^2)
varshot1=q*R*(Pase+Psig1)*Belec; % variance of shot noise for logical ones (A^2)
Id1=R*(Psig0+Pase); % Id1 and Id2 traps the root Idopt
Id2=R*(Psig1+Pase);
eps=1e-20; % maximum absolute error
I0=Id2-Id1; % interval contains the root
N=round(log10(I0/eps)/log10(2)-1); % number of iterations
A0=R*Psig0;
B0=(R*Pase)/M;
C0=(varthermal+varshot0)/2;
F0p1=1; % coefficients for the polynomial F(u)=0

```

```

F0p3=-M*B0^2/(2*C0);
F0p4=-A0*B0/(2*C0);
A1=R*Psig1;
B1=(R*Pase)/M;
C1=(varthermal+varshot1)/2;
F1p1=1;
F1p3=-M*B1^2/(2*C1);
F1p4=-A1*B1/(2*C1);
for n=1:N
    Id0=(Id1+Id2)/2;
    F0p2=B0*Id0/(2*C0)-1;
    F0p=[F0p1 F0p2 F0p3 F0p4];
    rootF0p=roots(F0p); % solve for the roots of F'(u)=0
    u0=rootF0p(find(rootF0p>0)); % the saddle point
    F0dp=(2*A0/B0)/u0^3+M/u0^2+2*C0/B0^2; % second derivative of F(u)
    Fu0=-A0*(u0-1)/(B0*u0)+(C0/B0^2)*(u0-1)^2+(Id0/B0)*(u0-1)-M*log(u0);
    F1p2=B1*Id0/(2*C1)-1;
    F1p=[F1p1 F1p2 F1p3 F1p4];
    rootF1p=roots(F1p);
    u1=rootF1p(find(rootF1p>0));
    F1dp=(2*A1/B1)/u1^3+M/u1^2+2*C1/B1^2;
    Fu1=-A1*(u1-1)/(B1*u1)+(C1/B1^2)*(u1-1)^2+(Id0/B1)*(u1-1)-M*log(u1);
    FId0=1-(sqrt(F0dp)/exp(Fu0))*(exp(Fu1)/sqrt(F1dp))*(prob1/prob0);
    F0p2=B0*Id1/(2*C0)-1;
    F0p=[F0p1 F0p2 F0p3 F0p4];
    rootF0p=roots(F0p); % solve for the roots of F'(u)=0
    u0=rootF0p(find(rootF0p>0)); % take positive root
    F0dp=(2*A0/B0)/u0^3+M/u0^2+2*C0/B0^2; % second derivative of F(u)
    Fu0=-A0*(u0-1)/(B0*u0)+(C0/B0^2)*(u0-1)^2+(Id1/B0)*(u0-1)-M*log(u0);
    F1p2=B1*Id1/(2*C1)-1;
    F1p=[F1p1 F1p2 F1p3 F1p4];
    rootF1p=roots(F1p);
    u1=rootF1p(find(rootF1p>0));
    F1dp=(2*A1/B1)/u1^3+M/u1^2+2*C1/B1^2;
    Fu1=-A1*(u1-1)/(B1*u1)+(C1/B1^2)*(u1-1)^2+(Id1/B1)*(u1-1)-M*log(u1);
    FId1=1-(sqrt(F0dp)/exp(Fu0))*(exp(Fu1)/sqrt(F1dp))*(prob1/prob0);
    if FId1*FId0<0
        Id2=Id0;
    else
        Id1=Id0;
    end
end
end
Id=Id1;
% Probability of error for logical zeros
F0p2=B0*Id/(2*C0)-1;
F0p=[F0p1 F0p2 F0p3 F0p4];
rootF0p=roots(F0p);
u0=rootF0p(find(rootF0p>0));
%Fu0=-A0*(u0-1)/(B0*u0)+(C0/B0^2)*(u0-1)^2+(Id/B0)*(u0-1)-M*log(u0);
Fu0=-A0*(u0-1)^2/(B0*u0^2)-(C0/B0^2)*(u0-1)^2+M*(u0-1)/u0-M*log(u0);
Gu0=Fu0+0.5*log(2*A0/u0^3+M*B0/u0^2+2*C0/B0);
Gu0p1=(2*A0/B0)*((1-u0)/u0^3);
Gu0p2=(2*C0/B0^2)*(1-u0);
Gu0p3=M*((1-u0)/u0^2);

```



```

Gu0p4=-(3*A0+M*B0*u0)/(2*A0*u0+M*B0*u0^2+2*C0*u0^4/B0);
Gu0p=Gu0p1+Gu0p2+Gu0p3+Gu0p4;
P0=exp(Gu0)*(1-exp(-Gu0p*u0))/(sqrt(2*pi*B0)*Gu0p);
% Probability of error for logical ones
F1p2=B1*Id/(2*C1)-1;
F1p=[F1p1 F1p2 F1p3 F1p4];
rootF1p=roots(F1p);
u1=rootF1p(find(rootF1p>0));
%Fu1=-A1*(u1-1)/(B1*u1)+(C1/B1^2)*(u1-1)^2+(Id/B1)*(u1-1)-M*log(u1);
Fu1=-A1*(u1-1)^2/(B1*u1^2)-(C1/B1^2)*(u1-1)^2+M*(u1-1)/u1-M*log(u1);
Gu1=Fu1+0.5*log(2*A1/u1^3+M*B1/u1^2+2*C1/B1);
Gu1p1=(2*A1/B1)*((1-u1)/u1^3);
Gu1p2=(2*C1/B1^2)*(1-u1);
Gu1p3=M*((1-u1)/u1^2);
Gu1p4=-(3*A1+M*B1*u1)/(2*A1*u1+M*B1*u1^2+2*C1*u1^4/B1);
Gu1p=Gu1p1+Gu1p2+Gu1p3+Gu1p4;
P1=exp(Gu1)/(sqrt(2*pi*B1)*(-Gu1p));
BER=prob0*P0+prob1*P1;

```

Program 9

```

% This program uses the Gaussian approximation to calculate the probability of error and
% BER.
function[BERg]=BERgauss(Bopt,Belec,mt,Nsp,Go,Pinlb,delta,prob1,prob0)
M=round(Bopt/Belec); % ratio of filter bandwidths
M=mt*M; % correction to M
Rin=50; % input resistance of electrical amplifier (Ohm)
Tk=273+25; % temperature (Kelvin)
F=10^(7/10); % noise figure of electrical amplifier
varthermal=(2*k*Tk*F/Rin)*Belec; % variance of thermal noise (A^2)
Psat=30e-3; % EDFA saturation power (W)
eff=0.8; % detector quantum efficiency
R=eff*q/(h*f); % responsivity of PIN diode (A/W)
Pinl=muin*Pinlb; % input power to EDFA for logical ones after loss (W)
Pin0=delta*Pinl; % input power to EDFA for logical zeros after loss (W)
Pinav=prob1*Pinl+prob0*Pin0; % average input power to EDFA after loss (W)
% Use Newton Raphson Method to solve for the EDFA gain
G=Go; % starting point
g=G-Go*exp((1-G)*Pinav/Psat); % function to be solved
gp=1+(Go*Pinav/Psat)*exp((1-G)*Pinav/Psat); % first derivative of g(G)
eps=1e-10; % error limit
while abs(g)>eps
    G=G-g/gp;
    g=G-Go*exp((1-G)*Pinav/Psat); % g(G)
    gp=1+(Go*Pinav/Psat)*exp((1-G)*Pinav/Psat); % g'(G)
end
Psig1=L*muout*G*Pinl; % output signal power of EDFA for logical ones (W)
Psig0=L*muout*G*Pin0; % output signal power of EDFA for logical zeros (W)
Pase=L*muout*mt*Nsp*(G-1)*h*f*Bopt; % ASE power (W)
varshot0=q*R*(Pase+Psig0)*Belec; % variance of shot noise for logical zeros (A^2)
varshot1=q*R*(Pase+Psig1)*Belec; % variance of shot noise for logical ones (A^2)
% Gaussian approximation
Imo=R*(Psig0+Pase); % mean current for logical zeros (A)

```

```

var0=(2*R^2*Pasc*Psig0)+(R*Pasc)^2)/M+varthermal+varshot0; % variance-logical
zeros (A^2)
Im1=R*(Psig1+Pasc); % mean current for logical ones (A)
var1=(2*R^2*Pasc*Psig1+(R*Pasc)^2)/M+varthermal+varshot1; % variance-logical
ones (A^2)
A=var1-var0;
B=2*(Im1*var0-Imo*var1);
C=var1*Imo^2-var0*Im1^2-var1*var0*log(prob0^2*var1/(prob1^2*var0));
Idg=roots([A B C]);
Idgauss=Idg(find(Idg>Imo));
% For logical zeros
argerfc0=(Idgauss-Imo)/sqrt(2*var0);
P0g=0.5*erfc(argerfc0);
% For logical ones
argerfc1=(Im1-Idgauss)/sqrt(2*var1);
P1g=0.5*erfc(argerfc1);
BERg=prob0*P0g+prob1*P1g;

```

The End